STOCHASTIC PREDICTION OF
SHEAR STRESS DISTRIBUTIONS AT THE BED OF
OPEN CHANNEL BENDS

by

MAMDOUH ALY NOUH

Submitted in partial fulfillment
of the requirements for the degree
of Doctor of Philosophy

Department of Civil Engineering
School of Graduate Studies
University of Ottawa
Ottawa, Canada

March 1978

To my mother

and to the spirit of my father

in loving gratitude

One can learn much from a river

From the river I have learned too:

everything comes back

H. Hesse-Siddhartha.

ACKNOWLEDGEMENT

During the thirty-month period of work on this project, the writer received assistance and suggestions from many people, to whom he would like to express appreciation. Special gratitude is due Dr. D. R. Townsend, Associate Professor in the Civil Engineering Department of the University of Ottawa and the advisor of the project, for his comments and counsel throughout the study and particularly his assistance concerning the preparation and reviews of the thesis; and Professor R. G. Warnock, Chairman of the Civil Engineering Department of the University of Ottawa, for his advice and encouragement.

Appreciation is extended to Professor A. Shukry, Chairman of the Civil Engineering Department of Alexandria University, Alexandria, Egypt; to Professor N. Ahmed, Professor of Stochastic Systems in the Electrical Engineering Department of California University, Berkeley, California; to Dr. K. Adamowski, Associate Professor of Hydrology in the Civil Engineering Department of the University of Ottawa, for their suggestions in developing the stochastic model.

The author gratefully acknowledges the Civil Engineering Department, University of Ottawa for providing laboratory and computing facilities to conduct this program of study; and the National Research Council of Canada for providing funds under Grant No. A-7443.

ABSTRACT

A stochastic-type numerical model is developed to predict the stable bed shear stress distributions and related bed topography in the vicinity of open channel bends having large radius of curvature to flow depth ratios. The flow regions described by the model include the bend sections and those portions of the downstream straight channel reaches along which the strong secondary flow mechanisms, generated in the former, remain an influential flow feature.

In addition to the theoretical and numerical analyses the overall investigation included comprehensive laboratory studies on a representative physical model of the system. The physical model consisted of a 10 m long plexiglass channel, having a rectangular cross section 30 cm wide by 6 cm deep, that contained an adjustable bend (test) section approximately 2 m downstream from the entrance to the channel. Central bend angles of 45°, 60° and 75° with a mean radius of curvature to channel width ratio = 3 were adopted for the studies. The bed material used throughout the tests was a coarse sand having a median grain size (d_{50}) = 0.7 mm and standard deviation (σ) = 2.05.

Point velocity and turbulence measurements were obtained using a Lazer Doppler Anemometer system. The major advantage of this particular system, over other velocity-measuring systems, is the remote sensing (optical) techinque it employs. Since local disturbance of the flow field, at the point of measurement, is eliminated overall accuracy is enhanced.

Measured shear stress distributions within the test sections were expressed in dimensionless format, i.e., local boundary shear stress was related to the corresponding theoretical uniform shear stress for a

straight infinitely-wide rectangular channel operating under similar flow conditions.

In the numerical analyses different models were employed to generate steady state bed shear stress distributions in the various test sections along selected pathlines that were parallel to the channel walls and comparison between predicted and measured stress distributions were used to examine the relative merits of the models developed for this purpose.

The results of these comparative studies indicate that shear stress distributions, along any pathline parallel to the channel walls, can be predicted to any require accuracy using a finite Fourier series approach. Furthermore, to ensure an acceptable degree of accuracy in the prediction, a minimum number of harmonics in the analysis is recommended. This number was found to depend on the position of the respective pathlines (relative to the channel's inner wall) and also on channel geometry; for example the number increases as the radius of curvature of the pathlines and the bend angle decrease.

Moreover, a second order autoregressive process appears appropriate in the analysis and the auto correlation function for all pathlines is found to be of the damped sine wave or damped exponential wave character. This conclusion is reflected in the periodic behaviour of the change in the bed shear stress along any pathline in the channel test section.

TABLE OF CONTENTS

LIST OF FIGURES

Figure		Page

NOTATIONS

The following symbols are used in this thesis:

A_c = cross-sectional area of channel;

A_e = logarithmic velocity distribution law constant;

A_m = coefficient of Fourier series corresponding to the <u>mth</u> harmonic;

a_t = white noise;

a_1 = constant;

B_e = logarithmic velocity distribution law constant;

B_m = coefficient of Fourier series corresponding to the <u>mth</u> harmonic;

b = channel width;

C = Chezy coefficient;

C_k = estimated sample variance at lag k;

C_v = volumetric concentration of total sediment load transported;

D_{16} = median size of sediment (letter D with numerical subscript denotes particle size in sediment for which percentage by weight corresponding to subscript is finer, i.e., D_{16} is size for which 16% by weight of sediment is finer);

d = flow depth;

e_i = unit vector in laser light scattering direction;

e_s = unit vector in laser light incident direction;

F = $v/\sqrt{gd}$ = Froude number;

F' = $(1 + R'^2/(1 - R'^2)).\tan 2\pi f_o$ = phase in AR model;

f_D = Doppler frequency;

f_o = frequency which is defined as $\cos 2\pi f_o = \phi_1/(2\sqrt{-\phi_2})$;

= fixed value;

f_1 = $1/N$ = fundamental frequency;

f_i = frequency of incident laser light;

f_s = frequency of scattered laser light;

G_1^{-1}, G_2^{-1} = roots of the characteristic equation in AR(2);

g = acceleration of gravity;

h = mean depth of flow;

I = limiter;

I_r = transverse slope of free water surface;

I_θ = longitudinal slope of free water surface;

κ = von Karman's universal constant;

L = length of channel;

N = number of observations;

n = refractive index of medium;

p = pressure;

P_w = wetted perimeter of channel;

Q = water discharge;

R = hydraulic radius of channel (= A_c/P_w);

R' = $-\phi_2$ = damping factor;

R_m = amplitude at <u>mth</u> harmonic;

r = radius of curvature of channel;

r = coordinate, transverse to main flow direction (horizontal);

r_k = estimated <u>kth</u> autocorrelation coefficient;

S = channel slope;

s_n = distance of a point from the wall;

T = duration period;

T_f = turbulent correction factor;

T_o = time constant;

t = time;

t = length lag;

u = velocity at distance s_n from the wall;

u = DC output;

u_* = $\sqrt{\tau_o/\rho}$ = shear velocity;

u' = instantaneous turbulence fluctuation of u at a point;

V = mean velocity;

$\overline{V}$ = velocity vector;

v = velocity;

v_ξ = velocity at distance ξ from the wall;

v_{av} = mean velocity at vertical;

v_{max} = maximum velocity at vertical;

v_{*o} = shear velocity;

v'_{*o} = grain-roughness shear velocity;

v''_{*o} = form drag shear velocity;

v' = instantaneous turbulence fluctuation of v at a point;

v'_z = transformed variable defined as $v_z \frac{r}{h}$;

v_r, v_θ, v_z = velocity projections along the coordinate lines of r, θ and z respectively;

w_k = lag window function;

w_{16} = fall velocity of the bed material D_{16} at a given viscosity;

X = variable length or distance;

x = coordinate in flow direction;

y = coordinate normal to water surface (vertical);

y_α = normal deviate corresponding to probability α;

z = coordinate transverse to flow (horizontal);

z' = transformed variable defined as $z \frac{r}{h}$;

α = angle;

γ = unit weight of water;

γ_k = autocovariance at k lag;

θ = angle;

θ = coordinate in the flow direction;

θ_k = kth parameter of MA;

λ = wave length of laser light;

μ = dynamic coefficient of turbulent viscosity;

μ' = dynamic viscosity of water;

ν = kinematic coefficient of turbulent viscosity (= μ/ρ);

ν_r = kinematic coefficient of turbulent viscosity in r direction;

ν_{ro} = kinematic viscosity of water surface in r direction;

ν'_r = transformed variable defined as ν_r/ν_{r_o};

ρ, ρ_f = mass density of water;

ρ_k = kth population autocorrelation coefficient;

ρ_s = mass density of sediment;

σ = gradation of bed material;

σ^2_τ = population variance of a series;

τ = bed shear stress;

$\bar{\tau}_o$ = average shear stress acting on channel boundary area (defined by its wetted perimeter, P_w, and length, L);

$\bar{\tau}$ = average bed shear stress acting on a series path;

τ = estimated bed shear stress;

ϕ_k = kth parameter of AR;

ϕ_{kj} = jth coefficient in an autoregressive process of order k;

ϕ_m = arc tan $-\frac{B_m}{A_m}$ = phase at mth harmonic;

ξ = z/h = dimensionless variable.

CHAPTER 1

INTRODUCTION

Boundary shear stress distribution, in a fully-developed open channel flow, is predominantly a function of the velocity distribution in the flow field. The velocity distribution in a curved channel section (river bend) differs substantially from that in the preceding "straight". This is largely due to the presence of a strong helicoidal flow pattern in the bend (generated by the flowline curvature) - the effects of which may persist for a considerable distance downstream from same.

These so-called "secondary currents", which govern the distribution of boundary shear stress (and hence the general bed topography) in the vicinity of channel bends, constitute only one factor in a highly complex problem in river engineering, namely that of sediment transportation.

In an alluvial stream, where non-cohesive materials constitute a large percentage of the total sediment complex, this secondary flow phenomenon is the prime mechanism responsible for the establishment of the "meander" profile of the main channel. This has become, in many instances, an important economic consideration (in overall river management) in that substantial areas of valuable agricultural lands are lost in the erosion process.

Furthermore, subsequent deposition of material, (initially eroded along the outer bank of a river bend), near the inner bank downstream from the bend can present problems of equal importance. For example: dredged navigation channels may become blocked through silting and river intake/outfall structures might suffer similar consequences.

These complex interrelated processes of erosion, transportation and deposition of material are governed, to a large degree, by the shear stress distribution at the sediment/water interface as is the stable channel bed configuration under "regime" flow conditions.

A major criticism that can be made concerning recent fundamental studies in this area is the fact that theories[16,28,45] developed for the prediction of boundary shear stress distribution are only applicable to the bend sections themselves. They do not extend to the straight channel reaches (immediately following the bends) where, as has been mentioned earlier, the secondary currents remain a significant flow feature. Moreover, these same theories are based on an assumed uniform tractive force distribution on the channel bed - an assumption that normally does not reflect the true situation in a natural watercourse.

Another recent laboratory investigation[42], while reporting boundary shear stress values in channel bends, does not provide a methodology to facilitate prediction of the steady-state distribution therein. Furthermore, the data reported in these studies may be subject to inherent errors introduced by the nature of the instrumentation employed in the investigations.

In view of the aforementioned limitations in existing theories and related laboratory studies on this subject it was felt that further work in this area was warranted. In particular there was a need to develop a more comprehensive predictive model that would include those portions of the straight channel reaches, downstream from the bends, that continue to be influenced by the secondary currents generated in the latter.

In the present study bed shear stress distributions in channel bends, and in the straights following the former, were determined using a "single-point" measurement technique and predictions of the steady-state stress distribution were obtained from a stochastic-type numerical model developed for this purpose.

CHAPTER 2

LITERATURE REVIEW

Boundary shear is the tractive force exerted by water flowing over the wetted perimeter of a channel or river cross section. It is defined by Lane[53] as a force exerted over a unit area of the channel perimeter. It is believed that the concept of average shear stress for an entire flow cross-section was first introduced into hydraulic literature by duBoys in 1879 (Chow[12]). If uniform flow exists in a channel the average shear stress, $\bar{\tau}_o$, acting on the channel-boundary area (defined by the wetted perimeter, P_w, and length, L) must evidently balance the corresponding weight component of the volume of water contained in the channel section of length L.

i.e. $$\bar{\tau}_o P_w L = \gamma \sin\theta A_c L$$

or $$\bar{\tau}_o = \gamma \frac{A_c}{P_w} S = \gamma RS \quad (1)$$

where γ is the unit weight of water; S is the channel slope defined by $S = \sin\theta$; A_c is the cross-sectional area of the channel; and R is the hydraulic radius ($= A_c/P_w$).

This equation, while supplying the mean value of boundary shear stress in the section, does not provide a means for determining the distribution of same over the channel bed. Moreover, the necessary condition for generating a uniform stress distribution is that where an "infinitely wide rectangular channel" situation is applicable. Accordingly this particular distribution is rarely approached in a natural watercourse.

Localized erosion and sedimentation processes in a river cross section are due , largely, to the presence of an inherently non-uniform stress distribution at the sediment/water interface caused by local accelerations and secondary currents in the flow field.

The degree to which these interrelated flow phenomena influence and govern the complex sediment transport processes constitutes an important aspect of overall river management and, in this regard, application of Equation (1) requires some method of differentiating the expression over the wetted perimeter.

This problem becomes even more complex when curved channel sections (river bends) are encountered insofar as the aforementioned secondary currents in the flow field become a dominant feature.

In recent years several researchers(16,28) have attempted, through analysis and experiment, to solve this particular problem. Their investigations center on the nature and development of the secondary currents in channel bends and their resulting effect on the velocity (and hence boundary shear stress) distribution therein.

2.1 Secondary Currents in Curved Streams

In the field of fluid dynamics there are a number of flow phenomena that are collectively described as "secondary (currents) flows". Although, in general, the term secondary flow may be used to describe any flow that has velocity components perpendicular to its mean flow path, Prandtl[88] identifies three basic flow categories where strong secondary currents will normally develop as follows:

(a) flow in conduit bends, between curved guide vanes, and in open channel (river) bends;

(b) flow in straight open channels, and in conduits of non-circular section; and

(c) oscillating flows produced by either a solid body vibrating in a still fluid, or a fluid oscillating near a solid, stationary boundary (e.g. standing waves near a vertical wall).

A common example of the first category is the double-spiral (helicoidal) flow pattern that initially develops in a bend of an open channel. James Thompson[47], in 1877, was the first to conduct, with the aid of flow visualization techniques, a qualitative investigation of this flow phenomenon in a curved experimental channel. Subsequently, Hinderks[40], using a similar technique, clearly demonstrated that the secondary current near the outer wall of the bend is the dominant flow feature insofar as it tends to grow rapidly at the expense of the other secondary current in the flow field.

The secondary flows associated with the second category, (namely flow in straight channel sections), take the form of two contra-rotating spiral currents that are symmetrically distributed about the centreline of the channel cross section. Whereas this particular motion is difficult to show experimentally, (since it is not usually as dominant a feature as the first category), Einstein and Li[21], using Lamb's form of the Navier-Stokes equations, have shown that this type of flow occurs spontaneously in a turbulent flow field but not in laminar flows.

In channel stabilization work, the study of flow processes in stream channel bends (secondary flow of the first kind) is of primary importance. This is because the erosive patterns characteristic of river channels, such as downstream migration of meanders, are essentially due to the non-uniform flow created by river bends. Studies of this type supply the answers to many important questions, such as, which areas of the stream bed require protection and to what depth?

One of the important characteristics of flow in bends is the presence of a spiral flow pattern which was analyzed by Joseph Boussinesq about 1868 and independently discovered and demonstrated by James Thompson[47] a few years later. It owes its existence to the interaction of frictional, centrifugal and inertial forces on the fluid passing through the curve. Near the bottom of a channel the local velocities are greatly retarded by boundary resistance. The surface particles, which have much greater inertia because of their higher velocities, tend to maintain their direction down the channel while the slower moving fluid near the bottom is forced to follow a more sharply curved path to maintain a balance between centrifugal and pressure forces. To maintain continuity of the fluid mass, water flows upward from the bottom along the inner bank while it is being forced downward at the outer bank. This induced spiral current tends to transport eroded channel material laterally across the bend, depositing some of it to form "point bars".

Ideally, if flow approaching a bend first traverses a sufficiently long upstream tangent, the lateral distribution of velocity at the entrance to the bend will be essentially uniform except close to the boundaries where friction is important. Upon entering the bend the tendency will be to conserve the momentum of fluid, leading to accelerations along the inner bank where the radius of curvature is smaller, and to deceleration along the outer bank. Were it not for the effect of the boundary influences, which diffuse through the flow, the tendency would be to develop across the bend a free vortex velocity distribution, in which the product of velocity and radial distance is constant. Boundary effects are most prevalent along the inner bank and across the bottom where, in the latter case, a continuous boundary layer is formed by the laterally inward movement of fluid induced by the spiral flow[22]. This bottom boundary layer grows larger as the fluid traverses the width of the bend and approaches the inner bank Simultaneously, the resistive effect of the inner bank on the flow is diffused outward to form a region of retarded fluid growing in width with distance through the bend. Although boundary resistance is also important at the outer bank, the size of the boundary layer generated at the inner bank is larger owing to the existence of favourable pressure gradients. Thus, as a first approximation, the flow pattern may be considered to have two principal parts; firstly, a complex boundary region in which frictional effects are dominant and secondly, the remainder of the cross section (distant from the bottom and the inner bank) in which frictional effects are largely unimportant.

The lateral effects of the boundary layer growth along the inner bank is to force outward the filament of maximum velocity. The growing boundary layer becomes filled with ever-increasing quantities of relatively slow-moving fluid, and the velocities in the outer inviscid flow region must continually accelerate to satisfy continuity. As the exit of a bend is approached the influence of the downstream tangent redistributes velocities so that they tend to return to lateral uniformity.

In fact, the flow pattern in a natural bend tends to be considerably more complicated than this simple explanation. Residual circulation patterns arising from upstream bends and the generally irregular channel geometries are two of the important modifying factors. In addition, along the inner bank of a relatively short radius and shallow bend the flow may separate from the boundary, creating an essentially stagnant eddy zone. Despite these complicating factors the general flow pattern in almost all bends exhibits the secondary spiral pattern, the initially higher velocities along the inner bank, and the gradual outward deflection of the maximum velocity filament.

James Thompson[(46)] was the first to produce a cogent analysis of the behaviour of water flowing through a river bend. He concluded that:

(a) There must be a transverse inclination of the water surface,

(b) the layer of water along the bed, being retarded by friction has much less centrifugal force than fluid above and will consequently flow across the bottom towards the inner bank,

(c) part at least of this cross flow will rise up the inner bank and protect that bank against the faster main stream flow,

(d) along the outer bank, the tendency of descent will draw fast flowing surface water into the bank and accelerate erosion,

(e) transverse flow begins upstream of the bend, and

(f) mud and sand in motion in the bed layer will tend to be deposited at the inner bank and this material is more likely to come from upstream than the outer bank of the same bend.

The transverse inclination of the water surface in open channel bends has been well documented, Blue, Herbert and Lancefield[5], Eakin[19] and Leliavski[58], the amount of superelevation being proportional to v^2b/gr, where "v" is mean longitudinal velocity, "b" is the channel breadth, "g" is acceleration due to gravity and "r" is mean radius of curvature. A similar formula is obtained by Grashof[38] assuming that the velocity is uniform everywhere in the cross section. This formula has been modified by experiments for design purposes by Jobes and Douma[50].

Based on assumptions that the velocity varies directly as radius (forced vortex flow), and the mean velocity occurs at the centroid of the section Chatley[10] derived the formula for water superelevation. Ippen and Drinker[45] derived another formula assuming that the mean velocity occurs at the centerline of the section and for constant average specific head and constant cross section. This formula is modified(92) later to take into consideration the effect of the corrected angular velocity of the vortex for angle of bend being less than 90°. On the other hand, another formula is suggested(103) when the circulation constant of the vortex is corrected for the inclined angle of the bend being less than 90°. Woodward(105) derived another formula which is based on the assumption of parabolic distribution of velocities at any (radial) section in the channel bend with velocity equal to zero at banks and maximum at the center. When the velocity varies both directly and inversely with radius (combined vortex), Chatley(10) derived another formula for the superelevation of the water surface. However, Shukry(92) found that critical depth exists at the radius separating the zones of forced and free-vortex flow in the bend. The formula that is based on a combined vortex flow concept is considered best suited for computation of maximum superelevation in river bends, even though the zones of free and forced vortex are not completely defined in such sections.

Theoretical and experimental studies of flow in an open channel bend were made by Mockmore(66). In the laboratory investigation the motion of floats, suspended oil globules and rice grain were filmed and velocity distributions measured using a small current-meter. From his experiments Mockmore concluded that the spiral flow enunciated by James Thompson existed but was very complex, and that slack water developed at the inner bank due to the secondary motion. Mockmore found that the strong boundary motion caused the bed load to move from the outer to the inner bank. The thin layer of fluid which moves across the bed of smooth channels (and carries with it some particulate matter) appears not to form in rivers, probably due to the rough bed form common in natural water courses. (Friedkin[34] also showed that, in rough loose boundary models, sand does not cross the stream bed at bends.) Mockmore's contribution, however, ignores certain important geometric parameters, (including relative curvature of the bend, shape of the channel cross section, and the length of the bend), which undoubtedly have significant effects on the flow field generated therein. Moreover, his mathematical model of the system assumes that the spiral flow is initiated, suddenly, at the point of entrance to the bend and remains constant through the bend section. Several investigators[2,75,85] have proved, however, that the spiral flow starts at a certain distance upstream from the bend entrance, increases in intensity through part of the bend and then decays over the remaining portion of the bend and over a section of the straight channel reach immediately following the bend.

Shukry[91], using a pitot sphere to measure velocity components, was able to calculate the strength of the secondary flow at various sections around a channel bend. Defining strength of the secondary flow as the percentage ratio of mean kinetic energy of lateral motion to the total kinetic energy of the flow, Shukry studied the variation of the strength of the secondary flow with Reynold's number, radius to breadth ratio, depth to breadth ratio and bend length.

It was suggested, in the discussion following Shukry's paper, that the Froude number of the flow should be considered a factor in the development of the spiral currents. However, in the closing discussion Shukry countered that, since spiral currents are primarily a friction-related phenomenon, there is every reason to expect that, for Froude numbers well below critical, the development of these currents would be essentially independent of the Froude number.

Unfortunately, Shukry's experimental results must also be viewed with caution in view of the fact that he reported poor entrance conditions (to his bend test section) which ultimately influenced the secondary flow generated by the bend.

Chacinski[9] and Wadekar[102] investigated the effects of different "entrance" conditions in their experimental studies. They initially controlled (minimized) secondary motion in the straight channel section preceding the bend and compared data with similar observations obtained after deliberately introducing secondary motion in the flow upstream from the bend.

Einstein and Harder[22] introduced a parameter "$\frac{v}{r} \cdot \frac{dv}{dr}$", (where "r" is radius of curvature and "v" is velocity), which is a function of the horizontal velocity distribution and should lie between -1 and +1 for free and forced vortex flow respectively. Experimentally all values were in excess of +1 and this may be attributed to the distortion of the velocity distribution by the secondary flow.

After introducing experimental values in their theory they discovered that it was necessary for the friction slope, in the upper layers of the fluid, to be almost zero (i.e. bed shear stress was only effective in the fluid field very close to the bed). Their analysis assumed that vertical velocity components were negligible and that the velocity pattern did not change from section to section or with time (i.e., an equilibrium velocity distribution was assumed to exist). Although these assumptions appear to be reasonable they did not check the validity of these assumptions in the course of their experiments.

Fox and Ball(33) investigated the secondary flow generated in a bend of a rigid-boundary experimental channel with the aid of a finite-difference type mathematical model. While satisfactory agreement was obtained between theory and experiment, their model has a limited application in view of the rigid boundary condition examined.

A second major characteristic of the flow field in channel bends is the related superelevation of the water surface therein. Yen(107) studied this particular phenomenon, for flow in trapezoidal channel bends, and derived, from an examination of the equations of motion, simplified mathematical expressions for the longitudinal and transverse water surface slopes.

While reporting satisfactory agreement between computed and measured superelevations he stressed that calculations, based on mean velocities alone, are often inadequate and that cross sectional shape and helical motion in the flow field are important factors in the analysis. Consequently, in view of the complex nature of the latter, accurate determination of the water surface superelevation is difficult.

These added complications, (introduced by the presence of secondary currents in open channel bends), led Robert[81] to recommend two basic approaches to the problem-depending on the degree of sophistication required. In dealing with minor studies on small streams, for example, he suggests neglecting the effects of secondary currents and, in the case of detailed studies relating to major watercourses, he recommends the use of more sophisticated mathematical and physical models of the systems. Robert[81] also developed a formula which related maximum superelevation of the water surface in a channel bend to discharge in the channel. The methodology is based on the principle that transverse water surface slope is related to velocity head and bend geometry.

Ripley[80] used data collected from natural streams to produce empirical formulae by which one can estimate the depth of a stream corresponding to any natural curvature. He concluded from his analysis that whenever the radius of curvature is less than 40.0 times the square root of the area of the channel, no further deepening of the channel results from increased curvature. Also, whenever the radius of curvature is greater than about 50.0 times the square root of the sectional area, the cross-section profile does not conform strictly to that due to curvature.

Muramoto[68] studied the hydraulic characteristics of the upper layer in a fully developed region of curved flow, that had a uniform equilibrium velocity distribution in the main flow direction. He derived fundamental equations to compute the radial distribution of the tangential velocity and the surface profile in the upper and lower layers, from the Navier-Stokes equations of motion, and the continuity equation. He concluded, from his investigations, that the fully-developed region in a curved section of an open channel is restricted to the downstream portion of same.

Salamon(87) studied analytically and experimentally the turbulent properties of a fully developed two-dimensional flow of air in a curved channel with constant radius of curvature. He concluded from the results that the fully developed turbulent flow occurred at an angle of 170.0° from the entrance to his bend section. Also, the intensity of turbulence as well as the energy dissipated through the curve were found to be greater at the inner wall than corresponding measurements near the outer wall.

Mostafa(67), using the principle of moment of momentum for flow through a bend, tried to find the radius of curvature which gave minimum loss of energy. He found that the loss due to the bend approached that for the straight channel when the ratio of the width to the double radius of curvature is equal to or less than 0.15, and Froude number is equal to or less than 0.60. He found from both his analytical and experimental results that the bend losses depend mainly on Froude number.

Muramoto(69), in his study of the complex structure of the flow field in a bend, divided the flow into three distinct zones, namely: a generating region, a developing region, and a fully-developed region. The analysis, which was based on measurements of the three velocity components and computed vorticity components of the bend flow, produced expressions for the distribution of velocity and vorticity in the initial and final regions of the flow field.

A study of laminar flow through pipes of circular cross section with small curvature was conducted by Murata and Inaba[70]. They concluded from their studies that, at sufficiently low Reynold's number, the axial flow shifts laterally to the inner part of a curved section and is accompanied by minimum energy dissipation. At higher Reynold's number the flow shifts to the outer boundary. The adaptation of the flow to curvature in the direction of flow is more and more delayed as the Reynold's number increases; the delay also increases with wave number in the case of a sinosoidally-curved pipe.

Chikwendu[11] performed a series of laboratory experiments to study the patterns, magnitudes and mixing effects of secondary currents in curved density-stratified rivers. Hot water and cold water were used to simulate the upper and lower layers respectively. He found that in the case of simple underflow, (which is free from entry secondary currents), two helical motions exist in the cold layer. In the overflow-with underflow case three helical motions are generated; one in each fluid layer and one in the intermediate mixing layer. He concluded that the helices are essentially confined within the density layers where they are formed. Also, he concluded that although these currents are responsible for transporting heat and mass from one layer to another they affect mixing to a small extent only.

In general the complex nature of the flow field in river bends is due, firstly, to the non-alignment of the channel (which results in centrifugal forces, superelevation of the water surface and related secondary currents) and secondly to the presence of the mobile boundaries. These various factors are, in turn, responsible for the development of the well-known meandering profile of the main channel of alluvial rivers where they cross their respective flood plains. While many researchers have examined these secondary flow processes with the aid of numerical models, until recently few laboratory studies have been performed using mobile-bed models.

Engels[(25)] revealed the essential meandering tendency of river channels by passing a flow over an initially flat sand bed. He found that a sinusoidal profile was developed by the flow.

Boussinesq[(6)], in assuming similarity between flow in pipe bends and open channel bends, produced a relationship for the mean flow depth in a bend as a function of the bend radius of curvature. A similar relationship, based on field observations, was reported by Fargue[(31)].

Rozovskii[(86)] performed experiments in an experimental channel having a mobile bed and a single 90.0° bend section. He found that significant erosion of the bed material occurred near the exit of the bend section.

Based on an assumed velocity distribution and critical shear stress for incipient motion of the bed material, Suga[(96)] obtained the static equilibrium lateral bed profile in a bend as a function of radial position in the bend. Moreover, for an assumed bed shear stress distribution, he produced similar relationships for dynamic equilibrium conditions.

An approximate theoretical analysis (through dimensional analysis) has been developed by Yen[106]. In his study, the bed-topography was obtained by passing water along a fixed-wall meandering channel with an initially flat sand bed until the latter reached a stable bed configuration. He found that, in fully developed curved channel flow, the transverse slope at a given point on the stabilized bed is directly proportional to the parameter which characterizes the relative importance of fluid inertia versus gravity acting on a particle, moving along the bed. Also, the pattern of bed-topography in a fixed-wall meander with a given plane channel geometry is a function of width: depth ratio, the Froude number and the ratio of particle fall velocity to the mean flow velocity.

Callander[8] developed a linearized stability mathematical analysis for the flow of water in a channel with a loose bed and vertical banks. His analysis is based on the assumption that the wave length of the perturbations, which develop into meanders or braids, is longer than the width of the channel. He found that instability is interpreted as leading to a meandering or braided channel. He concluded that all natural channels are unstable. Wave lengths calculated for channels expected to meander are compatible with those given for Inglis' empirical rule and wave lengths calculated for channels which become braided are approximately the same as those observed.

Engelund[26,27,28] adopted the vorticity transport equation to study mathematically the stability of a sand bed in an alluvial channel. He and Skovgaard[27] developed a mathematical model describing the three-dimensional flow leading to instability of an initially straight channel. Their analysis indicated that for given hydraulic resistance and depth the river will exhibit meandering if the width is smaller than some threshold value, while a wider river will braid in two or more courses; the more, the wider it is. They found their results seem to agree with observations reported by Leopold and Wolman (1957) (Lane[53]). In 1974, Engelund[28] developed a theory to predict the bed topography in sinusoidal open channel bends with erodible beds. The agreement between his theory and Hooke's observations[42] was satisfactory especially in the zone upstream of the point bar formation.

Langbein and Leopold[54] have suggested a "random walk" technique which can be made to produce a meander-like profile. They claim that such a pattern is more stable and minimizes energy losses. In a study of five Wyoming rivers, they found that the variances in the bed shear and in the friction factor were uniformly lower in the curved than in the straight reaches. Einstein and Shen[24] observed two types of meandering patterns in straight alluvial channels. They postulated that the first type (i.e. alternating diagonal bar patterns) resulted from surface waves on the water, and that the second type, namely alternating scour hole patterns, could be caused by the difference between the shear stresses at the two sides of the flow cross section.

Einstein and Li[23], and Shen and Komura[90] have argued that meandering is an instability phenomenon. Exner[53] argues that meandering is due to reflection of the stream by dunes and the eddies which form in their lee. However, this argument appears to be inadequate in that it can explain erosion but does not deal adequately with deposition. Quick[78] proposed that the principal of meandering depends on a stream-wise spiral flow which changes its direction of rotation in a cyclical manner. Furthermore, he postulated that the entrainment and subsequent deposition of bank material produce deflections in the main channel direction.

From this summary of recent contributions in this area of research it would appear that both mathematical deterministic and empirical-type approaches to solve the problem have failed to simulate, adequately, the complex flow field in river bends. In view of the inherently random nature of stream turbulence and related transport phenomena numerical models, based on stochastic processes, were favoured in the present study.

2.2 Shear Stress Distributions in Curved Open Channels

Bed shear stress determination is a very important aspect of any investigations relating to channel stabilization. Du Buat was the first scientist to introduce the concept of boundary shear stress as the main factor in analyzing the erosion process. His contribution led, eventually, to the well-known "Tractive-Force" theory by the French engineer DuBoys[18] about 100 years later.

In fact bed sediment movement increases with increasing shear stress once the critical value of shear stress (corresponding to the state of incipient motion of the individual particles) is exceeded. Therefore, it can be argued that, at any point on the bed of an otherwise stable (regime) channel, the local geometry adjusts to provide precisely the shear stress necessary to transport the sediment load supplied to that point. This adjustment takes the form of either erosion or deposition of material.

In river bends sediment transported by the flow tends to deposit in the 'slack water' zone (near the inner bank) causing the depth of flow to decrease there. This, in turn, results in a corresponding increase in the local velocity gradient (and hence shear stress). This process continues until a state of balance, or equilibrium, is reached. On the other hand, shear stress distribution along the outside bank of the bend is relatively low, initially, and a negligible amount of sediment is moved to this area of the bed from the upstream source. Because the shear stress can remove more sediment than is supplied, erosion occurs. As the outside of the bend becomes deeper, the local shear stress decreases and the lateral slope off the point bar increases, thereby increasing the sediment supply to this area of the bed. In due course equilibrium conditions are established.

Ippen and Drinker[45] have measured the shear stress distributions on the bed of a trapezoidal rigid boundary bend with a constant angle of 60°. They concluded, in general, that the distribution and relative magnitudes of the local boundary shear stress appear to be a function of the stream geometry for subcritical flows. Although they determined, from the measured shear patterns, the total head loss for the curve as well as the locations of the shear maxima, their analysis is based on one-dimensional flow in a smooth trapezoidal channel which is not the case in natural streams. Besides, the data obtained were subject to experimental error introduced by the fact that a pitot tube was used to measure velocities in the flow field.

Engelund[28] developed a theory to predict the distribution of sediment and hence bed topography in sinusoidal open channel bends with erodible beds. His theory is based on a mathematical approach which takes into account the theory of helical flow in circular bends. It provides a simplified, but non-axisymmetric computational method for the prediction of flow and bed configurations in such channels. Although the prediction was good upstream of the point bar area, it was noticed that there were non-satisfactory differences between the predicted and the measured values of shear stresses and bed topography downstream of the point bars. These differences were due to the flow separation zone downstream of the point bars, which had not been taken into consideration in the analytical model.

An attempt was made by Varshney and Garde[100] to determine the magnitude of maximum local shear stress in rigid bends. They approached the problem both analytically and experimentally. Their analysis was based on the assumption of a forced vortex condition for the radial variation of the depth-averaged tangential velocity of the flow. However, such a velocity distribution did not exist in the experiments conducted by the authors. Several studies(15,41,91) have shown that, for a fully developed bend flow in a long wide channel with zero lateral bed slope, the depth averaged longitudinal velocity, v_r, varies approximately with $\frac{1}{r}$ if the flow is laminar and with $r^{-0.5}$ if the flow is turbulent. On the other hand, shear stresses were computed from Preston tube measurements, which introduced some systematic errors in the latter that are very difficult to overcome.

De Vriend(16) developed a theory for secondary flow profiles for non-axisymmetric steady flow in shallow curved channels with fixed beds. The theory is based on the assumption that the main flow has a logarithmic longitudinal velocity profile in the vertical plane. However, it was found by Mahmood(64) that the velocity profile in a vertical can be divided, generally, into three regions of different velocity distribution. Only in the case of a flat bed without any "cut-back" at the water surface, could the logarithmic law be suitably applied over the entire vertical. In such channel bends, the computed shear stress values, using De Vriend's theory, are not in satisfactory agreement with the measured shear stress values. This disagreement increases rapidly in the downstream direction. In addition, the computational procedures are both tedious and complicated.

Hooke(42) measured the shear stress distributions, bed topography and helical strength in open channel bends with erodible beds. The centerline geometry of his flume was based on the sine-generated curve of Langbein and Leopold(54). His work established the shear stress distribution patterns corresponding to the stabilized bed condition for such bends. However, these patterns have not, as yet, been described by a theory which could make it possible to predict the shear stress at a point on the bed of a curved channel. Besides, shear stress measurements were obtained using a Preston tube which, in turn, affected the reliability of the data since systematic and random errors were introduced by the presence of the instrument in the flow field. These errors are due to one or more of the following sources:

1. In a mobile bed system, the height of the Preston tube above dune crests may vary. In Hooke's experiments, the tube was lowered to the point where scour of the crest was imminent. It is possible, therefore, to assume that the tube might have been systematically lower in zones of low shear stress. This, then, would have artificially accentuated the change in shear stress across the channel at stations (sections) in the straighter reaches. If, for example, the tube was located 1.50 mm above the dune crest near the inside bank and 3.00 mm near the outside bank, the relative shear stress, $\tau/\overline{\tau}$, would have been underestimated by 15% to 20% near the inside bank and overestimated by about 10% near the outside bank[42].

2. Dune geometry changes with position in a channel. In Hooke's experiments, all measurements were made on dune crests to ensure that the computed shear stress was maximum for any given position. Therefore, the error in underestimating the shear stress on the inside of the bend and overestimating it on the outside of the bend would be magnified.

3. Von Karman's coefficient, κ, is not a constant. It varies as the sediment concentration changes, (Vanoni and Nomicos[99], have established that its value increases as sediment concentration increases). Moreover, Rozovskii[86], in 1957, showed theoretically that under certain conditions κ may increase substantially through a bend section.

Since the erosion process is initially governed by boundary shear stress distribution, a methodology to facilitate the estimation of shear stress distribution (in the vicinity of channel bends and in the straight sections immediately downstream from them) is a fundamental requirement for studies relating to the problem of channel stabilization. In view of the apparent lack of fundamental research in this particular area, the present investigation was initiated.

2.3 Analytical Approach to Shear Stress Distribution

A mathematical model for shear stress distribution has been developed by Olsen and Florey[74], using the membrane analogy, analytical techniques and finite difference methods. The model was based on the assumption that turbulent mixing and momentum transfer, which modify a laminar velocity profile from its parabolic shape to the characteristic turbulent flow shape, can be achieved by taking some power of the velocity for the laminar case. This approach implies that the shearing stresses present in a flowing stream depend in some way on the velocity gradient. Although the method gives fair results for wide channels, it fails to predict the true shear stress distribution for narrow rectangular channels and the fact that the maximum velocity filament is located below the free surface. This is because the mechanisms of turbulent mixing and momentum transfer are not properly represented in the model.

An alternative approach is presented by Deissler and Taylor[15]. This approach depends on the assumption of neglecting the magnitude of secondary currents to simplify the equation of motion. They assumed that "uv-type" turbulent shear stresses appear only on surfaces normal to those where there is a finite gradient of $\overline{u}$, (the usual classical concept of mixing length theory), and that a velocity fluctuation $\overline{v}'$ moving through a y-gradient of $\overline{u}$-momentum produces a correlation between $\overline{v}'$ and $\overline{u}'$ and hence a stress $\overline{u'v'}$. Therefore, they devised a model involving the "law-of-the-wall" correlation and an "isovel" coordinate system which was solved iteratively to determine the wall shear stress from the axial pressure gradient. However, it is not necessarily true that the converse situation of no correlation holds if no gradient of $\overline{u}$ exists in the direction of $\overline{v}'$.

2.4 Experimental Methods for Shear Stress Calculations

There are several methods, based on velocity data, that are available for the determination of boundary shear stress. These methods are: direct methods, heat transfer techniques, and pitot tube methods.

2.4.1 Shear Stress Calculations from Velocity Data

Shear stress distributions, using velocity measurements, may be grouped into two general classes. The first is based on the entire velocity mapping of the channel cross-section such as the mapping presented in the Bazin[4] data (see Wien and Harms[104], page 286, or Nikuradse[71]). This method, adopted by Leighly[57] for data on three streams in Europe, involves drawing lines perpendicular to the isovels (lines connecting points of equal velocity) which divide the boundary into small segments. These perpendiculars terminate either at the point of maximum velocity or on the line which connects points of maximum velocity on vertical lines throughout the cross section. Thus the channel area is divided into several prisms defined by two of the perpendiculars, a unit length of channel, and the top line formed by the maximum velocity point in each vertical. Each prism contributes drag to that part of the boundary between the perpendiculars. The remaining prisms formed above the line of maximum velocities are assigned by Leighly to the dissipation by the surface. However, this method gives increased value of p_w in Equation (1), (since the surface is considered as an area of dissipation), and therefore the value of average shear stress, $\overline{\tau}_o$, is lower than that calculated using only the channel perimeter. On the other hand the assumed velocity-distribution approach, re: tractive force distribution, (i.e. that the perpendiculars constructed as described above define surfaces of equilibrium), in the presence of secondary currents and asymmetric velocity distributions can no longer be assumed.

The second method of determining shear stress distributions from velocity data consists of using a logarithmic velocity law. O'Brien[73] used a form of the velocity-distribution law for pipes proposed by Von Karman (Schlichting[88], page 488). He wrote the appropriate equations for two points in the flow field at different distances from the wall, and solved the equations by eliminating the maximum velocity term. The resulting equation can therefore be solved for τ_o, if two point velocity measurements on a velocity profile are known. Several investigators have adopted this particular approach. Taylor[97] used the universal velocity-distribution law for pipes and solved it for two different distances from the wall. Enger[29] used the equation, developed by Einstein[20] for both rough and smooth walls, in much the same way as O'Brien and Taylor. His equation indicates that the shear stress varies with the square of the velocity gradient and that two points from the velocity profile are sufficient to determine this shear stress.

In 1938, Keulegan[52] presented equations for smooth, wavy and rough channels based on the Prandtl and Von Karman velocity-distribution laws. Using these equations, one can compute the shear stress if one point on the velocity-profile and its distance from the wall are known.

2.4.2 Tractive-Force (Shear Stress) Determination from Inner-Law Velocity Data

Prandtl[88] was the first to suggest that the velocity distribution near the wall should be independent of more distant boundary conditions and should be a function only of the wall distance, the kinematic wall shearing stress, and the viscosity. Beyond the very thin viscous sublayer Prandtl assumed a constant shear and a linear mixing length to derive the following logarithmic expression:

$$\frac{u}{u_*} = A_e + B_e \log \frac{u_* s_n}{\nu} \qquad (2)$$

where the constants A_e and B_e are experimentally determined, u is the longitudinal velocity at distance s_n from the wall, ν is the kinematic viscosity, and $u_* = \sqrt{\tau_o/\rho}$ is the shear velocity.

In 1956 Ross[83] observed that the previous velocity laws (that attempted to describe the entire turbulent velocity profile with one equation) were deficient and failed to agree with measured velocity profiles. He proposed a division of the profile into a wall region and a main-flow region. The wall region was further divided into three parts: the viscous sublayer, the buffer zone, and a wall turbulence region; the first two usually being thin. He derived Equation (2) for the wall turbulence region from dimensional analysis by assuming that the most important influence on the eddy viscosity is the distance from the wall.

In the earliest formulation of the "law-of-the-wall" the constants A_e and B_e were based on observations of pipe flow (Coles[13]). The law-of-the-wall in boundary-layer studies was first proposed (and the constants A_e and B_e determined) by Ludweig[61,62] who stated that, for smooth walls, A_e and B_e are universal constants independent of the pressure gradients, the Reynolds number, or the past history of the flow. Ross[83] examined several cases where wall shear and velocity were measured. He concluded that there is no difference between the coefficients for various types of flow, and that both A_e and B_e can be taken as 5.6. However, other investigators, (Nikuradse[72], Clauser[36], Laufer[55], Leutheusser[59], Ludweig and Tillmann[62] and Townsend[98] have variously reported values of 4.9 to 6.9 for A_e and 5.53 to 5.8 for B_e. Therefore, Ross' value of 5.6 for both A_e and B_e could be justified.

Ross[83] found that the wall region, where the law-of-the-wall applies, extends out to about 10 to 15 percent of the boundary layer thickness, and for the main-flow region the Von Karman velocity-deficiency law could be applied if the value of the Von Karman coefficient κ is taken as 0.30. His equation is solved by O'Brien[73] for the shear stress, τ_o, if two points from the velocity profile are known. The solution gives satisfactory results for data points in the wall region if $\kappa = 0.41$, or in the main-flow region if $\kappa = 0.30$, and in case of smooth boundaries.

For "rough-wall" conditions Glauser[36] presented an analysis of the roughness effects by considering them as a velocity shift which is numerically identical to a shift of the wall position. The equation representing this velocity shift was used by Robertson to analyze the Nikuradse rough-pipe data. He presented the results as a function of the roughness height.

In the case of flow over a movable bed material, the problem of determining shear stresses from velocity profiles becomes complicated. This is due to the separation of the flow from the large scale boundary roughness elements and the generation of eddies in the flow field. However, Mahmood[64] found that the velocity profile over a channel sand bed can be divided into three regions.

Each region follows a different shape of the logarithmic velocity law. Thus, the determination of the velocity at a certain point depends on its location with respect to the bed.

Therefore, it would seem that these velocity-profile methods, for computing boundary shear stress, should be valid for both smooth and rough wall conditions if point velocity measurements are taken from the region described by the respective equation.

2.4.3 Direct Methods of Shear Stress Measurements

Direct skin-friction measurements were first taken by Kemf(51) who used a floating element on the bottom of a barge to obtain skin-friction values at high Reynolds numbers. A similar technique was used by Schultz-Grunow(89) to measure the frictional force on a wind-tunnel wall. Dhawan(17), Leipmann and Skinner(60), and Hakkinen(39), obtained, recently, direct measurements of the force on a small surface element of a flat plate at medium Reynolds numbers and over a range of Mach numbers. The measured skin friction was found to agree well with Blasius' theory for laminar flow at low Mach numbers. When the flow was turbulent, the measurements agreed with the semi-empirical formula of Von Karman(88). In these methods, linear variable differential transformers were used as the transducers to convert physical displacements of the small floating element into electrical signals. For various reasons it would be difficult to employ, and obtain valid results from, this particular measurement technique in the case of flow over a mobile boundary.

2.4.4 Heat Transfer Methods

These methods utilize the Reynolds analogy between transport of momentum and the transfer of heat near a solid boundary. Ludweig[61] developed an indirect method of obtaining skin friction by measuring the heat transfer from a small heated element mounted flush with the surface of a flow boundary. An extension of Ludweig's heated element technique was reported by Liepmann and Skinner[60]. They used a simple hot wire embedded in the surface to determine the skin friction coefficients for low-velocity air flow. However, in addition to its requirement for frequent calibration, this technique, like the direct-shear measurement technique, lacks mobility. Also, because the hot wire is very sensitive, it cannot be used in situations where flows have a suspended sediment content. Moreover, the presence of the wire sensor in the body of flow disturbs the latter and, as a result, significant errors are introduced in the measurements. In addition, its application has been substantially limited to constant property flows of low temperature, low speed and low turbulence intensity.

2.4.5 Pitot-Tube Techniques

Stanton, Marshall and Bryant[95] were the first to introduce the surface-impact-probe measurement technique. This instrument was developed to study boundary layers in turbulent pipe flow. The device was a "half-pitot" which was essentially a small square tube inserted perpendicularly through the flow boundary. The upstream wall of the tube was open and its end was covered with a razor-sharp plate to form one side of a rectangular opening. The flow boundary formed the other side of the very small rectangular opening that skimmed the viscous sublayer. This device was used by Fage and Falkner[30] to measure skin friction on airfoil shapes.

Preston[76] was the first to deduce that, if a law-of-the-wall velocity profile exists near a solid boundary, then a unique relationship should exist between the parameter $(p_t-p_o){s_n}^2/\rho\nu^2$ and $\tau_o {s_n}^2/\rho\nu^2$. He showed that when (p_o-p_t) is measured by any impact probe immersed in the appropriate part of the boundary layer, τ_o can be determined if the dynamic pressure of the free stream and the Reynolds number are known.

In 1955, Hsu[43] derived theoretically the relationship found experimentally by Preston for round tubes. He showed that the wall thickness of the probe was unimportant and that surface-impact probes could be used to measure the total turbulent skin friction of external boundary layers. Fenter and Stalmach[32] extended the principle to include the effects of compressible flow over insulated surfaces and Leadon and Barlle[56] extended it to include incompressible, plane, turbulent, boundary layer flow over a porous, flat plate surface.

However, Granville[37] examined the velocity of Preston tube approach on the basis of the log-similarity law and the displacement effect of the tubes. He concluded that the tubes were not suited for the rough surface conditions found in practice.

In fact, although Preston tubes are inexpensive, easily calibrated and mobile, the errors introduced in the measurements can not be considered negligible. These inherent errors are due, largely, to the physical presence of the probe in the flow field. Therefore, in order to remove this type of error from the present study, a measurement system that does not require the presence of a probe in the flow was considered essential.

CHAPTER 3

FORMULATION OF THE PROBLEM

Since the secondary currents generated in channel bends are largely responsible for the asymmetrical distribution of velocity and boundary shear stress in the straight channel sections, (in the immediate vicinity of the bend sections), a theory is developed to predict corresponding stress distributions in zones where these currents are strong. In fact these zones extend from a limited distance in the straight channel upstream from the bend entrance, where the growth of transverse circulation originates, to a certain distance in the straight channel downstream from the bend exit, after which the flow is not affected by the presence of the bend existence.

However, for all practical purposes, it can be assumed that the zone of influence of the secondary currents, (on the velocity distribution, etc.), begins at the bend entrance section and ends a certain distance along the straight reach downstream from the bend. Consequently the study section adopted for this investigation consists of a single channel bend followed by a straight channel section.

In the experimental investigation local boundary shear stress values in the study section are determined for the stable state condition (i.e. no sediment movement). In the numerical analysis a theory is developed to facilitate prediction of the stable boundary shear stress distribution within the study section.

3.1 Theoretical Considerations

3.1.1 Decay of Transverse Circulation

The mechanisms governing the decay process of transverse circulation in open channel bends have been investigated by many researchers in the past. Pioneer works include those of Potapov(75), Ananyan(2), Makkavyev(65) and others.

When flow passes through a bend, and enters a straight reach downstream from the former, a gradual transition from secondary flow to parallel flow takes place. The complex velocity distribution in a bend section can be explained if it is assumed that the transverse flow arises from the influence of centrifugal forces (generated by the stream curvature) and then begins to decay under the influence of viscous forces.

The equations of dynamic equilibrium of a continuous medium given in cylindrical coordinates can be written as

$$\rho \frac{dv_r}{dt} = \frac{\partial p_{rr}}{\partial r} + \frac{\partial \tau_{r\theta}}{r\partial\theta} + \frac{\partial \tau_{rz}}{\partial z} + \frac{p_{rr}-p_{\theta\theta}}{r} \; ;$$

$$\rho \frac{dv_\theta}{dt} = \frac{\partial \tau_{r\theta}}{\partial r} + \frac{\partial P_{\theta\theta}}{r\partial\theta} + \frac{\partial \tau_{\theta z}}{\partial z} + \frac{2\tau_{r\theta}}{r} \; ; \qquad (3.1.1.1)$$

and

$$\rho \frac{dv_z}{dt} = - g + \frac{\partial \tau_{rz}}{\partial r} + \frac{\partial \tau_{\theta z}}{r\partial\theta} + \frac{\partial p_{zz}}{\partial z} + \frac{\tau_{rz}}{r}$$

If a linear relationship exists between the stress and strain velocity components, one can write(63):

$$
\begin{aligned}
p_{rr} &= -p + 2\mu \frac{\partial v_r}{\partial r} &;\quad \tau_{r\theta} &= \mu\left(\frac{1}{r}.\frac{\partial v_r}{\partial r} + \frac{\partial v_\theta}{\partial r} - \frac{v_\theta}{r}\right) ; \\
p_{\theta\theta} &= -p + 2\mu \left(\frac{1}{r}.\frac{\partial v_\theta}{\partial \theta} + \frac{v_r}{r}\right) &;\quad \tau_{\theta z} &= \mu\left(\frac{\partial v_\theta}{\partial z} + \frac{1}{r}.\frac{\partial v_z}{\partial \theta}\right) ; \qquad (3.1.1.2) \\
p_{zz} &= -p + 2\mu \left(\frac{\partial v_z}{\partial z}\right) &;\quad \tau_{zr} &= \mu\left(\frac{\partial v_z}{\partial r} + \frac{\partial v_r}{\partial z}\right)
\end{aligned}
$$

Combining Equations (3.1.1.1) and (3.1.1.2) gives, in cylindrical coordinates, the equations for the flow of an incompressible fluid as:

$$
\begin{aligned}
&\frac{\partial v_r}{\partial t} + v_r \frac{\partial v_r}{\partial r} + \frac{v_\theta}{r} . \frac{\partial v_r}{\partial \theta} + v_z \frac{\partial v_r}{\partial z} - \frac{v_\theta^2}{r} = \frac{1}{\rho} . \frac{\partial p}{\partial r} + \\
&\quad + \nu_r \left(\frac{\partial^2 v_r}{\partial r^2} + \frac{1}{r} . \frac{\partial^2 v_r}{\partial \theta^2} + \frac{\partial^2 v_r}{\partial z^2} + \frac{1}{r} . \frac{\partial v_r}{\partial r} - \frac{2}{r^2} - \frac{\partial v_\theta}{\partial \theta} - \frac{v_r}{r^2}\right) + \\
&\quad + 2 \frac{\partial \nu_r}{\partial r} . \frac{\partial v_r}{\partial r} + \frac{\partial \nu_r}{r\partial \theta} \left(\frac{1}{r} . \frac{\partial v_r}{\partial \theta} + \frac{\partial v_\theta}{\partial r} - \frac{v_\theta}{r}\right) + \frac{\partial \nu_r}{\partial z} \left(\frac{\partial v_z}{\partial r} + \frac{\partial v_r}{\partial z}\right) ;
\end{aligned}
$$

$$
\begin{aligned}
&\frac{\partial v_\theta}{\partial t} + v_r \frac{\partial v_\theta}{\partial r} + \frac{v_\theta}{r} . \frac{\partial v_\theta}{\partial \theta} + v_z \frac{\partial v_\theta}{\partial z} + \frac{v_r v_\theta}{r} = - \frac{1}{\rho} . \frac{\partial p}{r\partial \theta} + \\
&\quad + \nu_r \left(\frac{\partial^2 v_\theta}{\partial r^2} + \frac{1}{r^2} . \frac{\partial^2 v_\theta}{\partial \theta^2} + \frac{\partial^2 v_\theta}{\partial z^2} + \frac{1}{r} . \frac{\partial v_\theta}{\partial r} + \frac{2}{r^2} . \frac{\partial v_r}{\partial \theta} - \frac{v_\theta}{r^2}\right) + \qquad (3.1.1.3) \\
&\quad + \frac{\partial \nu_r}{\partial r} \left(\frac{1}{r}.\frac{\partial v_r}{\partial \theta} + \frac{\partial v_\theta}{\partial r} - \frac{\partial \theta}{r}\right) + 2 \frac{\partial \nu_r}{r\partial \theta}\left(\frac{\partial v_\theta}{r\partial \theta} + \frac{v_r}{r}\right) + \frac{\partial \nu_r}{\partial z} \left(\frac{\partial v_\theta}{\partial z} + \frac{1}{r}.\frac{\partial v_z}{\partial \theta}\right);
\end{aligned}
$$

and

$$
\begin{aligned}
&\frac{\partial v_z}{\partial t} + v_r \frac{\partial v_z}{\partial r} + \frac{v_\theta}{r} . \frac{\partial v_z}{\partial \theta} + v_z \frac{\partial v_z}{\partial z} = - g - \frac{1}{\rho} . \frac{\partial p}{\partial z} + \\
&\quad + \nu_r \left(\frac{\partial^2 v_z}{\partial r^2} + \frac{1}{r^2} . \frac{\partial^2 v_z}{\partial \theta^2} + \frac{\partial^2 v_z}{\partial z^2} + \frac{1}{r} . \frac{\partial v_z}{\partial r}\right) + \\
&\quad + \frac{\partial \nu_r}{\partial r} \left(\frac{\partial v_z}{\partial r} + \frac{\partial v_r}{\partial z}\right) + \frac{\partial \nu_r}{r\partial \theta} \left(\frac{\partial v_\theta}{\partial z} + \frac{\partial v_z}{r\partial \theta}\right) + 2 \frac{\partial \nu_r}{\partial z} . \frac{\partial v_z}{\partial z}
\end{aligned}
$$

The equation of continuity should be added to describe the motion completely, therefore,

$$\frac{\partial v_r}{\partial r} + \frac{v_r}{r} + \frac{\partial v_\theta}{r\partial\theta} + \frac{\partial v_z}{\partial z} = 0 \qquad (3.1.1.4)$$

where

r,θ,z	are the cylindrical coordinates of a point,
v_r, v_θ, v_z	are the velocity projections along the coordinate lines,
$\nu_r = \mu/\rho$	is the kinematic coefficient of turbulent viscosity,
μ	is the coefficient of turbulent viscosity, and
ρ	is the mass density of the fluid.

In the case of a curved open channel, (large radius of curvature), the transverse velocity components, v_r and v_z, are small compared with the longitudinal velocity component v_θ (85).

Integrating Equation (3.1.1.4) leads to

$$\begin{aligned} v_z &= \int_o^z \frac{\partial v_z}{\partial z}\, dz = -\int_o^z \left(\frac{\partial v_r}{\partial r} + \frac{v_r}{r} + \frac{\partial v_\theta}{r\partial\theta}\right) dz \\ &= -\, r\left(\frac{\partial v_r}{\partial r} + \frac{v_r}{r} + \frac{\partial v_\theta}{r\partial\theta}\right)_m \frac{z}{r} \end{aligned} \qquad (3.1.1.5)$$

where "m" represents the averaging within the limits of integration. Therefore, if the radius of curvature is large compared to the depth of flow, v_z will be of the order of magnitude $(\frac{h}{r})$ and can be ignored.

Define the variables z', v_z' and ν_r' such that

$$z' = z\,\frac{r}{h} \quad ; \quad v_z' = v_z\,\frac{r}{h} \quad \text{and} \quad \nu_r' = \frac{\nu_r}{\nu_{ro}}$$

in order to obtain variables of the same order of magnitude as r, v_θ and v_r.

Introducing these variables into Equation (3.1.1.3), leads in case of steady flow to:

$$
\begin{aligned}
& v_r \frac{\partial v_r}{\partial r} + \frac{v_\theta}{r} \cdot \frac{\partial v_r}{\partial \theta} + v'_z \frac{\partial v_r}{\partial z} - \frac{v_\theta^2}{r} = -\frac{1}{\rho} \cdot \frac{\partial p}{\partial r} + \nu_{r_o} \left[\frac{\partial}{\partial r}\left(2\nu'_r \frac{\partial v_r}{\partial r}\right) + \right. \\
& \quad + \frac{1}{r^2} \cdot \frac{\partial}{\partial \theta}\left(\nu'_r \frac{\partial v_r}{\partial \theta}\right) + \frac{r^2}{h^2} \cdot \frac{\partial}{\partial z'}\left(\nu'_r \frac{\partial v_r}{\partial z'}\right) + \frac{\partial}{r\partial \theta}\left(\nu'_r \frac{\partial v_\theta}{\partial r}\right) + \\
& \quad \left. + \frac{\partial}{\partial z'}\left(\nu'_r \frac{\partial v'_z}{\partial r}\right) + \frac{1}{r} \nu_r \frac{\partial v_r}{\partial r} - \frac{2}{r^2} \nu'_r \frac{\partial v_\theta}{\partial \theta} - \nu'_r \frac{v_r}{r^2}\right] \; ;
\end{aligned}
$$

$$
\begin{aligned}
& v_r \frac{\partial v_\theta}{\partial r} + \frac{v_\theta}{r} - \frac{\partial v_\theta}{\partial \theta} + v'_z \frac{\partial v_\theta}{\partial z'} + \frac{v_r v_\theta}{r} = -\frac{1}{\rho} - \frac{\partial p}{r\partial \theta} + \\
& \quad + \nu_{r_o} \left[\frac{\partial}{\partial r}\left(\nu'_r \frac{\partial v_\theta}{\partial r}\right) + \frac{\partial}{r\partial \theta}\left(2\nu'_r \frac{\partial v_\theta}{r\partial \theta}\right) + \frac{r^2}{h^2} \cdot \frac{\partial}{\partial z'}\left(\nu'_r \frac{\partial v_\theta}{\partial z'}\right) + \right. \\
& \quad \left. + \frac{\partial}{\partial z'}\left(\nu'_r \frac{\partial v'_z}{r\partial \theta}\right) + \frac{\partial}{\partial r}\left(\nu'_r \frac{\partial v_r}{r\partial \theta}\right) + 2 \frac{\nu'_r}{r^2} \cdot \frac{\partial v_r}{\partial \theta} - \nu'_r \frac{\partial \theta}{r^2}\right] \; ; \text{ and} \qquad (3.1.1.6)
\end{aligned}
$$

$$
\begin{aligned}
& \frac{h}{r}\left[v_r \frac{\partial v'_z}{\partial r} + \frac{v_r}{r} \cdot \frac{\partial v'_z}{\partial \theta} + v'_z \frac{\partial v'_z}{\partial z}\right] = -g - \frac{1}{\rho} \cdot \frac{\partial p}{\partial z} + \\
& \quad + \nu_{r_o} \left[\frac{h}{r} \cdot \frac{\partial}{\partial r}\left(\nu'_r \frac{\partial v'_z}{\partial r}\right) + \frac{h}{r} \cdot \frac{\partial}{r\partial \theta}\left(\nu'_r \frac{\partial v'_z}{r\partial \theta}\right) + \nu'_r \frac{\partial v'_z}{\partial z'} + \right. \\
& \quad \left. + \frac{r}{h} \cdot \frac{\partial}{\partial r}\left(\nu'_r \frac{\partial v_r}{\partial z'}\right) + \frac{r}{h} \cdot \frac{\partial}{r\partial \theta}\left(\nu'_r \frac{\partial v_\theta}{\partial z'}\right) + \frac{\partial'_r}{r} \cdot \frac{\partial v_r}{\partial r}\right]
\end{aligned}
$$

All those terms, between the square brackets on the right hand side of the first and the second equations of (3.1.1.6) may be dropped with an error of the order of $\frac{h^2}{r^2}$ except the term which contains $\frac{r^2}{h^2}$ (since this term is much larger than the others). In the square bracket of the right-hand side of the third equation, it may be possible, with an error of the order of $\frac{h}{r}$, to retain only the terms that contain the factor $\frac{r}{h}$. After dropping terms of small magnitude, the following system of equations is obtained:

$$v_r \frac{\partial v_r}{\partial r} + \frac{v_\theta}{r} \cdot \frac{\partial v_r}{\partial \theta} + v'_z \frac{\partial v_r}{\partial z'} - \frac{v_\theta^2}{r} = -\frac{1}{\rho} \cdot \frac{\partial p}{\partial r} + \nu_{r_o} \frac{r^2}{h^2} \cdot \frac{\partial}{\partial z'} (\nu'_r \frac{\partial v_r}{\partial z'});$$

$$v_r \frac{\partial v_\theta}{\partial r} + \frac{v_\theta}{r} \cdot \frac{\partial v_\theta}{\partial \theta} + v'_z \frac{\partial v_\theta}{\partial z'} + \frac{v_r v_\theta}{r} = -\frac{1}{\rho} \cdot \frac{\partial p}{r \partial \theta} + \nu_{r_o} \frac{r^2}{h^2} \cdot \frac{\partial}{\partial z'} (\nu'_r \frac{\partial v_\theta}{\partial z});$$

and (3.1.1.7)

$$\frac{h}{r} (v_r \frac{\partial v'_z}{\partial r} + \frac{v_r}{r} \cdot \frac{\partial v'_z}{\partial \theta} + v'_z \frac{\partial v'_z}{\partial z'}) = -g - \frac{1}{\rho} \cdot \frac{\partial p}{\partial z'} +$$

$$+ \nu_{r_o} \frac{r}{h} [\frac{\partial}{\partial r} (\nu'_r \frac{\partial v_r}{\partial z'}) + \frac{\partial}{r \partial \theta} (\nu'_r \frac{\partial v_\theta}{\partial z'})]$$

If the viscosity, ν_{r_o}, has a small magnitude whose order does not exceed $\frac{h^2}{r^2}$, one can write (to an accuracy of $\frac{h}{r}$):

$$g + \frac{1}{\rho} \cdot \frac{\partial p}{\partial z} = 0 \qquad (3.1.1.8)$$

If the pressure is assumed to be hydrostatic in the case of wide streams, one can write:

$$p = \rho g (z_o - z) \qquad (3.1.1.9)$$

where "z_o" is the coordinate of a point on the free surface of the stream, "p" is the excess pressure above atmospheric. Therefore:

$$\frac{\partial p}{\partial r} = \rho g \frac{\partial z_o}{\partial r} = \rho g \, I_r \qquad (3.1.1.10)$$

$$\frac{\partial p}{\partial \theta} = \rho g \frac{\partial z_o}{r \partial \theta} = -\rho g r \, I_\theta \qquad (3.1.1.11)$$

where I_r and I_θ are the transverse and longitudinal slopes of the free water surface, respectively.

Introducing Equations (3.1.1.10) and (3.1.1.11) into Equations (3.1.1.7) leads, after dropping the quantities of small order of magnitude and returning to the original variables, to the following system of equations:

$$v_r \frac{\partial v_r}{\partial r} + \frac{v_\theta}{r} \cdot \frac{\partial v_r}{\partial \theta} + v_z \frac{\partial v_r}{\partial z} - \frac{v_\theta^2}{r} = - g\, I_r + \frac{\partial}{\partial z} (\nu_r \frac{\partial v_r}{\partial z}); \qquad (3.1.1.12)$$

$$v_r \frac{\partial v_\theta}{\partial r} + \frac{v_\theta}{r} \cdot \frac{\partial v_\theta}{\partial \theta} + v_z \frac{\partial v_\theta}{\partial z} + \frac{v_r v_\theta}{r} = g\, I_\theta + \frac{\partial}{\partial z} (\nu_r \frac{\partial v_0}{\partial z}) \qquad (3.1.1.13)$$

Dropping the terms $v_r \frac{\partial v_r}{\partial r}$ and $v_z \frac{\partial v_r}{\partial z}$, being of the order of magnitude $(\frac{h}{r})^2$, equation (3.1.1.12) reduces to

$$\frac{v_\theta}{r} \cdot \frac{\partial v_r}{\partial \theta} - \frac{v_\theta^2}{r} = - g\, I_r + \frac{\partial}{\partial z} (\nu_r \frac{\partial v_r}{\partial z}) \qquad (3.1.1.14)$$

Ignoring the inertia forces of transfers flows, which are of the order of magnitude $(\frac{h}{r})^2$, the absence of centrifugal forces on the straight channel length beyond the bend must lead to the disappearance of the transverse slope of the free water surface. Therefore, Equation (3.1.1.14) can be written, after replacing r_θ by x and v_θ by v_x, as:

$$v_x \frac{\partial v_r}{\partial x} = \frac{\partial}{\partial z} (\nu_r \frac{\partial v_r}{\partial z}) \qquad (3.1.1.15)$$

For channel bends, with radii of curvature many times larger than stream depths, the change in the velocity-field at the bend are insignificant in comparison with an equivalent straight reach[2,3], the distribution of longitudinal velocity components and of turbulent exchange coefficients on the bend, approximately, will remain the same as in the straight channel upstream. Therefore, the transverse velocity components v_r and v_z can be neglected in comparison with v_θ and Equation (3.1.1.12) can be written as:

$$\frac{\partial}{\partial z}\left(\nu_r \frac{\partial v_r}{\partial z}\right) = g\ I_r - \frac{v_\theta^2}{r} \tag{3.1.1.16}$$

Introducing the variable ξ into Equation (3.1.1.16) such that,

$$\xi = \frac{z}{h},$$

leads, after rearrangement, to:

$$\frac{1}{h^2} \cdot \frac{\partial}{\partial \xi}\left(\nu_r \frac{\partial v_r}{\partial \xi}\right) = g\ I_r - \frac{v_\theta^2}{r} \tag{3.1.1.17}$$

Integrating, with respect to ξ, gives

$$\nu_r \frac{\partial v_r}{\partial \xi} = h^2 \int \left(g\ I_r - \frac{v_\theta^2}{r}\right) d\xi \tag{3.1.1.18}$$

According to the stated assumptions, v_θ can be substituted from Prandtl's equation :

$$v_\theta = v_{max} + \frac{1}{\kappa} v_* \ln \xi \tag{3.1.1.19}$$

This equation gives the coefficient of turbulent viscosity μ as:

$$\nu_r = \mu/\rho = \kappa h v_m \frac{\sqrt{g}}{C} (\xi - 1)\xi \tag{3.1.1.20}$$

Integrating Equation (3.1.1.17) after substituting the value of v_θ

from Formula (3.1.1.19) leads to

$$\nu_r \frac{\partial v_r}{\partial \xi} = \frac{g v_m^2 h^2 \xi}{C^2 r} \{[\frac{C^2 I_r \cdot r}{v_m^2} - \frac{(\kappa C+\sqrt{g})^2}{\kappa^2 g}] + \frac{2(\kappa C+\sqrt{g})}{\kappa^2\sqrt{g}} (1-\ln\xi) -$$

$$- \frac{(\ln^2\xi - 2\ln\xi + 2)}{\kappa^2} \} + \text{constant} \qquad (3.1.1.21)$$

The radial component of frictional stress, τ_r, can be represented by $\nu_v \frac{\partial v_r}{\partial \xi}$. Therefore

$$\frac{\tau_r}{\rho} = \frac{\nu_r}{h} \cdot \frac{\partial v_r}{\partial \xi} \qquad (3.1.1.22)$$

Based on the boundary condition that the friction at the free surface is equal to zero (no wind effect), the constant of integration can be determined

$$\text{i.e.,} \qquad (\frac{\tau_r}{\rho})_{\xi=1} = \frac{\nu_r}{h} (\frac{\partial v_r}{\partial \xi})_{\xi=1} = 0 \quad , \text{ therefore}$$

$$\frac{g v_m^2 h^2}{C^2 r} \{\frac{C^2 I_r \cdot r}{v_m^2} - \frac{(\kappa C+\sqrt{g})^2}{\kappa^2 g} + \frac{2(\kappa C+\sqrt{g})}{\kappa^2\sqrt{g}} - \frac{2}{\kappa^2} \} + \text{constant} = 0$$

Substituting by this constant and by the turbulent viscosity coefficient from Equation (3.1.1.20) in Equation (3.1.1.21) we get

$$\frac{\partial v_r}{\xi \partial} = \frac{\sqrt{g} v_m h}{C\kappa r} \{[(\frac{C}{\sqrt{g}} + \frac{1}{\kappa})^2 - \frac{r I_r C^2}{v_m^2 g}] \frac{1}{\xi} + \frac{2C}{\kappa\sqrt{g}} (1 + \frac{\sqrt{g}}{\kappa C}) \frac{\xi \ln - \xi + 1}{\xi(\xi-1)} +$$

$$\frac{1}{\kappa^2} \cdot \frac{\xi \ln^2\xi - 2\xi\ln\xi + 2\xi - 2}{\xi(\xi-1)} \} \qquad (3.1.1.23)$$

Integrating this equation, with respect to the condition $\int_0^h v_r dz = 0$, leads to

$$v_r = \frac{\sqrt{g}\, v_m h}{C\kappa r} \{ [\frac{C}{\sqrt{g}} + \frac{1}{\kappa})^2 - \frac{r I_r C^2}{v_m^2 g}] (\ln\xi+1) -$$

$$- \frac{2}{\kappa} (\frac{C}{\sqrt{g}} + \frac{1}{\kappa}) A(\xi) + \frac{1}{\kappa^2} B(\xi) \} \qquad (3.1.1.24)$$

where

$$A(\xi) = + \int \frac{\xi \ln\xi - \xi + 1}{\xi(\xi-1)} d\xi ,$$

and

$$B(\xi) = - \int \frac{\xi \ln^2\xi - 2\xi\ln\xi + 2\xi - 2}{\xi(\xi-1)} d\xi$$

The transverse slope of the free surface, I_r, can be expressed as:

$$I_r = \frac{dh}{dr} = \alpha_o \frac{v_m^2}{gr} + \frac{\tau r_o}{\rho g h} \qquad (3.1.1.25)$$

The coefficient α_o can be determined from:

$$\alpha_o = \frac{\int_o^1 \frac{\bar{v}_\theta^2}{gr} d\xi}{v_m^2/gr}$$, which leads to

$$\alpha_o = 1 + \frac{g}{\kappa^2 C^2} \qquad (3.1.1.26)$$

Substituting the value of "I_r" into Equation (3.1.1.24) leads to

$$v_r = \frac{v_m h}{\kappa^2 r} [F(\xi) - \frac{\sqrt{g}}{\kappa C} G(\xi)] \qquad (3.1.1.27)$$

where

$$F(\xi) = 2 \{\ln\xi + 1 - A(\xi)\}$$, and

$$G(\xi) = 2 A(\xi) - B(\xi)$$

At the surface, the radial velocity component can be expressed, from Equation (3.1.1.27), as

$$v_{r_o s} = \frac{v_m h}{\kappa^2 r} \{1.25 - 0.44 \frac{\sqrt{g}}{\kappa C}\} \tag{3.1.1.28}$$

On the assumption that, in the process of circulation decay, the profiles of velocities v_r remain similar to one another one can express v_r as

$$v_r = v_{rs} f(\xi) \tag{3.1.1.29}$$

In the section of steady circulation, the right-hand side of Equation (3.1.1.15) can be determined from Equations (3.1.1.21), (3.1.1.25) and (3.1.1.26). After substitution the following equation is arrived at

$$\frac{\partial}{\partial z}(\nu_r \frac{\partial v_{r_o}}{\partial z}) = \frac{-2\sqrt{g}\, v_m^2}{\kappa C r} \{1 + (1 + \frac{\sqrt{g}}{\kappa C}) \ln\xi + \frac{\sqrt{g}}{2\kappa C} \ln^2\xi\} \tag{3.1.1.30}$$

Assuming that, for the zone of circulation decay, the longitudinal velocity components v_x and the coefficient ν_r remain unchanged, then the magnitude $\frac{\partial}{\partial z}(\nu_r \frac{\partial v_r}{\partial z})$ will vary in proportion to v_{r_n}; where v_{r_n} is the radial velocity component at the surface, therefore:

$$\frac{\partial}{\partial z}(\nu_r \frac{\partial v_r}{\partial z}) = \frac{v_{r_n}}{v_{r_{o_s}}} \cdot \frac{\partial}{\partial z}(\nu_r \frac{\partial v_{r_o}}{\partial z}) \tag{3.1.1.31}$$

or

$$\frac{\partial}{\partial z}(\nu_r \frac{\partial v_r}{\partial z}) = -\frac{v_{r_s}}{v_{r_{o_s}}} \cdot \frac{2v_m^2\sqrt{g}}{\kappa C r} [1 + (1 + \frac{\sqrt{g}}{\kappa C}) \ln\xi + \frac{\sqrt{g}}{2\kappa C} \ln^2\xi] \tag{3.1.1.32}$$

substituting the value of $v_{r_{o_s}}$ from (3.1.1.28) into (3.1.1.32) leads to the following equation

$$\frac{\partial}{\partial z}\left(\nu_r \frac{\partial v_r}{\partial z}\right) = - \frac{2\sqrt{g}\, v_m\, v_{r_s}\, [1 + (1 + \frac{\sqrt{g}}{\kappa C})\ \ln\xi + \frac{\sqrt{g}}{2\kappa C}\ \ln^2\xi]}{\frac{C}{\kappa}\,(1.25 - \frac{\sqrt{g}}{\kappa C})} \qquad (3.1.1.33)$$

From Prandtl's equation, the velocity, v, at any depth ξ can be related to the average velocity, v_m, as:

$$v = v_m\ [1 + \frac{\sqrt{g}}{\kappa C}\,(1 + \ln\xi)] \qquad (3.1.1.34)$$

Adopting the longitudinal velocity component $v_\Theta = v_x$ from Prandtl's equation, and substituting expression (3.1.1.33) into Equation (3.1.1.14) gives:

$$\frac{\partial v_{r_s}}{\partial x} = - \frac{2v_m\kappa\sqrt{g}}{} \cdot \frac{[1 + (1 + \frac{\sqrt{g}}{\kappa C})\ \ln\xi + \frac{\sqrt{g}}{2\kappa C}\ \ln^2\xi]}{[1 + \frac{\sqrt{g}}{\kappa C}\,(1 + \ln\xi)][f(\xi) - \frac{\sqrt{g}}{\kappa C}\,G(\xi)]} \qquad (3.1.1.35)$$

$$= - \frac{2v_m\kappa\sqrt{g}}{hC} \cdot M(\xi)$$

For a first approximation, if one assumes that the Chezy's coefficient, C = 50, and Von Karmans coefficient $\kappa = 0.50$; and for $\xi = 0.1$ (i.e., close to the bed), the function $M(\xi) = 1.30$. Therefore, Equation (3.1.1.35) reduces to

$$\frac{\partial v_{r_s}}{\partial x} = - 2.6\ \frac{v_m\kappa\sqrt{g}}{Ch} \qquad (3.1.1.35)$$

Integrating this equation leads to

$$\ln v_{r_s} = -2.6\ \frac{\kappa\sqrt{g}x}{Ch} + \ln C_1 \qquad (3.1.1.36)$$

or

$$v_{r_s} = C_1 e^{\frac{-2.6\kappa\sqrt{g}x}{Ch}}$$

At the bend exit $v_r\big|_{x=0} = v_{r_o}$, then

$$v_r = v_{r_o} e^{\frac{-2.6\kappa\sqrt{g}x}{Ch}} \tag{3.1.1.37}$$

Choosing $\kappa = 0.5$, and considering the length at which the decay of circulation takes place terminates where the intensity of circulation amounts to only 10% of the original intensity, i.e., $v_r = 0.1\ v_{r_o}$, the length over which the circulation decays can be expressed as:

$$x = \frac{1.77\ Ch}{\sqrt{g}} \tag{3.1.1.38}$$

Therefore, in the channel system adopted the total length T (in the longitudinal direction) affected by the secondary flow can be expressed as

$$T = \frac{1.77\ Ch}{\sqrt{g}} + \frac{\pi r \theta}{180} \tag{3.1.1.39}$$

where

- g is the gravitational acceleration,
- C is the Chezy's coefficient,
- h is the mean depth of flow,
- θ is the central angle of the bend in degrees, and
- r is the radius of curvature of the bend.

3.1.2 Velocity Distributions in Straight Sand Bed Channels

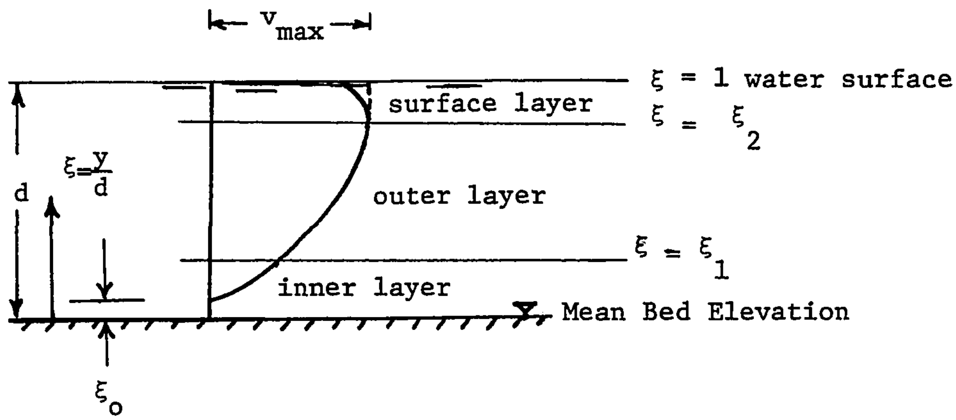

The vertical distributions of velocity over sand bed channels can be divided, generally, into three regions(64). This division corresponds to differences in turbulence characteristics in the three regions. In the first layer (surface layer), the secondary flow causes a "cut-back" in the velocity profile. The zone close to the bed, (inner layer), is affected by the location of the vertical with respect to the bed form. The difficulty concerning measurements in this region relates to separation of the flow from the irregular boundary and the presence of eddies. These flow phenomena make the definition of the flow depth difficult. In the middle zone, (outer layer), the velocity profile is less affected by the location of the origin for "y" (because of larger absolute values of y) or by the secondary flow.

Mahmood(64) concludes that, in case of a plane-bed, there is no eddy zone, but the effects of contact load and the uncertainty about the location of the origin introduce a curvature in the velocity profile. Therefore, there is no individual velocity profile in sand bed channels that can be representative of the flow. However, for average flow conditions, it is possible to adopt the concept of an average velocity profile based on the spatial average of velocities observed in a vertical plane along the mean direction of flow at specific heights above the mean bed elevation.

It is found[64] that the vertical velocity distributions over sand bed channels can be expressed thus:

For $\xi_o \le \xi \le \xi_1$ $$\frac{v_\xi}{v_{*_o}} = \frac{1}{\kappa_o} \ln \left(\frac{\xi}{\xi_o}\right) \; ; \; v_{\xi_o} = 0 \qquad (3.1.2.1)$$

For $\xi_1 \le \xi \le \xi_2$ $$\frac{v_{max} - v_\xi}{v_{*_o}} = -\frac{1}{\kappa} \ln\xi \qquad (3.1.2.2)$$

For $\xi_2 \le \xi \le \xi_1$ $$\frac{v_{max} - v_\xi}{v_{*_o}} = -\frac{1}{\kappa} \ln\xi + f(\xi) \qquad (3.1.2.3)$$

where

v_{*_o} is the shear velocity,

v_ξ is the velocity at depth ξ from the bed,

v_{max} is the maximum velocity in a vertical,

κ is the Von Karman's coefficient,

$f(\xi)$ is a correction factor which takes into account the effect of cut-back and can be expressed as

$$f(\xi) = a_1 \left(1 - \frac{\xi}{0.80}\right)^2 \; ; \quad (a_1 = 35.0, \; 0.80 \le \xi \le 1)$$

Based on statistical analysis Von Karman's coefficient, κ, is found[64] to vary according to the following relationship:

$$\kappa = 0.446 \frac{\sigma^{0.34}}{F^{0.15} (\frac{C}{\sqrt{g}})^{0.15} T_f^{\ 0.11}} \tag{3.1.2.4}$$

where

σ is the gradation of the bed material,

F is the Froude number of the flow,

$\frac{C}{\sqrt{g}}$ is the Chezy's roughness coefficient, and

T_f is the turbulence correction factor derived from the consideration of two-phase flow and is defined as

$$T_f = [1 + (30\{\rho_s - \rho_f\}/\rho_f)\ v_m\ w_{16}\ C_v/v_{*_o}^2\ ] \tag{3.1.2.5}$$

where

v_m is the average velocity of flow,

C_v is the volumetric concentration of total transported load (including the fine material load),

w_{16} is the fall velocity of the bed material D_{16} at the given viscosity, and

ρ_s, ρ_f are the mass density of the sediment and water respectively.

In the case of flow over coarse sand stable channels (no sediment in motion), C_v can be assumed to be negligible. Therefore, Equation (3.1.2.4) reduces to

$$\kappa = 0.446 \frac{\sigma^{0.34}}{F^{0.15}\ (\frac{C}{\sqrt{g}})^{0.15}} \tag{3.1.2.6}$$

In general, the shear velocity, v_{*_o}, can be considered[93] as the sum of two components v'_{*_o} and v''_{*_o} such that

$$v_{*_o} = \bar{v}'_{*_o} + v''_{*_o} \tag{3.1.2.7}$$

This subdivision corresponds to the flow resistance due to skin friction and bed forms respectively. Therefore, for channels with flat beds the value v''_{*_o} is negligible and $v_{*o} = v'_{*o}$.

According to our earlier assumption that the components of the tensor of stress are in a linear relation to the components of the tensor of rate of strain, and in case of a flat uniform turbulent stream, where $v_y = v_z = 0$, the following relationship can be derived

$$\tau_{xz} = \tau = \mu \frac{\partial v_x}{\partial z} \tag{3.1.2.8}$$

On the other hand, the slope can be expressed with the aid of the Chezy's formula as

$$v_m = C\sqrt{hs} \tag{3.1.2.9}$$

Combining Equations (3.1.2.8) and (3.1.2.9) leads to

$$v_{*o} = v_m \frac{\sqrt{g}}{C} \tag{3.1.2.10}$$

Therefore, Equation (3.1.2.2) can be expressed as

$$v_\xi = v_{max} + \frac{\sqrt{g}}{\kappa C} v_m \ln\xi \tag{3.1.2.11}$$

Neglecting the eddy zone close to the bed surface, in case of stable channels (no sediment in motion) with flat-beds, the average velocity along the vertical velocity profile, v_m, can be expressed as

$$v_m = \int_0^1 v_\xi \, d_\xi = v_{max} - \frac{\sqrt{g}}{\kappa C} v_m$$

Then,

$$v_{max} = v_m \left(1 + \frac{\sqrt{g}}{C}\right) \qquad (3.1.2.12)$$

and Equation (3.1.2.2) becomes

$$v_\xi = v_m \left[1 + \frac{\sqrt{g}}{\kappa C} (1 + \ln\xi)\right] \qquad (3.1.2.13)$$

3.2 Stochastic Approach

3.2.1 Theory

As stated beforehand, a major objective of this study was the development of a numerical model to describe the complex flow field in the vicinity of open channel bends and also to assist in the prediction of steady-state distribution of boundary shear stress therein.

To this end the system was initially viewed as consisting of a series of similar channels, each having an overall length T (Equation 3.1.1.39) made up of a single bend followed by a straight-channel reach. Accordingly in the system adopted, once the secondary flow influences the boundary shear stress, the following (time-invariant) relationship can be written for stable-state conditions:

$$\tau_m(t) = \tau_m(t+T) \qquad (3.2.1.1)$$

where

$\tau_m(t)$ is the dimensionless shear stress, at length "t" (from the bend entrance to the point where the bed shear stress is calculated,

or alternately

$$\tau_m(t) = \tau_{m1}(t)/\tau_o \tag{3.2.1.2}$$

where

$\tau_{m1}(t)$ is the bed shear stress at the length "t" (from the bend entrance to the point where the bed shear stress is measured);

τ_o is the uniform shear stress in case of wide rectangular channel of equivalent mean flow properties.

Equation (3.2.1.1) is a periodic function (of period "T"). The function between the length "t" and "t+T" can be of any shape whatsoever. This section, in analyzing the structure of this functional relationship, describes the various stochastic-type processes employed in the investigation.

3.2.2 Assumptions

1. For any path parallel to the channel centreline of length T (Equation 3.1.1.39), along which changes in sand bed elevation take place gradually and smoothly, the resistance to flow is assumed to be due to skin friction only.

2. Based on a mean radius of bend curvature to flow depth ratio

$(\frac{R}{d}) = 22.5$ used in the experiments, it is assumed that the velocity field in the bend is essentially similar to that in a straight reach of the channel. Therefore, as a first approximation, it is assumed that the distribution of longitudinal velocity components (and turbulent exchange coefficients) in the bend section and in the "decay" region (downstream from the bend) will be the same as that in the straight reach upstream of the bend.

3. The zone, in which secondary currents have significant effect on the system velocity distribution, originates at the entrance to the bend and extends over a length T (Equation 3.1.1.39) into the straight channel section downstream from the bend.

4. For a stable bed condition the process governing the change in bed shear stress, along any path (length T), can be considered a stationary stochastic process.

3.2.3 Mathematical Techniques

The discrete shear stress values can be considered as having been derived from a continuous signal $\tau(t)$ of duration "T" by sampling the values of the signal at spacing Δ. This produces $N = T/\Delta$ sample values τ_t, where

$$\tau_t = \tau(t=r\Delta) \qquad (3.2.3.1)$$

The periodic function which passes through the sample values may be chosen as the finite Fourier series:

$$\hat{\tau}(t) = \bar{\tau}+2\sum_{m=1}^{n-1} \{Am \cos 2\pi m f_1 t + Bm \sin 2\pi m f_1 t\} +$$

$$+ An \cos 2\pi n f_1 t; \quad (n = \frac{N}{2}) \qquad (3.2.3.2)$$

or

$$\hat{\tau}(t) = \bar{\tau} + 2 \sum_{m=1}^{n-1} \{A_m \cos 2\pi m f_1 t + B_m \sin 2\pi m f_1 t\}; \quad (N = 2n - 1) \tag{3.2.3.3}$$

where

$\bar{\tau}$ is the mean value of the series along the length T,

f_1 is the fundamental frequency which is equal to $\frac{1}{N\Delta}$,

A_m, B_m are coefficients which can be determined so that the discrete and continuous values coincide at points $t = r\Delta$. This provides an approximation to the original continuous function $\tau(t)$ in the interval $-T/2 \leq t \leq T/2$.

Substituting $t = r\Delta$, and setting $\tau(r\Delta) = \tau_t$, Equations (3.2.3.2) can be written as

$$\hat{\tau}_t = \bar{\tau} + 2 \sum_{m=1}^{n-1} \{A_m \cos 2\pi m f_1 r\Delta + B_m \sin 2\pi m f_1 r\Delta\} + $$
$$+ A_n \cos 2\pi n f_1 r\Delta, \quad (r = -n, \ldots, 0, 1, \ldots, n-1) \tag{3.2.3.4}$$

It has been proven(7) that

$$A_m = \frac{1}{N} \sum_{t=-n}^{n-1} \tau_t \cos \frac{2\pi m t}{N}, \tag{3.2.3.5}$$

and

$$B_m = \frac{1}{N} \sum_{t=-n}^{n-1} \tau_t \sin \frac{2\pi m t}{N} \tag{3.2.3.6}$$

Equations (3.2.3.2) can now be expressed(7) thus:

$$\hat{\tau}(t) = R_o + 2 \sum_{m=1}^{n-1} R_m \cos (2\pi m f_1 t + \phi_m) + R_n \cos 2\pi n f_1 t \tag{3.2.3.7}$$

where R_m and ϕ_m are the amplitude and the phase respectively of the mth harmonic relative to an arbitrary origin of time. They can be obtained[7] from the following relationships:

$$R_m = \sqrt{A_m^2 + B_m^2} \quad ; \quad \phi_m = \text{arc tan} - \frac{B_m}{A_m} \tag{3.2.3.8}$$

and

$$A_m = R_m \cos \phi_m \quad ; \quad B_m = - R_m \sin \phi_m \tag{3.2.3.9}$$

Length dependence

This refers to the degree of linear association between observations that are separated by "k" length units. It is measured by an auto-correlation coefficient. The population value of the lag "k" auto-correlation coefficient is defined[7] by

$$\rho_k = \frac{E(\tau_t - \bar{\tau})(\tau_{t-k} - \bar{\tau})}{\sigma^2_{\tau_t}} \tag{3.2.3.10}$$

where $\sigma^2_{\tau_t}$ is the variance of the series τ_t. The unbiased sample estimate can be written[3] as

$$r_k = \frac{\sum\limits_{t=1}^{N-k} \tau_t \tau_{t-k} - \frac{1}{N-k} (\sum\limits_{t=1}^{N-k} \tau_t)(\sum\limits_{t=k-1}^{N} \tau_t)}{\sum\limits_{t=1}^{N-1} \tau_t^2 - \frac{1}{N-1} (\sum\limits_{t=1}^{N-1} \tau_t)]^{1/2} [\sum\limits_{t=z}^{N} \tau_t - \frac{1}{N-1} (\sum\limits_{t=z}^{N} \tau_t)^2]^{1/2}} \tag{3.2.3.11}$$

For the hypothesis that $\rho_1 = 0$, and based on the assumptions that the series is stationary and the observations are normally distributed (i.e., it was found by Ghosh and Misra[35] in 1977 that the frequency distribution of shear stress values can be considered to follow a normal distribution pattern), the confidence limits can be given as[7]

$$\frac{-1 - y_\alpha\sqrt{N-2}}{N-1} < \rho_1 < \frac{-1 + y_\alpha\sqrt{N-2}}{N-1} \qquad (3.2.3.12)$$

where y_α is the normal deviate corresponding to probability α.

Variance spectrum

The theory of variance spectrum analysis postulates that the observed time series is a random sample of a process in time (length in this study) that is made up of oscillations of all possible frequencies. A single series spectrum partitions the variance into a number of intervals or bands of frequency. The power spectrum can be estimated from the auto-covariance function[7], namely:

$$p(f) = 2[\sigma_o + 2 \sum_{k=1}^{N-1} \sigma_k \cos 2\pi fk] \qquad (3.2.3.13)$$

where σ_o and σ_k are the variances at lags of zero and k respectively.

On the other hand, the spectral density function can also be estimated from the auto-correlation function[7] as

$$g(f) = 2[1 + 2 \sum_{k=1}^{N-1} \rho_k \cos 2\pi fk] \qquad (3.2.3.14)$$

The irregular spectrum estimated from the auto-correlation or the auto-covariance functions may be smoothed by using special functions. Such functions are equivalent to the application of a filter on the auto-covariance function. One of these functions is the "lag window" function, w_k. The smoothed estimate of spectral density can be written[7] as

$$\hat{p}(f) = 2[C_o + 2 \sum_{k=1}^{N-1} w_k C_k \cos 2\pi fk] \qquad (3.2.3.15)$$

where

C_o and C_k are the estimated sample variances at lags from zero and k respectively, and

w_k is the "lag window" function which is defined[7] as

$$w_k = \begin{cases} 1 - \frac{k}{M} & \text{for } k \leq M \\ 0 & \text{for } k > M \end{cases} \qquad (3.2.3.16)$$

where "M" is the maximum number of lags used in computing the auto-covariance function.

Assuming that the process is stationary, the population variance spectra is determined by considering the Autoregressive processes and the Moving average processes as linear stationary stochastic models.

A. Linear Auto-Regressive Models

In these models, the current value of the process, τ_t, is expressed as a finite linear combination of the previous values and a random part a_t, by the following representation

$$\tau_t = \phi_1 \tau_{t-1} + \phi_2 \tau_{t-2} + \dots + \phi_p \tau_{t-p} + a_t \qquad (3.2.3.17)$$

Using the backward operator shift B, the autoregressive process can be expressed as

$$\phi(B)\ \tau_t = a_t \tag{3.2.3.18}$$

where

$$\phi(B) = 1-\phi_1 B-\phi_2 B^2-\ldots-\phi_p B^p \tag{3.2.3.19}$$

The order of the auto-regressive process for a given series can be determined by computing the partial autocorrelation function with two standard error limits. Denote by ϕ_{kj}, the j<u>th</u> coefficient in an autoregressive process of order k, so that ϕ_{kk} is the last coefficient. From Equation (3.2.3.17), ϕ_{kk} satisfies the set of equations (in general).

Therefore:

$$\rho_j = \phi_{k1}\rho_{j-1} + \ldots + \phi_{k(k-1)}\rho_{j-k+1} + \phi_{kk}\rho_{j-k} \tag{3.2.3.20}$$

This leads to the Yule-Walker[7] equations which may be written as:

$$\begin{vmatrix} 1 & \rho_1 & \rho_2 & \rho_{k-1} \\ \rho_1 & 1 & & \rho_{k-2} \\ \rho_2 & & 1 & \rho_{k-3} \\ & & & \\ \rho_{k-1} & & & 1 \end{vmatrix} \begin{vmatrix} \phi_{k1} \\ \phi_{k2} \\ \\ \\ \phi_{kk} \end{vmatrix} = \begin{vmatrix} \rho_1 \\ \rho_2 \\ \\ \\ \rho_k \end{vmatrix} \tag{3.2.3.21}$$

or

$$P_k\ \phi_k = \rho_k$$

Solving the system of Equations (3.2.3.21) gives the partial auto-correlation function as:

$$\emptyset_k = \rho_k/p_k \qquad (3.2.3.22)$$

It was shown by Quenouille[77], that on the hypothesis that the process is autoregressive of order p, the estimated partial auto-correlation of order p+1, and higher, are approximately independently distributed with variance

$$\text{var}\ [\emptyset_{kk}] \simeq \frac{1}{N}\ , \qquad k \geq p+1$$

Therefore, the standard error (S.E.) of the estimated partial auto-correlation $\emptyset_{kk}$ is

$$\text{S.E.}[\emptyset_{kk}] \simeq \frac{1}{\sqrt{N}}\ , \qquad k \geq p+1 \qquad (3.2.3.23)$$

An examination of all the series in this study indicated that the auto-regressive process of maximum second order is satisfactory.

A-1. First Order Markov Model AR(1)

This model can be written as

$$\tau_t = \emptyset_1\tau_{t-1} + a_t \qquad (3.2.3.24)$$

For stationarity condition

$$-1 < \emptyset_1 < 1 \qquad (3.2.3.25)$$

According to this model, the auto-correlation function can be expressed[7] as

$$\rho_k = \emptyset_1{}^k \qquad (3.2.3.26)$$

where $\phi_1 = \rho_1$

and the spectrum is given[7] as

$$p(f) = \frac{2\sigma_a^2}{1 + \phi_1^2 - 2\phi_1 \cos 2\pi f}, \quad 0 \leq f \leq 0.5 \tag{3.2.3.27}$$

where

$$\sigma_a^2 = \sigma_\tau^2 (1 - \phi_1^2)$$

and σ_τ^2 is the variance of the process.

A-2. Second Order Markov Model AR(2)

This model can be expressed as

$$\tau_t = \phi_1 \tau_{t-1} + \phi_2 \tau_{t-z} + a_t \tag{3.2.3.28}$$

For stationarity condition

$$\begin{aligned} \phi_1 + \phi_2 &< 1 \\ \phi_2 - \phi_1 &< 1 \\ -1 < \phi_2 &< 1 \end{aligned} \tag{3.2.3.29}$$

The characteristic equation for this model can be written as

$$\phi(B) = 1 - \phi_1 B_1 - \phi_2 B^2 = 0 \tag{3.2.3.30}$$

Depending on the roots of this equation, the auto-correlation function can be computed. If the roots are real, the auto-correlation function can be written[7] as

$$\rho_k = \frac{G_1(1-G_2^2)G_1^k - G_2(1-G_1^2)G_2^k}{(G_1-G_2)(1+G_1G_2)} \qquad (3.2.3.31)$$

where G_1^{-1} and G_2^{-1} are the roots of the characteristic equation. If the roots are complex, then the auto-correlation function can be written[47] as

$$\rho_k = \frac{R^{|k|}\cos(2\pi f_o kF)}{\cos F} \qquad (3.2.3.32)$$

where

R' is the damping factor and is equal to $\sqrt{-\phi_2}$,

f_o is the frequency which is defined as $\cos 2\pi f_o = \phi_1/(2\sqrt{-\phi_2})$, and

F is the phase which is defined as $\tan F = \frac{1+R'^2}{1-R'^2} \tan 2\pi f_o$.

If the characteristic Equation (3.2.3.30) has equal roots, the correlation function can be computed from Equation (3.2.3.26). According to this model, the spectrum can be written[5] as

$$p(f) = \frac{2\sigma_a^2}{\{1 + \phi_1^2 + \phi_2^2 - 2\phi_1(1-\phi_2)\cos 2\pi f - 2\phi_2 \cos 4\pi f\}}, \qquad (3.2.3.33)$$

$$0 \le f \le 0.5$$

where σ_a^2 can be computed[7] from the variance of the process, σ_τ^2, as

$$\sigma_a^2 = \sigma_\tau^2 (1 - \rho_1\phi_1 - \rho_2\phi_2) \qquad (3.2.3.34)$$

Using Yule-Walker Equations (3.2.3.21) with k = 2, gives the following expressions:

$$\rho_1 = \phi_1 + \phi_2\rho_1$$
$$\rho_2 = \phi_1\rho_1 + \phi_2 \qquad (3.2.3.35)$$

Solving for ϕ_1 and ϕ_2 gives

$$\phi_1 = \frac{\rho_1(1-\rho_2)}{1-\rho_1^2} \quad ; \quad \phi_2 = \frac{\rho_2-\rho_1^2}{1-\rho_1^2} \qquad (3.2.3.36)$$

In estimating these parameters, the theoretical autocorrelations ρ_k are replaced by the estimated autocorrelations r_k. Therefore, Equations (3.2.3.36) can be written as:

$$\phi_1 = \frac{r_1(1-r_2)}{1-r_1^2} \quad ; \quad \phi_2 = \frac{r_2-r_1^2}{1-r_1^2} \qquad (3.2.3.37)$$

B. Moving Average Processes

The moving average process of order p, MA(p), is defined as

$$\tau_t = a_t - \theta_1 a_{t-1} - \theta_2 a_{t-2} - \dots - \theta_p a_{t-p} \qquad (3.2.3.38)$$

where

$\theta_1, \theta_2, \dots, \theta_p$ are parameters, and

a_t is an independent "white noise" of mean equal to $\bar{a}$ and constant variance σ_a^2.

B.1. First Order Process MA(1)

This model is defined as:

$$\tau_t = a_t - \theta_1 a_{t-1} \qquad (3.2.3.39)$$

or

$$\tau_t = (1 - \theta_1 B)\, a_t$$

According to this model, the auto-covariance function is defined as:

$$\gamma_k = E[a_t - \theta_1 a_{t-1}][a_{t-k} - \theta_1 a_{t-k-1}] \qquad (3.2.3.40)$$

and the variance is

$$\gamma_o = (1 + \theta_1^2)\, \sigma_a^2 \qquad (3.2.3.41)$$

Therefore, the auto-correlation function can be written as

$$\rho_k = \frac{\gamma_k}{\gamma_o} = \begin{cases} -\theta_1/(1+\theta_1^2) & \text{for } k = 1 \\ 0 & \text{for } k \geq 2 \end{cases} \qquad (3.2.3.42)$$

and the spectrum is defined[7] as

$$p(f) = 2\sigma_a^2\, (1 + \theta_1^2 - 2\theta_1 \cos 2\pi f), \qquad 0 < f < 0.5 \qquad (3.2.3.43)$$

The partial auto-correlation function[7] is

$$\phi_{kk} = -\,\theta_1^k\, \{1 - \theta_1^2 \,/\, 1 - \theta_1^{2(k+1)}\}$$

B-2. Second Order Process MA(2)

This model is defined as

$$\tau_t = a_t - \theta_1\, a_{t-1} - \theta_2\, a_{t-2}$$

The auto-covariance function, $_k$, is given[7] as

$$\gamma_k = \begin{cases} (-\theta_k + \theta_1\theta_{k+1} + \theta_2\theta_{k+2})\,\sigma_a^2 & \text{for } k = 1,2 \\ 0 & \text{for } k > 2 \end{cases}$$

where σ_a^2 can be computed from the variance of the process, γ_o, as

$$\sigma_a^2 = \frac{\gamma_o}{1+\theta_1^2+\theta_2^2}$$

The auto-correlation function, ρ_k, is defined[7] as

$$\rho_k = \begin{cases} \dfrac{-\theta_1(1-\theta_2)}{1+\theta_1^2+\theta_2^2} & \text{if } k = 1 \\ -\theta_1/(1+\theta_1^2+\theta_2^2) & \text{if } k = 2 \\ 0 & \text{if } k \geq 3 \end{cases}$$

and the spectrum can be written as:

$$p(f) = 2\sigma_a^2[1 + \theta_1^2 + \theta_2^2 - 2\theta_1\,(1-\theta_2)\cos 2\pi f - 2\theta_2 \cos 4\pi f]$$

$$0 \leq f \leq 0.5$$

The parameters θ_1 and θ_2 can be estimated by replacing the theoretical auto-correlation, ρ_k, by the estimated auto-correlations r_k.

The characteristics equation in this model is

$$1 - \theta_1 B - \theta_2 B^2 = 0$$

The behaviour of the auto-correlation function depends on the roots of this equation.

CHAPTER 4

COMPUTATIONAL PROCEDURES

Two computer programmes were prepared to facilitate the study of boundary shear stress distributions in the study section of the channel. The first one (Appendix B.1) was used to compute flow properties and local shear stress values from given channel geometry and velocity measurements in the flow field.

The second programme, (which is an extension of the former), was used for the stochastic analysis of the computed shear stresses along any path parallel to the centreline of the channel. This included the use of finite Fourier series, Auto-regressive processes, and Moving-Average process as linear stationary stochastic models of the system.

The analysis reflected both the aforementioned theoretical considerations and the assumptions listed in Section 3.2.2. Figures 4.1 and 4.2 are the flow charts for the first and second programmes respectively:

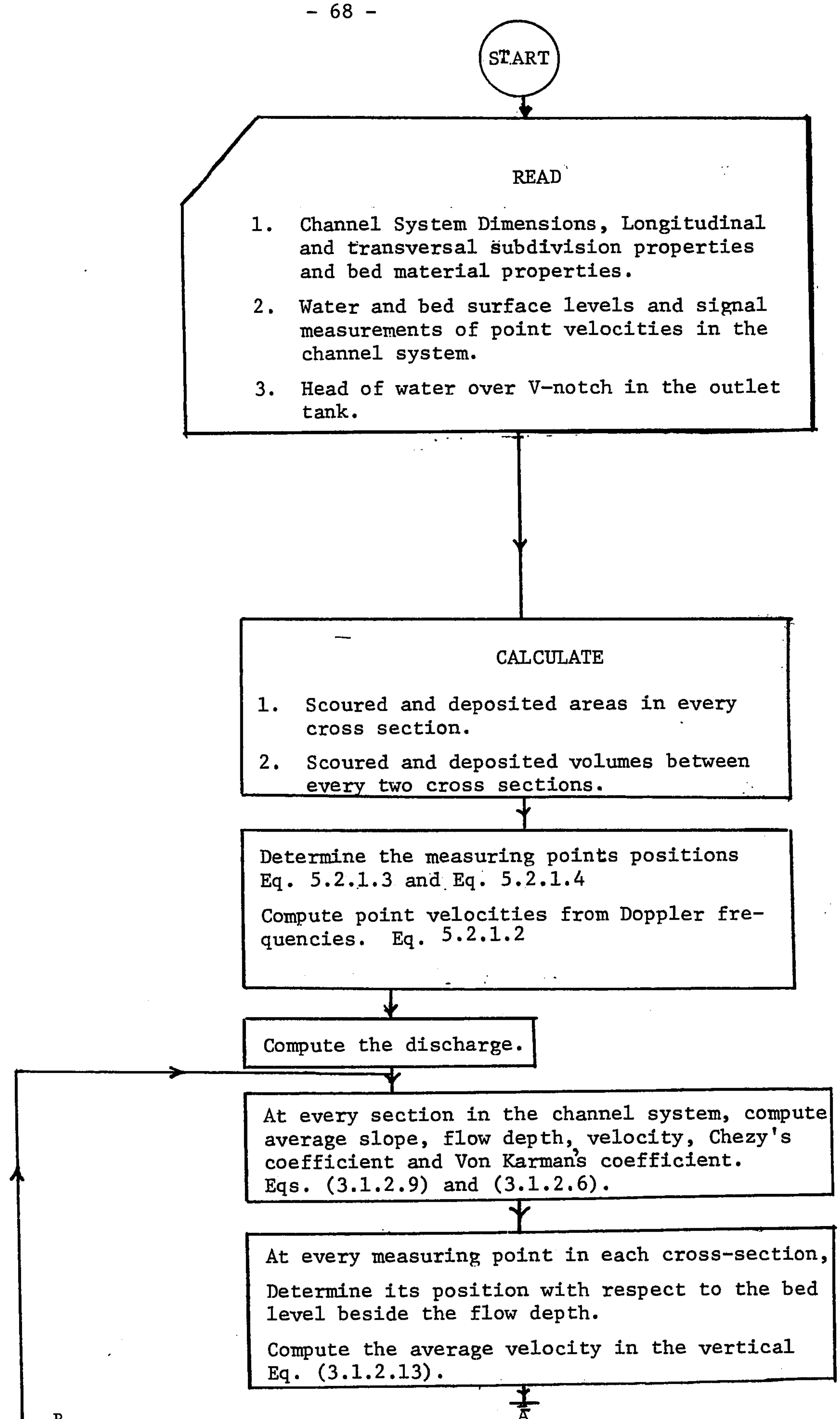
START
READ
1. Channel System Dimensions, Longitudinal and transversal subdivision properties and bed material properties.
2. Water and bed surface levels and signal measurements of point velocities in the channel system.
3. Head of water over V-notch in the outlet tank.
CALCULATE
1. Scoured and deposited areas in every cross section.
2. Scoured and deposited volumes between every two cross sections.
Determine the measuring points positions Eq. 5.2.1.3 and Eq. 5.2.1.4
Compute point velocities from Doppler frequencies. Eq. 5.2.1.2
Compute the discharge.
At every section in the channel system, compute average slope, flow depth, velocity, Chezy's coefficient and Von Karman's coefficient. Eqs. (3.1.2.9) and (3.1.2.6).
At every measuring point in each cross-section,
Determine its position with respect to the bed level beside the flow depth.
Compute the average velocity in the vertical Eq. (3.1.2.13).
B
A

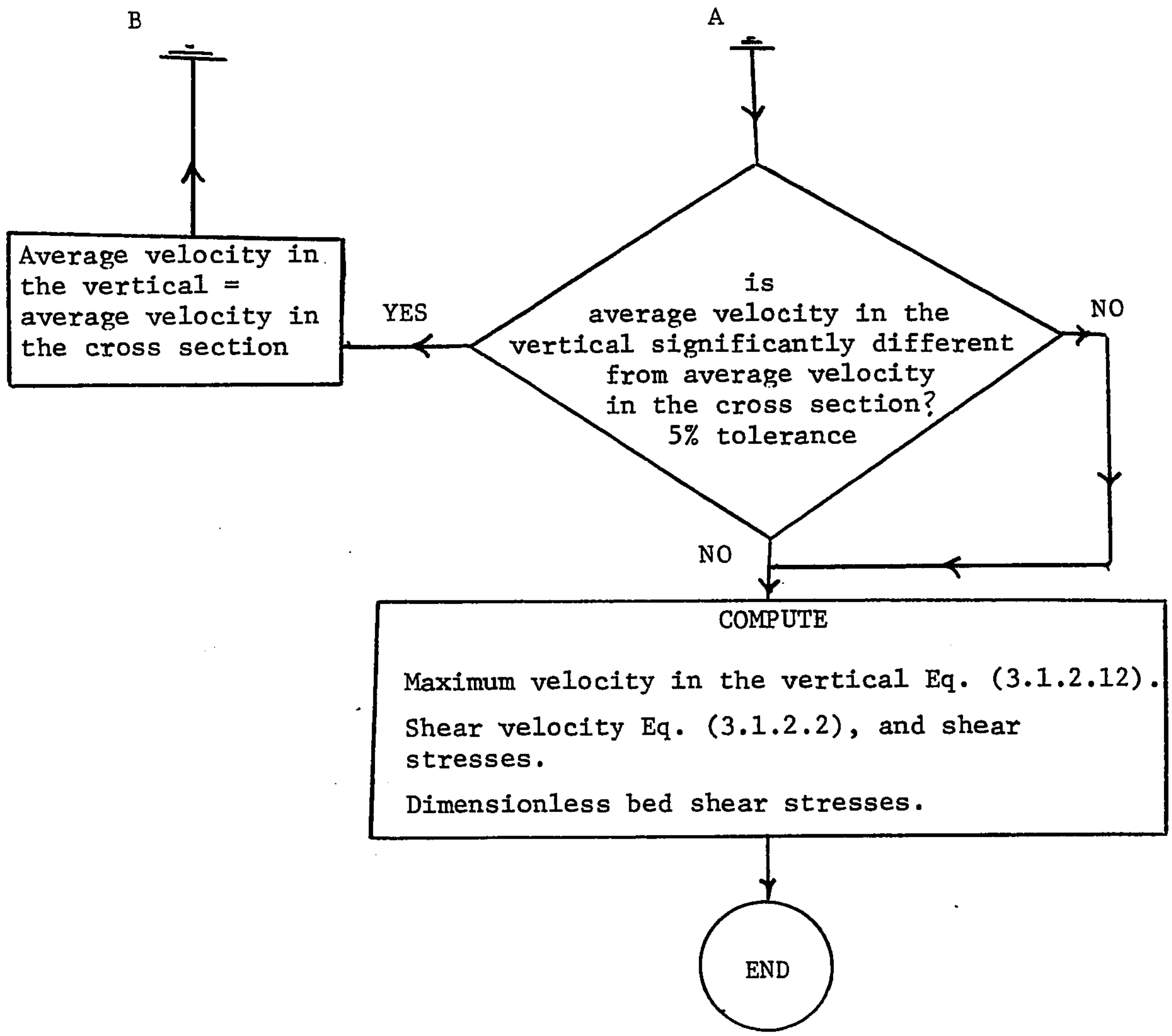

Figure 4.1: Flow Chart: Flow Properties in the Channel System.

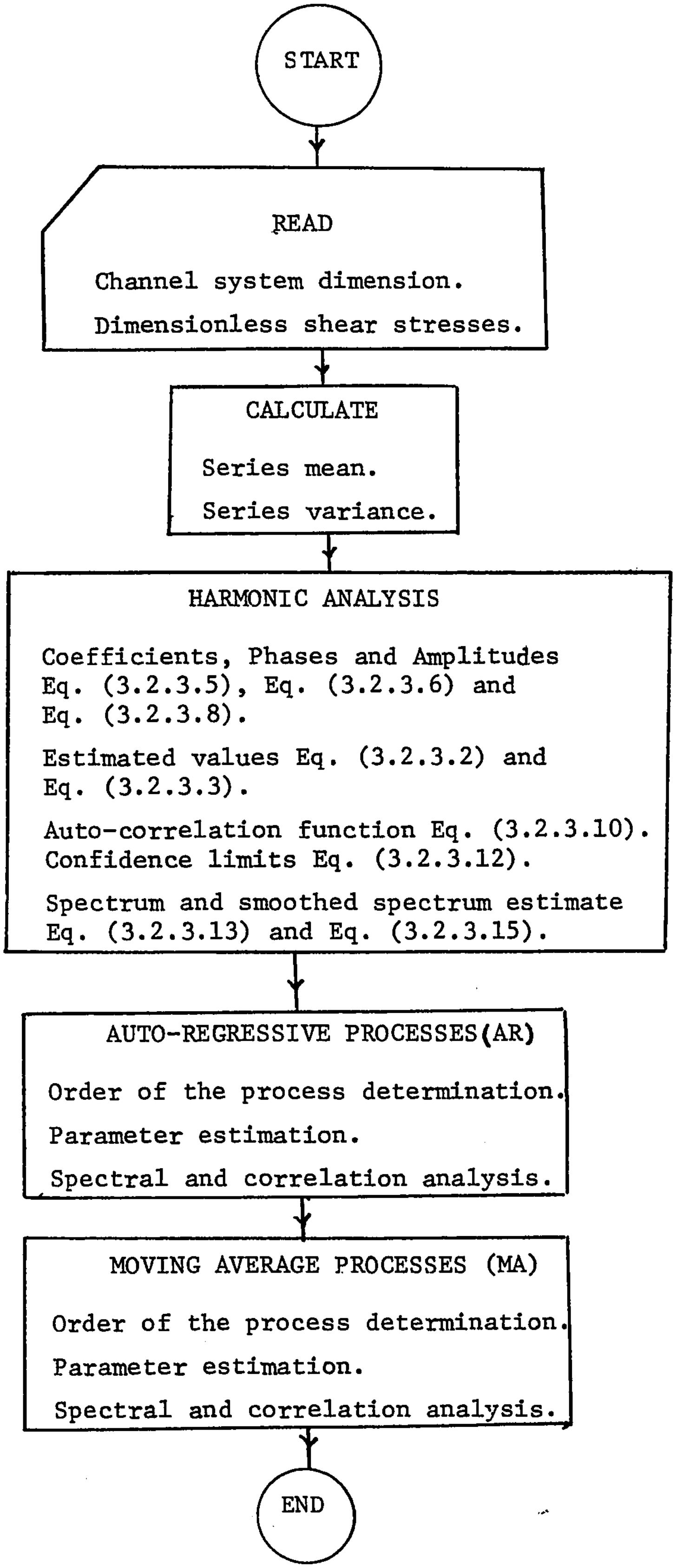

Figure 4.2: Flow Chart: Stochastic Stationary Linear Models.

The theory developed in this study is based, primarily, on the assumptions that the variation in boundary shear stress (within the zones of secondary circulation generation and decay) is a stationary process and that local values of shear stress can be determined from point velocity measurements. The following statements are made in support of these assumptions:

1. In view of the inherent inaccuracies associated with other known deterministic methods, (re: evaluation of boundary shear stress in curved open channels with movable bed material), it is believed that, in this instance, the best approach is to compute such values from point velocity measurements.

2. The logarithmic velocity distribution law is assumed to apply to any vertical in the channel system adopted. This is because the radius of bend curvature is many times larger than the depth of the flow (22.5 times) which supports the earlier assumption that modifications in the velocity field at the bend are insignificant when compared with that for a straight reach. In addition, it was found that changes in the bed elevation, (throughout the study section), take place gradually (Fig. 6.4). Moreover, this supports the premise that the (vertical) velocity distribution, at any location in the study section, differs little from that in the immediate neighbourhood of same.

3. The logarithmic velocity distribution law is found by many investigators (Sections (2.4.1) and 2.4.2)) to be applicable to flow

in streams with either smooth or rough surfaces. Recently, it was shown[64] that such a law could be used in the case of flow over flat sand bed. Therefore, the bed shear stress at a point in the channel system can be determined, using this law, from a point velocity measurement.

4. The approach used in this study (to determine bed shear stress) has the following major advantages:

(i) Changes in Von Karman's coefficient (k), due to relative position in the study section, are accounted for (Equation 3.1.2.6),

and

(ii) point velocity measurements in the flow field are obtained without disturbance to the latter (Laser-Doppler Anemometer system).

It should be noted, at this point, that the validity of the assumption, (concerning the logarithmic-type distribution of velocity in a vertical) was checked by comparing actual velocity measurements with computed values. Moreover, differences between shear stress values, computed using one and two-point velocity measurements, were considered negligible hence the "one point" velocity measurement approach was deemed to be valid in this instance.

CHAPTER 5

EXPERIMENTAL APPARATUS

5.1 Physical Model

5.1.1 Experimental Channel

The laboratory programme was performed in a plexiglass channel having a rectangular cross section 30 cm wide and 15 cm deep with an overall length of approximately 10.0 m. The channel was assembled using straight and curved sectional units (each approximately 1.2 m long).

The central angles of the three bends tested during the investigation were 45°, 60° and 75° and the mean radius of bend curvature to channel width ratio was 3.0. This particular range of bend geometries was considered to be reasonably representative of the more common bend conditions found in "stable" rivers.

The "entrance" section (to the bend) was a straight length of channel, approximately 1.8 m long, and the "exit" section (downstream from the bend) was a similar channel reach approximately 5 m long. The former was made sufficiently long to promote good entrance conditions (symmetrical flow field) upstream of the bend (test) section, and the long exit section length was required to remove any possibility of the zone of secondary circulation decay being affected by flow conditions in the vicinity of the channel outlet structure.

The channel walls were made from 0.3 cm thick plexiglass sheeting and were supported against lateral deflection (water and sediment pressures) by external plexiglass brackets at 12.5 cm spacing along the straight sections (and at 5° intervals within the bend sections).

The entire channel was supported on a number of identical and equally-spaced wooden 'box' units (0.5 m x 1.5 m) above a wooden platform which, in turn, was supported 1 m above the laboratory floor on an adjustable-sloping steel frame. Thesspacing between adjacent boxes allowed the "Optical Bench" (Laser Doppler Anemometer System) to span the channel (from below) for the purpose of measuring velocity components at points in the flow field.

5.1.2 Control Sections

In view of the changes in channel alignment, (resulting from the three different bend geometries considered), the "inlet" and "outlet" tanks were supported on steel frames fitted with casters to enable them to be easily relocated in the event of a change in bend geometry.

The function of the inlet tank (100 cm long x 100 cm wide x 120 cm deep) was to supply relatively smooth, parallel flow to the channel. Water entered the base of the tank through two (circular) orifices located at the upstream end and placed symmetrical about the tank's axis. Screens and baffles were installed downstream of the orifices to dissipate large-scale turbulence (surface 'boils') and circulation in the tank and a variable height overflow pipe was located on the tank's axis to provide additional control over the water surface elevation generated therein. The downstream portion of the tank was a smooth streamlined transition section leading to the channel which produced a uniform acceleration in the flow as it passed along it.

The outlet tank, which measured 100 cm x 100 cm x 200 cm long, provided a means for monitoring the discharge in the system during the experiments. A rectangular channel unit, measuring 40 cm x 40 cm, was suspended inside the tank, parallel to three sides of the tank. Water in the experimental channel discharged to the upstream end of this unit, passed through screens located at the two corners of the unit, and finally discharged over a sharp-edged "V"-notch (installed at the downstream end of the unit) to the main tank. Head above the "V"-notch was measured some 10 cm upstream of the notch by point gauge.

5.2 Instrumentation

5.2.1 Velocity Measurements

As stated before, a Laser Doppler Anemometer System was employed to measure local longitudinal velocity components in the test section of the channel. Each test section included the bend section and a downstream 'straight' of overall length T (Equation 3.1.1.39).

The various units of the system were arranged according to the "reference-beam" mode of operation (Fig. A.1) since this particular mode best suited the physical arrangement of the experimental facility.

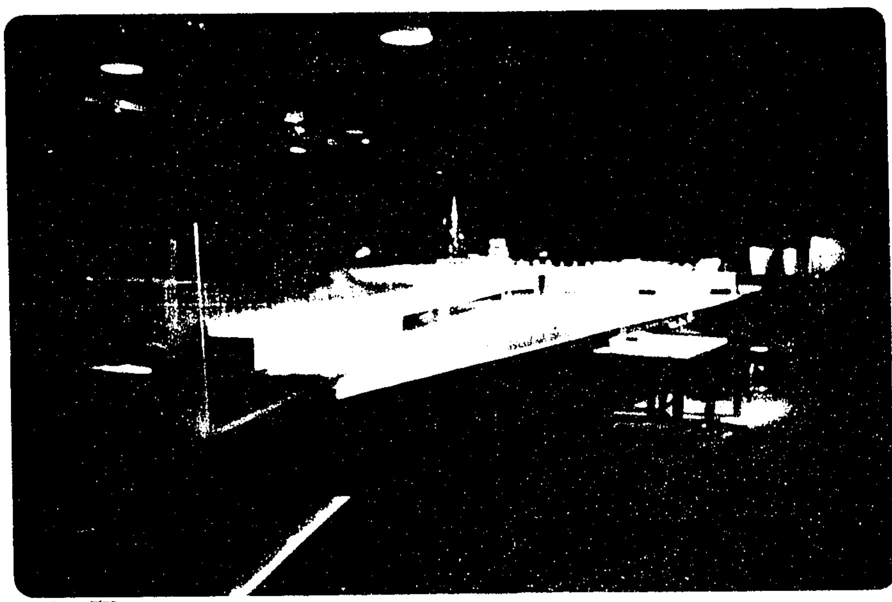

Fig. 5.1 -General View of the Model

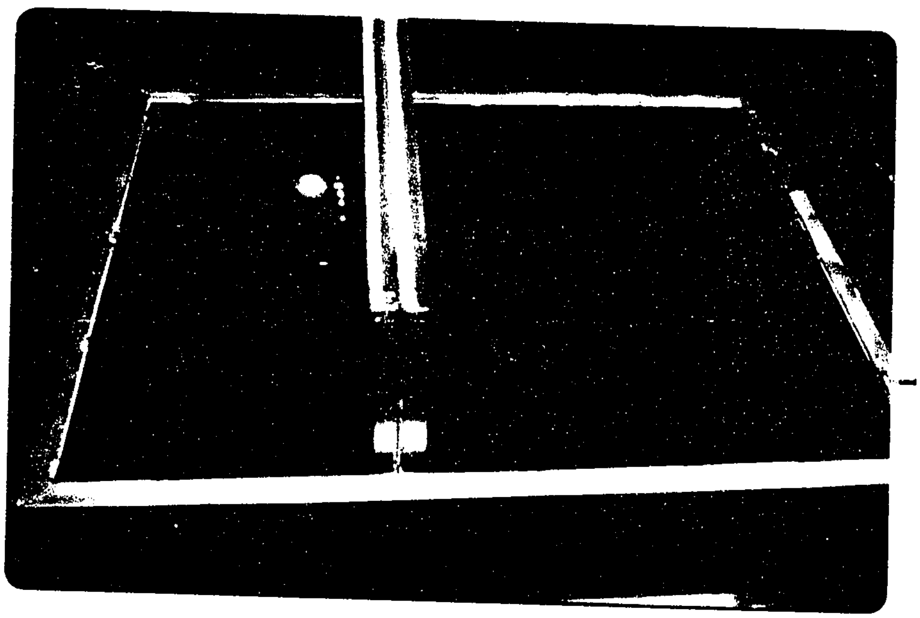

Fig. 5.2 - Inlet Tank : Top View.

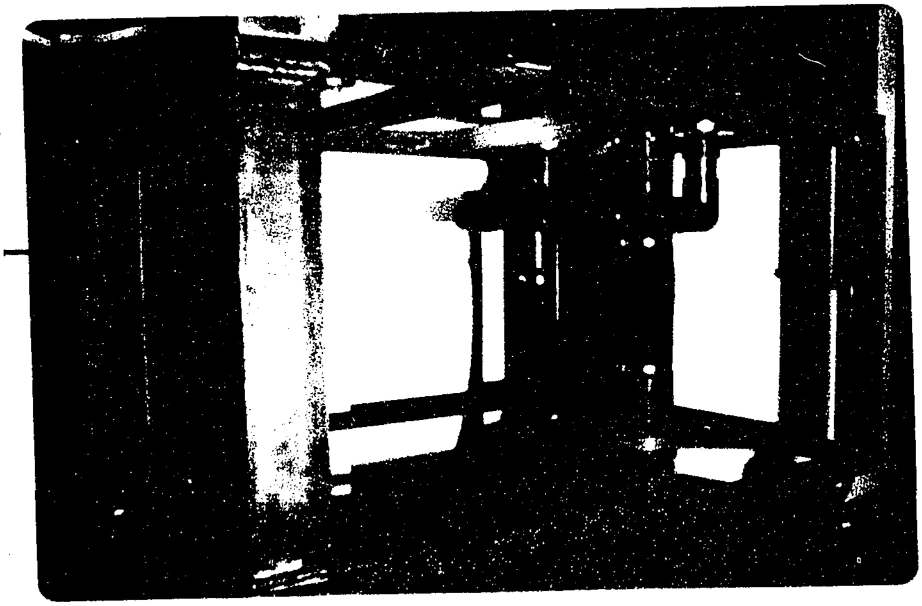

Fig. 5.3 – Inlet Tank : Water Supply and Regulation

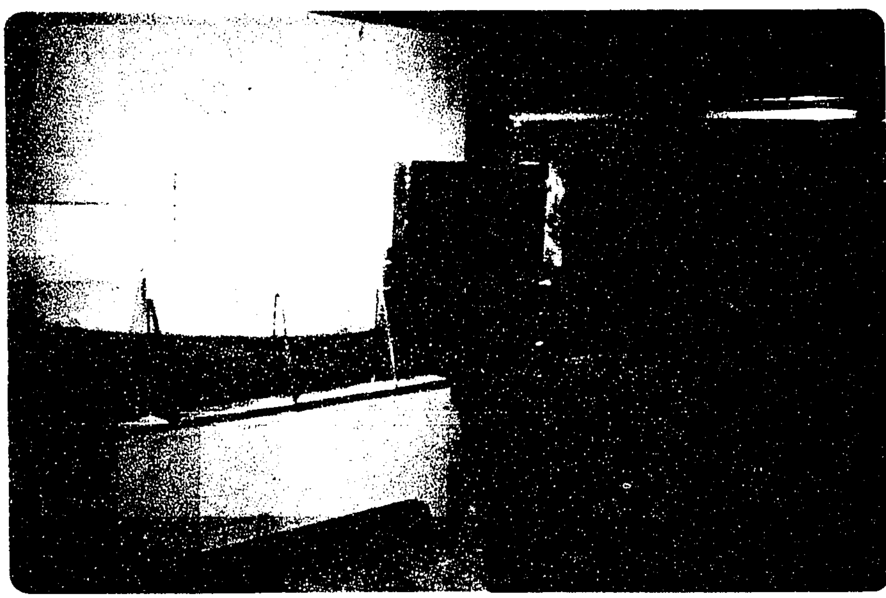

Fig. 5.4 –Inlet Tank : Connection to the Flume Entrance.

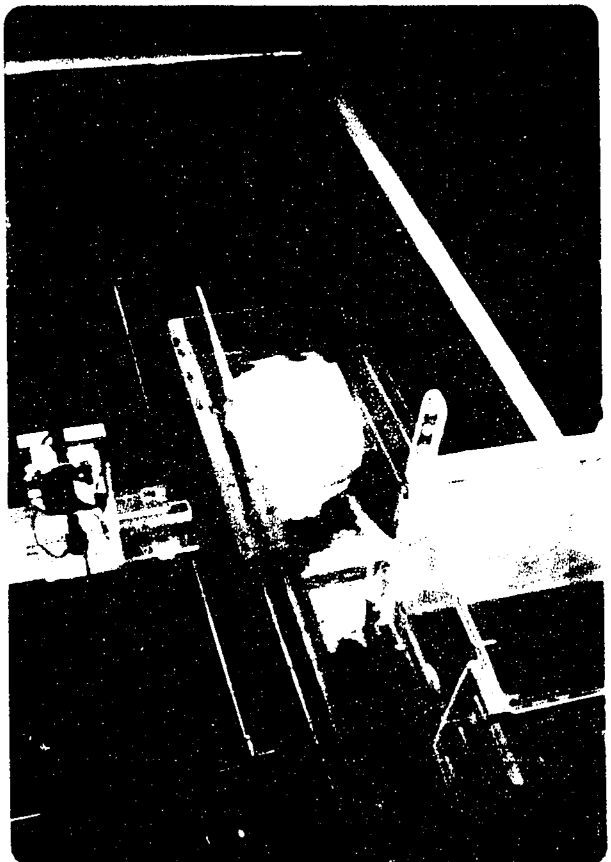

Fig. 5.5 -Outlet Tank : Top View.

Fig. 5.6 -Outlet Flume Gate.

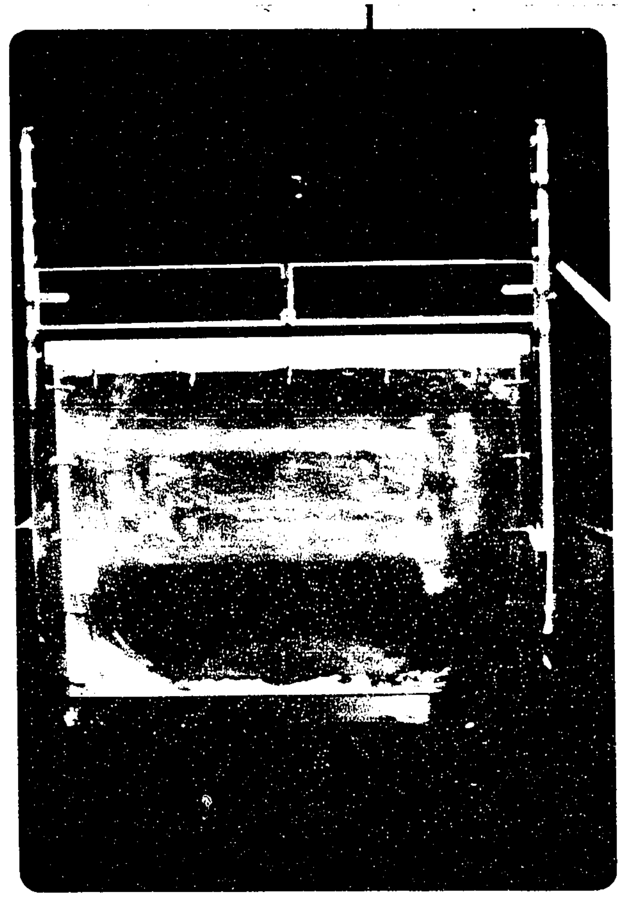

For the purpose of data collection the test sections were divided, lengthwise, into approximately 30 sections and each section was subdivided into 6 cross-section compartments to form a grid for point velocity measurements.

The following procedures were followed prior to actual velocity measurements:

(i) The direction of the bisector of the two laser beams was adjusted so that it was aligned perpendicular to the channel at the section under investigation.

(ii) The laser units, (which ran on the optical bench traversing the channel from below), were then moved back and forth along the bench until the beams intersected precisely at the required measuring point in the flow field.

(iii) Finally the "elevation screws" on the optical units were adjusted, where necessary, to keep the laser beams in a horizontal plane.

Since the purpose of the velocity measurements was to compute boundary shear stress within the test section, the measuring points were chosen as close as possible to the channel bed.

It was found[44] that the velocity component, v, in the direction normal to the bisector of the beam intersection angle θ, and parallel to the beam plane can be calculated from the formula:

$$v = \frac{f_D \cdot \lambda}{2 \sin \theta/2} \qquad (5.2.1.1)$$

where

v = Local flow velocity,

f_D = Doppler frequency which can be read directly on the Meter Unit incorporated in the Doppler Signal Processor,

λ = Wave length of Laser light which is found[44] to be equal to 0.6328×10^{-6} m, in the system adopted, and

θ = Angle of beam intersection.

In fact, the above formula is valid for measurements in air (vacuum). Besides, the accuracy of the analog output of the Doppler Signal Processor is reported[44] to be approximately 1% fsd. Therefore, in order to determine the flow velocity with the same accuracy, modifications are introduced into Equation 5.2.1.1 to take into consideration the effect of flow temperature and the refractive index of the medium as well.

Because the two light beams pass through mediums of different refractive index, the crossing of the two beams is expected to be displaced. This displacement must be perpendicular to the interface as soon as the two beams are symmetric to the normal of the plane of such interface. Therefore, the law of refraction gives in case of measurements in a liquid with refractive index n_2:

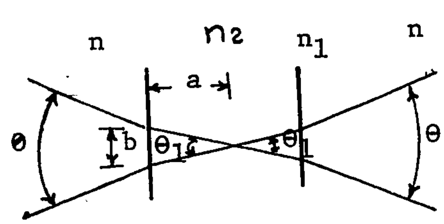

Fig.5.7.Position of the measuring point

$$\lambda_2 = \frac{n}{n_2} \lambda \quad , \text{ and}$$

$$\sin \theta_2/2 = \frac{n}{n_2} \sin \theta/2$$

Thus

$$v = \frac{f_D \cdot \lambda}{2 \sin \theta/2} = \frac{f_D \cdot \lambda_2}{2 \sin \theta_2/2} \tag{5.2.1.2}$$

and

$$a = \frac{b}{2} \cot \theta_2/2$$

where

v = velocity,

f_D = Doppler frequency,

λ_2 = wave length of Laser light in liquid, and

θ_2 = intersection angle in liquid.

The refractive index of air is found [44] to be:

$$n_{air} \text{ (760 mm Hg, 20°C)} = 1.000277$$

and for water

$$n_{water} \text{ (0°C)} = 1.334;$$

and temperature dependence of n_{water} is approximately

$$\Delta_n = 0.0001/\text{C°} \ .$$

However, a new method is adopted to determine the exact location of the beam crossing (i.e., not only its distance from the channel wall but also its depth from the water surface). Accordingly, for each crossing four measurements, (YI, YO, XI and XO), were taken

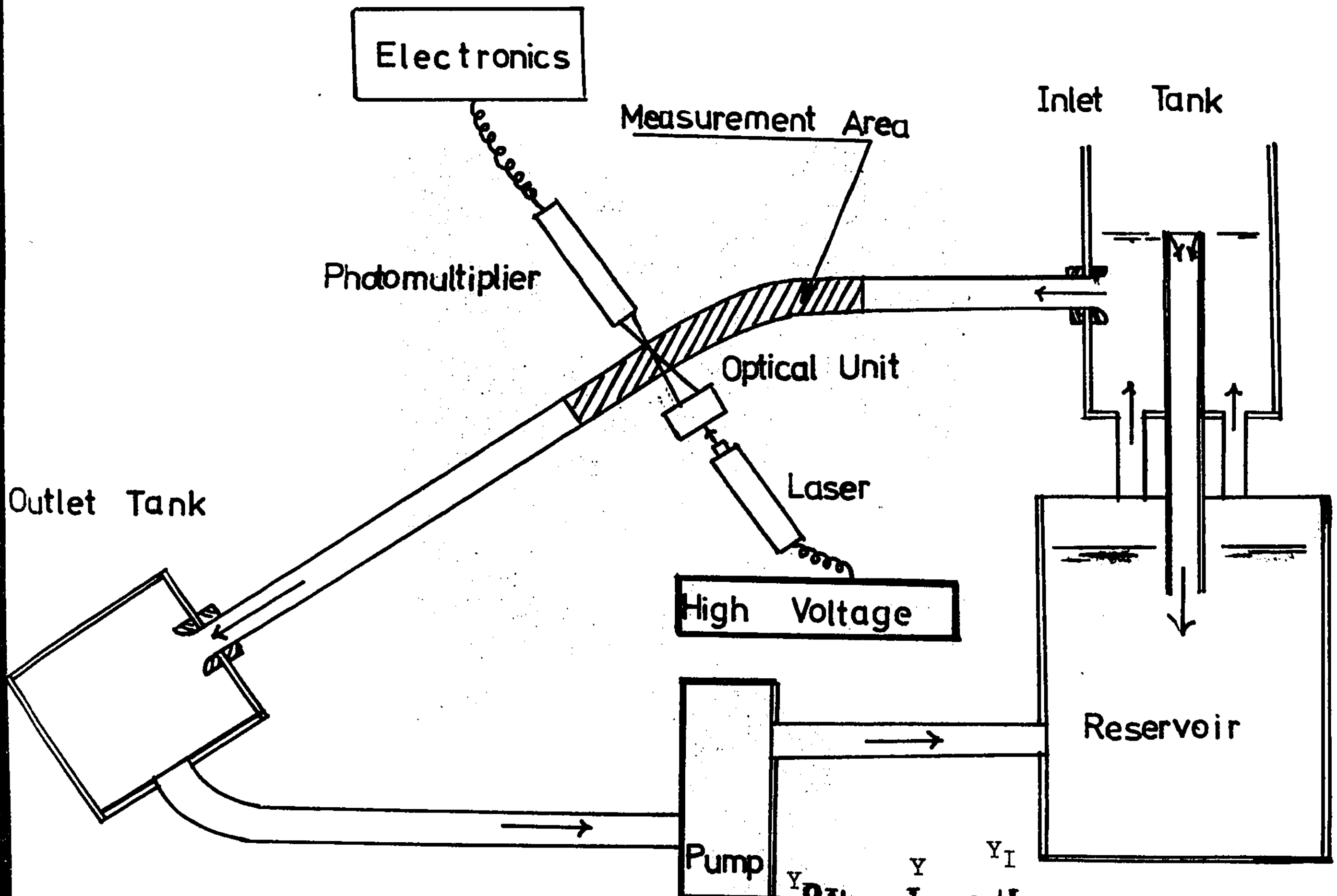

$$x = w/(1 + \frac{x_o}{x_1})$$

$$y = y_I + \frac{y_o - y_I}{w}.x$$

$$\theta = 2 \tan^{-1} (\frac{x_I}{2x})$$

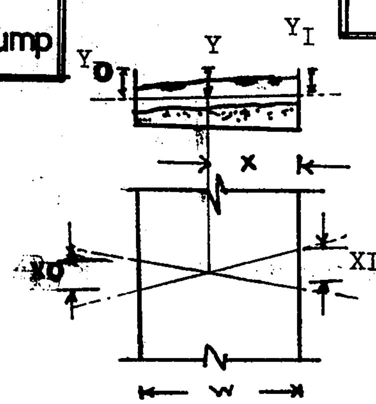

FIG. 5.8 — Installation of the Equipment.

Fig. 5.9- Installation of Laser Set With the Flume.

(Fig. 5.8). The position of the crossing can be determined from:

$$\left.\begin{aligned} x &= w/(1 + \frac{XO}{XI}) , \quad \text{and} \\ y &= YI + \frac{YO - YI}{w} x \end{aligned}\right\} \qquad (5.2.1.3)$$

Therefore, the beam intersection angle, θ, can be computed from:

$$\theta = 2 \tan^{-1} (\frac{XI}{2x}) \qquad (5.2.1.4)$$

5.2.2 Depth Measurements

In order to compute bed shear stresses from point velocities the position of the measuring point, with respect to the channel bed (and the water surface), must be determined. Furthermore, accuracy in depth measurements is extremely important if error in computations of related bed shear stress are to be minimized. In order to achieve accurate readings of local water surface levels and bed elevations, an electronic point gauge was used which measured to an accuracy of 0.01 cm.

In stable channels, where there is no bed sediment in motion, the bed-configuration does not change with time. Therefore, it is assumed that the mean velocity at a point (as well as water surface configuration) also does not change with time. Accordingly, at each point of the reference grid (test section), longitudinal velocity components were measured (LDA System) and local water surface elevations were recorded at these same points. Following each test run corresponding elevations for the bed were recorded (in the dry) at the grid point locations.

5.3 Reliability of the Theory

While the methodology adopted to estimate the bed shear stress distribution in the test section is subject to a number of errors, these errors can be minimized (as stated earlier) by increasing the number of harmonics and/or increasing the period length T in the analysis.

Errors are introduced as a result of the following observations: It is assumed, for example, that the first portion of the system to be affected by the secondary currents is the upstream limit of the bend section, and the portion over which the decay of secondary circulation takes place terminates where the intensity of circulation amounts to 10% of the original intensity.

In fact experimental observations indicate that secondary currents begin to develop upstream from the bend entrance section. Furthermore, the length of channel, in which the decay process takes place, can be considered, theoretically, to approach infinity.

The aforementioned assumptions, therefore, would necessarily lead to an underestimation for the actual period length T, with a corresponding underestimation in boundary shear stress. Moreover, point velocity measurements, water surface and bed elevation measurements are not taken instantaneously, consequently small errors may be introduced as a result of not taking velocity and elevation measurements in the exact same vertical plane.

Finally random perturbations in Doppler signal may occur from time to time during the tests; this can result for example from poor beam intersection and associated shift in the "measuring-volume" zone in the flow field. This instability in the signal output introduces errors in point velocity measurements, consequently a corresponding error in the computed shear stress value is to be expected. However, in view of the characteristically smooth and gradually-changing bed profiles within the test section, it can be argued that small displacements (of the actual point of measurement) from the true grid point will result in negligible error.

CHAPTER 6

DATA ANALYSES AND RESULTS

6.1 Introduction

As stated beforehand the laboratory programme consisted of three series of tests on similar channel bend units having central angles of 45°, 60° and 75° respectively. The initial (boundary) conditions in each of the test series were similar; namely, flow was over a uniform flat sand bed (d_{50} = 0.7 mm; σ = 2.05)*. After equilibrium conditions were established in the test section the following measurements were taken:

(i) point velocity measurements (LDA system) in that portion of the channel in which secondary currents were a significant flow feature;

(ii) water surface elevations; and

(iii) bed elevations.

In view of the close similarity of the three test sections, and the same initial flow conditions used in all tests, the basic steady-state flow patterns that developed in each test section were similar and hence the observed velocity and boundary shear stress distributions were comparable also. Accordingly, for the purpose of presentation and discussion of experimental observations, detailed results for one of the test series (i.e., θ_{bend} = 60°) are presented in Appendix C.1.

---

*All experimental observations are available on request from the Department of Civil Engineering, University of Ottawa, Ottawa, Canada.

6.2 Bed Topography

The observed steady-state bed topography, for both straight and curved portions of the test section, are shown in Fig. C1.1 and Fig. C1.2 respectively for test series number 2.* The initial "flat bed" elevation provided a reference line for subsequent measurements of local erosion and deposition of bed material.

For steady state conditions in the test section it was observed that:

(i) maximum scour occurred near the outer wall of the channel a short distance downstream from the bend section (for test series no. 2 this amounted to -5.3 cm);

(ii) maximum deposition, (+1.85 cm for this same test series), occurred near the inner wall of the bend section; and

(iii) longitudinal profiles of the stable sand bed, along any path line (parallel to the channel centre line), are smooth - i.e., they exhibit gradual change in bed elevation, lengthwise, through the test section.

Use of a flow visualization technique (dye injection) indicated that deposition occurs within a zone of flow deceleration - caused by flow separating from the inner bank near the entrance to the bend.

At this point it is also worth noting that the third observation (above) strongly supports the argument for adopting the logarithmic velocity distribution law when computing bed shear stress from point velocity measurements - especially if such measurements are taken close to the sediment/water interface and without disturbance to the flow field.

---

*Stable bed topography for all experimental runs are presented in Figs. 6.1, 6.2 and 6.3.

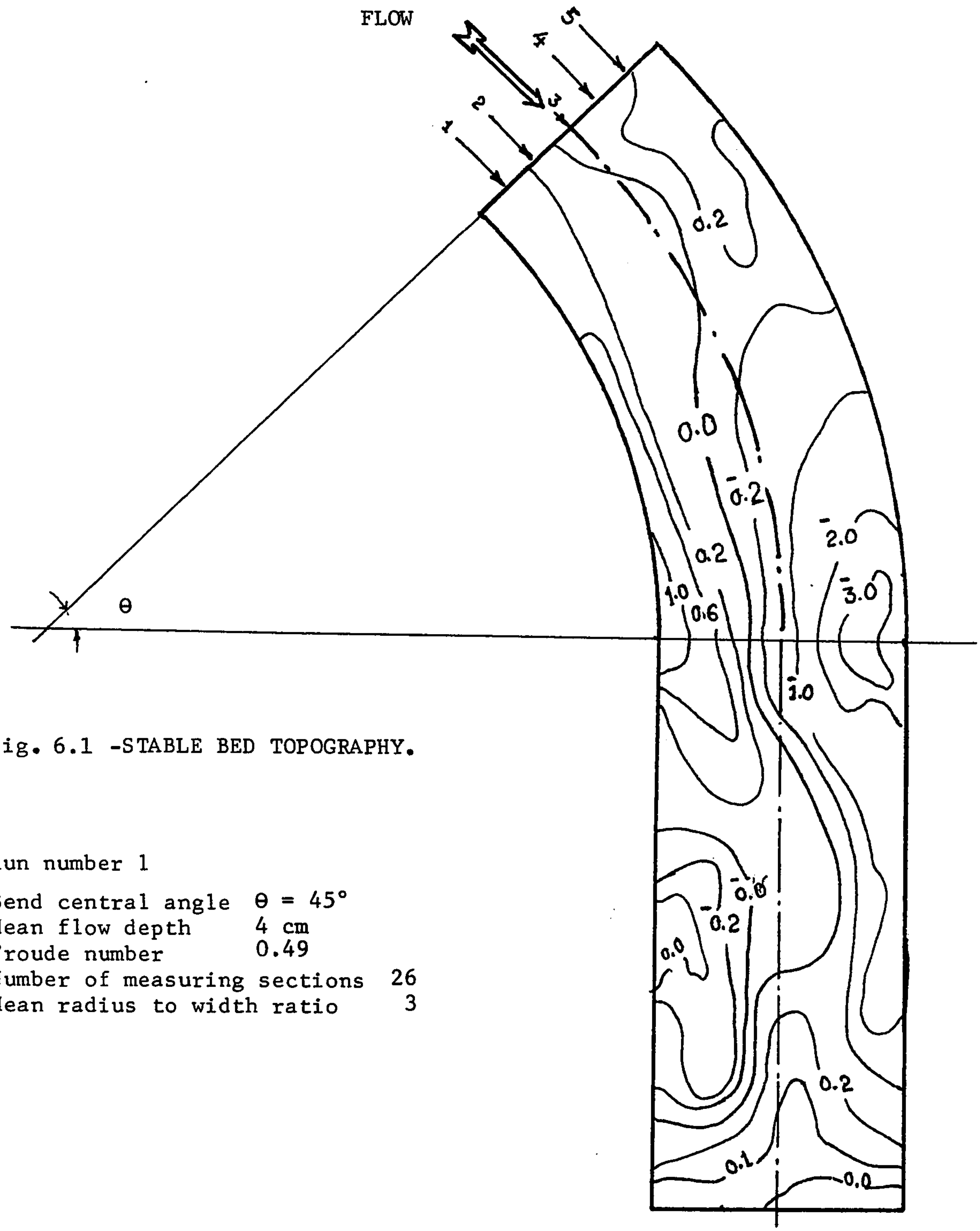

Fig. 6.1 -STABLE BED TOPOGRAPHY.

Run number 1

Bend central angle θ = 45°
Mean flow depth 4 cm
Froude number 0.49
Number of measuring sections 26
Mean radius to width ratio 3

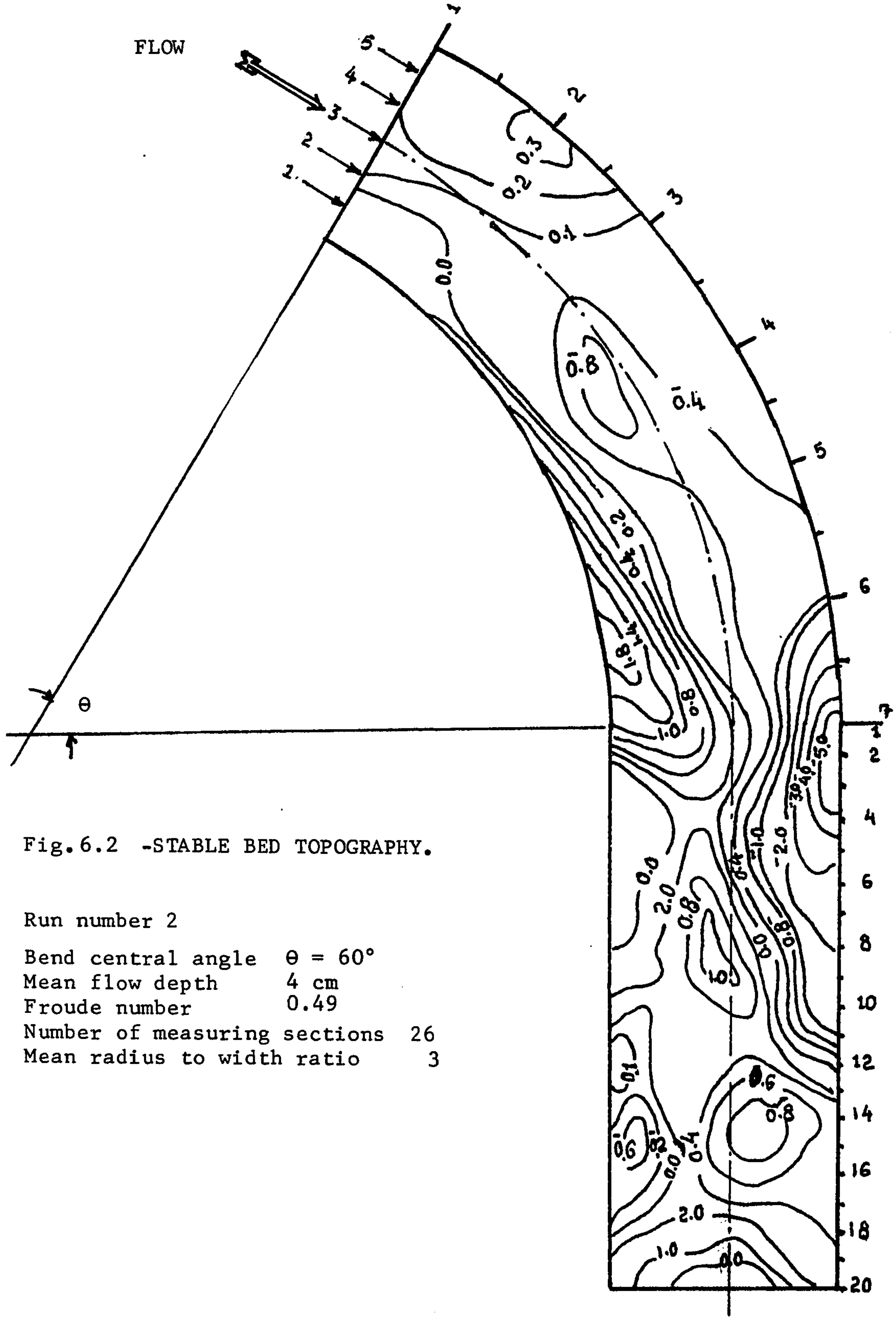

Fig.6.2 -STABLE BED TOPOGRAPHY.

Run number 2

Bend central angle θ = 60°
Mean flow depth 4 cm
Froude number 0.49
Number of measuring sections 26
Mean radius to width ratio 3

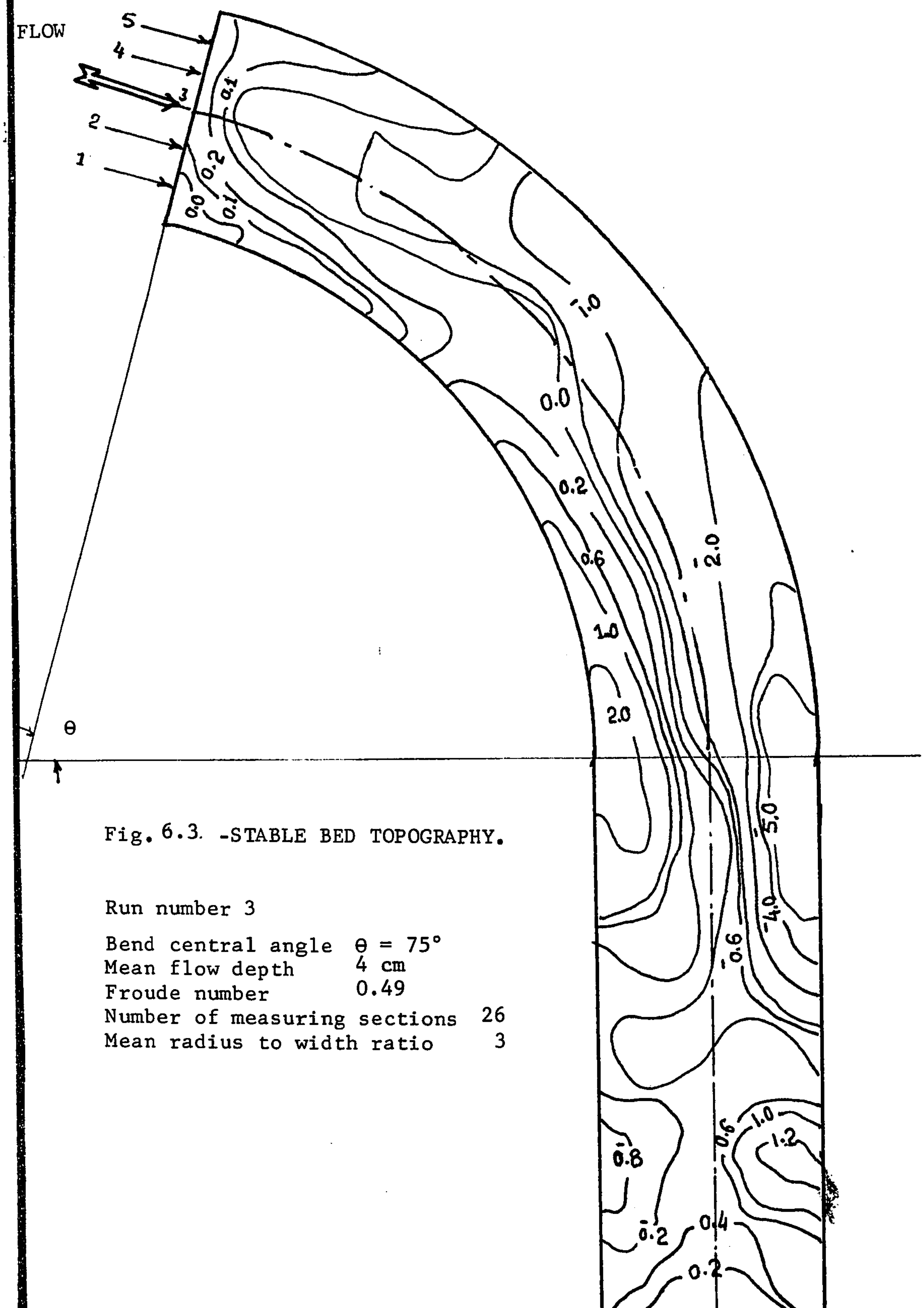

Fig. 6.3. -STABLE BED TOPOGRAPHY.

Run number 3

Bend central angle	θ = 75°
Mean flow depth	4 cm
Froude number	0.49
Number of measuring sections	26
Mean radius to width ratio	3

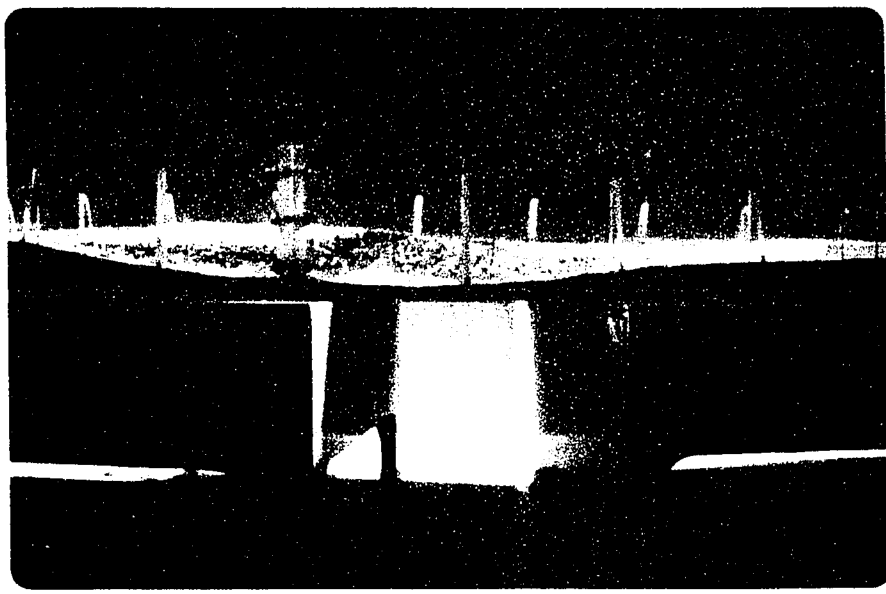

Fig. 6.4 – Sand Bed Elevations.

6.3 Water Surface Profiles

Water surface elevations, for the straight and curved portions of the test section, are shown in Fig.C1.3 and Fig.C1.4 respectively. Values represent the recorded water surface elevations relative to the initial horizontal water surface level. The following observations were noted:

(i) maximum superelevation of the water surface occurred near the exit from the bend, (in the fully-developed turbulent flow region), and had a value of +0.55 cm in the second test series;

(ii) since erosion occurred over much of the bed in the test section, most of the "steady-state" water surface elevations had negative signs (i.e., the water surface was generally lower than the initial water surface elevation at the beginning of the tests), however local water depths, (Figs.C.1.9 and C1.10), were approximately the same as the initial values. This particular observation was supported by the computed changes in the cross-sectional areas of flow and the computed changes in sediment volume at any point in the system (Figs. C.1.5,C.1.6,C.1.7,C.1.8)

(iii) the ratio of the "steady-state" cross sectional area of flow to the "initial" flow area had two maximum values at bend sections 3 and 4 and a minimum value atssection 19 in the straight channel reach downstream from the bend, (Fig.C.1.11 and Fig. C.1.12)

6.4 Bed Shear Stresses

Local bed shear stresses, which were computed from point velocity measurements using the logarithmic velocity distribution law, were expressed in dimensionless form (i.e., stresses were divided by the uniform boundary shear stress value obtained for similar flow conditions in a correspondingly infinitely wide channel. The observed boundary shear stress distributions, for each of the test series, are presented in Figs. 6.5, 6.6, 6.7, 6.8, 6.9 and 6.10.*

Inspection of these diagrams indicates two areas of maximum shear stress and two areas of minimum shear stress in the test sections. The former occur near the inner wall of the channel (at the entrance to the bend) and near the outer wall (at the downstream end of the bend); whereas the latter occur near the outer wall (at entry to the bend) and near the inner wall (at the bend exit section). Moreover, in general it may be stated that change in boundary shear stress (along the walls of the test section), takes place gradually.

Furthermore, in the straight portion of the channel (following the bend section), bed shear stress tends to decrease along the outer wall and increase along the inner wall until a section is reached (some distance downstream from the bend) where the stress distribution becomes more or less uniform across the bed.

These characteristics patterns of maxima and minima stress distribution in the test section can be considered manifestations of the flow being deflected, diagonally, to and fro across the channel by

---

* τ_o, the theoretical uniform bed shear stress value for an equivalent straight infinitely-wide channel, is found to be equal to 0.073 gm/cm^2.

FIGURE 6.5

Shear Stress Distributions (τ/τ_o)

Run Number 1

Central Bend Angle = 45°

Dimensionless Shear Stress				
Path 1	Path 2	Path 3	Path 4	Path 5
1.09	1.05	1.0	0.9	1.0
1.25	1.15	1.05	1.07	1.0
1.20	1.13	1.09	1.0	0.96
1.15	1.25	1.30	1.25	1.25
1.15	1.35	1.45	1.55	1.55
1.15	1.12	1.25	1.55	1.66
1.09	1.04	1.25	1.50	1.65
0.90	1.05	1.30	1.62	1.72
1.0	1.10	1.50	1.70	1.81
1.03	1.10	1.50	1.65	1.75
1.05	1.10	1.45	1.62	1.72
1.06	1.40	1.40	1.62	1.69
1.07	1.14	1.30	1.60	1.67
1.08	1.20	1.30	1.60	1.65
1.09	1.20	1.35	1.6	1.65
1.10	1.25	1.35	1.55	1.64
1.25	1.29	1.35	7.5	1.62
1.28	1.28	1.35	1.55	1.62
1.28	1.27	1.35	1.50	1.61
1.25	1.26	1.35	1.45	1.60
1.22	1.35	1.34	1.45	1.50
1.20	1.22	1.27	1.40	1.50
1.17	1.20	1.25	1.30	1.45
1.16	1.17	1.20	1.35	1.45
1.14	1.12	1.15	1.22	1.25
1.10	1.08	1.11	1.15	1.22
1.0	1.02	1.05	1.10	1.15
0.8	0.9	1.0	0.8	0.80
0.70	0.80	1.0	0.90	0.75
0.8	0.80	0.90	1.0	0.70

FIGURE 6.6

Shear Stress Distributions (τ/τ_o)

Run Number 2

Central Bend Angle = 60°

Dimensionless Shear Stress				
Path 1	Path 2	Path 3	Path 4	Path 5
1.0	0.9	0.8	1.0	1.0
1.40	1.50	1.50	0.9	0.8
1.85	1.65	1.00	0.85	0.65
2.10	1.70	1.30	0.95	0.90
1.90	1.80	1.50	1.20	0.95
1.80	1.30	1.40	1.25	0.95
1.25	1.20	1.40	1.30	0.97
1.10	1.30	1.40	1.30	1.00
0.95	1.30	1.60	1.65	1.45
0.80	1.30	1.60	1.70	1.80
0.80	1.15	1.40	1.90	2.10
0.80	1.30	1.50	2.0	2.20
0.80	1.40	1.80	2.20	2.40
0.80	1.30	1.65	2.20	2.45
0.80	1.40	1.70	2.15	2.40
1.0	1.40	1.70	2.0	2.20
1.0	1.35	1.65	2.05	2.10
1.10	1.30	1.70	2.0	2.10
1.15	1.30	1.70	1.90	2.05
1.20	1.30	1.65	1.90	2.05
1.20	1.30	1.60	1.85	2.0
1.20	1.30	1.60	1.85	2.0
1.25	1.30	1.60	1.80	1.90
1.27	1.30	1.45	1.60	1.85
1.28	1.40	1.40	1.38	1.50
1.40	1.50	1.40	1.35	1.37
1.45	1.40	1.30	1.32	1.34
1.40	1.30	1.25	1.25	1.28
1.10	1.10	1.15	1.18	1.20
1.05	1.08	1.08	1.10	1.12
1.0	1.04	1.05	1.07	1.10
0.90	1.05	1.05	1.06	1.08

FIGURE 6.7

Shear Stress Distribution (τ/τ_o)

Run Number 3

Central Bend Angle = 75°

Dimensionless Shear Stress				
Path 1	Path 2	Path 3	Path 4	Path 5
1.0	1.0	1.0	1.10	1.30
2.00	1.8	1.70	1.30	1.0
2.10	1.75	1.70	1.20	0.80
2.10	1.90	1.70	1.30	1.10
2.15	1.80	1.70	1.50	1.20
2.10	1.80	1.70	1.70	1.20
1.90	1.7	1.70	1.70	1.30
1.75	1.70	1.70	1.70	1.40
1.70	1.20	1.40	1.70	1.30
1.10	1.10	1.50	1.70	1.50
0.80	1.10	1.50	1.75	1.80
0.80	1.10	1.70	1.90	2.0
0.80	1.30	1.80	2.0	2.10
0.90	1.50	1.80	2.0	2.10
1.10	1.50	1.80	2.15	2.40
1.10	1.50	1.70	2.30	2.60
1.10	1.50	1.80	2.30	2.65
1.10	1.60	1.85	2.30	2.65
1.20	1.75	1.85	2.00	2.40
1.10	1.70	1.80	1.90	2.10
1.10	1.70	1.80	1.90	2.10
1.10	1.60	1.80	1.85	2.00
1.50	1.70	1.80	1.85	1.95
1.60	1.75	1.80	1.85	1.90
1.70	1.50	1.40	1.50	1.80
1.40	1.30	1.35	1.50	1.70
1.30	1.20	1.20	1.35	1.50
1.20	1.20	1.20	1.30	1.45
1.08	1.08	1.15	1.25	1.30
0.90	1.02	1.05	1.07	1.10
0.9	1.00	1.02	1.06	1.08
0.80	0.90	1.00	1.05	1.08

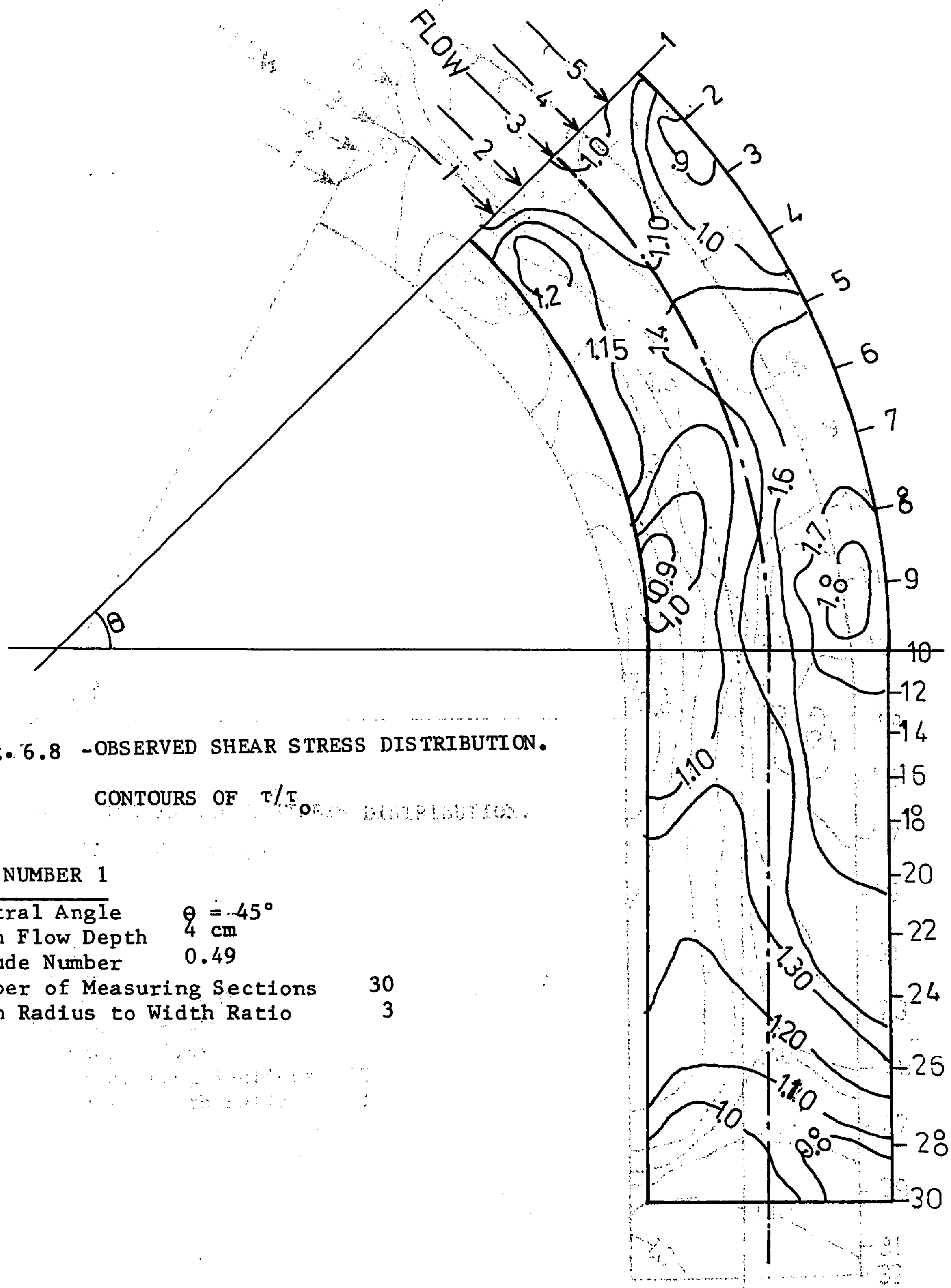

Fig. 6.8 -OBSERVED SHEAR STRESS DISTRIBUTION.

CONTOURS OF τ/τ_o

RUN NUMBER 1

Central Angle	θ = 45°
Mean Flow Depth	4 cm
Froude Number	0.49
Number of Measuring Sections	30
Mean Radius to Width Ratio	3

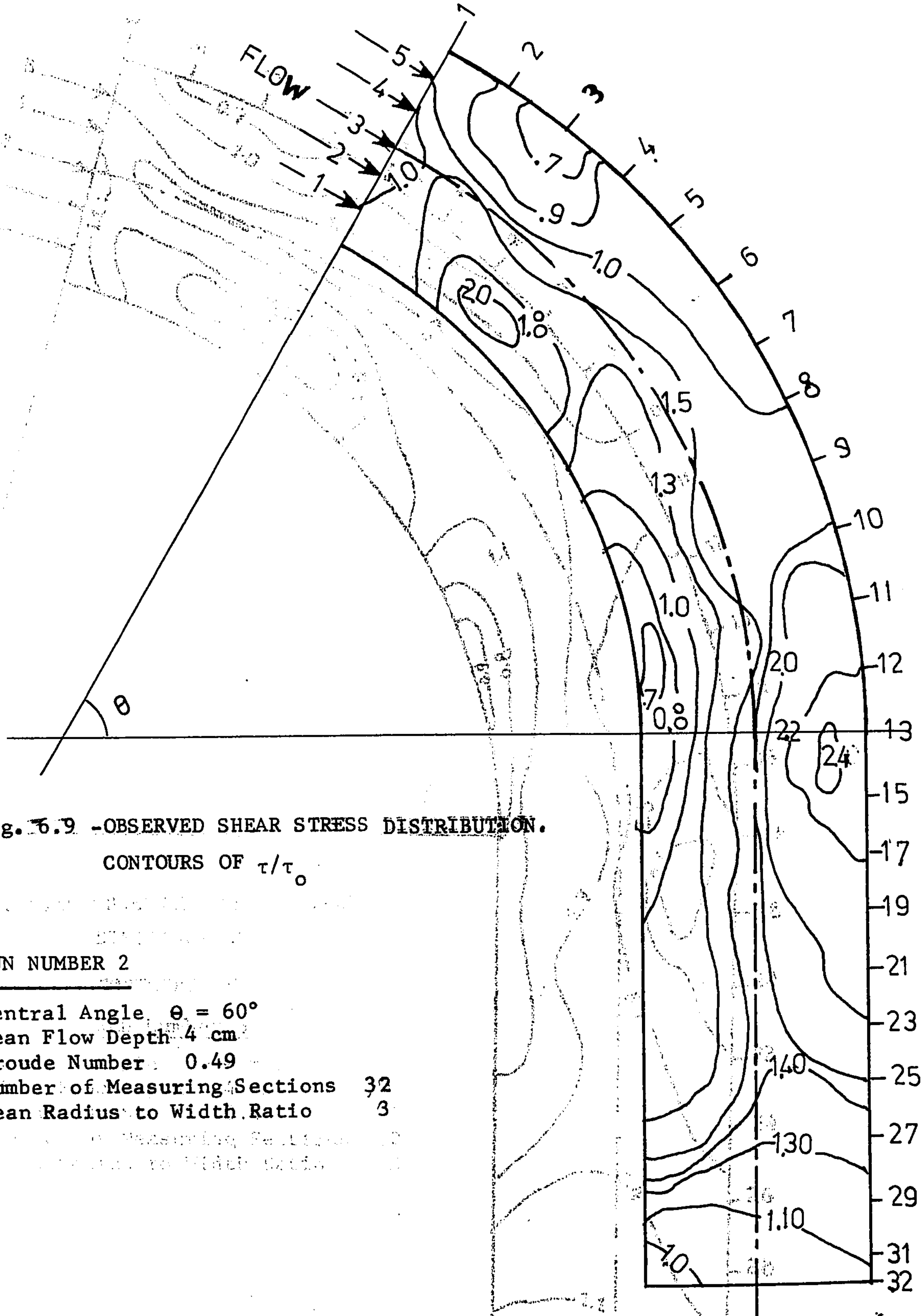

Fig. 6.9 -OBSERVED SHEAR STRESS DISTRIBUTION.
CONTOURS OF τ/τ_o

RUN NUMBER 2

Central Angle $\theta = 60°$
Mean Flow Depth 4 cm
Froude Number 0.49
Number of Measuring Sections 32
Mean Radius to Width Ratio 3

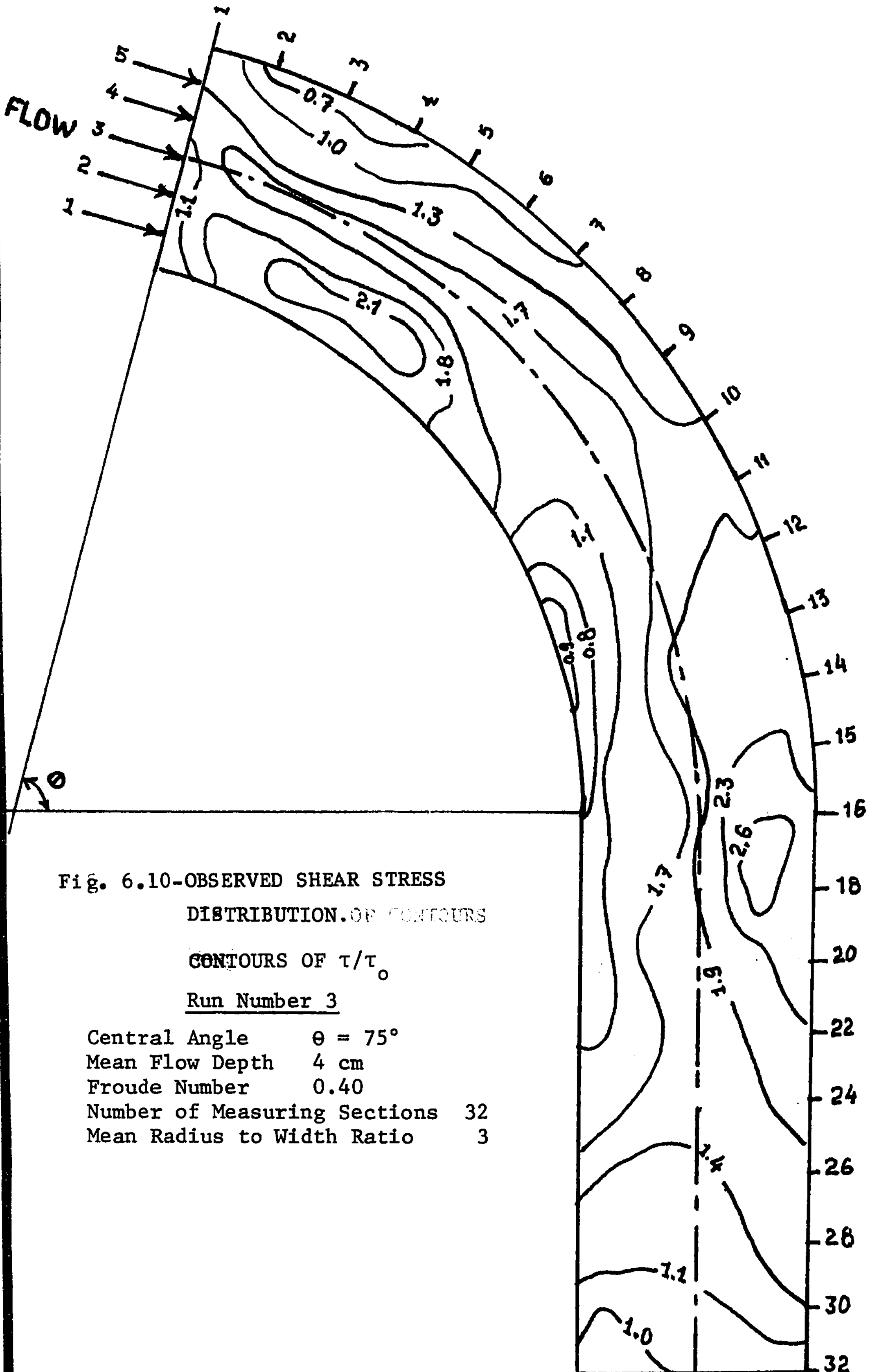

Fig. 6.10-OBSERVED SHEAR STRESS DISTRIBUTION.OF CONTOURS

CONTOURS OF τ/τ_o

Run Number 3

Central Angle	$\theta = 75°$
Mean Flow Depth	4 cm
Froude Number	0.40
Number of Measuring Sections	32
Mean Radius to Width Ratio	3

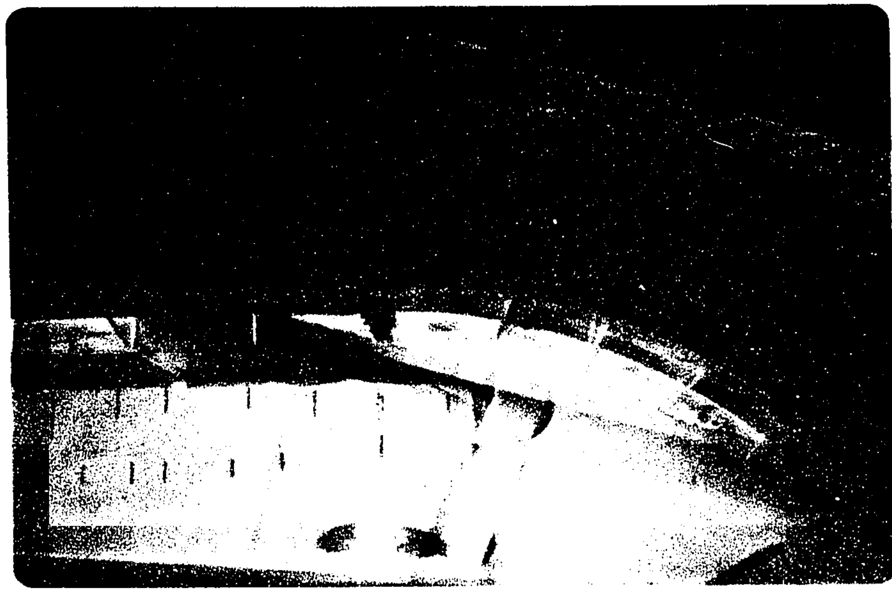

Fig. 6.11 –Zones of Maximum and Minimum Bed Shear Stress in the Bend Sections (Flow From Right to Left)

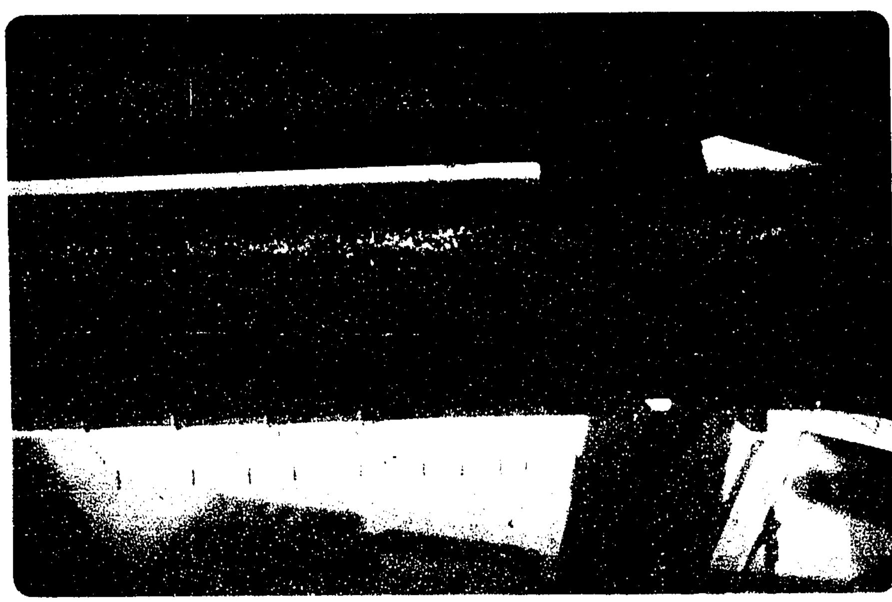

Fig. 6.12 –Zones of Maximum and Minimum Shear Stress in the Straight Reach Immediately after the Bend (Flow From Right to Left)

the wall curvature in the bend section. Moreover the portion of the straight channel section (downstream from the bend), in which an essentially uniform stress distribution is re-established, represents the flow zone where decay of secondary circulation takes place.

In comparing Figs. 6.9 and 6.2 it should be noted that zones of maximum shear stress on the bed correspond closely to zones of maximum scour; also zones of minimum shear stress are compatible with areas of maximum deposition of material in the test sections.

It is also clear that the maximum value of bed shear stress occurs near the outer bank, (at bend exit), where the forced vortex law can be reasonably applied for determination of local longitudinal velocities. Furthermore, it was noted that this maximum value increased as the bend angle increased. This can be explained by the fact that the flow becomes fully developed (i.e., has a uniform velocity distribution in the main flow direction) at larger bend angles.

6.5 Stochastic Analysis

The dimensionless shear stresses, presented in Fig.C2.3 were obtained using stochastic-type predictive models. Finite Fourier Series, Autoregressive and Moving Average Models were employed to predict shear stress on thebbed along any path parallel to the channel centre line.

Since the computational procedures used in a test series were the same for all tests, a general discussion of the procedures is included in this section. However, in view of the similarity in data obtained for the various tests, only detailed results for pathline no. 1; test series no. 2, are presented as a representative example and are tabulated in Appendix C.2. In addition, a summary of the main characteristics, for all paths in each of the test series, is presented in Figs. 6.13 and 6.14.

6.5.1 Finite Fourier Series

The "analysis of variance" table (Finite Fourier Series Model) for the selected test series is shown in Fig. C.2.2. The variables shown were calculated, for the different harmonics chosen, using Equations (3.2.3.2).

Referring to Fig. C.2.2 it was noticed that the variance of the chosen series could be explained by increasing the number of harmonics (a number of harmonics equal to half the total observations in the path is required to explain all the variance[7]). However, for practical application of the method, it is believed that a number of harmonics which explains about 80%, or more, of a series variance is adequate for dimensionless bed shear stress prediction. Accordingly, in this instance, a number of harmonics = 4 was considered suitable for predictive purposes (since this gave an explained variance of 96.1%). It was felt that the increased amount of explained variance (obtained from a corresponding increase in the number of harmonics employed) did not warrant the related increase in calculations required. Furthermore, by comparing the estimated and measured values (Fig. C.2.3)

FIGURE 6.13
Series Characteristics

		Series			Fourier Analysis		Autoregressive Process Parameters		
Angle	Path	b/B	Mean	Variance	No. of Harmonics	Ex.Var.%	AR(1)	AR(2)	Characteristic Eq. Roots
45°	1	1/6	1.09	0.02	4	89.54	0.78	1.08-0.39	Complex
	2	1/3	1.14	0.02	4	89.48	0.74	0.89-0.21	Complex
	3	1/2	1.25	0.02	2	86.40	0.74	0.84-0.13	Real
	4	2/3	1.37	0.07	2	94.26	0.82	0.90-0.11	Real
	5	5/6	1.42	0.10	2	95.10	0.82	1.01-0.22	Real
60°	1	1/6	1.19	0.11	4	96.10	0.84	1.22-0.46	Complex
	2	1/3	1.32	0.03	4	86.20	0.49	0.57-0.155	Complex
	3	1/2	1.43	0.06	2	79.80	0.55	0.32-0.41	Real
	4	2/3	1.54	0.18	2	97.10	0.91	1.20-0.30	Real
	5	5/6	1.57	0.30	2	94.10	0.93	1.35-0.45	Complex
75°	1	1/6	1.33	0.19	3	90.26	0.80	0.92-0.14	Real
	2	1/3	1.43	0.09	3	86.14	0.69	0.67-0.04	Real
	3	1/2	1.56	0.08	3	77.68	0.71	0.62-0.13	Real
	4	2/3	1.66	0.14	1	91.94	0.87	0.93-0.07	Real
	5	5/6	1.68	0.27	1	93.16	0.92	1.31-0.42	Real

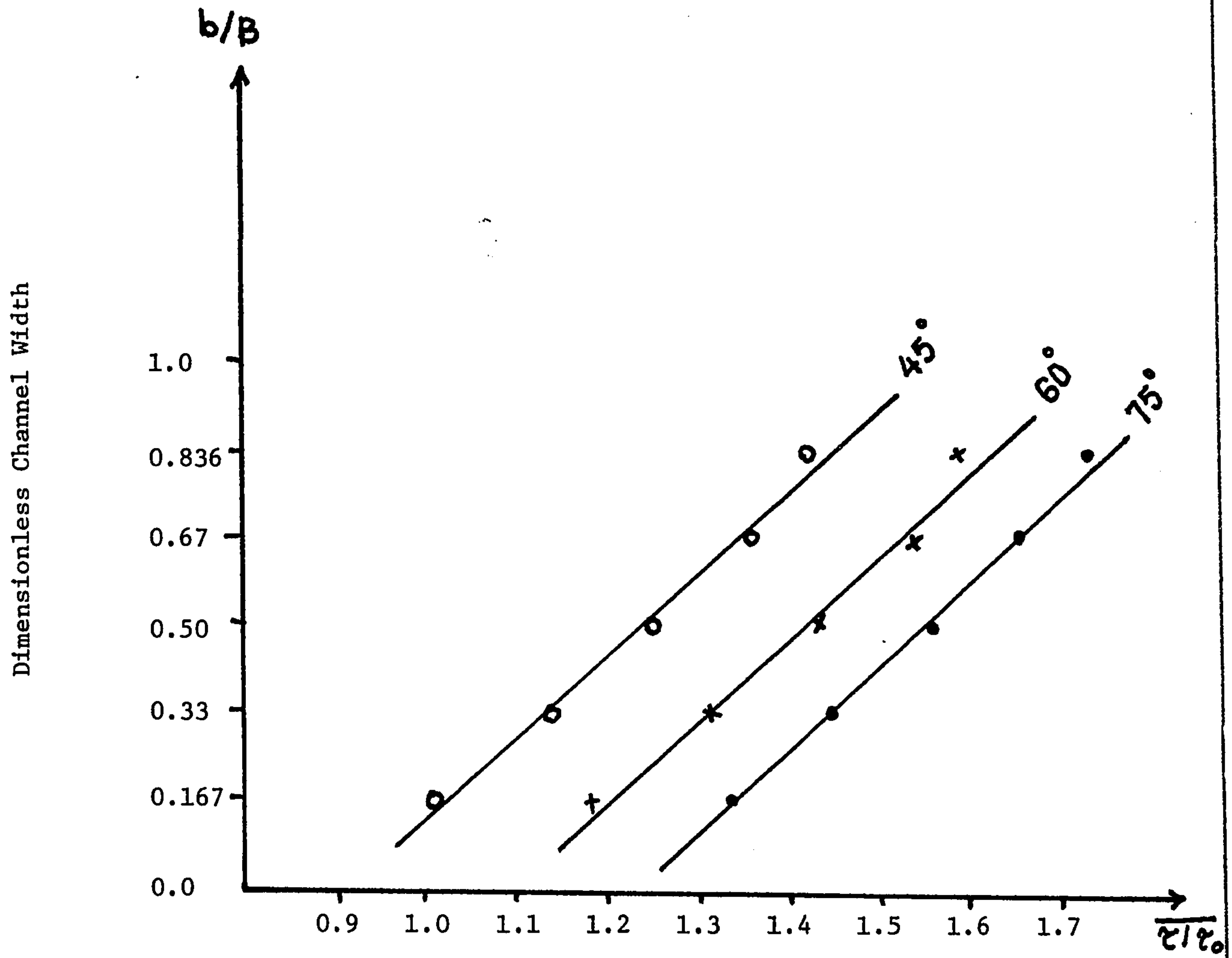

Mean Values of Dimensionless Shear Stress

Fig. 6.14 - Dimensionless Shear Stresses

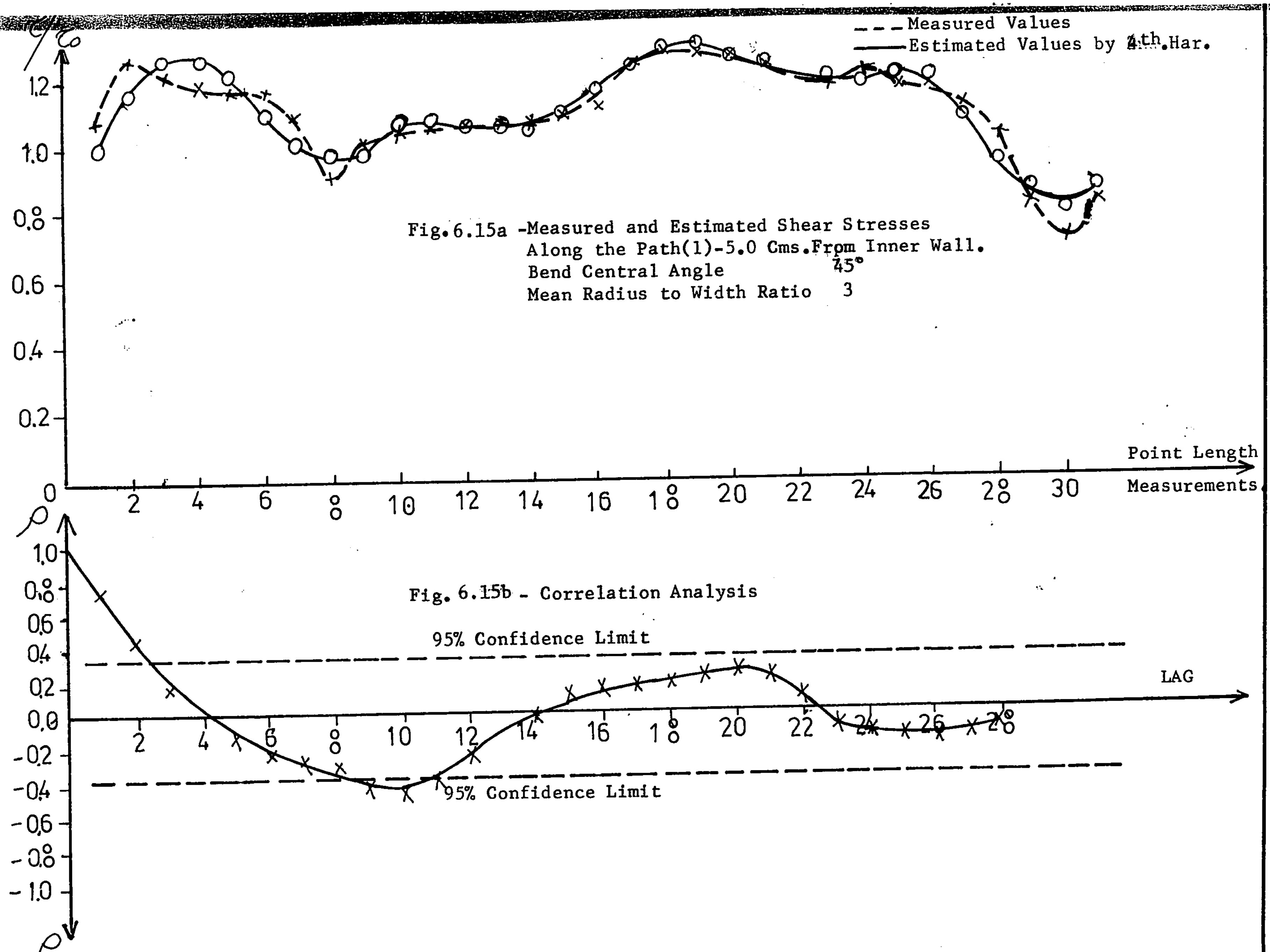

Fig.6.15a -Measured and Estimated Shear Stresses
Along the Path(1)-5.0 Cms.From Inner Wall.
Bend Central Angle 45°
Mean Radius to Width Ratio 3

Fig. 6.15b - Correlation Analysis

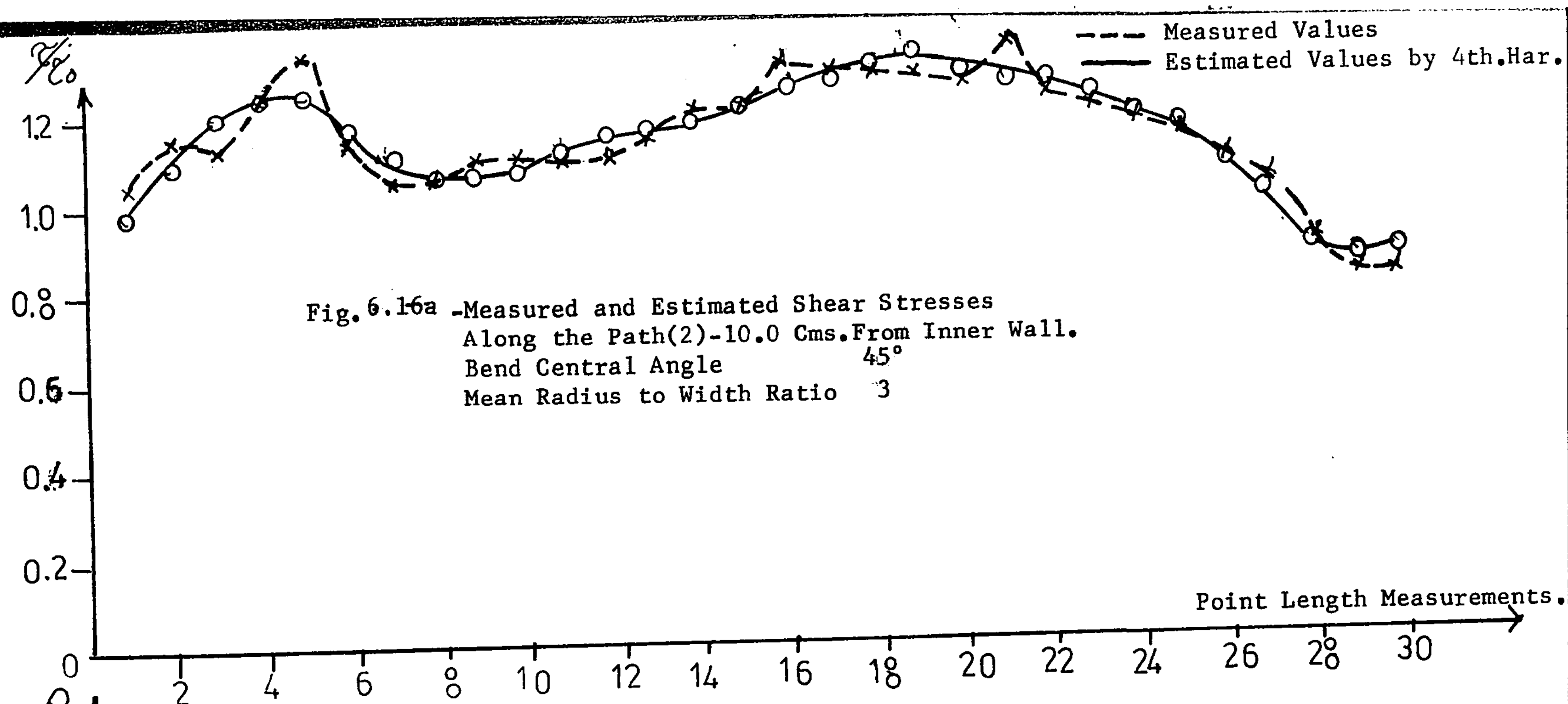

Fig. 6.16a -Measured and Estimated Shear Stresses
Along the Path(2)-10.0 Cms.From Inner Wall.
Bend Central Angle 45°
Mean Radius to Width Ratio 3

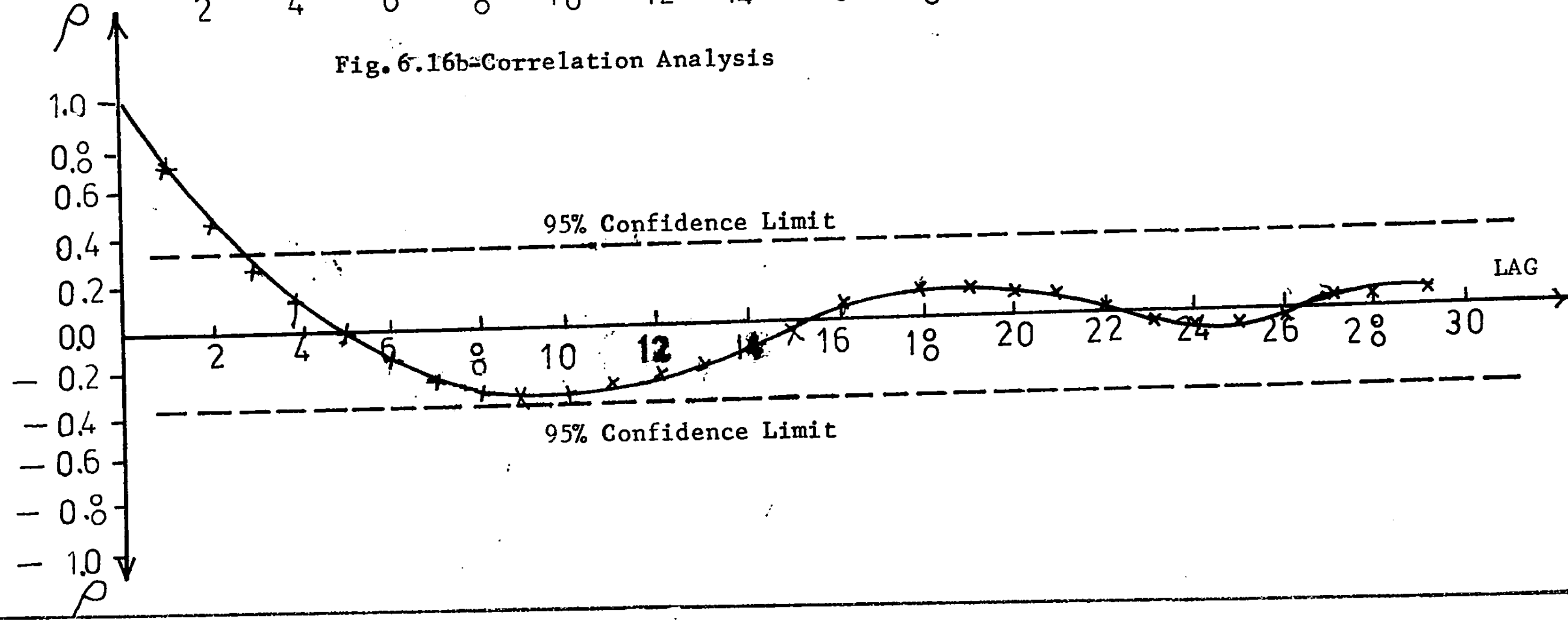

Fig. 6.16b-Correlation Analysis

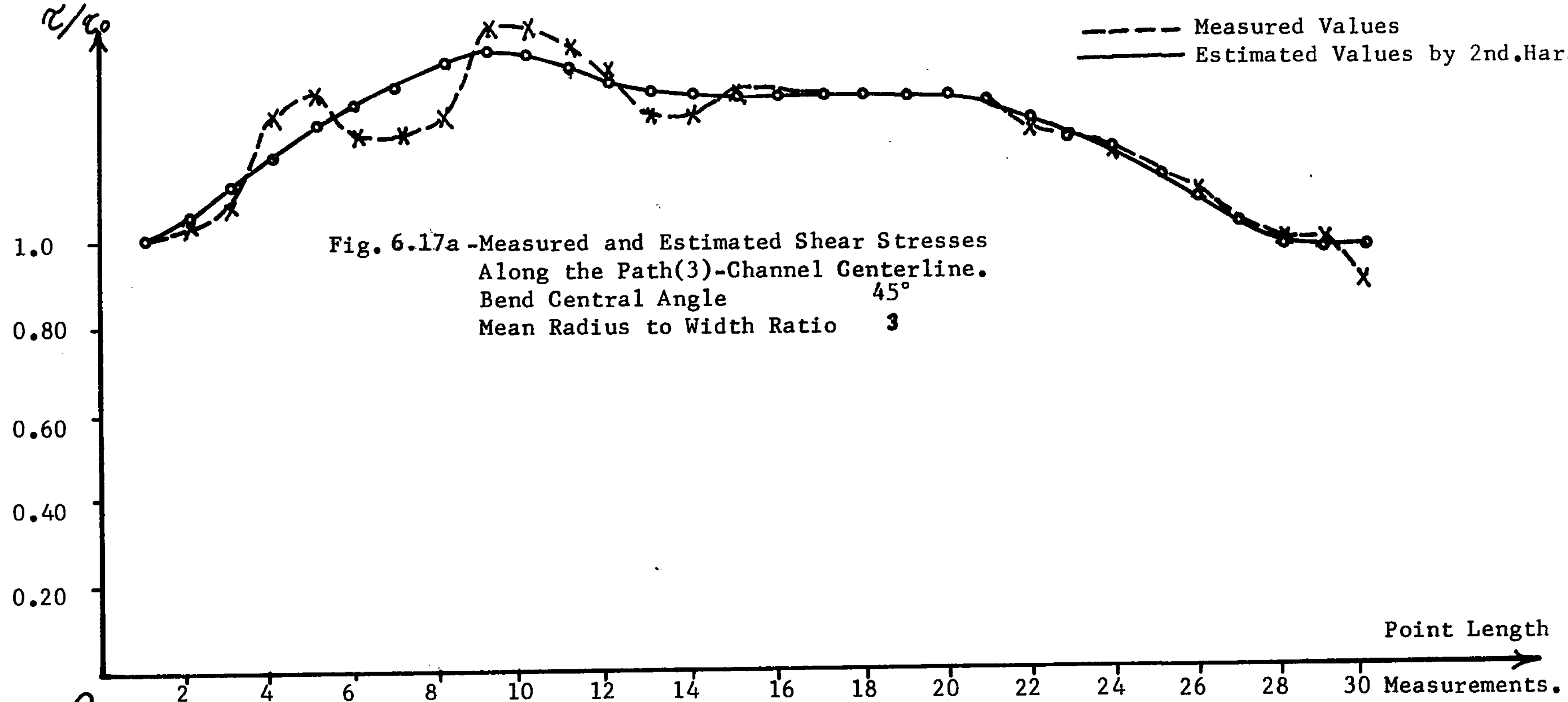

Fig. 6.17a -Measured and Estimated Shear Stresses
Along the Path(3)-Channel Centerline.
Bend Central Angle 45°
Mean Radius to Width Ratio 3

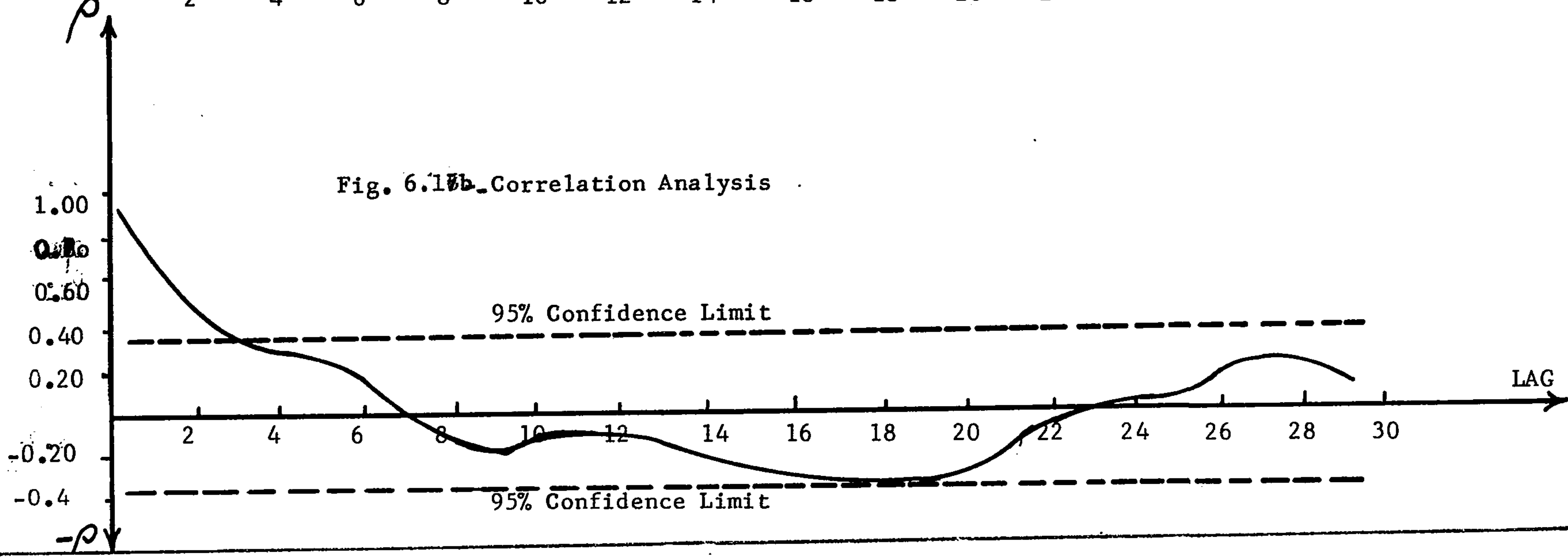

Fig. 6.17b Correlation Analysis

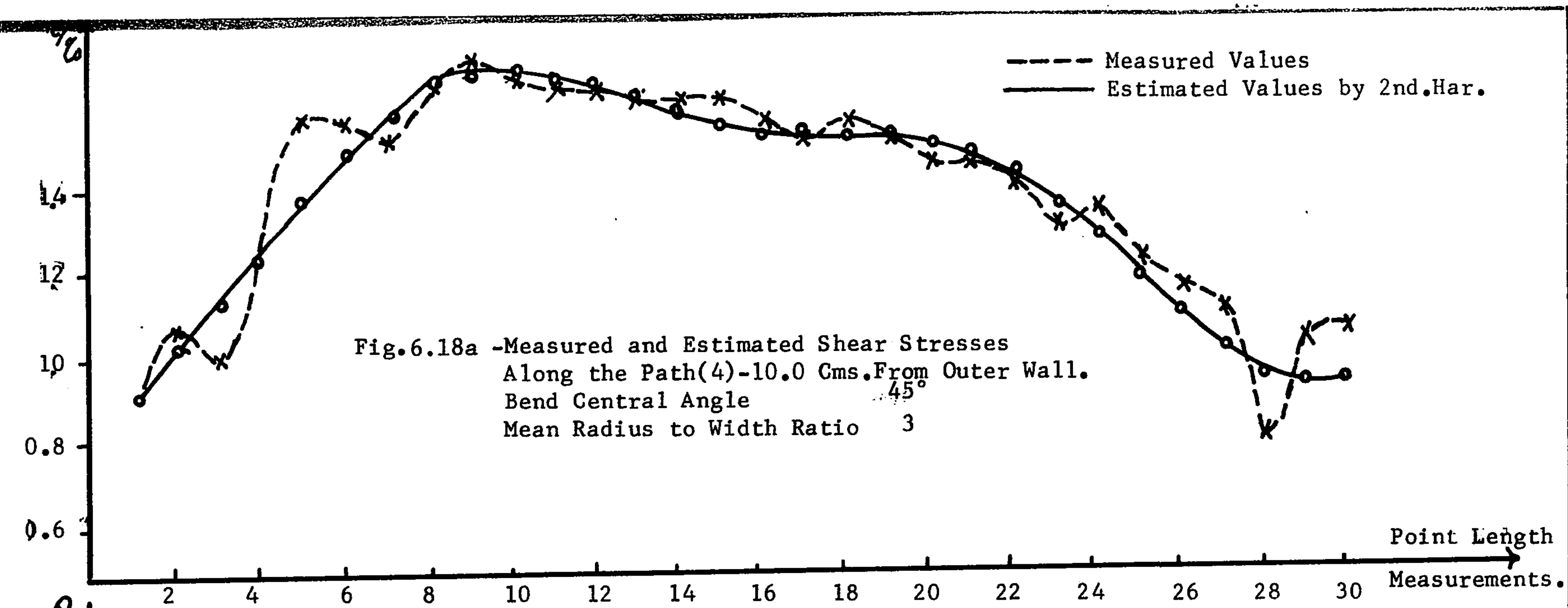

Fig.6.18a -Measured and Estimated Shear Stresses
Along the Path(4)-10.0 Cms.From Outer Wall.
Bend Central Angle 45°
Mean Radius to Width Ratio 3

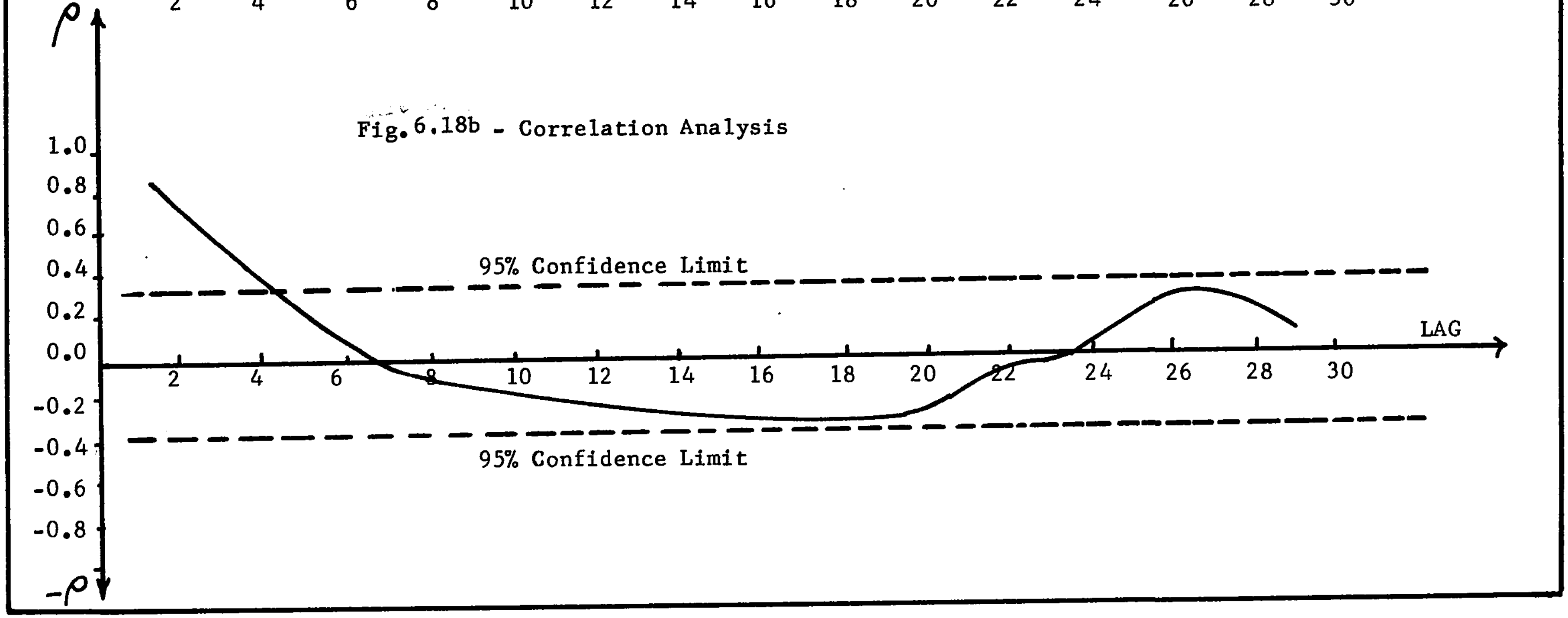

Fig.6.18b - Correlation Analysis

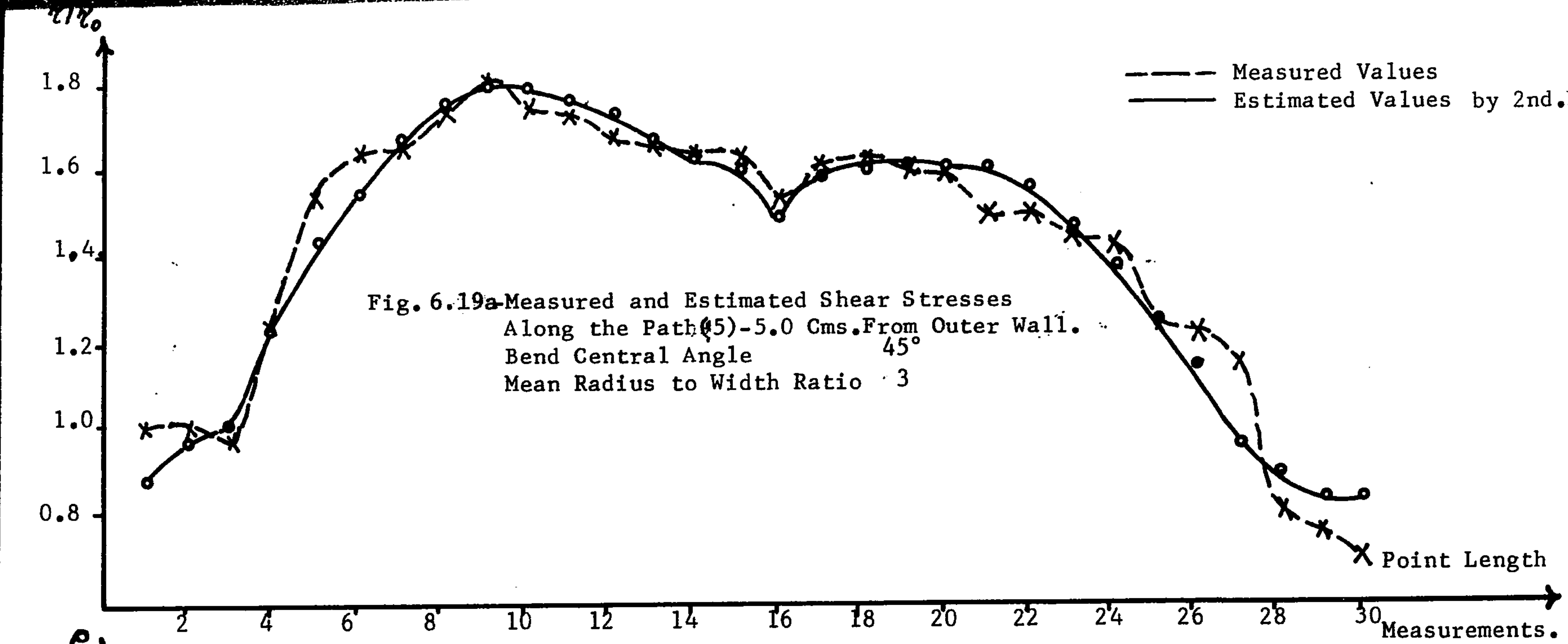

Fig. 6.19a-Measured and Estimated Shear Stresses
Along the Path(5)-5.0 Cms.From Outer Wall.
Bend Central Angle 45°
Mean Radius to Width Ratio 3

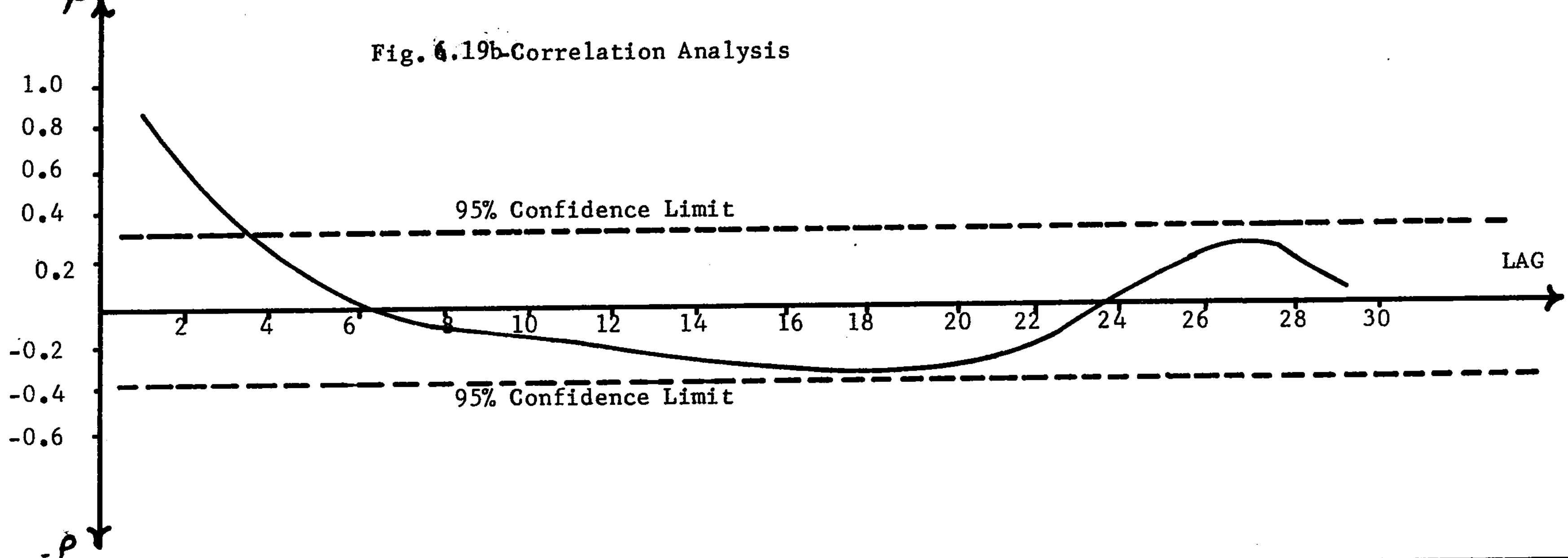

Fig. 6.19b-Correlation Analysis

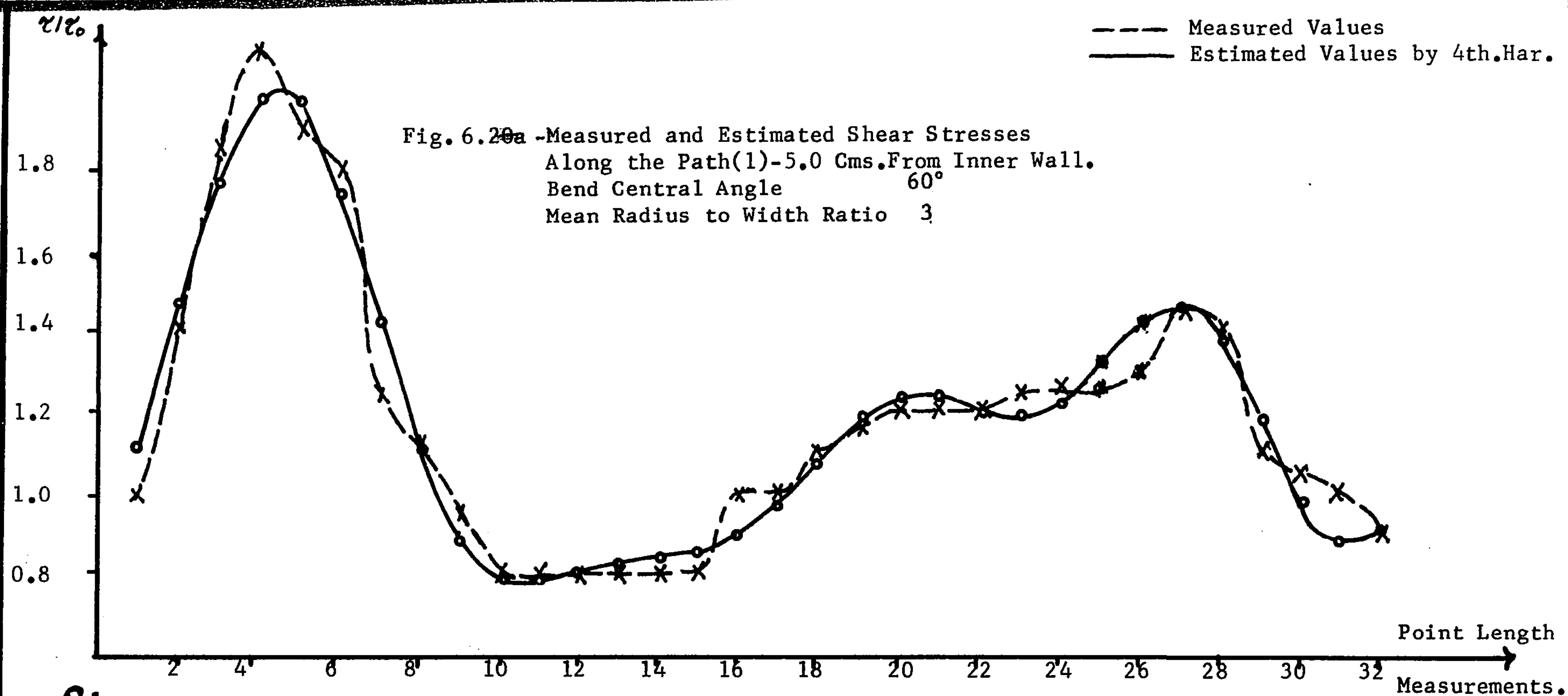

Fig. 6.20a -Measured and Estimated Shear Stresses Along the Path(1)-5.0 Cms.From Inner Wall. Bend Central Angle 60° Mean Radius to Width Ratio 3

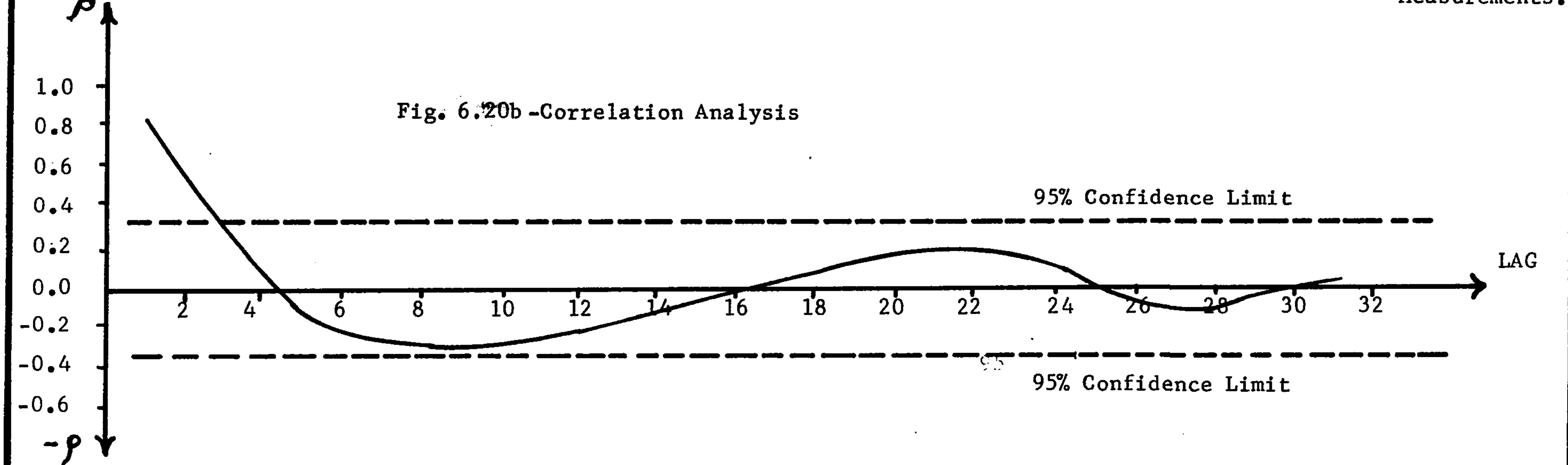

Fig. 6.20b -Correlation Analysis

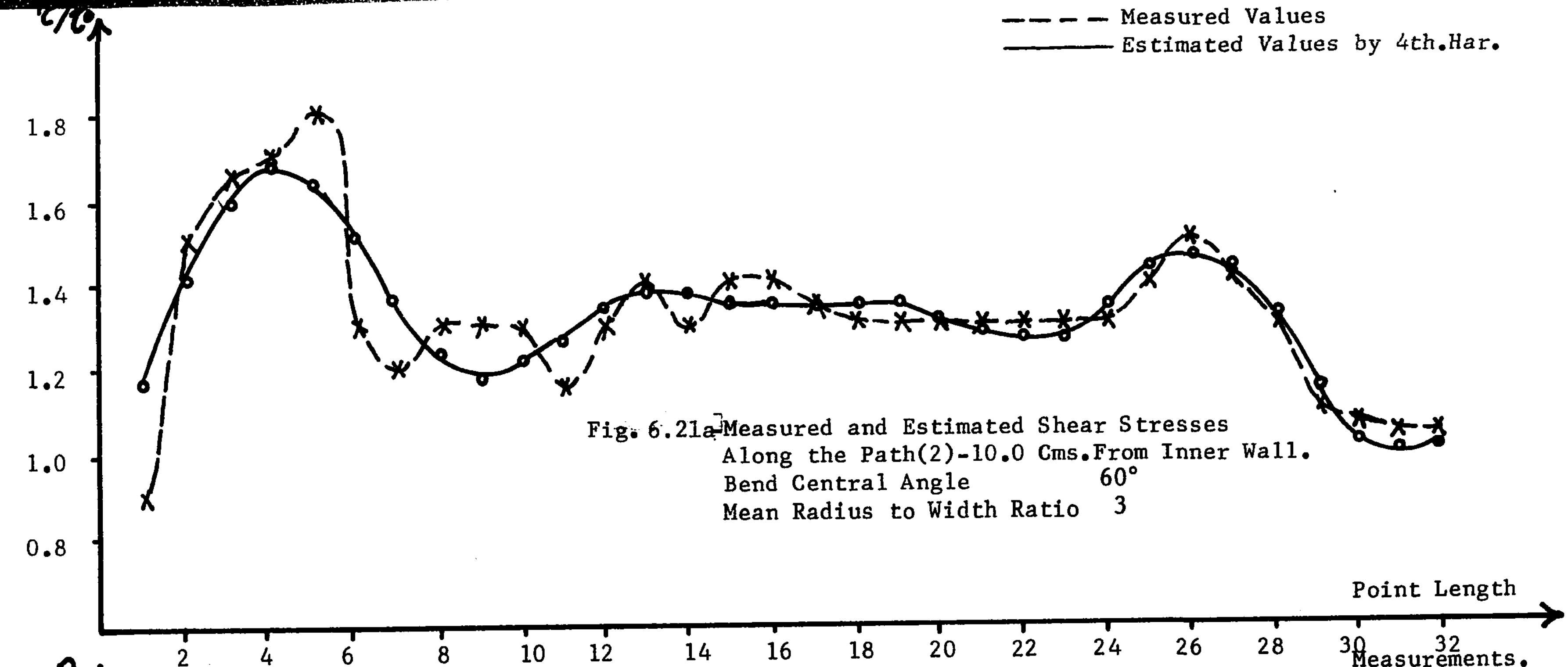

Fig. 6.21a-Measured and Estimated Shear Stresses
Along the Path(2)-10.0 Cms.From Inner Wall.
Bend Central Angle 60°
Mean Radius to Width Ratio 3

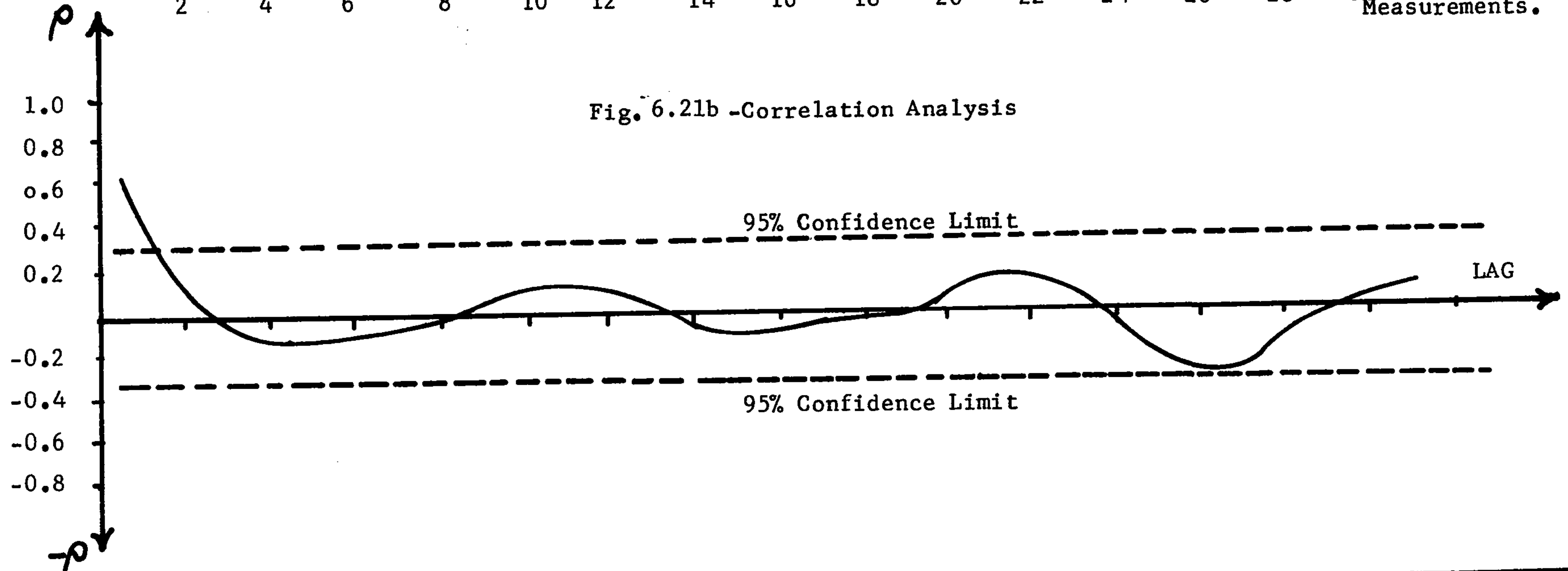

Fig. 6.21b -Correlation Analysis

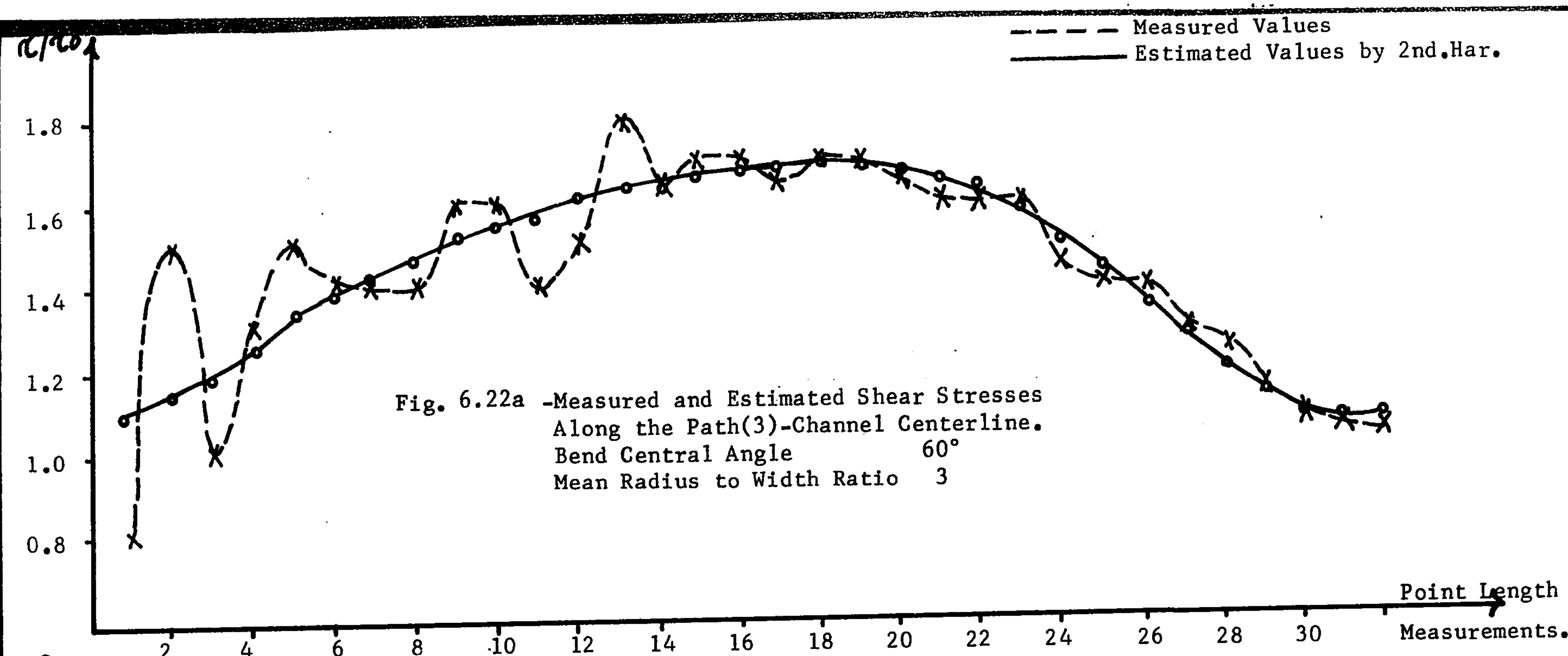

Fig. 6.22a -Measured and Estimated Shear Stresses
Along the Path(3)-Channel Centerline.
Bend Central Angle 60°
Mean Radius to Width Ratio 3

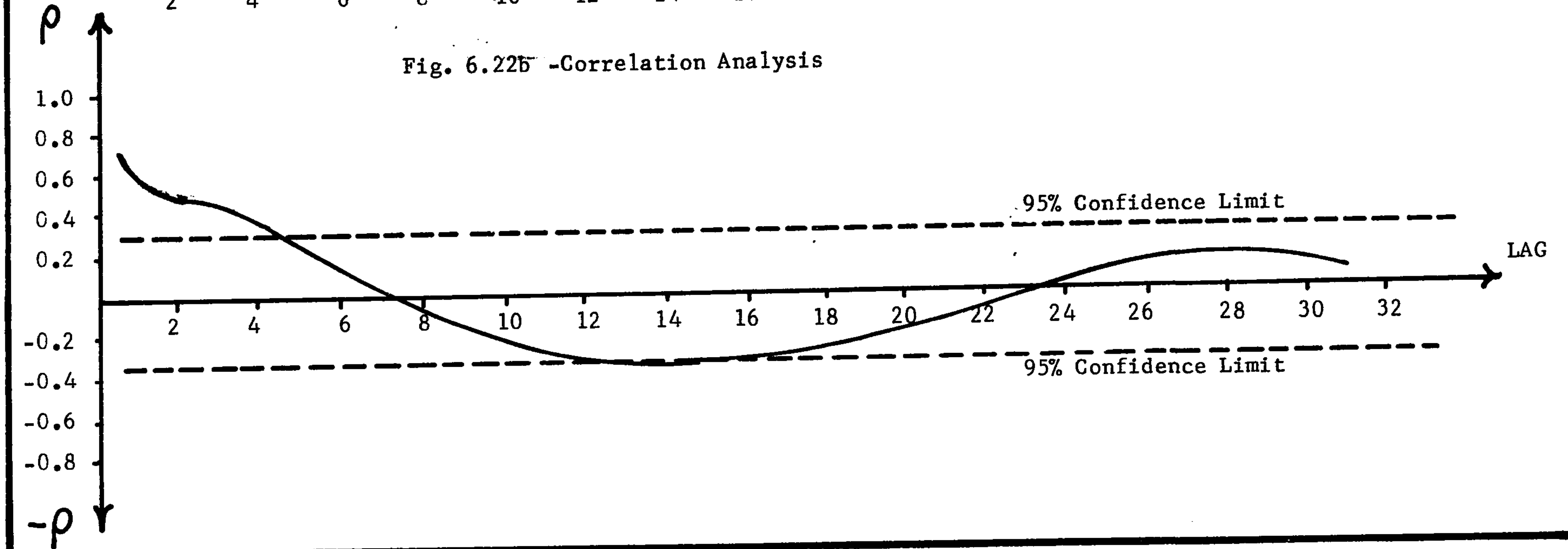

Fig. 6.22b -Correlation Analysis

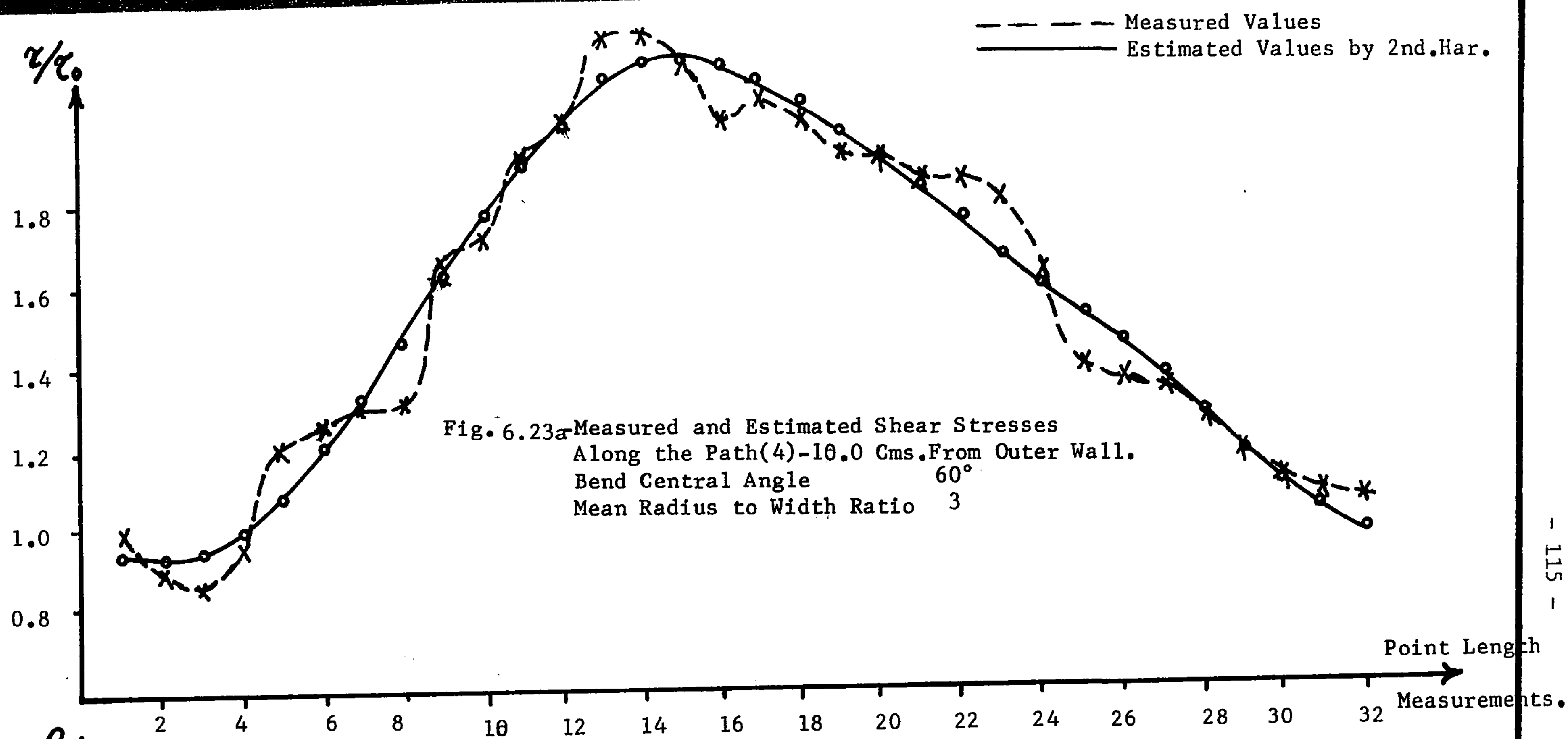

Fig. 6.23a-Measured and Estimated Shear Stresses Along the Path(4)-10.0 Cms.From Outer Wall.
Bend Central Angle 60°
Mean Radius to Width Ratio 3

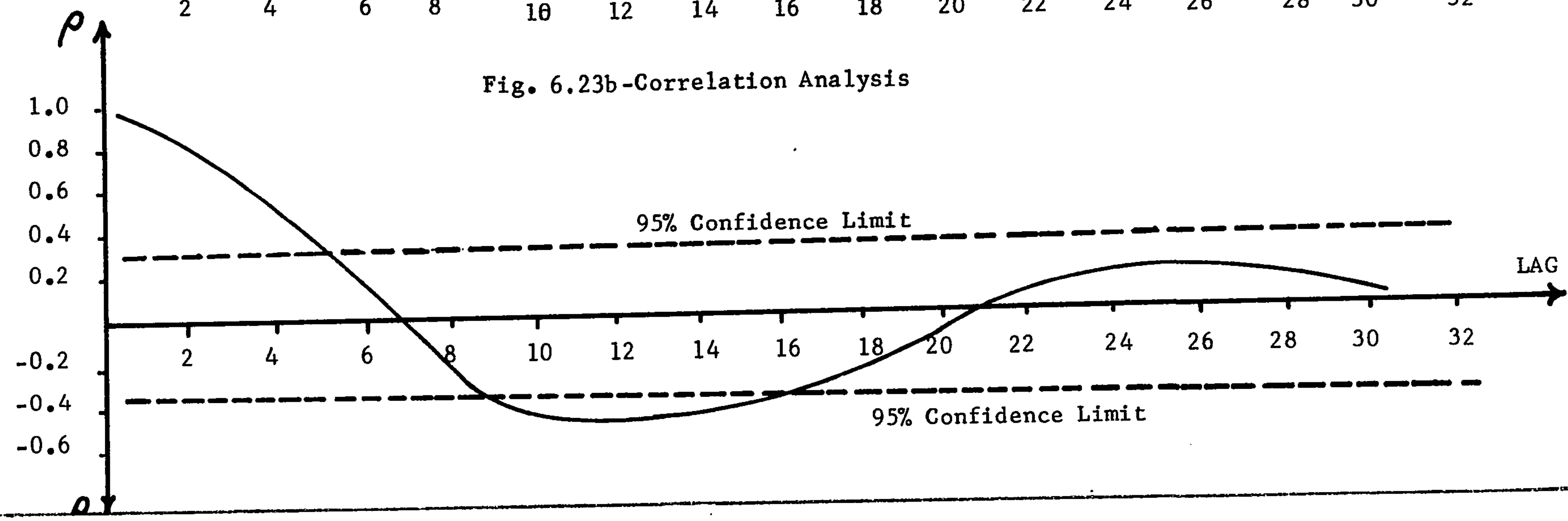

Fig. 6.23b-Correlation Analysis

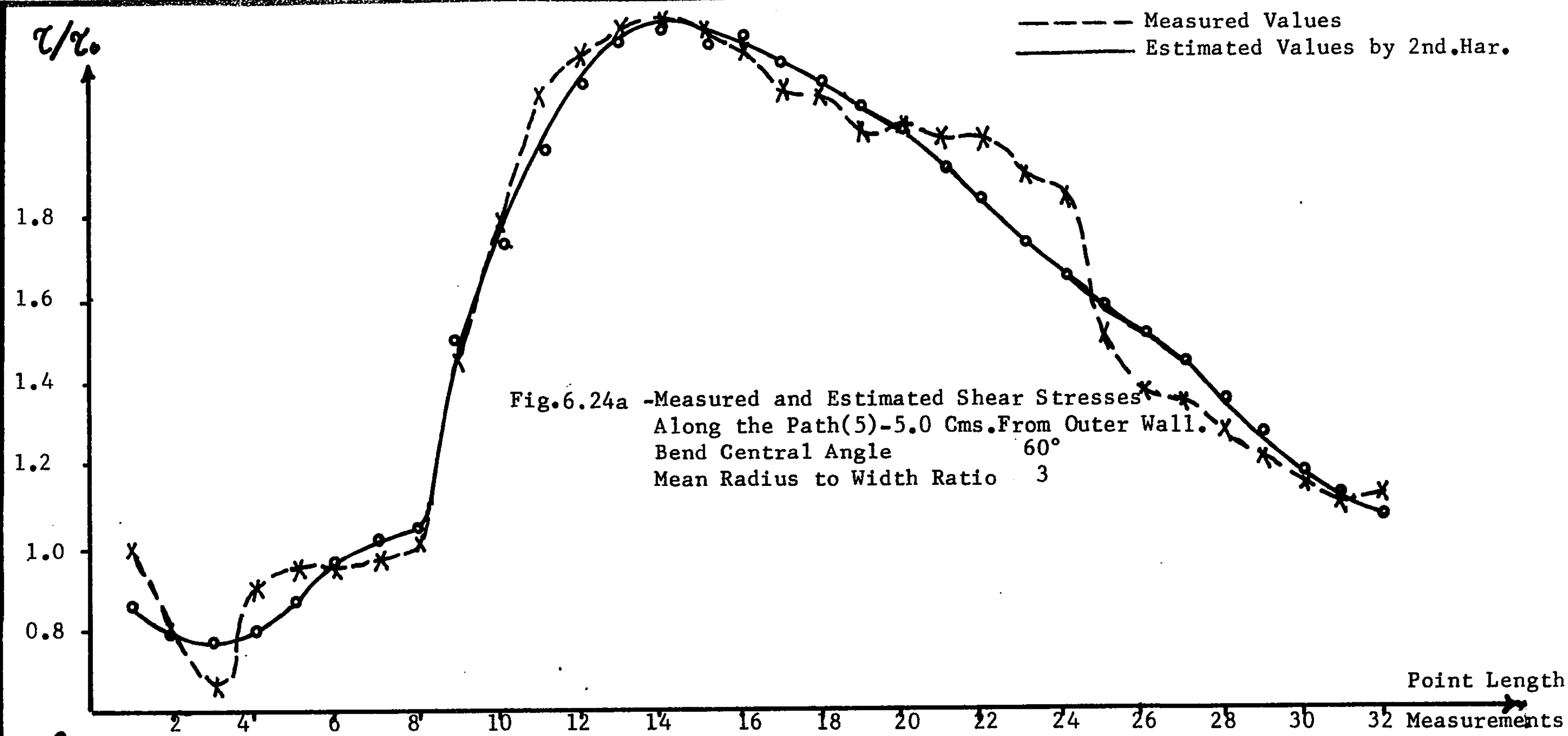

Fig.6.24a -Measured and Estimated Shear Stresses
Along the Path(5)-5.0 Cms.From Outer Wall.
Bend Central Angle 60°
Mean Radius to Width Ratio 3

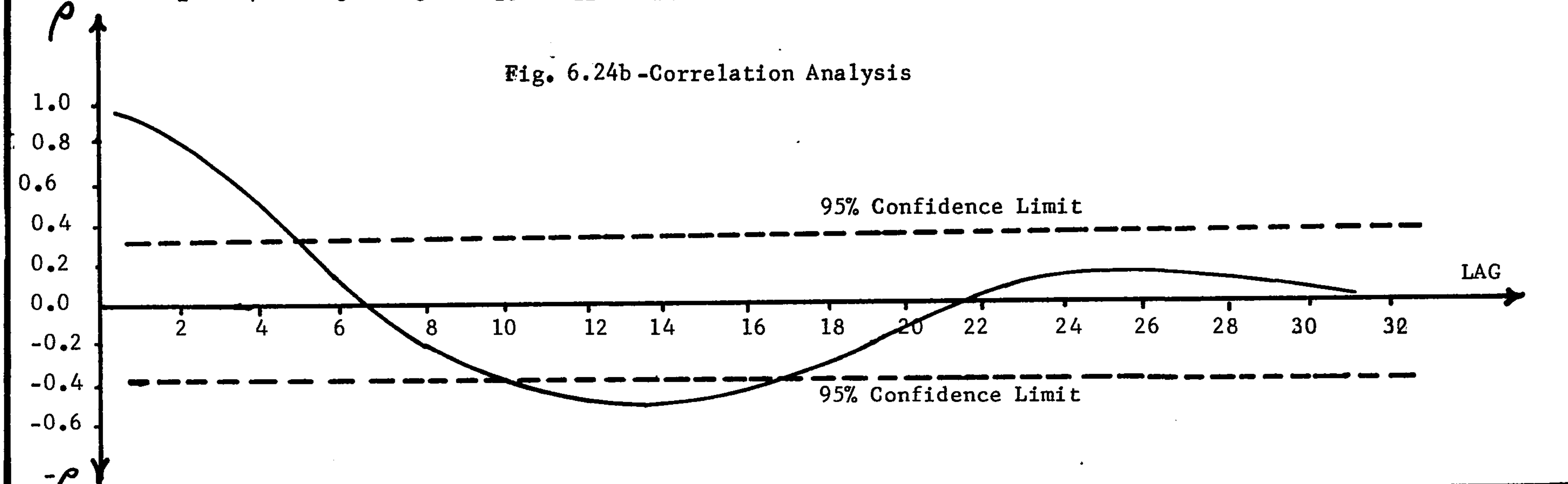

Fig. 6.24b -Correlation Analysis

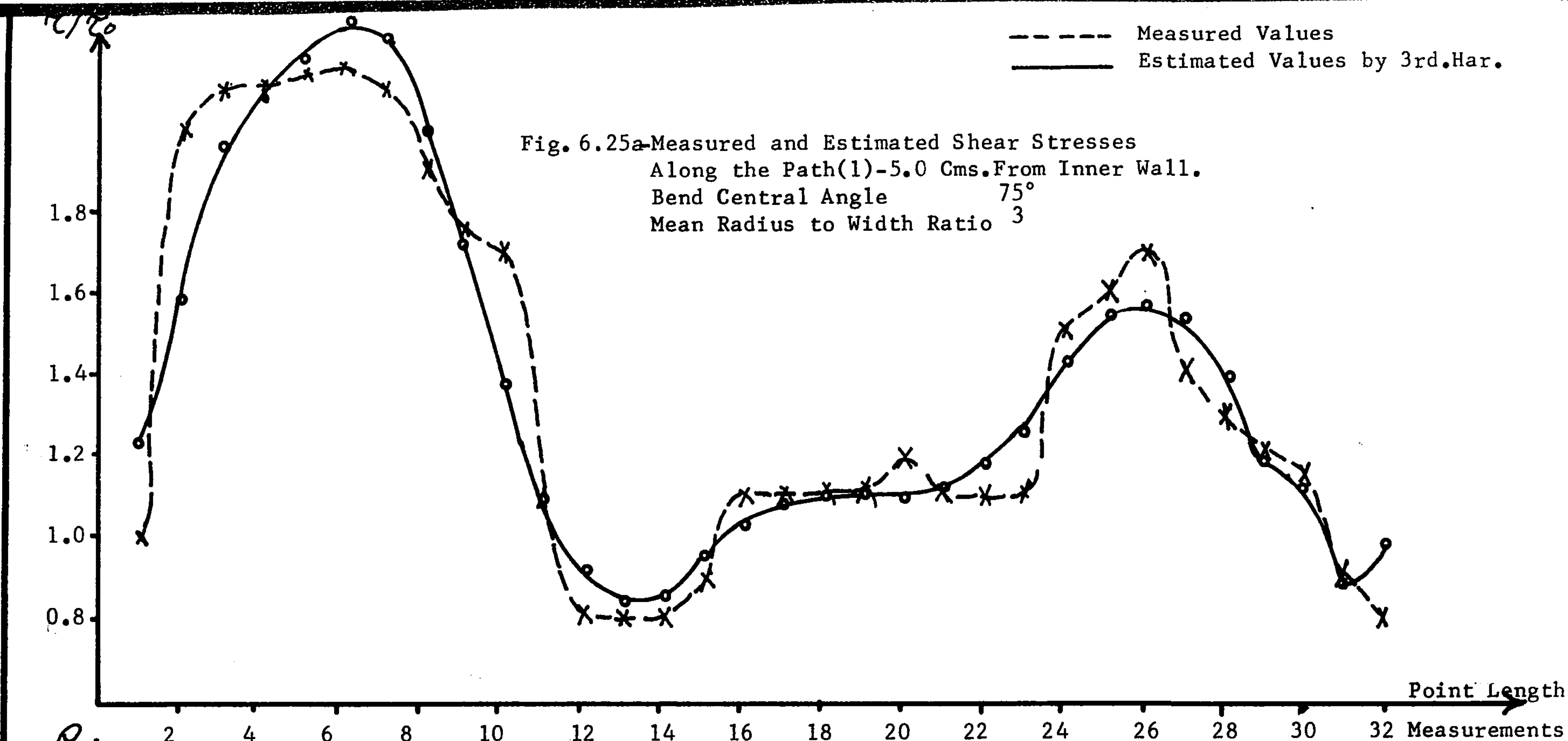

Fig. 6.25a-Measured and Estimated Shear Stresses
Along the Path(1)-5.0 Cms. From Inner Wall.
Bend Central Angle 75°
Mean Radius to Width Ratio 3

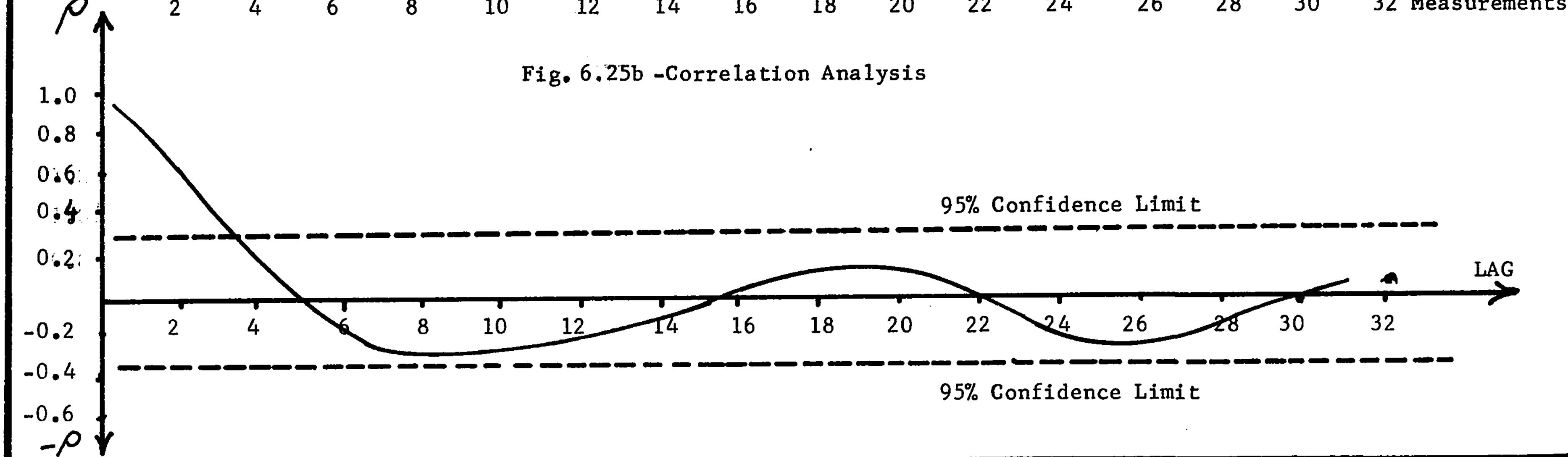

Fig. 6.25b -Correlation Analysis

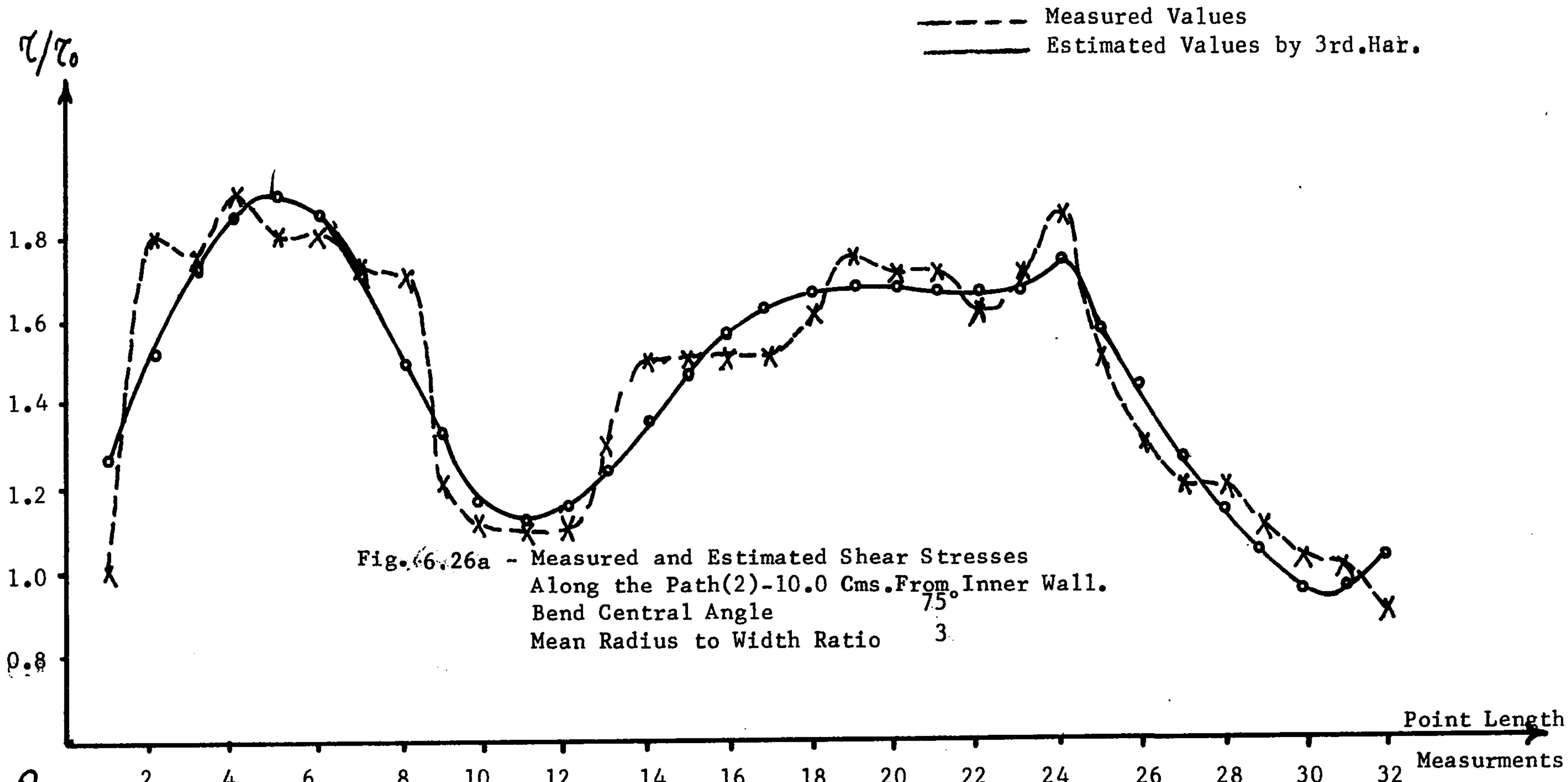

Fig. 6.26a - Measured and Estimated Shear Stresses
Along the Path(2)-10.0 Cms.From Inner Wall.
Bend Central Angle 75°
Mean Radius to Width Ratio 3

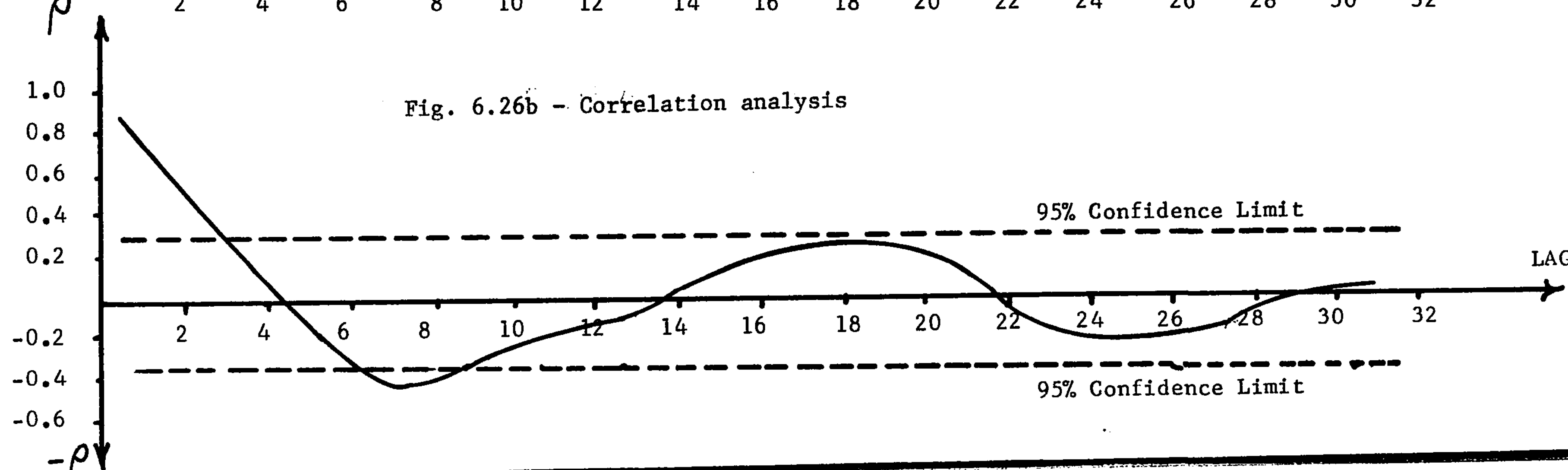

Fig. 6.26b - Correlation analysis

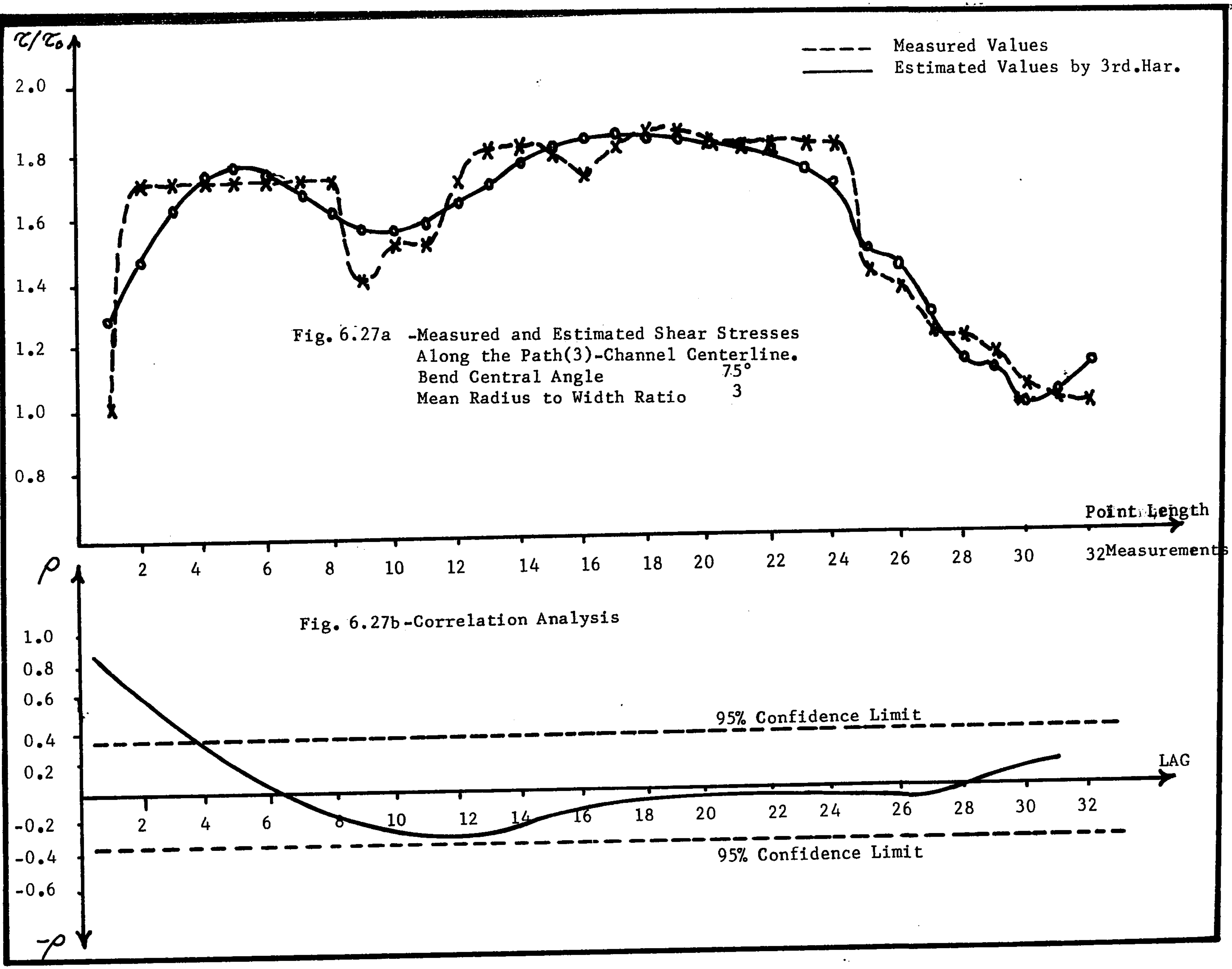

Fig. 6.27a -Measured and Estimated Shear Stresses Along the Path(3)-Channel Centerline.
Bend Central Angle 75°
Mean Radius to Width Ratio 3

Fig. 6.27b-Correlation Analysis

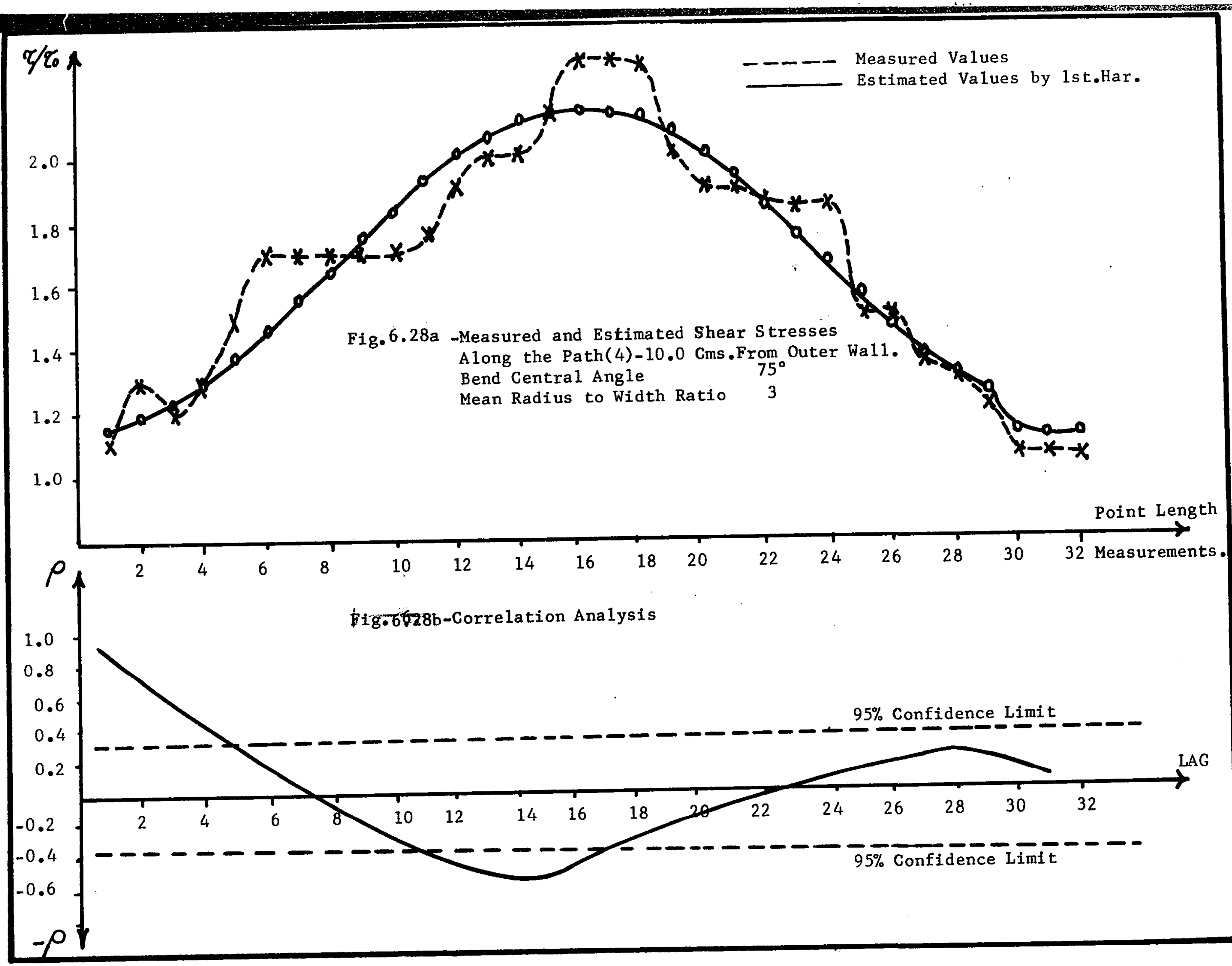

Fig. 6.28a -Measured and Estimated Shear Stresses
Along the Path(4)-10.0 Cms.From Outer Wall.
Bend Central Angle 75°
Mean Radius to Width Ratio 3

Fig. 6.28b-Correlation Analysis

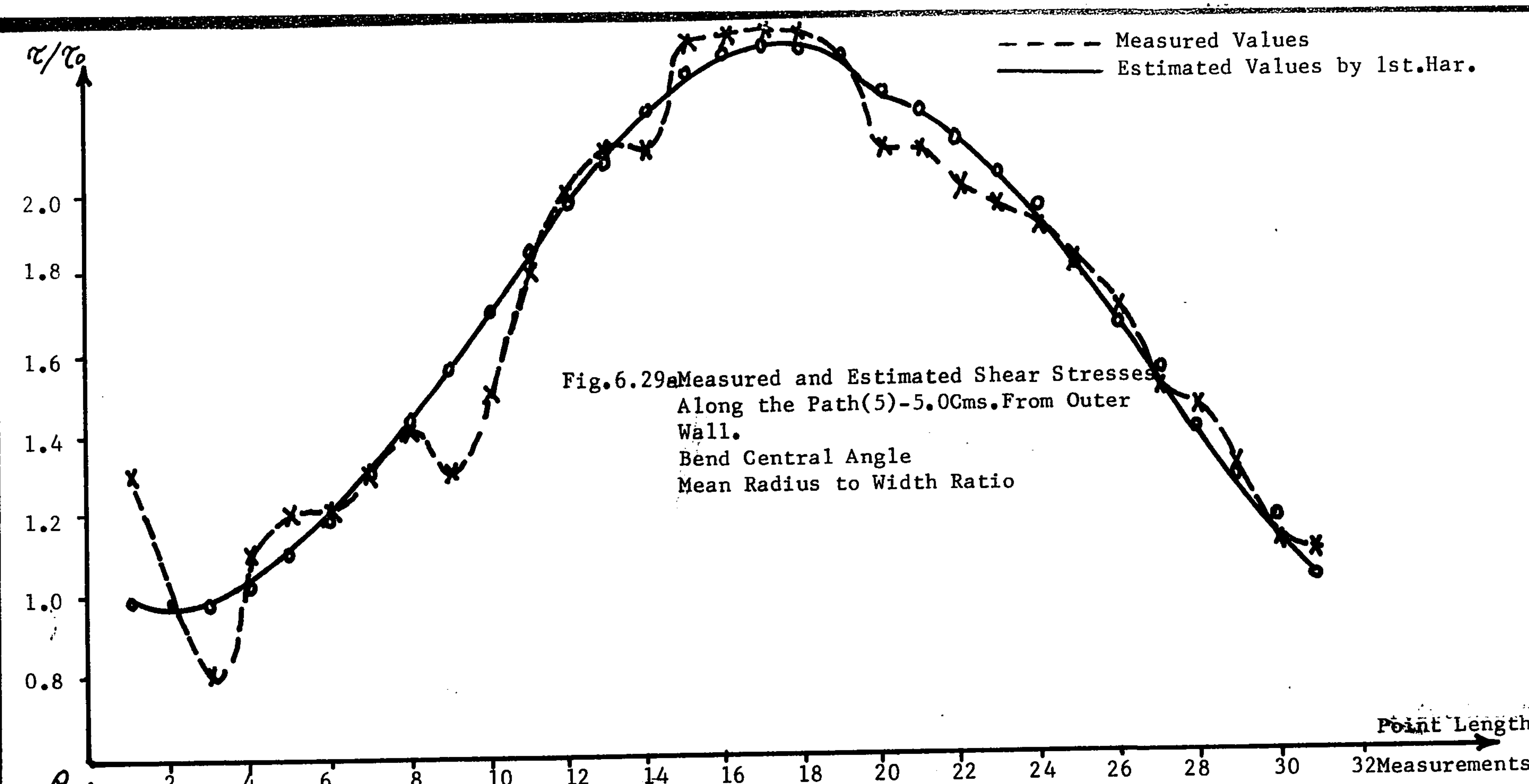

Fig.6.29aMeasured and Estimated Shear Stresses Along the Path(5)-5.0Cms.From Outer Wall.
Bend Central Angle
Mean Radius to Width Ratio

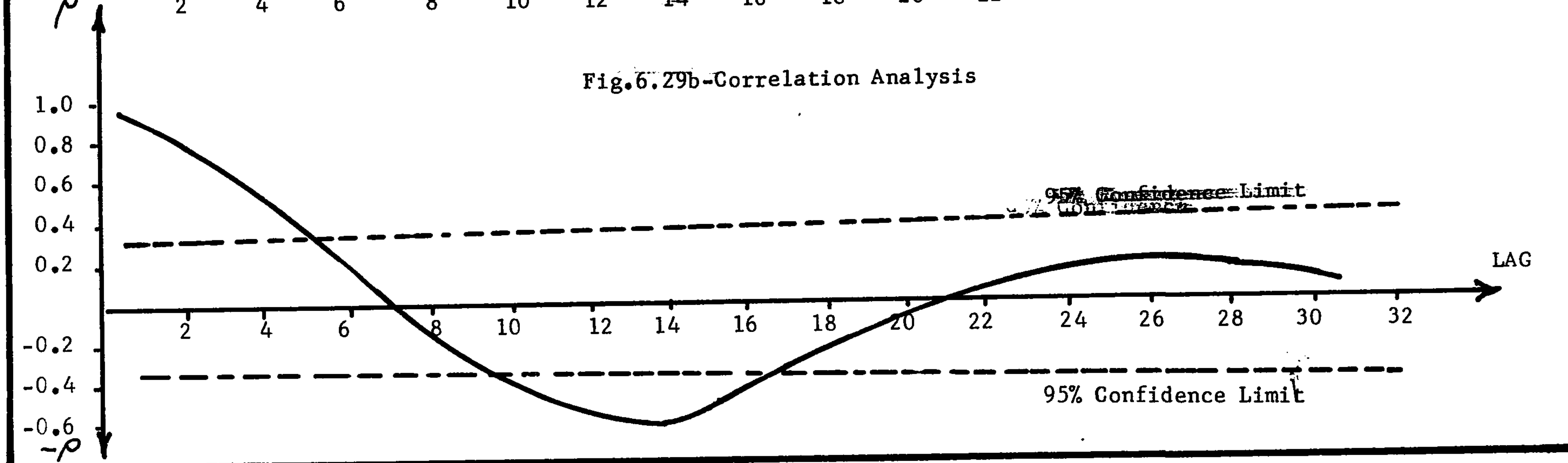

Fig.6.29b-Correlation Analysis

for different numbers of harmonics it was clear that the selected number of harmonics, (i.e., 4 for that particular path line), was valid.

A correlation analysis, with a confidence limit of 95% for path line no. 1, is presented in Fig. C.2.4. Similar analyses for all path lines are shown in Figs. 6.15b to 6.29b. It is clear, from these data, that the correlation of dimensionless bed shear stress values is significant only at small length lags. This, in turn, reflects thedependence of each bed shear stress value on its "neighbourhood" values of bed shear stress.

The spectrum and smoothed spectrum for path line no. 1 were calculated and are shown in Fig. 6.30. A peak value at the third harmonic in the periodogram is observed. Furthermore, a decreasing trend in the rate of explained variance (as the number of harmonics increases) reflects the fact that observations along this particular path line have a periodic structure. Moreover a study of the spectrum within the 95% confidence limit indicated that an increase in the number of harmonics, over four, is not warranted for the purpose of series analysis (Fig. 6.30). This spectral analysis was based on the assumption that the red noise Markov spectrum could be used as an appropriate null continuum; this is because the hypothesis: that the population correlation coefficient ρ_1 is as small as zero, was tested and rejected using Fisher's method and performing z-transformation (at a 0.05 level of significance and using a one-tailed test of the normal distribution). Based on the spectral analysis the choice of 4 as the harmonic number

Fig. 6.30- Spectral Analysis

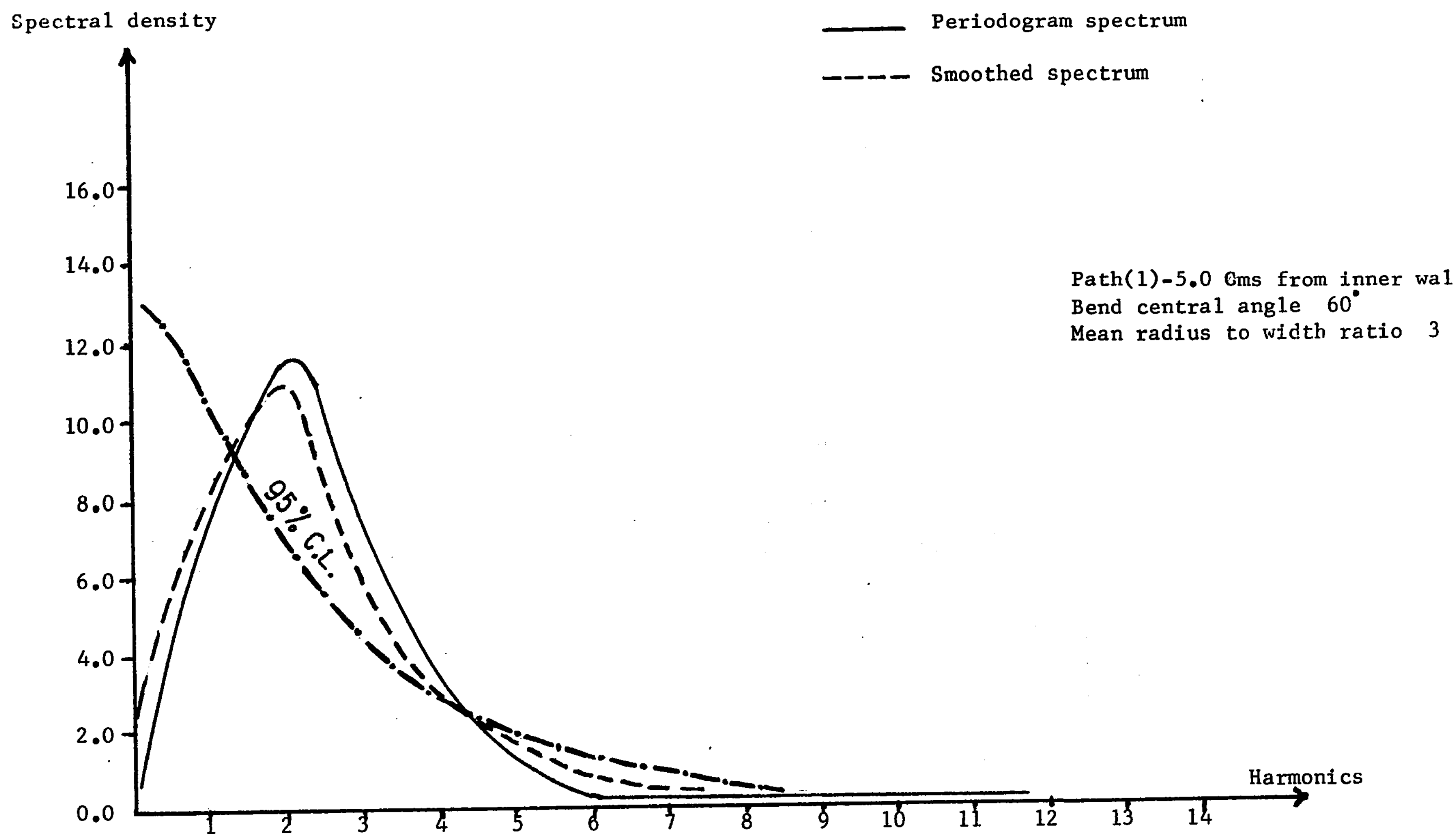

strongly supports the use of the selected number which was obtained from the analysis of variance table (Fig. C.2.2).

6.5.2 Autoregressive Models

Another type of numerical model investigated was the Autoregressive model. The order of the model, that best fitted observations along path line no. 1, was determined from a study of the partial autocorrelation function, Fig. 6.31. The second-order autoregressive model was found to be the more appropriate model for this particular study.

The complex roots of the characteristics equation, if the second-order autoregressive model is adopted, reflect the following facts:

(i) the second order (AR(2)) model displays pseudo periodic behaviour;

(ii) this behaviour is reflected in the autocorrelation function (the autocorrelation function then is damped sine wave with $0 \leq$ phase ≤ 90); and

(iii) this condition means that the autocorrelation starts by being positive for a few length lags and then is damped in a typical sine wave profile (Fig. C.2.7).

The spectrums of AR(1) and AR(2) were analyzed. It was noted that the spectrum damps out more or less exponentially if the AR(1) model is used. However, it shows a large proportion of the series variance (accounted for by the frequencies) in the neighbourhood of the most significant frequency, in the series analysis, if the AR(2) model is used.

FIG. 6.31 — AR Order Estimation

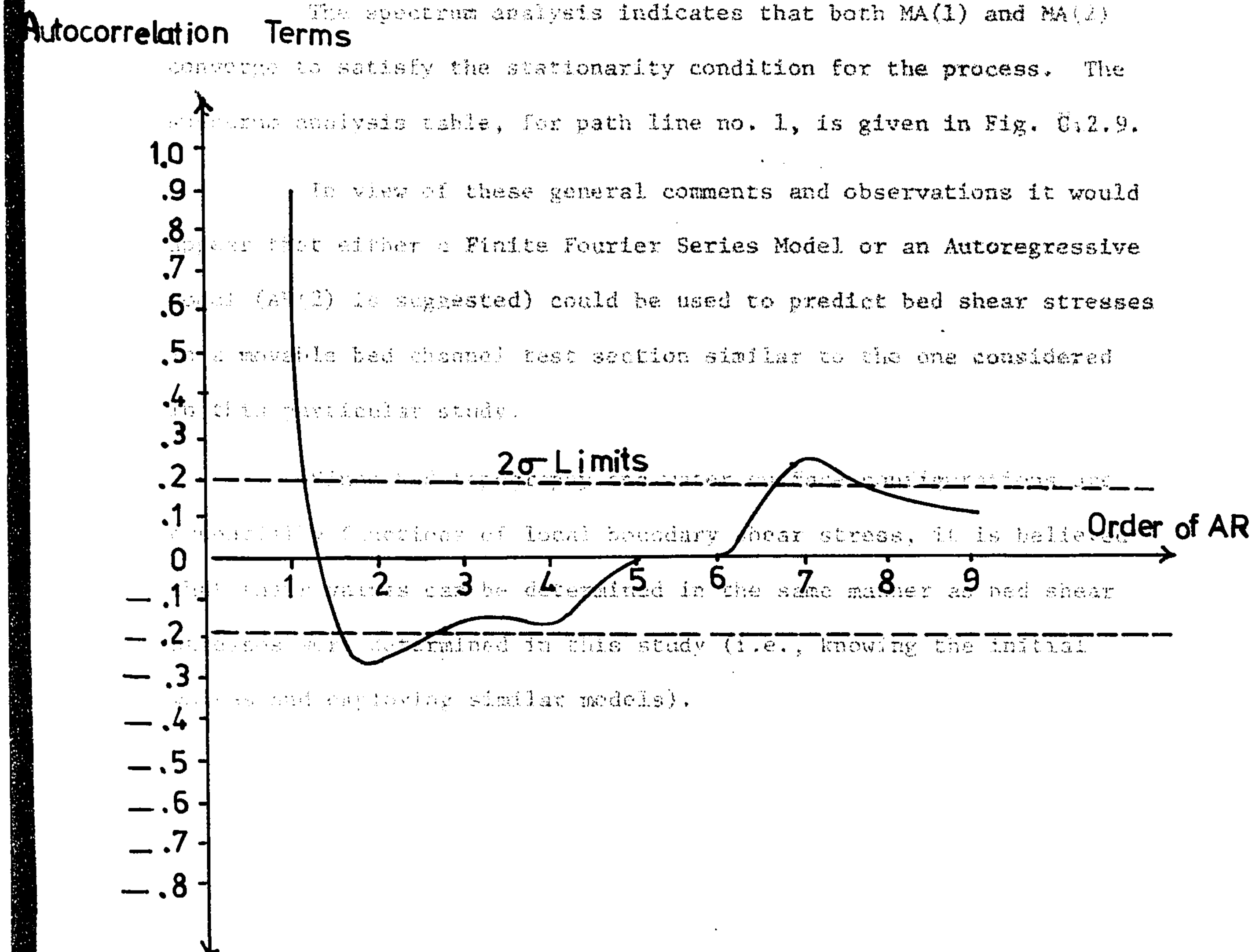

6.5.3 Moving Average Models

First and second order moving average models were used to predict dimensionless shear stress at any point on any path parallel to the channel system centerline. The parameters of these models were estimated from the observations, and the results, for path line no. 1, are given by Fig. 6.13a.

The spectrum analysis indicates that both MA(1) and MA(2) converge to satisfy the stationarity condition for the process. The spectrum analysis table, for path line no. 1, is given in Fig. 6.2.9.

In view of these general comments and observations it would appear that either a Finite Fourier Series Model or an Autoregressive model (AR(2) is suggested) could be used to predict bed shear stresses in a movable bed channel test section similar to the one considered in this particular study.

Since bed topography and water surface configurations are essentially functions of local boundary shear stress, it is believed that their values can be determined in the same manner as bed shear stresses were determined in this study (i.e., knowing the initial values and employing similar models).

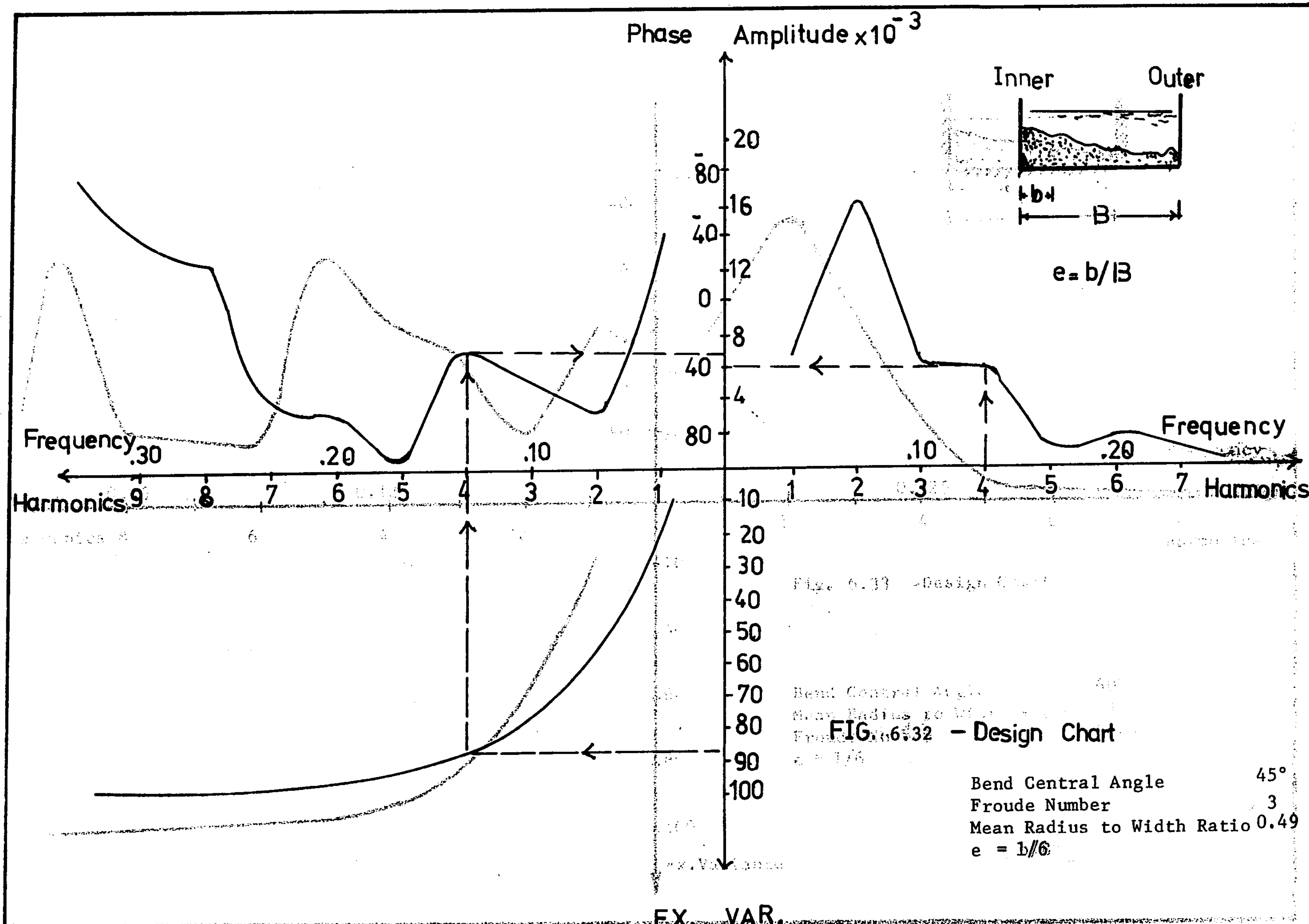

FIG. 6.32 – Design Chart

Bend Central Angle 45°
Froude Number 3
Mean Radius to Width Ratio 0.49
e = b/6

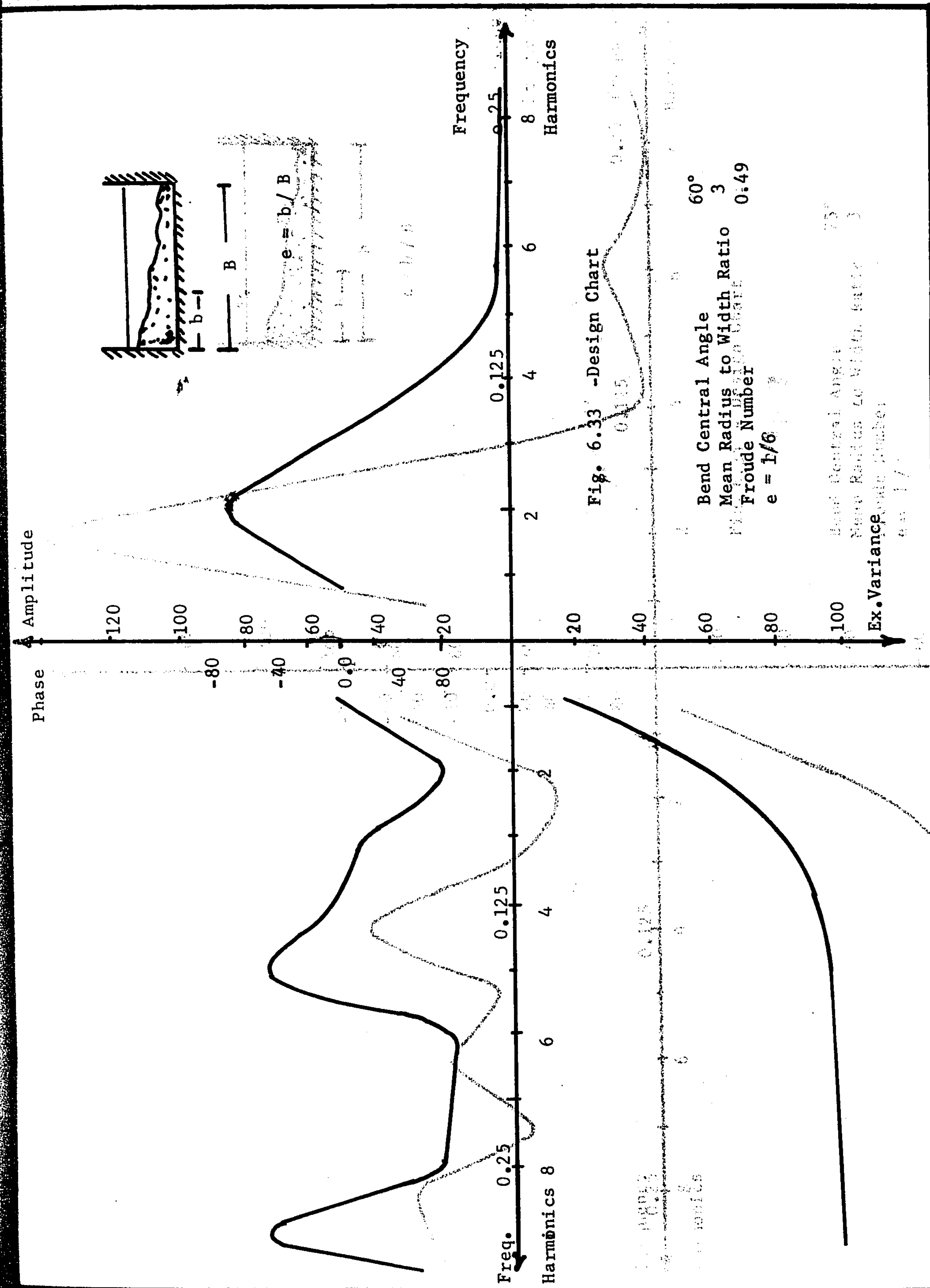

Fig. 6.33 -Design Chart

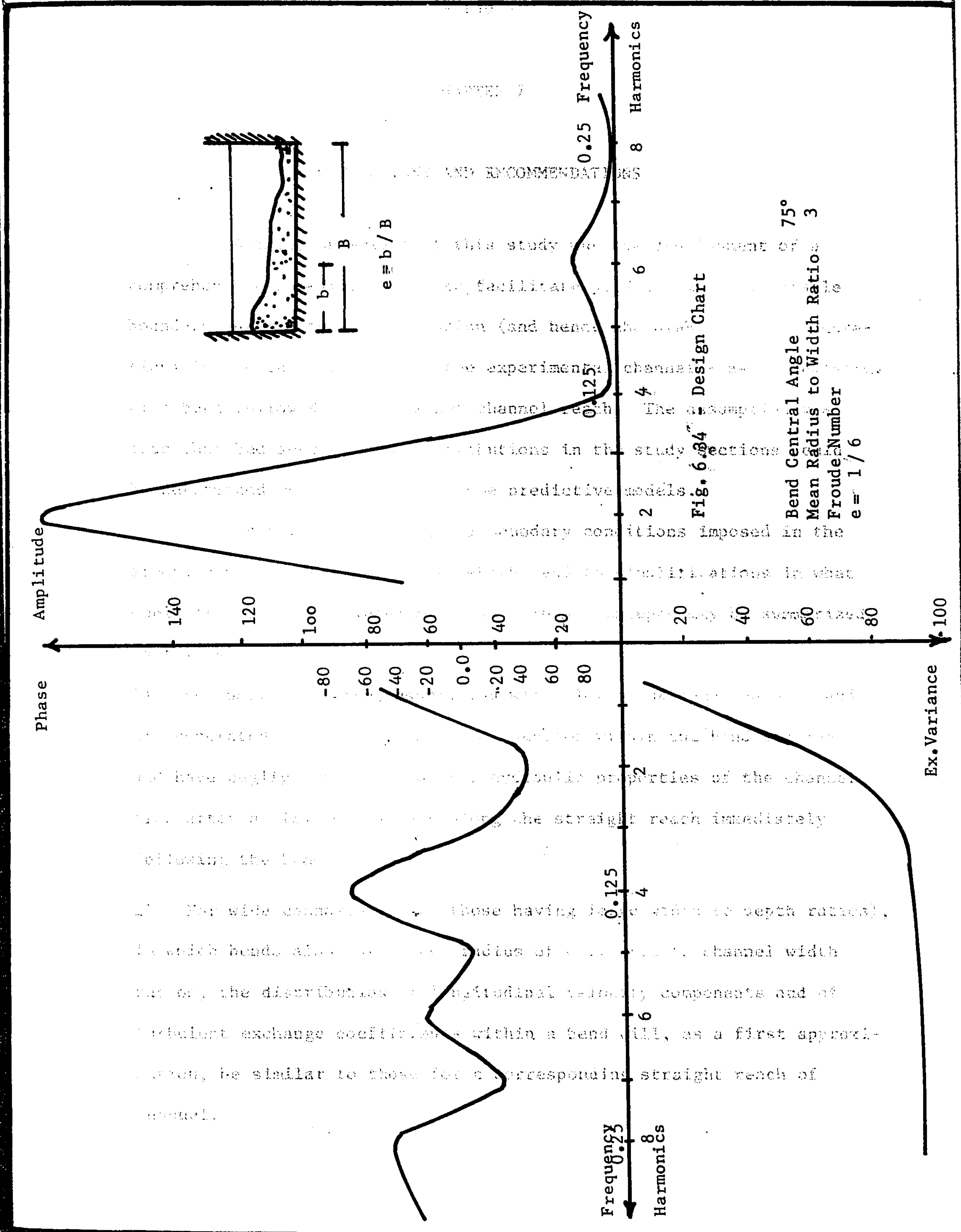

Fig. 6.34 Design Chart

Bend Central Angle 75°
Mean Radius to Width Ratio 3
Froude Number
e = 1/6

CHAPTER 7

CONCLUSIONS AND RECOMMENDATIONS

A major objective of this study was the development of a comprehensive numerical model to facilitate prediction of the stable boundary shear stress distribution (and hence the stable bed configuration) in the test sections of the experimental channel - each consisting of a bend followed by a straight channel reach. The assumption was made that bed shear stress distributions in the study sections could be determined using stochastic-type predictive models.

In view of the limiting boundary conditions imposed in the study, concepts were introduced which lead to simplifications in what would otherwise be complex analyses. These concepts may be summarized as follows:

1) Secondary currents, associated with flow in an open channel bend, are generated at entry to the bend, develop within the bend section and have negligible effect on the hydraulic properties of the channel flow after a limited distance along the straight reach immediately following the bend.

2) For wide channels (i.e., those having large width to depth ratios), in which bends also have large radius of curvature to channel width ratios, the distribution of longitudinal velocity components and of turbulent exchange coefficients within a bend will, as a first approximation, be similar to those for a corresponding straight reach of channel.

With regard to the experimental programme the selection of the measuring techniques employed in the tests was governed by a desire to minimize, where possible, experimental error in the observations. Accordingly, in view of the remote-sensing concept associated with the Laser Doppler Anemometry system, this instrumentation was adopted for point velocity measurements in the flow field. Moreover, the methodology used to determine bed shear stress distribution in the study sections took into account change in the value of von Karman's coefficient (K) with location in the cross section.

The following are the main conclusions drawn from a review (and comparison) of results obtained in the numerical and experimental studies:

1) For the stable-bed condition considered in this study of bed shear stress distribution in an open channel bend, the zone of maximum shear stress occurs near the outer wall of the bend and towards the downstream end of the bend. Moreover the maximum value increases, and its location tends to move downstream, as the length of the bend section increases. This trend might be explained by a similar tendency of the zone of flow separation (at the inner wall of the bend) to move downstream with increasing bend length - thereby causing the zone of accelerated flow to move downstream also.

2) At the bend exit section the longitudinal velocities tend to increase in proportion to the radii of curvature. This tendency increases as the length of the curve increases in a zone where the flow is essentially fully developed.

3) A basic assumption: that bend secondary currents are effective over a length of channel bounded by the bend entrance section (upstream limit) and a section in straight reach following the bend where residual circulation amounts to approximately 10% of the original intensity (downstream limit): appeared a valid concept for all practical purposes. This was supported by the observed (essentially uniform) bed topography and absence of superelevation of the water surface above and below these limiting sections.

4) Within this zone of influence (as defined in 3, above) the analyses performed, using linear autoregressive and moving average models, indicated that change in bed shear stress, along any path parallel to the channel system centerline, could be considered as stationary.

5) The mean value of dimensionless bed shear stress, along any path line, increases linearly as the radius of curvature increases, Fig. 6.14.

6) Of the various models considered, the stress distribution prediction obtained using the second order autoregressive model gave the best overall results. The roots of the characteristic's equation were found to be either complex or real - which indicated that, along any path, the change in boundary shear stress is periodic with an autocorrelation function of damped sine wave (in the case of the former) and damped exponential wave (in the case of the latter).

7) Bed shear stress distribution in the system can be predicted, with reasonable accuracy, using a finite Fourier series (stationary stochastic) model.

8) For design purposes a minimum number of harmonics is suggested, Fig. 6.13, to provide an acceptable explained variance in the analysis. Design charts, such as that presented in Figs. 6.32 and 6.33, could be prepared to supply the constants in the Fourier analysis for any required accuracy in the prediction exercise.

9) The minimum number of harmonics required depends on the point location in the system (where shear stress is to be determined) as well as on channel geometry. For example, the number increases as the point approaches the inside wall of the bend and as the bend angle decreases. This may be explained by the large-scale flow pattern in the bend section; namely that the main stream separates from the inner wall (at entrance to the bend), is forced towards the outer wall by centrifugal action and is then reflected back across the channel towards the inner wall downstream of the bend before the decay process is accomplished. As a result bed shear stress, being a function of local velocity in the flow field, is subject at the inner bank to a decaying wave of frequency larger than the frequency of the decaying wave at the outer bank of the bend section.

10) For stable open channel systems, that contain bends which approach the geometry of the test sections considered in this study, the general distribution of bed shear stress (and related bed topography) in the bends can be predicted, with reasonable accuracy, as follows:

(a) Determine the effective bend angle and define the location of the data points (selected grid pattern) in the study section; (i.e., the distance from the inner bank to a point, (b), and the distance from the bend entrance section to the point, (L)).

(b) From the relevant field data (channel and flow characteristics) determine the overall length (T), (Eq. (3.1.1.39)), of each of the longitudinal path lines contained in the grid which, taken together, define the effective zone of influence of the secondary currents in the system.

(c) Divide the path lengths into a number of subdivisions, ND, so that the mean subdivision length N along a path is given by: N = T/ND and count the number of subdivisions (N_e) up to the point in question, i.e.,

$$N_e = L/N$$

(d) Determine the transverse width parameter (B_d) for the point, where

$$B_d = b/B \; ; \quad (B = \text{channel width})$$

(e) Calculate the dimensionless bed shear stress value from Fig. 6.14.

(f) Employ a design chart (e.g., Fig. 6.32) to determine the recommended number of harmonics to use, (to achieve the desired accuracy), as well as the phase and amplitude of each harmonic.

(g) Use Equation (3.2.3.2) to predict the dimensionless bed shear stress value at the point in question (i.e., relative to the uniform bed shear stress value for an infinitely wide channel condition).

Recommendations for Future Research

The present study was limited to an investigation of the effects of secondary currents, generated in a single channel bend, on the stable bed shear stress distribution (and related bed topography) in the vicinity of same.

A single bend configuration was adopted to isolate the flow, entering and leaving the test sections, from residual bend secondary flow mechanisms that would otherwise exist if the test sections were to include two or more bends. While this arrangement obviously simplified the problem, from both an analytical and experimental viewpoint, it also limits, to some extent, the applicability of the predictive model to field situations where conditions approach those examined in the study.

Therefore, in view of the meandering nature of most alluvial river channels, it is recommended that this work be extended in the future to include the "multiple-bend" condition.

Another limitation imposed on the study was the stable bed condition examined. (It should be noted that this condition was, to a large extent, necessary since application of the Laser Doppler Anemometer System (point velocity measurement) is virtually restricted to "clear-water" flows). Accordingly it is further recommended that, for comparison purposes, future work in this area should examine the behaviour of such systems under dynamic conditions (i.e., sediment in motion).

BIBLIOGRAPHY

These are the writer's readings which helped, indirectly, to accomplish the study.

BIBLIOGRAPHY

1. Allen, J.R.L., "Asymmetrical ripple marks and the origin of water-laid closets of cross-strata", Liverpool and Manchester Geological Journal, Vol. 3, 1963.

2. Allen, J.R.L., "Current Ripples; their relation to patterns of water and sediment motion", North-Holland Publishing Co., Amsterdam, 1968.

3. Allen, J.R.L., "Physical processes of sedimentation", American Elsevier Publishing Company, Inc., New York,1970.

4. Akalank, K.J., "Accurate explicit equation for friction factor", Jour. of Hy. Div., ASCE, No. HY5, May 1976.

5. Ananian, A.K., "An approximate theory of secondary flows at the bend of the river course", Proc.12th Congress of Inter. Assoc. for Hy. Res., Sept. 1967.

6. Asher, J.R. and Chow, V.T., "Tractive force distribution in open channels", Jour. of Hy. Div., ASCE, No. HY2, March 1966.

7. Baum, K.L. and Harvey, E.J., "Stochastic analysis of dune bed profiles", Jour. of Hy. Div., ASCE, No. HY7, July 1974.

8. Bogardi, J., "Sediment transport in alluvial streams", Akademiai Kiado, Budapest, 1974.

9. Camp, T.R., "Civil Engineering classics", ASCE, 1973.

10. Chao, L.C. and McSparran, J.E., "Effect of secondary flow on sediment transport", Jour. of Hy. Div., ASCE, No. HY5, Sept. 1966.

11. Chi, E., "Resistance to flow in alluvial channels", Jour. of Hy. Div., ASCE, No. HY6, June 1975.

12. Chiu, C.L., "The role of secondary currents in hydraulics", Proc. 12th Congress of Inter. Assoc. for Hy. Res., Sept. 1967.

13. Ciray, C., "On secondary currents", Proc. 12th Congress of the Inter. Assoc. for Hy. Res., Sept. 1967.

14. Clark, W.J., "Flow measurements by square-edged orifice plate using corner tappings", Pergamon Press Ltd., 1965.

15. Colby, B.R., "Relationship of unmeasured sediment discharge to mean velocity", Trans. American Geophysical Union, Aug. 1957.

16. Durst, F. and Melling, A. and Whitelaw, J.H., "Principles and practice of laser-doppler anemometry", Academic Press Inc., London, England, 1976.

17. Einstein, H.A., Anderson, A.G. and Johnson, J.W., "A distinction between bed load and suspended load in natural stream", Trans. AGU, 1940.

18. Einstein, H.A., "Formulae for transportation of bed load", Trans. ASCE, Vol. 107, 1942.

19. Einstein, H.A. and El-Samni, "Hydrodynamic forces on a rough wall", Revies of Modern Physics, Vol. 21, No. 3, July 1949.

20. Einstein, H.A. and Banks, R.B., "Fluid resistance of composite roughness", Trans, AGU, Vol. 31, No. 4, Aug. 1950.

21. Einstein, H.A., "The bed-load function for sediment transportation in open channel flows", Tech. Bulletin No. 1026, U.S. Dept. of Agriculture, Soil Conservation Service, Washington, D.C., Sept. 1950.

22. Einstein, H.A. and Barbarossa, N.A., "River channel roughness", Trans. ASCE, Vol. 117, 1952.

23. Engelund, F., "Hydraulic resistance of alluvial streams", Jour. of Hy. Div., ASCE, No. HY2, March 1966.

24. Garde, R.J. and Ranga Raju, K.G., "Resistance relationships for alluvial channel flow", Jour. of Hy. Div., ASCE, No. HY4, July 1966.

25. Graf, W.H., "Hydraulics of sediment transport", McGraw-Hill Book Co., Inc., 1971.

26. Grunaer, D. and IPST Staff, "Handbook of hydraulic resistance", Published pursuant to an agreement with the U.S. Atomic Energy Commission and the National Science Foundation, Washington, D.C., 1966.

27. Gupta, R.D., "Total sediment transport as a parameter in the design of stable channels", Thesis presented to the University of Roorkee in partial fulfillment of the requirements for M.Eng., Roorkee, India, 1967.

28. "Handbook for Hydraulic Resistance", Translated from Russian by Israel Program for Scientific Translations, Jerusalem, 1966.

29. Harry, J.E., "Industrial lasers and their applications", McGraw-Hill Book Co. Ltd., 1974.

30. Hinze, J.O., "Turbulence", McGraw-Hill Book Co., New York, 1959.

31. "Hydraulic engineering and the environment", Proc. of the 21st Annual Hy. Div. Specialty Conference held at Montana State University, Bozeman, Montana, ASCE, 1973.

32. Kalinske, A.A., "Criteria for determining sand-transport by surface creep and saltation", Trans. AGU, 1942.

33. Kaminow, I.P., and Siegman, A.E., "Laser devices and applications", The Institute of Electrical and Electronics Engineers, Inc., New York, 1973.

34. Kennard, E.H., "Irrotational flow of frictionless fluids, mostly of invariable density", David Taylor Model Basin Report 2299, Washington, D.C., Feb. 1967.

35. Kenneth, C.W., "Bed load transport at high shear stress", Jour. of Hy. Div., ASCE, No. HY6, Nov. 1966.

36. Kenneth, V.H.S., "Alluvial channel resistance related to bed form", Jour. of Hy. Div., ASCE, No. HY1, Jan. 1968.

37. Lacey, G., "Stable channels in alluvium", Proc. Inst. of Civil Engrs, Vol. 229, London, England, 1929-1930.

38. Lebreton, J.C. and Nicollet, G., "Etude des courants secondaires induits par un panneau immerge et de leurs effects sur un fond mobil", Proc. 12th Congress of Inter. Assoc. for Hy. Res., Sept. 1967.

39. Liu, H.K. and Hwang, S.Y., "Discharge formulae for straight alluvial channels", Trans. ASCE, Vol. 226, 1961.

40. Lucas, A.H., "Secondary currents in the Newcastle Harbour Siltation investigation", Proc. 12th Congress of Inter. Assoc. for Hy. Res., Sept. 1967.

41. MacDougall, C.H., "Bed sediment transportation in open channels", Trans. AGU, 1934.

42. Micheal, A.S. and Simons, D.B., "Non-equilibrium river form", Jour. of Hy. Div., ASCE, No. HY5, May 1975.

43. Micheal, D.G., "Bed form response to nonsteady flows", Jour. of Hy. Div., ASCE, No. HY3, March 1975.

44. Moddock, T.J., "Equations for resistance to flow and sediment transport in alluvial channels", W.R.R., Vol. 12,No. 1, Feb. 1976.

45. Mohammed, S.M., "Flow in open channels with smooth curved boundaries", Jour. of Hy. Div., ASCE, Dec. 1973.

46. Morgan, J.P., "Deltaic sedimentation; modern and ancient", The Society of Economic Paleontologists and Mineralogists, Nov. 1970.

47. Mostafa, M.S. and Tinney, R., "Flow around 180° bends in open rectangular channels", Jour. of Hy. Div., ASCE, No. HY4, July 1968.

48. Myers, R.C. and Elsawy, E.M., "Boundary shear in channel with flood plain", Jour. of Hy. Div., ASCE, No. HY7, July 1975.

49. Öner, Y. and Graf, W.H., "Wall shear measurement in sand-water mixture flow", Jour. of Hy. Div., ASCE, No. HY7, July 1975.

50. Pettijohn, F.J., "Sedimentary rocks", Harper and Row Publishers, Inc. Third Edition, 1975.

51. Prus-chacinski, T.M., "Patterns of motion in open channel bends", Inter. Union of Geol. and Geophys., Rome, Italy, Sept. 1954, and Proc. Inst. of Water Engrs., London, England, Vol. 10, No. 5, Aug. 1958.

52. Raichlen, F. and Kennedy, J.F., "The growth of sediment bed forms from an initially flattened bed", Proc. 11th Congress of Inter. Assoc. for Hy. Res., Vol. 3, No. 37, Union of the Soviet Socialist Republic, Leningrad, 1965.

53. Rathbun, R.E. and Guy, H.P., "Effect of non-equilibrium flow conditions on sediment transport and bed roughness in a lab. alluvial channel", Proc. 12th Congress for Hy. Res., Sept. 1967.

54. Raudkivi, A.J., "Loose boundary hydraulics", Pergamon Press Ltd., London, 1967.

55. Roa, B.V. and Seetharamiah, K., "Development and role of secondary currents in alluvial streams", 12th Congress of Inter. Assoc. for Hy. Res., Sept. 1967.

56. Roger, L.H., "Shear stress and sediment distribution in a meander bend", University of Uppsala, Dept. of Physical Geography, Uppsala, Sweden, 1974.

57. Rouse, H., "Fluid mechanics for engineering hydraulics", Eng. Societies Monographs, McGraw-Hill Book Co. Inc., New York 1938.

58. Rouse, H., "Critical analysis of open channel resistance", Jour. of Hy. Div., ASCE, 1965.
Discussions: Proc., ASCE, Vol. 92, March 1966.

59. Ruh-ming, L. and Shen, H.W., "Solid particle settlement in open channel flow", Jour. of Hy. Div., ASCE, No. HY7, July 1975.

60. Salamon, E., "An investigation of fully developed turbulent flow in a curved channel", Thesis submitted to the Advisory Board of the School of Engrg of the Johns Hopkins University in conformity with the requirements for the Ph.D. Degree, Baltimore, Maryland, 1954.

61. Sam, S. and Hill, R.D., "Bed load formulas", Soil and Water Conservation Research Div., Agricultural Research Services, U.S. Dept. of Agriculture, Dec. 1968.

62. Schenck, H., "Theories of engineering experimentation", McGraw-Hill Book Co. Inc., 1961.

63. Schwarzacher, W., "Sedimentation models and quantitative stratigraphy", Elsevier Scientific Publishing Company, Inc., 1975.

64. Shen, H.W., "Development of bed roughness in alluvial channels", Jour. of Hy. Div., ASCE, Vol. 88, No. HY3, Proc. Paper 3113, May 1962.

65. Shen, H.W., and Komura, S., "Meandering tendencies in straight alluvial channels", Jour. of Hy. Div., ASCE, No. HY4, July 1968.

66. Shen, H.W., "River Mechanics - Vol. 1", W.R.P., Fort Collins, Colorado, U.S.A., 80521, 1971.

67. Shen, H.W., "River Mechanics - Vol. 2", W.R.P., Fort Collins, Colorado, U.S.A., 80521, 1971.

68. Shen, H.W., "River Mechanics - Vol. 3; Environmental impact on rivers", W.R.P., Fort Collins, Colorado, U.S.A. 80521, 1973.

69. Shen, H.W., "Sedimentation", Symposium to honor Professor H.A. Einstein, Fort Collions; Colorado, 1972.

70. Simons, D.B., Richardson, E.V. and Hausild, W.L., "Depth discharge relations in alluvial channels", Jour. of Hy. Div., ASCE, Vol. 88, No. HY5, Proc. Paper 3263, 1962.

71. Simons, D.B., Stevens, M.A. and Duke, J.H., "Predicting stages on sand bed rivers", Jour. of the Waterways, Harbors and Coastal Engineering, Div., ASCE, Vol. 99, No. WW2, Proc. Paper 9731, May 1973.

72. Simons, D.B. and Senturk, F., "Sediment transport technology", W.R.P., Fort Collins, Colorado, 1977.

73. Sobey, I.J., "Inviscid secondary motions in a tube of slowly varying ellipticity", Jour. of Fluid Mechanics, Vol. 73, Part 4, 1976.

74. Stoll, H.W., "Flow: its measurement and control in science and industry", Vol. 1, Part 1, Instrument Society of America, 1971.

75. Suga, K., "The stable profiles of the curved open channel beds", Proc. 12th Congress of Inter. Assoc. for Hy. Res., Sept. 1967.

76. Swift, D., Duane, D. and Pilkey, O.H., "Shelf sediment transport: process and pattern", Dowden, Hutchinson & Ross, Inc., 1972.

77. "Task Committee of Preparation of the Sedimentation Manual", Sediment transportation mechanics: H. Sediment discharge formulas", Jour. of Hy. Div., ASCE, Vol. 97, No. HY4, Proc. Paper 8076, April 1971.

78. Task Committee for the Preparation of the Manual on Sedimentation, "Sedimentation engineering", ASCE, 1975.

79. "The Accuracy of Flow Measurements by Laser Doppler Methods", Proc. of the LDA-Symposium, Copenhagen, 1975.

80. Thermosciences Division, Department of Mechanical Engineering, Stanford University, "Computation of turbulent boundary layers", Vol. 1 and 2, Proc. Afosr-IFP-Standord Conference, California, 1969.

81. Troskolanski, A.T., "Hydrometry-theory and practice of hydraulic measurements", Pergamon Press Ltd.; 1960.

82. Tsuchiya, A. and Ishizaki, K., "The mechanics of dune formation in erodible bed channels", Proc. 12th Congress of Inter. Assoc., for Hy. Res., Sept. 1967.

83. Yang, C.T., "Unit stream power and sediment transportation", Jour. of Hy. Div., ASCE, Vol. 98, No. HY10, Proc. Paper 9295, Oct. 1972.

84. Yang, C.T., "Incipient motion and sediment transport", Jour. of Hy. Div., ASCE, Vol. 99, No. HY10, Proc. Paper 10067, Oct. 1973.

85. Yang, C.T., "Applicability of unit stream power equation", Jour. of Hy. Div., ASCE, No. HY4, May 1976.

86. Yalin, M.S., "Theory of hydraulic models", Macmillan Press Ltd., 1971.

87. Yalin, M.S., "Mechanics of sediment transport", Pergamon Press Ltd., 1972.

88. Yasuo, O., Sublash, C.J., and Kennedy, J., "Effects of meandering on sediment discharges and friction factors of alluvial streams", Report No. 141, Iowa Inst. of Hy. Res., The University of Iowa, Iowa City, Iowa, Sept. 1972.

89. Yen, B.C., "Characteristics of subcritical flow in a meandering channel", Inst. of Hy. Res., University of Iowa, Iowa City, 1965.

90. Yen, B.C., "Some aspects of flow in meandering channels", Proc. 12th Congress of Inter. Assoc. for Hy. Res., Vol. 1, Sept. 1967.

91. Yen, C.H., "Determination of best proportions for canal bend", Thesis submitted in partial fulfillment of the requirements for the degree of Ph.D. in the Dept. of Mechanics and Hydraulics in the Graduate College of the State University of Iowa, Feb. 1941.

92. Yen, C.L., "Bed configuration and characteristics of subcritical flow in a meandering channel", Dissertation presented to the University of Iowa in partial fulfillment of the requirements for the Degree of Ph.D., Iowa City, 1967.

93. Yen, C.L., "Bed topography effect on flow in a meander", Jour. of Hy. Div., ASCE, Vol. 96, No. HY1, Jan. 1970.

94. Vannah, W.E. and Wayland, H., "Flow: its measurement and control in science and industry", Vol. 1, Part 3, Instrument Society of America, 1974.

95. "Water Resources Instrumentation; Vol. 1 - Measuring and sensing methods; Vol. 2 - Data acquisition and analysis", Proc. of the Inter. Seminar and Exposition on Water Resources Instrumentation, Chicago, Illinois, 1975.

96. Wendt, R.E., "Flow: its measurement and control in science and industry", Vol. 1, Part 2, Instrument Society of America, 1974.

REFERENCES

1. Adamowski, K. and Smith, A.F., "Stochastic generation of rainfall", Jour. of Hy. Div., ASCE, No. HY11, Nov. 1972.

2. Ananyan, A.K., "Transverse circulation in bend of turbulent stream", Doctor's Dissertation and Lecture, Erevan, 1952.

3. Ananyan, A.K., "An approximate theory of secondary flows at the bend of the river course", Proc. 12th Congress of Inter. Assoc., for Hy. Res., Sept. 1967.

4. Bazin, H., "Recherches experimentales sur l'ecoulemont de l'eau dans les canaux decouverts", Memoires Presentes par Divers Savants a l'Academic de Sciences, Paris, Vol. 19, 152 (with separate atlas containing 33 plates), 1865.

5. Blue et al., "Flow around a river bend investigated", Civil Engineering, Vol. 4, p.258, 1934.

6. Boussinesq, J., "Essai sur la theoric des eaux courants", Memoires Presentes par Divers Savants a l'Academic des Sciences, Paris, Vol. 23, Ser. 2, No. 1, Supplement 24, 1877.

7. Box, G.E. and Jenkins, G.M., "Time series analysis-forecasting and control", Holden Day, Inc., 1970.

8. Callander, R.A., "Instability and river channels", Jour. of Fluid Mechanics, Vol. 36, Part 3, pp.465-480, 1969.

9. Chacinski, T.M., "The secondary flow in a meandering channel", Unpublished Ph.D. thesis, London, 1956.

10. Chatley, H., "Curvature effects in alluvial channels", Engineering, London, England, pp.260-261, Feb. 20th, 1931.

11. Chikwendu, L.N., "Secondary currents in curved stratified rivers", Proc. 12th Congress of Inter. Assoc. for Hy. Res., Sept. 1967.

12. Chow, Ven Te, "Open channel hydraulics", McGraw-Hill Book Company, Inc., New York, 1959.

13. Coles, D., "The law of the wake in the turbulent boundary layer," Jour. of Fluid Mechanics, Vol. 1, pp.191-226, 1956.

14. Daniels, H.E., "The approximate distribution of serial correlation coefficients", Biometrika, 43, 169, 1956.

15. Deissler, R.G. and Taylor, M.F., "Analysis of turbulent flow and heat transfer in noncircular passages", National Aeronautics and Space Administration, Technical Report R-31, p.18, 1959.

16. DeVriend, H.J., "A mathematical model of steady flow in curved shallow channels", Jour. of Hy. Res., No. 1, 1977.

17. Dhawan, S., "Direct measurements of skin friction", National Advisory Committee for Aeronautics, Report No. 1121, pp.281-300, 1953.

18. DuBoys, P., "Etudes du regime du rhone et l'action exercee par les eaux sur un lit a fond de graviers indefiniment affouillable", Annales des Ponts et Chaussees, Ser. 5, 18, 141-95 (1879).

19. Eakin, H.M., "Diversity of current direction and load distribution in channel bends," T.A.G.U., Vol. 16, pp.467, 1935.

20. Einstein, H.A., "The bed-load function for sediment transportation in open channel flows", U.S. Department of Agriculture, Technical Bulletin No. 1026, pp.71, Sept. 1950.

21. Einstein, H.A. and Li, H., "Secondary currents in straight channels", T.A.G.U., Vol. 32, pp.898, 1951.

22. Einstein, H.A. and Harder, J.A., "Velocity distribution and the boundary layer at channel bends", Trans American Geophysical Union, Vol. 35, No. 1, pp.114-120, 1954.

23. Einstein, H.A. and Li, H., "Secondary currents in straight channels", Trans AGU, Vol. 39, No. 6, 1958.

24. Einstein, H.A. and Shen, H.W., "A study of meandering in straight alluvial channels", Jour. of Geophysical Research, Vol. 69, No. 34, Dec. 15, 1964.

25. Engels, H., "Das flussbau-Laboratorium der kgl.technischen hochschute in dresden", Berlin, 1900.

26. Engelund, F., "Instability of erodible beds", Jour. of Fluid Mechanics, Vol. 42, Part 2, pp.225-244, 1970.

27. Engelund, F. and Skovgaard, O., "On the origin of meandering and braiding in alluvial streams", Jour. of Fluid Mechanics, Vol. 57, Part 2, pp.289-302, 1973.

28. Engelund, F. "Flow and bed topography in channel bends", Jour. of Hy. Div., ASCE, No. HY11, Nov. 1974.

29. Enger, P.F., "Tractive force fluctuations around an open channel perimeter as determined from point velocity measurements", pp.21, Presented at the Convention of ASCE at Phoenix, Arizona, April 1961.

30. Fage, A. and Faulkner, V.M. "An experimental determination of the intensity of friction on the surface of an airfoil", Proc. Royal Society of London, Ser. A, Vol. 129, pp.378-410, 1930.

31. Fargue, O., "La forme du lit des riveres a fond mobile", Gauthorvillars, Paris, 1908.

32. Fenter, F.W. and Stalmuch, C.J., "The measurement of turbulent boundary layer shear stress by means of surface impact pressure probes", Jour. of the Aero/Space Sciences, Vol. 25, No. 12, pp.793-794, Dec. 1958.

33. Fox, J.A. and Ball, D.J., "The analysis of secondary flow in bends in open channels", Proc. Inst. Civil Engrs., London, Vol. 39, paper 7087, March 1968.

34. Friedkin, J.F., "A laboratory study of the meandering of alluvial rivers", U.S. Waterways Experimental Station, Vicksburg, 1945.

35. Ghosh, S.N. and Misra, L.K., "The frequency distribution of boundary shear and effect of non-uniformity on shear distribution in open channel flow resistance", Proc. Inst. Civil Engrs., Part 2, pp.701-709, Sept. 1977.

36. Glauser, F.H., "Turbulent boundary layers in adverse pressure gradients", Jour. of Aeronautical Sciences, Vol. 21, No. 2, pp.91-108, 1954.

37. Granville, P.S., "The determination of the local skin friction and the thickness of the turbulent boundary layer from the velocity similarity laws", David Taylor Model Basin Report 1340, October 1959.

38. Grashof, F., "Theoretische maschinenlehre hydraulik, L. Voss, Leipzig, Germany, pp.748-751, 1875.

39. Hakkinen, R.J., "Measurements of turbulent skin friction on a flat plate at transonic speeds", National Advisory Committee for Aeronautics, Technical Note TN-3486, pp.41, 1955.

40. Hinderks, A., "Neben stromungen in gekrummten kanalen", V.D.I. Zeitschrift, V.71, No. 51, p.1779, Dec. 1897.

41. Hoagland, L.C., "Fully developed flow in straight rectangular ducts-secondary flow, its cause and effect on the primary flow", Unpublished Ph.D. Thesis, Department of Mechanical Engineering, MIT, p.156, Sept. 1960.

42. Hooke, R.L., "Shear stress and sediment distribution in a meander bend", Ungi Report 30, University of Uppsala, Sweden, 1974.

43. Hsu, E.Y., "The measurement of local turbulent skin friction by means of surface pitot tubes", David Taylor Model Basin Report, 957, p.18, Aug. 1955.

44. Instruction Manual, "DISA type 55L Laser Doppler Anemometer", DISA. Information Department, Denmark, Sept. 1973.

45. Ippen, A.T. and Drinker, P.A., "Boundary shear stresses in curved trapezoidal channels", Jour. of Hy. Div., ASCE, Vol. 88, No. HY5, Proc. Paper 3273, Sept. 1962, pp.143-179.

46. James T., "On the origins of windings of rivers in alluvial plains with remarks on the flow of water around bends in pipes", Proc. Royal Soc., V.A.25, p.5, May 1876.

47. James T., "Experimental demonstration in respect to the origin of windings of rivers in alluvial plains and the mode of flow of water around bends in pipes", Proc. Royal Soc., V.A.26, p.356, June 1877.

48. Jenkins, G.M. and Watts, D.G., "Spectral analysis and its applications", Holden Day, Inc., 1968.

49. Jenkins, G.M., "Tests of hypotheses in the linear autoregressive model", I. Biometrika, 41, 405, 1954; II. Biometrika, 43, 186, 1956.

50. Jobes, J.G. and Douma, J.N., "Testing theoretical losses in open channel flow", Part I: Superelevation at bends, Civil Engineering, ASCE, Vol. 12, No. 11, p.613, 1942.

51. Kempf, G., "Neue ergebnisse der widerstandsforschung", Werft Reederet, Hafen, Jahrgang 10, Heft 11, June 7, 1929, pp.234-239; Jahrgang 12, Heft 20, pp.247-253, October 15, 1931.

52. Keulegan, G.H., "Laws of turbulent flow in open channels", Jour. of Res. of National Bureau of Standards, U.S. Department of Commerce, National Bureau of Standards, Research Paper RP 1151, Vol. 21, pp.707-741, Dec. 1938.

53. Lane, E.W., "Progress report on results of studies on design of stable channels", U.S. Bureau of Reclammation, Hydraulic Laboratory Report No. Hyd-352, 36p. June 1952.

54. Langbein, W.B. and Leopold, L.B., "River meander - theory of minimum variance", Professional Paper 422-H, U.S. Geological Survey, 1966.

55. Laufer, J., "The structure of turbulence in fully developed pipe flow", National Advisory Committee for Aeronautics, Report 1174, 18p., 1954.

56. Leaden, B.M. and Barlle, E.R., "On the measurement of local skin friction by means of a surface probe in the case of low speed turbulent flow over a porous flat plate with mass injection", Proc. of the Sixth Midwestern Conference on Fluid Mechanics at the University of Texas, Austin, pp.350-361, Sept. 1959.

57. Leighly, J.B., "Toward a theory of the morphologic significance of turbulence in the flow of water in streams", University of California, Publications in Geography, Vol. 6, No. 1, pp.1-22, Berkeley, 1932.

58. Leliavski, S., "An introduction to fluvial hydraulics", Dover Publications, Inc., New York, 1959.

59. Leutheusser, H.J., "Turbulent flow in rectangular ducts", Jour. of Hy. Div., ASCE, Vol: 89, No. HY3, May 1963.

60. Liepmann, H.W. and Skinner, G.T., "Shearing stress measurements by use of a heated element", National Advisory Committee for Aeronautics, Technical Note TN-3268, pp.27, 1954.

61. Ludwieg, H., "Instrument for measuring the wall stress of turbulent boundary layers", Translated as National Advisory Committee for Aeronautics Technical Memorandum TM-1284, 22p., 1950.

62. Ludwieg, H. and Tillmann, W., "Investigations of the wall-shearing stress in turbulent boundary layers", National Advisory Committee for Aeronautics, Technical Memorandum TM-1285, 25p., May 1950.

63. Lyav, A., "Matematicheskaya teoriya uprugosti (Mathematical theory of elasticity), ONTI, 1935.

64. Mahmood, K., "Flow and resistance charactertistics of sand bed channels", Inter. Assoc. for Hy. Res., Inter. Symposium on River Mechanics, Bangkok, Thailand, Jan. 1973.

65. Makkaveev, V.M., "Transverse flows in prismatic channel and their initiation", IBID, 1953.

66. Mockmore, C.A., "Flow around bends in stable channels", Trans., ASCE, Vol. 109, pp.593, 1944.

67. Mostafa, M.S. and Tinney, R., "Flow around 180° bends in open rectangular channels", Jour. of Hy. Div., ASCE, No. HY4, July 1968.

68. Muramoto, Y., "Flow through curved open channels", Bulletin of the Disaster Prevention Research Inst., Vol. 14, Part 2, Feb. 1965.

69. Muramoto, Y., "Secondary flow in curved open channels", Proc. 12th Congress of Inter. Assoc. for Hy. Res., Sept. 1967.

70. Murata, Y.M. and Inaba, T., "Laminar flow in a curved pipe with varying curvature", Jour. of Fluid Mechanics, Vol. 73, Part 4, March 1976.

71. Nikuradse, J., "Untersuchung uber die geschwindigkeitsverteilung in turbulenten stromungen", Verein Deutscher Ingentieure Forschungeheft No. 281, Berlin, 36p, 1926.

72. Nikuradse, J., "Gesetzmassigkeiten der turbulenten stromung in glatten rohren", Verein Deutscher Ingenieure, Forschungsheft No. 356, Berlin, 36p. 1932.

73. O'Brien, M.P., "The vertical distribution of velocity in wide rivers", Trans. AGU, Vol. 18, Part, pp.467-470, 1937.

74. Olsen, O.J. and Florey, Q.L., "Sediment studies in open channels: boundary shear and velocity distribution by the membrane analogy, analytic and finite-difference methods", U.S. Bureau of Reclamation Structural Laboratory Report No. SP-34, 32p. 1952.

75. Potapov, M.V., "Concerning the question of fluid flow in channel bends", Sochineniya (Essay), Vol. II, Sel'kozgiz-Gosudar-Stvennoe Izdatel'stvo Sel'skokhozyaistvennoi Literatury (State Publishing House of Agricultural Literature), 1951.

76. Preston, J.H., "The determination of turbulent skin friction by means of pitot tubes", Jour. of the Royal Aeronautical Society, Vol. 58, No. 518, pp.109-121, Feb. 1954.

77. Quenouille, M.H., "Approximate tests of correlation in time series", Jour. Royal Stat. Soc., B11, 68, 1949.

78. Quick, M.C., "Mechanism for stream flow meandering", Jour. of Hy. Div., ASCE, No. HY6, June 1974.

79. Replogle, J., "Tractive-force distribution in sewers and channels", Ph.D. Thesis, University of Illinois, Civil Eng. Dept., Urbana, Illinois, 1964.

80. Ripley, H.C., "Relation of depth to curvature of channels", Trans. ASCE, Paper No. 1599, Feb. 1926.

81. Robert, P.A., "Flow processes in open channel bends", Jour. of Hy. Div., ASCE, No. HY 5, May 1972.

82. Robert, P.A., "Estimating discharge from superelevation in bends", Jour. of Hy. Div., ASCE, No. HY1, Jan. 1973.

83. Ross, D., "A physical approach to turbulent boundary layer problems", Trans. ASCE, Vol. 121, pp.1219-1254, 1956.

84. Rouse, H., "Laboratory instruction in the mechanics of fluids", State University of Iowa, Studies in Engineering, Bulletin 41, pp.60, 1961.

85. Rozovskii, I.L., "Concerning the question of velocity distribution in stream bends", Report of the Academy of Science of the Ukr., SSR, No. 6, 1954.

86. Rozovskii, I.L., "Flow of water in bends of open channels", Academy of Sciences of Ukranian, SSR, Kiev, 1957.

87. Salamon, E., "An investigation of fully developed turbulent flow in a curved channel", Thesis submitted to the Advisory Board of the School of Engg. of the Johns Hopkins University in Conformity with the Requirements for the Ph.D. Degree, Baltimore, Maryland, 1954.

88. Schlichting, H., "Boundary layer theory", McGraw-Hill Book Company, New York, 4th Edition, 1960.

89. Schultz-Grunow, F., "New frictional resistance law for smooth plates", Translated as National Advisory Committee for Aeronautics, Technical Memorandum TM-986, 23p. 1941.

90. Shen, H.W. and Komura, S., "Meandering tendencies in straight alluvial channels", Jour. of Hy. Div., ASCE, Vol. 94, No. HY4, Proc. Paper 6042, July 1968, pp.997-1016.

91. Shukry, A., "Flow around bends in an open flume", Proc. ASCE, Vol. 75, pp.751-779, Paper 2411, 1949.

92. Shukry, A., Discussion of "Boundary shear stresses in curved trapezoidal channels", by Ippen, A.T. and Drinker, P.A., Jour. of Hy. Div., ASCE, Vol. 89, No. HY3, Proc. Paper 3529, May 1963, pp.333-345.

93. Simons, D.B. and Senturk, F., "Sediment transport technology", WRP, pp.278-394, Fort Collins, Colorado, 1977.

94. Smerden, E.T. and Beasley, R.P., "The tractive force theory applied to stability of open channels in cohesive soils", University of Missouri Agricultural Experiment Station, Research Bulletin 715, 36p., October 1959.

95. Stanton, T.E., Marshall, D.S. and Bryant, C.N., "On the conditions at the boundary of a fluid in turbulent motion", Proc. Royal Society of London, Ser. A, Vol. 97, pp.413-434, 1920.

96. Suga, K., "Stable shape of bed in curved open channels", Symposium on Hydraulic Research, Japanese Society of Civil Engineers, Feb. 1965.

97. Taylor, E.H., "Velocity distribution in open channels", Trans. AGU, Vol. 20, Part 4, pp.641-643, 1939.

98. Townsend, A.A., "Equilibrium layers and wall turbulence", Jour. of Fluid Mechanics, Vol. 11, Part 1, pp.97-120, Aug. 1961.

99. Vanoni, V.S. and Nomicos, G.N., "Resistance properties of sediment laden streams", Jour. of Hy. Div., ASCE, Vol. 85, No. HY5, pp.77-107, 1959.

100. Varshney, D.V. and Garde, R.J., "Shear distribution in bends in rectangular channels", Jour. of Hy. Div., ASCE, No. HY8, Aug. 1975.

101. VonKarman, T., "Turbulence and skin friction", Jour. of Aeronautical Sciences, Vol. 1, No. 1, pp.1-20, Jan. 1934.

102. Wadekar, I., "Secondary flow in a curved channel", Unpublished Ph.D. Thesis, London, 1957.

103. Wattendorf, F.L., "A study of the effect of curvature on fully developed turbulent flow", Proc. Royal Soc. of London; Ser. A., Vol. 148, pp.565-598, 1934.

104. Wien, W. and Harms, F. (editors), "Handbuch der experimental physik", Band 4, Teil. 1, Leipzig, Akademische Verlagsgesellschaft, M.B.H., 1932.

105. Woodward, S.M., "Hydraulics of the Miami flood control project", Miami Conservancy District, Technical Report, Pt. VII, Dayton, Ohio, 1920.

106. Yen, C.L., "Bed topography effect on flow in a meander", Jour. of Hy. Div., ASCE, Vol. 96, No. HY1, Jan. 1970.

107. Yen, C.L., and Yen, B.C., "Water surface configuration in channel bends", Jour. of Hy. Div., ASCE, No. HY2, Feb. 1971.

Appendix (A)

Measuring point velocity with Laser Doppler Anemometer

MEASURING POINT VELOCITY WITH THE LASER DOPPLER ANEMOMETER SYSTEM

Experimental fluid mechanics has, for many years, made use of mechanical measuring probes to obtain information on fluid velocity. Total-pressure probes, in conjunction with static-pressure probes, have provided the principal means of measuring mean velocity and hot-wire or hot-film anemometers the principal means of measuring instantaneous velocity. The limitations of these instruments when, for example, measuring velocity near solid boundaries or near the water surface have emphasized the need for an alternative (remote sensing) measurement technique. An example of such a technique is the optical sensing method employed in the Laser Doppler Anemometry System.

While the application of this particular measuring technique is limited to certain flow categories and boundary conditions it, nevertheless, has one major advantage over all other "direct" sensing methods, namely: the fact that the region of the flow field being studied remains undisturbed. This, in turn, removes inherent errors associated with the physical presence of a probe (however small) in the flow.

In essence the technique works on the following principle: the instrumentation, which is positioned outside the test section, directs a laser beam at a point in the flow and the light scattered, by small particles suspended in the fluid, contains information that can be related to the velocity of these same particles.

Although the frequency of the scattered light waves (from the particles) is different from the frequency of the directed light wave, there is a vector relationship between these frequencies and the local velocity of the particles, namely:

$$f_s = f_i + \frac{1}{\lambda}\,\overline{V}\,(e_s - e_i) \tag{1}$$

where

f_s = frequency of scattered light,

f_i = frequency of incident light,

e_s = unit vector in the scattering direction,

e_i = unit vector in the incident direction,

$\overline{V}$ = velocity vector,

λ = wave length of incident light.

The frequency shift is equal to the Doppler frequency, f_D;

$$f_D = f_s - f_i$$

and thence

$$f_D = \frac{1}{\lambda}\,\overline{V}.(e_s - e_i) \tag{2}$$

Therefore, the Doppler frequency is directly proportional to the particle velocity (Equation 2).

The optical technique employes the interference patterns produced by the equipment to facilitate determination of the particle velocity (by measuring the "transit time" of a particle across a

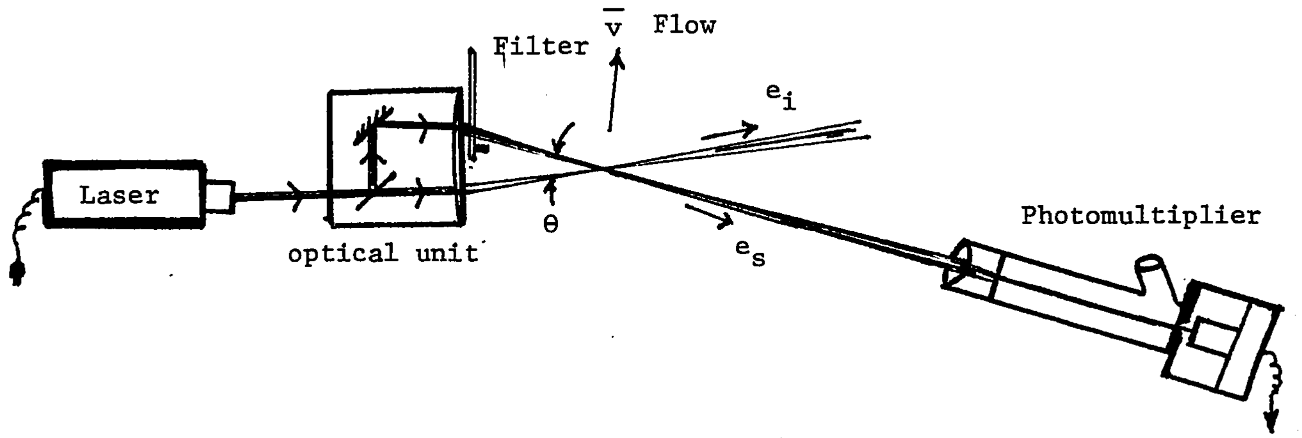

Fig. A.1.a Measurements using reference-beam mode

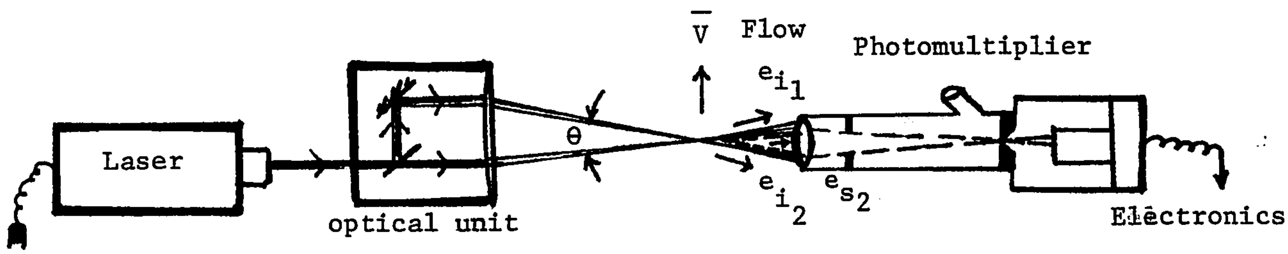

Fig. A.1.b Measurements using the differential-Doppler mode on forward scattered light

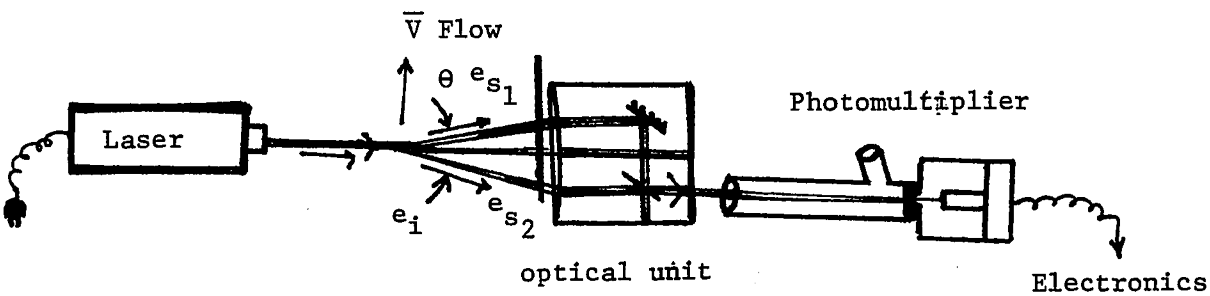

Fig. A.1.c Measurements using two scattered light beams with forward scattering (Dual-beam Mode)

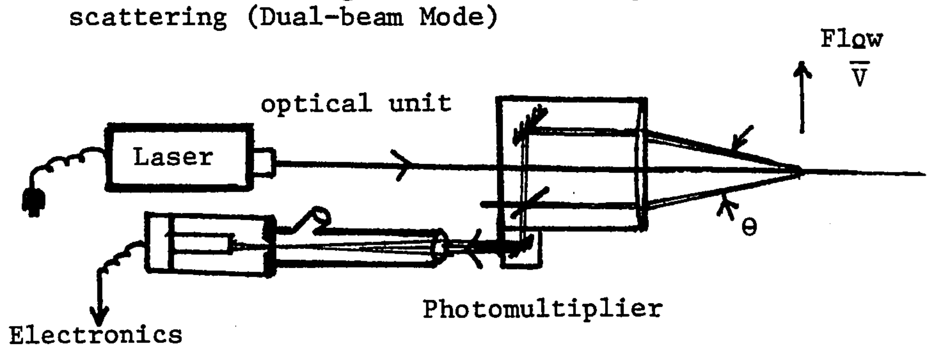

Fig. A.1.d Measurements using two scattered light beams on back scattered light

Fig. A.1. Modes of Operation

known number of interference "fringes"). These interference patterns are formed in three ways and are referred to as the "dual-beam" (or fringe), "feference-beam" and "two-scattered beam" modes (Fig. A.1).

Whichever mode is used, a Laser-Doppler anemometer comprises a light source (which is always a laser), optical arrangements to transmit and collect light, a photocathode and a signal processing arrangement Fig. A.2 represents a typical Laser-Doppler anemometer and identifies the various components. The laser is a source of coherent light of appropriate intensity, as indicated on the figure, its beam may be split into two parts which cross to provide an interference pattern in the local region of the flow where velocity measurements are required. Part of the volume of interference is observed by a light-collecting system and imaged on a photodetector. The photodetector converts the optical signal to an electronic signal which is, in turn, processed by an appropriate signal-processing arrangement.

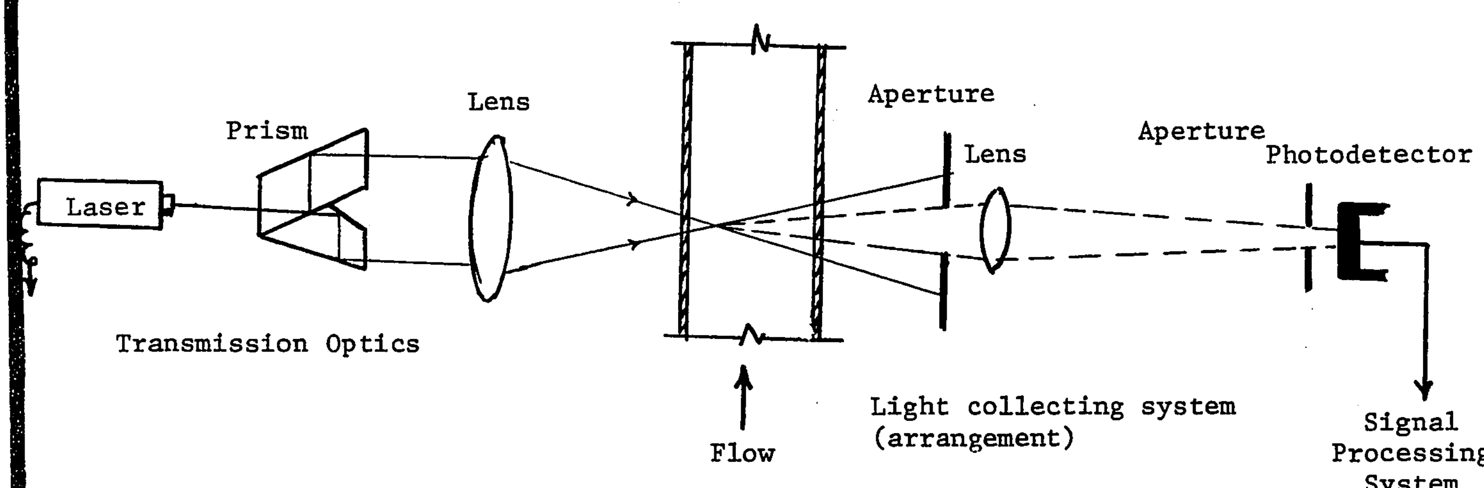

Fig. A.2. Laser-Doppler Anemometer System

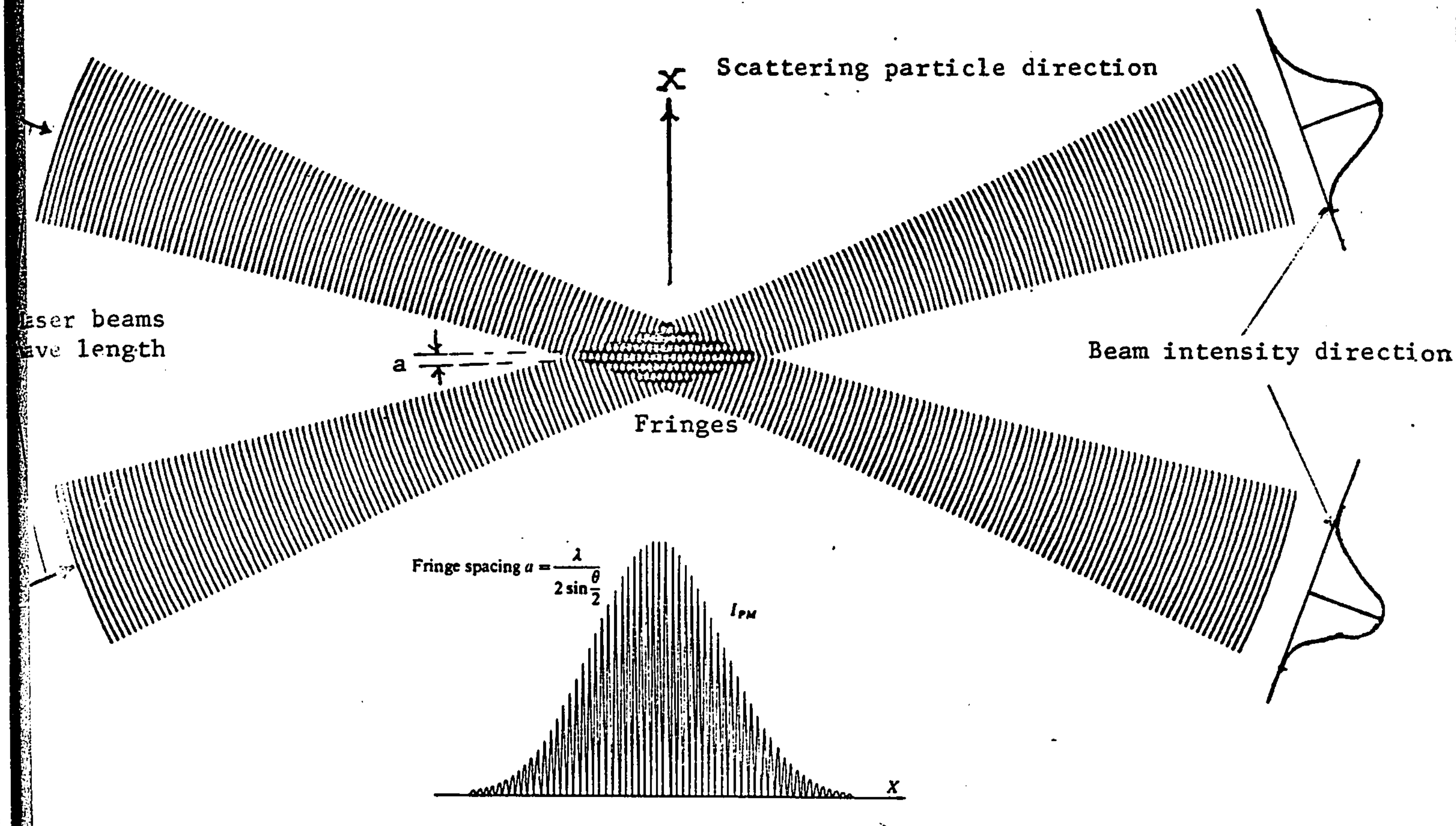

Fig. A.3.a Two intersecting laser beams forming an interference or fringe pattern at the intersection.

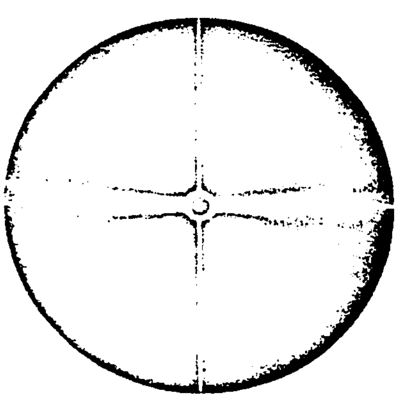

Fig. A.3.b Image of beam intersection on pinhole.

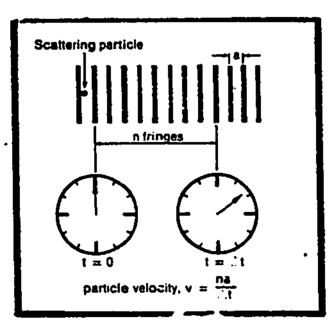

Fig. A.3.c LDA Counter principle

Fig. A.3 Beams intersection and counter principle.

A DISA Laser Doppler Anemometer System (type 55L) was used to measure velocity in this study. The system included the following basic units: (i) optical unit (type 55L01); (ii) photomultiplier (type 55L10); (iii) doppler signal processor (type 55L20); (iv) high voltage supply unit (type 55L15); (v) signal conditioner (type 55D26); (vi) digital voltmeter (type 55D31); and (vii) R.M.S. voltmeter (type 55D35).

It was established (44) that the laser source should be a continuously luminous type with a coherence length of not less than 20 cm and with a low noise factor, therefore a 5 mW Helium-Neon Laser (Spectra-Physics Model 120) was installed in the system.

The operation mode selected for the study was the "Differential-Doppler" (forward scattered light) mode, see Fig. A.1.b.

With this particular mode of operation the optical unit (Fig.A.4) focuses, via two beam adjusters, the laser beams at the required data point in the flow field. The beam adjusters are two glass wedge plates (with wedge angles of 3°) positioned next to each other, but with their direction of taper at 90° to one another. The wedge plates can be rotated by using two micrometer screws, a 25 mm movement of a screw turning a wedge plate through 40°. This micrometer adjustment ensures a high resolution of beam adjustment for perfect beam intersection.

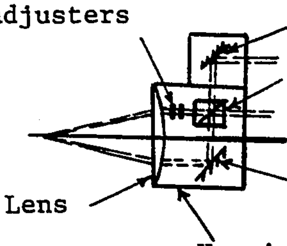

Fig. A.4 Diagram of the Optical Unit.

The photomultiplier (Fig. 4) has the function of detecting the doppler shifted light scattered from the point of measurement. It consists of a collecting light tube and a PM-tube containing a photocathode, an electro-optical input system, a secondary emission multiplier, and an anode.

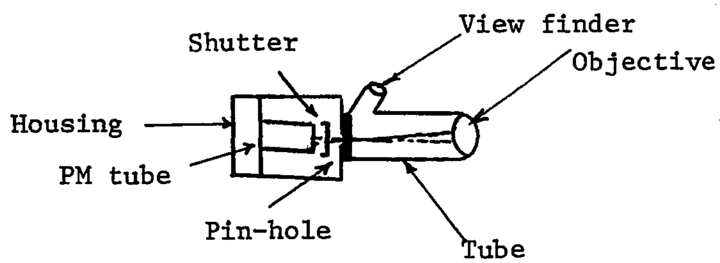

Fig. A.5 Diagram of the Photomultiplier.

Because the PM-tube is very sensitive to light, it is protected by a housing (Fig. A.5. The built-in shutter is controlled by the knob at the end of the housing and protects the PM-tubes photocathode from exposure to the intensive laser beam while setting up the LDA system.

The pin-hole aperture unit prevents undesired light from hitting the PM-tube during measurements, thus optimizing the PM-tube signal quality. The objective mounted on the view-finder tube is focussed on the point of measurement in the flow. Adjustment screws on the pin-hole aperture unit make centering of the scattered light on the pin-hole center possible.

In the PM-tube, photoelectrons from the desired area of the cathode must be guided onto the first dynode of the secondary emission multiplier with the maximum possible efficiency. This is achieved by the optimization of the cathode to first dynode geometry, and the maximization of the collecting field. Photoelectrons impinging on the first dynode produce a number of secondary electrons which are accelerated onto the next dynode of the multiplier where they, in turn, produce secondaries. A potential gradient is maintained between the successive dynode stages, by means of a suitable resistor chain.

The last dynode is in the form of a shallow box, within which the anode mesh is stretched. Electrons from the penultimate dynode pass through the anode mesh to strike the last dynode, the low energy secondaries produced are then collected at the mesh.

The Doppler signal processor contains the circuits of pre-amplifier (Type 55L30), Frequency tracer (Type 55L30), and meter unit (Type 55L40). Its purpose is to provide a Doppler signal, corresponding to mean flow velocity, with minimum noise. The Doppler signal can be filtered by using the pre-amplifier circuit. This circuit has two electronically switched filters for "top cut" and "bottom cut" of signal.

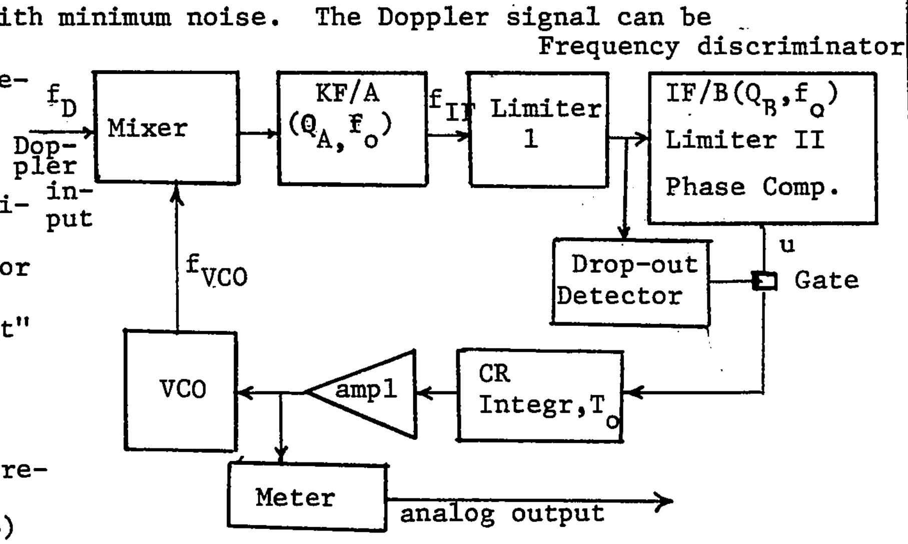

Fig. A.6 Block Diagram of the Tracker.

Then, in the frequency tracker (Fig. A.6) the incoming Doppler signal at a frequency which varies with time, is combined with the output of a voltage-controlled local oscillator in a mixer stage. The output signal at the difference frequency is narrow-band filtered (by IF/A), to remove as much noise as possible, then passed through Limiter I, in order to remove amplitude fluctuations inherent in the Doppler signal, and thence to a sensitive frequency discriminator. This provides a DC output (u) proportional to IF frequency deviation from a fixed center value f_o, after suitable smoothing with a long time constant T_o, and DC amplification, the resulting error voltage v is fed back to the control input of the VCO. The result of the feedback is that, provided a suitable value of loop gain is chosen, the oscillator frequency tracks that of the Doppler signal, maintaining a nearly constant difference equal to f_o. Thus voltage v provides an electrical analogy of "instantaneous" Doppler frequency, and hence of flow velocity.

The frequency discriminator consists of a second IF filter IF/B (also tuned to f_o) together with Limiter II and a Phase Comparator. IF/B selects only the fundamental (sinusoidal) component of the rectangular wave form delivered by Limiter I; the second IF circuit is arranged so that its output lags the input by 90° at resonance, and by more at higher frequencies and less at lower frequencies, the phase lag approaching zero at low frequencies and 180° at high frequencies. The Limiter II generates a rectangular waveform of defined amplitude, similar to that from Limiter I, and the Phase Comparator performs a simple analog multiplication, its output is therefore a rectangular wave, fundamentally at twice the IF frequency, whose mark/space ratio varies with the phase difference of the inputs. The mean DC level $\overline{u}$ of the output is proportional to $(\frac{\pi}{2} - \phi)$, where ϕ is the phase lage introduced by IF/B. Thus $\overline{u}$ (and hence v) is positive for IF frequencies below resonance, negative for frequencies above resonance and zero if $f = f_o$. Provided the oscillator operates at a frequency higher than the Doppler signal, theaamplified (non-inverted) voltage v is then the correct sense to give overall negative feedback, at least for slow modulation of the Doppler frequency.

The Signal Conditioner has the function[44] of converting an anemometer output signal so that the parameters of interest will stand clearly, whereas undesired signal components are suppressed. It may be used[44] as a filter, amplifier, zero suppressor, and summing and subtracting network. In this study it is used as filter of the anemometer output signals.

Two voltmeters have been used, Digital voltmeter[44] for mean flow velocity measurements, and RMS voltmeter[44] for turbulence level determinations. In the digital voltmeter, a built-in filter, (switchable in 7 steps), provides a choice of time constants between 0.1 and 100 seconds, thus permitting measurement of the mean value (and hence the mean flow velocity) of a signal from turbulent flows. On the other hand, the RMS voltmeter has 12 ranges between 1 mV and 300 volts and operates over the frequency range from 0.1 Hz to 400 kHz. The maximum permissible crest factor at full scale is 5, at smaller deflections it may be proportionally higher (for example 10 at 50% of full scale, etc.) without introducing distortion. Six different integrating time constants between 0.3 s and 100 s are available.

Appendix (B)

Computer program listing

Appendix (B-1)

Computation of bed shear stress from point velocity,amount of sediment scoured and deposited,and cross sectional area at any point in a system of"N"curved channels separated by straight channels.

```
      $JOB    SK329881,MAMDOUH*ALY*NOUH,PAGES=99,TIME=120,LIBLIST
      C       ***************************************************************
      C       ***************************************************************
      C       ***************************************************************
      C       ***************************************************************
      C
      C       THIS PROGRAM IS DONE BY MAMDOUH ALY NOUH AS A PART OF HIS PH.D. DEG
      C
      C       ***************************************************************
      C       ***************************************************************
      C
      C       FORMAT STATMENTS
      C
      C
      C       ***************************************************************
      C
 1          1 FORMAT(2I10,5F10.1)
 2          2 FORMAT(8F10.8)
 3          3 FORMAT('1',////////,25X,'NUMBER OF STRAIGHT CHANNELS=',I2,//,25X,'
             CNUMBER OF CURVED CHANNELS=',I2,//,25X,'MEAN RADIUS  TO  WIDTH RATI
             CO=',F5.2,//,25X,91('*'))
 4          4 FORMAT(////,25X,'ST. CHANNEL NO.',3X,'NO. OF CROSS SECTION',3X,'BE
             CD LEVELS ACROSS THE SECTION-INITIAL BED LEVEL IS A REFERANCE',/,25
             CX,103('*'),/,25X,103('*'))
 5          5 FORMAT(/,31X,I2,15X,I2,18X,7(F6.2,2X))
 6          6 FORMAT(////,21X,'ST. CHANNEL NO.=',3X,'NO. OF CROSS SECTION=',3X,'
             CWATER LEVELS ACROSS THE SECTION-INITIAL WATER LEVEL IS A REFERANCE
             C',/,21X,111('*'),/,21X,111('*'))
 7          7 FORMAT(////,23X,'CURVED CHANNEL NO.',3X,'NO. OF CROSS SECTION',3X,
             C'BED LEVELS ACROSS THE SECTION-INITIAL BED LEVEL IS A REFERANCE',/
             C,23X,106('*'),/,23X,106('*'))
 8          8 FORMAT(////,23X,'CURVED CHANNEL NO.',3X,'NO. OF CROSS SECTION',3X,
             C'WATER LEVELS ACROSS THE SECTION-INITIAL WATER LEVEL IS A REFERANC
             CE',/,23X,110('*'),/,23X,110('*'))
 9          9 FORMAT(////,15X,'ST. CHANNEL NO.',3X,'N. OF CROSS SECTION',3X,'TOT
             CAL CHANGE IN THE AREA',3X,'CHANGES IN THE AREAS 5-CMS INTERVAL',/,
             C15X,104('*'),/,15X,104('*'))
 10        11 FORMAT(/,20X,I4,16X,I5,13X,F8.2,8X,6(1X,F7.1))
 11        12 FORMAT(////,12X,'CURVED CHANNEL NO.',3X,'NO. OF CROSS SECTION',3X,
             C'TOTAL CHANGE IN THE AREA',3X,'CHANGES IN THE AREAS 5-CMS INTERVAL
             C',/,12X,106('*'),/,12X,106('*'))
 12        13 FORMAT(////,15X,'ST. CHANNEL NO.',3X,'N. OF CROSS SECTION',3X,'TOT
             CAL CHANGE IN THE VOL.',3X,'CHANGES IN THE VOLS. 5-CMS INTERVAL',/,
             C15X,102('*'),/,15X,102('*'))
 13        14 FORMAT(////,12X,'CURVED CHANNEL NO.',3X,'NO. OF CROSS SECTION',3X,
             C'TOTAL CHANGE IN THE VOL.',3X,'CHANGES IN THE VOLS. 5-CMS INTERVAL
             C',/,12X,106('*'),/,12X,106('*'))
 14        15 FORMAT('1')
 15        16 FORMAT(//////////,20X,'FLOW CHARACTERISTICS',/,20X,20('*'),/,20X,2
             C0('*'),/,20X,'AVARAGE CROSS SECTIONAL AREA=',F10.2,/,20X,'MEAN VEL
             COCITY=',F10.2,/,20X,'FROUDE NUMBER=',F10.2,/,20X,'NUMBER OF STRAIG
             CHT CHANNELS=',I2,/,20X,'NUMBER OF CURVED CHANNELS=',I2,/,20X,'MEAN
             CRADIUS TO WIDTH RATIO=',F5.2,/,20X,35('*'),/,20X,35('*'))
 16        17 FORMAT(//,20X,'ST. CHANNEL NO.',3X,'NO.OF CROSS SECTION',3X,'DIMEN
             CSIONLESS AREA OF WATER',2(/,20X,67('*')))
 17        18 FORMAT(/,25X,I5,18X,I5,18X,F10.2)
 18        19 FORMAT(//,17X,'CURVED CHANNEL NO.',3X,'NO. OF CROSS SECTION',3X,'D
             CIMENSIONLESS AREA OF WATER',2(/,17X,71('*')))
 19        22 FORMAT(/,I4,6X,I5,5X,F6.2,4X,F6.2)
 20        24 FORMAT(//,20X,'ST. CHANNEL NO.',3X,'NO. OF CROSS SECTION',3X,'CROS
             CS DISTANCE',3X,'WATER LEVEL',3X,'BED LEVEL',3X,'WATER DEPTH',2(/,2
```

```
     COX,95('*')))
   25 FORMAT(/,25X,I4,17X,I5,12X,F6.2,10X,F6.2,7X,F6.2,7X,F6.2)
   26 FORMAT(//,17X,'CURVED CHANNEL NO.',3X,'NO. OF CROSS SECTION',3X,'C
     CROSS DISTANCE',3X,'WATER LEVEL',3X,'BED LEVEL',3X,'WATER DEPTH',2(
     C/,17X,98('*')))
   27 FORMAT(F10.2)
   28 FORMAT(8F10.7)
   29 FORMAT(2F10.2)
   31 FORMAT(2I10)
   32 FORMAT(I10)
  611 FORMAT(15X,I2,8X,I2,8(4X,F6.2))
  612 FORMAT('1',///,11X,'ST.CH.NO. NO.CR.SE. BED LEVEL WATER LEV FREQUE
     CNCY     RMS      OUTER Y  OUTER X    INNER Y    INNER X',2(/,11X,97('*
     C')))
  613 FORMAT('1',///,11X,'CU.CH.NO. NO.CR.SE. BED LEVEL WATER LEV FREQUE
     CNCY     RMS      OUTER Y  OUTER X    INNER Y    INNER X',2(/,11X,97('*
     C')))
  614 FORMAT('1',//////,60X,'RUN CONSTANTS',2(/,60X,13('*')))
  615 FORMAT(//,20X,'NUMBER OF STRAIGHT CHANNEL=',I2,/,20X,'NUMBER OF CU
     CRVED CHANNELS=',I2,/,20X,'HEAD OF WATER OVER V-NOTCH=',F6.2,/,20X,
     C'INITIAL LEVEL OF SAND IN THE RUN=',F6.2,/,20X,'FLUME BED LEVEL=',
     CF6.2,/,20X,'INITIAL WATER SURFACE LEVEL=',F6.2,/,20X,'RADIUS TO WI
     CDTH RATIO=',F6.2)
  616 FORMAT(/,20X,'RADIUS OF CURVATURES OF CURVED CHANNELS IN THE RUN='
     C,2(F10.2,5X))
  617 FORMAT(20X,'STRAIGHT CHANNEL LENGTHS=',3(F10.2,5X))
  618 FORMAT(20X,'CENTRAL ANGLES OF CURVED CHANNELS=',2(F10.2,5X))
  619 FORMAT(20X,'NUMBER OF LONGITUDINAL SUBDIVISION S IN STRAIGHT CHANN
     CELS=',3(I10,5X))
  621 FORMAT(20X,'NUMBER OF LONGITUDINAL SUBDIVISIONS IN CURVED CHANNELS
     C',2(I10,5X))
  622 FORMAT(20X,'NUMBER OF CROSS SUBDIVISIONS IN STRAIGHT CHANNELS=',3(
     CI10,5X))
  623 FORMAT(20X,'NUMBER OF CROSS SUBDIVISIONS IN CURVED CHANNELS=',2(I1
     C0,5X))
  624 FORMAT(20X,'LONGITUDINAL SUBDIVISION LENGTHS IN STRAIGHT CHANNELS
     CARE:',/,30X,'NO. OF STRAIGHT CHANNEL  NO. OF CROSS SECTION  LONGL.
     C DISTANCES',/,30X,63('*'))
  626 FORMAT(40X,I2,20X,I2,17X,F6.2)
  627 FORMAT(20X,'LONGITUDINAL SUBDIVISION ANGLES  IN  CURVED  CHANNELS
     CARE:',/,30X,'NO. OF  CURVED  CHANNEL  NO. OF CROSS SECTION  CENTRA
     CL ANGLES',/,30X,61('*'))
  628 FORMAT(20X,'CROSS SUBDIVISION LENGTHS IN STRAIGHT CHANNELS ARE:',/
     C,30X,'NO. OF STRAIGHT CHANNEL  NO. OF SECTION',6X,'CROSS SUBDIVISI
     CONS',/,30X,73('*'))
  629 FORMAT(20X,'CROSS SUBDIVISION LENGTHS IN  CURVED  CHANNELS ARE:',/
     C,30X,'NO. OF  CURVED  CHANNEL  NO. OF SECTION',6X,'CROSS SUBDIVISI
     CONS',/,30X,73('*'))
  631 FORMAT(40X,I2,20X,I2,5X,7(F4.1,2X))
  632 FORMAT('1',////////)
C
C       ***************************************************************
C
C       DIMENSION STATMENTS
C
C       ***************************************************************
C
        DIMENSION R(2),SL(3),CA(2),NSL(3),NSC(2),NWS(6),NWC(6),DSL(3,20),D
       CSC(2,7),WSL(3,21,6),WSC(2,8,6),HBS(3,21,7),HBC(2,7,7),HWS(3,21,7),
       CHWC(2,7,7),PEOS(3,21,6),RMSS(3,21,6),YOS(3,21,6),YIS(3,21,6),XOS(3
```

```
      C,21,6),XIS(3,21,6),REQC(2,7,6),RMSC(3,7,6),YOC(2,7,5),YIC(2,7,6),X
      COC(2,7,6),XIC(2,7,6),AS(3,21,6),ASN(3,21),AC(2,7,6),ACN(2,7),B(2)
       DIMENSION RR(2,7,6),SUMS(20),XS(3,21),XSC(3,21),XC(2,7),XCC(2,7),X
      CISI(3,21,7),XICI(2,7,6),VOLTS(3,21,6),VOLTC(2,7,6),XWS(3,21,7),XWC
      C(2,7,7),SSL(3,21,7),SSC(2,7,7)
C
C        ******************************************************************
C
C        READ STATMENTS
C
C        ******************************************************************
C
         K1=5
         K2=6
         K3=7
         READ(K1,1)NS,NC,H,CI,CIB,WS,RAT
         READ(K1,27)(R(I),I=1,NC)
         READ(K1,29)(SL(I),I=1,NS)
         READ(K1,27)(CA(I),I=1,NC)
         READ(K1,31)(NSL(I),I=1,NS)
         READ(K1,32)(NSC(I),I=1,NC)
         READ(K1,31)(NWS(I),I=1,NS)
         READ(K1,32)(NWC(I),I=1,NC)
         DO 450 I=1,NS
         NN=NSL(I)
     450 READ(K1,28)(DSL(I,J),J=1,NN)
         DO 460 I=1,NC
         NN=NSC(I)
     460 READ(K1,28)(DSC(I,J),J=1,NN)
         DO 10 I=1,NS
         NN=NSL(I)+1
         MM=NWS(I)
      10 READ(K1,2)((WSL(I,J,K),K=1,MM),J=1,NN)
         DO 20 I=1,NC
         NN=NSC(I)+1
         MM=NWC(I)
      20 READ(K1,2)((WSC(I,J,K),K=1,MM),J=1,NN)
         DO 30 I=1,NS
         NN=NWS(I)+1
         MM=NSL(I)+1
      30 READ(K1,28)((HBS(I,J,K),K=1,NN),J=1,MM)
         DO 40 I=1,NS
         NN=NWS(I)+1
         MM=NSL(I)+1
      40 READ(K1,2)((HWS(I,J,K),K=1,NN),J=1,MM)
         DO 50 I=1,NC
         NN=NWC(I)+1
         MM=NSC(I)+1
      50 READ(K1,28)((HBC(I,J,K),K=1,NN),J=1,MM)
         DO 60 I=1,NC
         NN=NWC(I)+1
         MM=NSC(I)+1
      60 READ(K1,2)((HWC(I,J,K),K=1,NN),J=1,MM)
         DO 70 I=1,NS
         NN=NWS(I)-1
         MM=NSL(I)+1
      70 READ(K1,2)((REQS(I,J,K),K=1,NN),J=1,MM)
         DO 80 I=1,NS
         NN=NWS(I)-1
         MM=NSL(I)+1
```

```
   80 READ(K1,28)((RMSS(I,J,K),K=1,NN),J=1,MM)
      DO 530 I=1,NS
      NN=NWS(I)-1
      MM=NSL(I)+1
  530 READ(K1,2)((VOLTS(I,J,K),K=1,NN),J=1,MM)
      DO 90 I=1,NS
      NN=NWS(I)-1
      MM=NSL(I)+1
   90 READ(K1,2)((YOS(I,J,K),K=1,NN),J=1,MM)
      DO 100 I=1,NS
      NN=NWS(I)-1
      MM=NSL(I)+1
  100 READ(K1,2)((YIS(I,J,K),K=1,NN),J=1,MM)
      DO 110 I=1,NS
      NN=NWS(I)-1
      MM=NSL(I)+1
  110 READ(K1,2)((XOS(I,J,K),K=1,NN),J=1,MM)
      DO 120 I=1,NS
      NN=NWS(I)-1
      MM=NSL(I)+1
  120 READ(K1,2)((XIS(I,J,K),K=1,NN),J=1,MM)
      DO 130 I=1,NC
      NN=NWC(I)-1
      MM=NSC(I)+1
  130 READ(K1,2)((REQC(I,J,K),K=1,NN),J=1,MM)
      DO 140 I=1,NC
      NN=NWC(I)-1
      MM=NSC(I)+1
  140 READ(K1,28)((RMSC(I,J,K),K=1,NN),J=1,MM)
      DO 540 I=1,NC
      NN=NWC(I)-1
      MM=NSC(I)+1
  540 READ(K1,2)((VOLTC(I,J,K),K=1,NN),J=1,MM)
      DO 150 I=1,NC
      NN=NWC(I)-1
      MM=NSC(I)+1
  150 READ(K1,2)((YOC(I,J,K),K=1,NN),J=1,MM)
      DO 160 I=1,NC
      NN=NWC(I)-1
      MM=NSC(I)+1
  160 READ(K1,2)((YIC(I,J,K),K=1,NN),J=1,MM)
      DO 170 I=1,NC
      NN=NWC(I)-1
      MM=NSC(I)+1
  170 READ(K1,2)((XOC(I,J,K),K=1,NN),J=1,MM)
      DO 180 I=1,NC
      NN=NWC(I)-1
      MM=NSC(I)+1
  180 READ(K1,2)((XIC(I,J,K),K=1,NN),J=1,MM)
C
C     *******************************************************************
C
C     PRINT OUT THE DATA GIVEN AS INPUT
C
C     *******************************************************************
C
      WRITE(K2,614)
      WRITE(K2,615)NS,NC,H,CI,CIB,WS,RAT
      WRITE(K2,616)(R(I),I=1,NC)
      WRITE(K2,617)(SL(I),I=1,NS)
```

```
      WRITE(K2,618)(CA(I),I=1,NC)
      WRITE(K2,619)(NSL(I),I=1,NS)
      WRITE(K2,621)(NSC(I),I=1,NC)
      WRITE(K2,622)(NWS(I),I=1,NS)
      WRITE(K2,623)(NWC(I),I=1,NC)
      WRITE(K2,632)
      WRITE(K2,624)
      DO 650 I=1,NS
      NN=NSL(I)
      DO 650 J=1,NN
      WRITE(K2,626)I,J,DSL(I,J)
  650 CONTINUE
      WRITE(K2,632)
      WRITE(K2,627)
      DO 660 I=1,NC
      NN=NSC(I)
      DO 660 J=1,NN
      WRITE(K2,626)I,J,DSC(I,J)
  660 CONTINUE
      WRITE(K2,632)
      WRITE(K2,628)
      DO 670 I=1,NS
      NN=NSL(I)+1
      MM=NWS(I)
      DO 670 J=1,NN
  670 WRITE(K2,631)I,J,(WSL(I,J,K),K=1,MM)
      WRITE(K2,632)
      WRITE(K2,629)
      DO 680 I=1,NC
      NN=NSC(I)+1
      MM=NWC(I)
      DO 680 J=1,NN
  680 WRITE(K2,631)I,J,(WSC(I,J,K),K=1,MM)
      WRITE(K2,612)
      DO 610 I=1,NS
      NN=NSL(I)+1
      MM=NWS(I)-1
      DO 610 J=1,NN
      WRITE(K2,611)I,J,HBS(I,J,1),HWS(I,J,1)
      DO 630 K=1,MM
      M=K+1
      WRITE(K2,611)I,J,HBS(I,J,M),HWS(I,J,M),REOS(I,J,K),RMSS(I,J,K),YOS
     C(I,J,K),XOS(I,J,K),YIS(I,J,K),XIS(I,J,K)
  630 CONTINUE
      WRITE(K2,611)I,J,HBS(I,J,7),HWS(I,J,7)
  610 CONTINUE
      WRITE(K2,613)
      DO 620 I=1,NC
      NN=NSC(I)+1
      MM=NWC(I)-1
      DO 620 J=1,NN
      WRITE(K2,611)I,J,HBC(I,J,1),HWC(I,J,1)
      DO 640 K=1,MM
      M=K+1
      WRITE(K2,611)I,J,HBC(I,J,M),HWC(I,J,M),REOC(I,J,K),RMSC(I,J,K),YOC
     C(I,J,K),XOC(I,J,K),YIC(I,J,K),XIC(I,J,K)
  640 CONTINUE
      WRITE(K2,611)I,J,HBC(I,J,7),HWC(I,J,7)
  620 CONTINUE
C
```

```
C     ******************************************************************
C
C     RUN CONSTANTS
C
C     ******************************************************************
C
      W=12.*2.54
      PI=22./7.
      C=W/2.
      Q=(8./15)*0.62*TAN((30.*PI)/180.)*((2.*981.)**0.5)*(H**2.5)
      BI=CIB-CI
      STD=2.025
      ROO=1./981.
      GMA=1.0
C
C     ******************************************************************
C
C   1 SCOURED AND DEPOSITED AREAS
C
C     ******************************************************************
C
      DO 190 I=1,NS
      NN=NWS(I)+1
      MM=NSL(I)+1
      DO 190 J=1,MM
      DO 190 K=1,NN
      HBS(I,J,K)=CI-HBS(I,J,K)
      HWS(I,J,K)=WS-HWS(I,J,K)
  190 CONTINUE
      WRITE(K2,3)NS,NC,RAT
      WRITE(K2,4)
      DO 191 I=1,NS
      NN=NWS(I)+1
      MM=NSL(I)+1
      DO 191 J=1,MM
      WRITE(K2,5)I,J,(HBS(I,J,K),K=1,NN)
  191 CONTINUE
      WRITE(K2,3)NS,NC,RAT
      WRITE(K2,6)
      DO 192 I=1,NS
      NN=NWS(I)+1
      MM=NSL(I)+1
      DO 192 J=1,MM
      WRITE(K2,5)I,J,(HWS(I,J,K),K=1,NN)
  192 CONTINUE
      DO 550 I=1,NS
      NN=NWS(I)+1
      MM=NSL(I)+1
      DO 550 J=1,MM
      DO 550 K=1,NN
      HBS(I,J,K)=HBS(I,J,K)-CI+CIB
      HWS(I,J,K)=HWS(I,J,K)-WS+CIB
  550 CONTINUE
      DO 200 I=1,NC
      NN=NWC(I)+1
      MM=NSC(I)+1
      DO 200 J=1,MM
      DO 200 K=1,MM
      HBC(I,J,K)=CI-HBC(I,J,K)
      HWC(I,J,K)=WS-HWC(I,J,K)
```

```
  200 CONTINUE
      WRITE(K2,3)NS,NC,RAT
      WRITE(K2,7)
      DO 194 I=1,NC
      NN=NWC(I)+1
      MM=NSC(I)+1
      DO 194 J=1,MM
      WRITE(K2,5)I,J,(HBC(I,J,K),K=1,NN)
  194 CONTINUE
      WRITE(K2,3)NS,NC,RAT
      WRITE(K2,8)
      DO 195 I=1,NC
      NN=NWC(I)+1
      MM=NSC(I)+1
      DO 195 J=1,MM
      WRITE(K2,5)I,J,(HWC(I,J,K),K=1,NN)
  195 CONTINUE
      DO 560 I=1,NC
      NN=NWC(I)+1
      MM=NSC(I)+1
      DO 560 J=1,MM
      DO 560 K=1,NN
      HWC(I,J,K)=HWC(I,J,K)-WS+CIB
      HBC(I,J,K)=HBC(I,J,K)-CI+CIB
  560 CONTINUE
      DO 210 I=1,NS
      NN=NSL(I)+1
      DO 210 J=1,NN
      XA=0.
      KK=NWS(I)
      DO 220 K=1,KK
      AS(I,J,K)=0.5*((HBS(I,J,K)+HBS(I,J,K+1))*WSL(I,J,K))-WSL(I,J,K)*
  220 XA=XA+AS(I,J,K)
  210 ASN(I,J)=XA
      WRITE(K2,3)NS,NC,RAT
      WRITE(K2,9)
      DO 193 I=1,NS
      NN=NWS(I)
      MM=NSL(I)+1
      DO 193 J=1,MM
      WRITE(K2,11)I,J,ASN(I,J),(AS(I,J,K),K=1,NN)
  193 CONTINUE
      DO 230 I=1,NC
      NN=NSC(I)+1
      DO 230 J=1,NN
      KK=NWC(I)
      XX=0.
      DO 240 K=1,KK
      AC(I,J,K)=0.5*((HBC(I,J,K)+HBC(I,J,K+1))*WSC(I,J,K))-WSC(I,J,K)*
  240 XX=XX+AC(I,J,K)
  230 ACN(I,J)=XX
      WRITE(K2,3)NS,NC,RAT
      WRITE(K2,12)
      DO 196 I=1,NC
      MM=NSC(I)+1
      NN=NWC(I)
      DO 196 J=1,MM
      WRITE(K2,11)I,J,ACN(I,J),(AC(I,J,K),K=1,NN)
  196 CONTINUE
C
```

```
C         ******************************************************************
C
C    2    SCOURED AND DEPSITED VOLUMES
C
C         ******************************************************************
C
          DO 250 I=1,NS
          KK=NSL(I)
          DO 250 J=1,KK
          XV=0.
          KX=NWS(I)
          DO 260 K=1,KX
          AS(I,J,K)=0.50*(AS(I,J,K)+AS(I,J+1,K))*DSL(I,J)
      260 XV=XV+AS(I,J,K)
      250 ASN(I,J)=XV
          WRITE(K2,3)NS,NC,RAT
          WRITE(K2,13)
          DO 197 I=1,NS
          NN=NWS(I)
          MM=NSL(I)
          DO 197 J=1,MM
          WRITE(K2,11)I,J,ASN(I,J),(AS(I,J,K),K=1,NN)
      197 CONTINUE
          DO 270 I=1,NC
          B(I)=R(I)-W/2.
          KX=NSC(I)
          DO 270 J=1,KX
          KG=NWC(I)
          YV=0.
          DO 280 K=1,KG
          IF(K.EQ.1)GOTO 101
          KK=K-1
          SUM1=0.
          SUM2=0.
          DO 290 KC=1,KK
          SUM1=SUM1+WSC(I,J,KC)
      290 SUM2=SUM2+WSC(I,J+1,KC)
          B(I)=B(I)+0.5*(SUM1+SUM2)
      101 RR(I,J,K)=B(I)+0.25*(WSC(I,J,K)+WSC(I,J+1,K))
          AC(I,J,K)=0.5*(AC(I,J,K)+AC(I,J+1,K))*PI*DSC(I,J)*RR(I,J,K)/180.
      280 YV=YV+AC(I,J,K)
      270 ACN(I,J)=YV
          WRITE(K2,3)NS,NC,RAT
          WRITE(K2,14)
          DO 198 I=1,NC
          NN=NSC(I)
          MM=NWC(I)
          DO 198 J=1,NN
          WRITE(K2,11)I,J,ACN(I,J),(AC(I,J,K),K=1,MM)
      198 CONTINUE
C
C         ******************************************************************
C
C    3    TOTAL DISTANCES FROM THE RUN BEGINNING TO THE END AND SLICE CENTRE
C
C         ******************************************************************
C
          NN=NSL(1)+1
          SUMS(1)=0.
          DO 470 J=2,NN
```

```
      XS(1,J)=SUMS(J-1)+DSL(1,J-1)
      XSC(1,J)=XS(1,J)-0.5*DSL(1,J-1)
  470 SUMS(J)=XS(1,J)
      NP=NS-1
      DO 300 I=1,NP
      XC(I,1)=XS(I,NN)
      NN=NSC(I)+1
      DO 310 J=2,NN
      XC(I,J)=XC(I,J-1)+DSC(I,J-1)*R(I)*PI/180.
  310 XCC(I,J)=XC(I,J)-0.5*DSC(I,J-1)*R(I)*PI/180.
      XS(I+1,1)=XC(I,NN)
      NN=NSL(I+1)+1
      DO 320 J=2,NN
      XS(I+1,J)=XS(I+1,J-1)+DSL(I+1,J-1)
  320 XSC(I+1,J)=XS(I+1,J)-0.5*DSL(I+1,J-1)
  300 CONTINUE
C
C     ******************************************************************
C
C   5 MEAN AREA,VELOCITY,FROUDE NUMBER,AND DIMENSIONLESS AREAS
C
C     ******************************************************************
C
      S=0.
      X=0.
      XX=0.
      X1X=0.
      WRITE(K2,15)
      WRITE(K2,24)
      DO 370 I=1,NS
      NN=NSL(I)+1
      MM=NWS(I)+1
      XX=XX+NN*MM
      DO 370 J=1,NN
      DO 370 K=1,MM
      SSL(I,J,1)=0.
      IF(K.EQ.1)GOTO 351
      KK=K-1
      DO 350 M=1,KK
  350 X=X+WSL(I,J,M)
      SSL(I,J,K)=X
      X=0.
  351 XWS(I,J,K)=HWS(I,J,K)-HBS(I,J,K)
      WRITE(K2,25)I,J,SSL(I,J,K),HWS(I,J,K),HBS(I,J,K),XWS(I,J,K)
  370 S=S+XWS(I,J,K)
      X=0.
      WRITE(K2,15)
      WRITE(K2,26)
      DO 380 I=1,NC
      NN=NSC(I)+1
      MM=NWC(I)+1
      X1X=X1X+MM*NN
      DO 380 J=1,NN
      DO 380 K=1,MM
      SSC(I,J,1)=0.
      IF(K.EQ.1)GOTO 361
      KK=K-1
      DO 360 M=1,KK
  360 X=X+WSC(I,J,M)
      SSC(I,J,K)=X
```

```
      X=0.
  361 XWC(I,J,K)=HWC(I,J,K)-HBC(I,J,K)
      WRITE(K2,25)I,J,SSC(I,J,K),HWC(I,J,K),HBC(I,J,K),XWC(I,J,K)
  380 S=S+XWC(I,J,K)
      YAV=S/(XX+X1X)
      PARR=2.*YAV+W
      ARAV=W*YAV
      VAV=Q/ARAV
      F=VAV/((981.*YAV)**0.5)
      SUM=0.
      SUM1=0.
      NN=NSL(NS)+1
      MM=NWS(1)+1
      ML=NWS(NS)+1
      DO 770 K=1,MM
      SUM=SUM+HWS(1,1,K)
  770 SUM1=SUM1+HBS(1,1,K)
      SUM=SUM/MM
      SUM1=SUM1/MM
      SUM2=0.
      SUM3=0.
      DO 780 K=1,ML
      SUM2=SUM2+HWS(NS,NN,K)
  780 SUM3=SUM3+HBS(NS,NN,K)
      SUM2=SUM2/ML
      SUM3=SUM3/ML
      SUM=(SUM-SUM2)/XS(NS,NN)
      SUM1=(SUM1-SUM3)/XS(NS,NN)
      SLOPE=SUM-(F**2)*(SUM-SUM1)
      IF(SLOPE.LE.0)SLOPE=SUM
      SHEAR=GMA*YAV*SLOPE
C
C     ***********************************************************************
C
      WRITE(K2,15)
      WRITE(K2,16)ARAV,VAV,F,NS,NC,RAT
      DO 390 I=1,NS
      NN=NSL(I)+1
      MM=NWS(I)
      DO 390 J=1,NN
      XA=0.
      DO 400 K=1,MM
      XWS(I,J,K)=0.5*(XWS(I,J,K)+XWS(I,J,K+1))*WSL(I,J,K)
  400 XA=XA+XWS(I,J,K)
      ASN(I,J)=XA
  390 ASN(I,J)=ASN(I,J)/(YAV*W)
      WRITE(K2,17)
      DO 199 I=1,NS
      MM=NSL(I)+1
      DO 199 J=1,MM
      WRITE(K2,18)I,J,ASN(I,J)
  199 CONTINUE
      DO 410 I=1,NC
      NN=NSC(I)+1
      MM=NWC(I)
      DO 410 J=1,NN
      XX=0.
      DO 420 K=1,MM
      XWC(I,J,K)=0.5*(XWC(I,J,K)+XWC(I,J,K+1))*WSC(I,J,K)
  420 XX=XX+XWC(I,J,K)
```

```
      ACN(I,J)=XX
  410 ACN(I,J)=ACN(I,J)/(YAV*W)
      WRITE(K2,15)
      WRITE(K2,16)ARAV,VAV,F,NS,NC,RAT
      WRITE(K2,19)
      DO 201 I=1,NC
      MM=NSC(I)+1
      DO 201 J=1,MM
      WRITE(K2,18)I,J,ACN(I,J)
  201 CONTINUE
C
C     ******************************************************************
C
C     FIXED PARAMETERS
C
C     ******************************************************************
      DO 690 I=1,NS
      NN=NSL(I)+1
      MM=NWS(I)
      DO 690 J=1,NN
      ASN(I,J)=Q/(ASN(I,J)*YAV*W)
      SUM=0.
      DO 700 K=1,MM
      SUM=SUM+SQRT(ABS(HBS(I,J,K+1)-HBS(I,J,K))**2+WSL(I,J,K)**2)
  700 CONTINUE
      ASN(I,J)=ASN(I,J)/(SQRT(SUM+XWS(I,J,1)+XWS(I,J,7)))
  690 CONTINUE
      DO 730 I=1,NC
      NN=NSC(I)+1
      MM=NWC(I)
      DO 730 J=1,NN
      ACN(I,J)=Q/(ACN(I,J)*YAV*W)
      SUM=0.
      DO 740 K=1,MM
      SUM=SUM+SQRT(ABS(HBC(I,J,K+1)-HBC(I,J,K))**2+WSC(I,J,K)**2)
  740 CONTINUE
      ACN(I,J)=ACN(I,J)/(SQRT(SUM+XWC(I,J,1)+XWC(I,J,7)))
  730 CONTINUE
C
C
C     ******************************************************************
C
C   4 DETERMINATION OF MEASURING POINT POSITIONS
C
C     ******************************************************************
C
      DO 510 I=1,NS
      NN=NSL(I)+1
      DO 510 J=1,NN
      MM=NWS(I)-1
      DO 510 K=1,MM
      XIS(I,J,K)=W/(1.+(XOS(I,J,K)/XIS(I,J,K)))
      REQS(I,J,K)=REQS(I,J,K)/(2.*SIN(ATAN(XOS(I,J,K)/(2.*(W-XIS(I,J,K))
     C))))
      REQS(I,J,K)=REQS(I,J,K)*100000.
      YIS(I,J,K)=C-YIS(I,J,K)
      YOS(I,J,K)=C-YOS(I,J,K)
  510 YIS(I,J,K)=YIS(I,J,K)+((YOS(I,J,K)-YIS(I,J,K))/W)*XIS(I,J,K)
      DO 520 I=1,NC
      NN=NSC(I)+1
```

```
      DO 520 J=1,NN
      MM=NWC(I)-1
      DO 520 K=1,MM
      XIC(I,J,K)=W/(1.+(XOC(I,J,K)/XIC(I,J,K)))
      REOC(I,J,K)=REOC(I,J,K)/(2.*SIN(ATAN(XOC(I,J,K)/(2.*(W-XIC(I,J,K))
     C))))
      REOC(I,J,K)=REQC(I,J,K)*100000.
      YIC(I,J,K)=C-YIC(I,J,K)
      YOC(I,J,K)=C-YOC(I,J,K)
  520 YIC(I,J,K)=YIC(I,J,K)+((YOC(I,J,K)-YIC(I,J,K))/W)*XIC(I,J,K)
C
C     ******************************************************************
C
      DO 330 I=1,NS
      NN=NSL(I)+1
      MM=NWS(I)-1
      DO 330 J=1,NN
      X=0.
      DO 330 K=1,MM
  103 DO 104 M=1,MM
      X=X+WSL(I,J,M)
      IF(X.LT.XIS(I,J,K))GOTO 104
      XOS(I,J,K)=X
      N=M
      GOTO 329
  104 CONTINUE
  329 XISI(I,J,K)=XOS(I,J,K)-XIS(I,J,K)
      HBS(I,J,K)=HBS(I,J,N)+((HBS(I,J,N+1)-HBS(I,J,N))/WSL(I,J,N))*(WSL(
     CI,J,N)-XISI(I,J,K))
      HWS(I,J,K)=HWS(I,J,N)+((HWS(I,J,N+1)-HWS(I,J,N))/WSL(I,J,N))*(WSL(
     CI,J,N)-XISI(I,J,K))
      YOS(I,J,K)=HWS(I,J,K)-HBS(I,J,K)
  330 YIS(I,J,K)=YIS(I,J,K)-HBS(I,J,K)
      DO 340 I=1,NC
      NN=NSC(I)+1
      MM=NWC(I)-1
      DO 340 J=1,NN
      X=0.
      DO 340 K=1,MM
  106 DO 107 M=1,MM
      X=X+WSC(I,J,M)
      IF(X.LT.XIC(I,J,K))GOTO 107
      XOC(I,J,K)=X
      N=M
      GOTO 328
  107 CONTINUE
  328 XICI(I,J,K)=XOC(I,J,K)-XIC(I,J,K)
      HBC(I,J,K)=HBC(I,J,N)+((HBC(I,J,N+1)-HBC(I,J,N))/WSC(I,J,N))*(WSC(
     CI,J,N)-XICI(I,J,K))
      HWC(I,J,K)=HWC(I,J,N)+((HWC(I,J,N+1)-HWC(I,J,N))/WSC(I,J,N))*(WSC(
     CI,J,N)-XICI(I,J,K))
      YOC(I,J,K)=HWC(I,J,K)-HBC(I,J,K)
  340 YIC(I,J,K)=YIC(I,J,K)-HBC(I,J,K)
      WRITE(K2,15)
      WRITE(K2,16)ARAV,VAV,F,NS,NC,RAT
      WRITE(K2,24)
      DO 204 I=1,NS
      MM=NSL(I)+1
      NN=NWS(I)-1
      DO 204 J=1,MM
```

```
      DO 204 K=1,NN
      WRITE(K2,25)I,J,XIS(I,J,K),HWS(I,J,K),HBS(I,J,K),YOS(I,J,K)
  204 CONTINUE
      WRITE(K2,15)
      WRITE(K2,16)ARAV,VAV,F,NS,NC,RAT
      WRITE(K2,26)
      DO 205 I=1,NC
      NN=NSC(I)+1
      MM=NWC(I)-1
      DO 205 J=1,NN
      DO 205 K=1,MM
      WRITE(K2,25)I,J,XIC(I,J,K),HWC(I,J,K),HBC(I,J,K),YOC(I,J,K)
  205 CONTINUE
C     ******************************************************************
C
C   6 POINT LONGITUDINAL VELOCITIES
C
C     ******************************************************************
C
      ALAN=((1./1.334)*63.28)/1000000.
      DO 430 I=1,NS
      NN=NSL(I)+1
      MM=NWS(I)-1
      DO 430 J=1,NN
      DO 430 K=1,MM
      REQS(I,J,K)=REQS(I,J,K)*ALAN
  430 CONTINUE
      DO 440 I=1,NC
      NN=NSC(I)+1
      MM=NWC(I)-1
      DO 440 J=1,NN
      DO 440 K=1,MM
      REQC(I,J,K)=REQC(I,J,K)*ALAN
  440 CONTINUE
C
C     ******************************************************************
C
C   7 SHEAR STRESS DISTRIBUTIONS AT THE CHANNEL BED
C
C     ******************************************************************
C
      DO 720 I=1,NS
      NN=NSL(I)+1
      MM=NWS(I)-1
      DO 720 J=1,NN
      DO 720 K=1,MM
      IF(J.EQ.1)GOTO 721
      IF(J.EQ.NN)GOTO 722
      HBS(I,J,K)=(HBS(I,J-1,K)-HBS(I,J+1,K))/(DSL(I,J-1)+DSL(I,J))
      HWS(I,J,K)=(HWS(I,J-1,K)-HWS(I,J+1,K))/(DSL(I,J-1)+DSL(I,J))
      GOTO 723
  721 HBS(I,J,K)=(HBS(I,J,K)-HBS(I,J+1,K))/DSL(I,J)
      HWS(I,J,K)=(HWS(I,J,K)-HWS(I,J+1,K))/DSL(I,J)
      GOTO 723
  722 HBS(I,J,K)=(HBS(I,J-1,K)-HBS(I,J,K))/DSL(I,J-1)
      HWS(I,J,K)=(HWS(I,J-1,K)-HWS(I,J,K))/DSL(I,J-1)
  723 HBS(I,J,K)=HWS(I,J,K)-(F**2)*(HWS(I,J,K)-HBS(I,J,K))
      IF(HBS(I,J,K).LT.0)HBS(I,J,K)=ABS(HBS(I,J,K))
      HBS(I,J,K)=ASN(I,J)/SQRT(HBS(I,J,K))
      XK=0.446*(STD**0.34)/((F**0.15)*(HBS(I,J,K)/SQRT(981.))**0.15)
```

```
      YIS(I,J,K)=ALOG(YIS(I,J,K)/YOS(I,J,K))
      HBS(I,J,K)=(REQS(I,J,K)/(1.+(SQRT(981.)/(XK*HBS(I,J,K)))*(1.+YIS(I
     C,J,K))))*(1.+SQRT(981.)/(XK*HBS(I,J,K)))
      REQS(I,J,K)=XK*(HBS(I,J,K)-REQS(I,J,K))/YIS(I,J,K)
      REQS(I,J,K)=(REQS(I,J,K)**2)*ROO
      REQS(I,J,K)=REQS(I,J,K)/SHEAR
  720 CONTINUE
      DO 750 I=1,NC
      B(I)=R(I)-W/2.
      NN=NSC(I)+1
      MM=NWC(I)-1
      DO 750 J=1,NN
      DO 750 K=1,MM
      IF(K.EQ.1)GOTO 753
      KK=K-1
      SUM1=0.
      SUM2=0.
      DO 760 KC=1,KK
      SUM1=SUM1+WSC(I,J,KC)
  760 SUM2=SUM2+WSC(I,J,KC)
      B(I)=B(I)+0.5*(SUM1+SUM2)
  753 RR(I,J,K)=B(I)
      IF(J.EQ.1)GOTO 751
      IF(J.EQ.NN)GOTO 752
      HBC(I,J,K)=(HBC(I,J-1,K)-HBC(I,J+1,K))/((DSC(I,J-1)+DSC(I,J))*PI*R
     CR(I,J,K)/180.)
      HWC(I,J,K)=(HWC(I,J-1,K)-HWC(I,J+1,K))/((DSC(I,J-1)+DSC(I,J))*PI*R
     CR(I,J,K)/180.)
      GOTO 754
  751 HBC(I,J,K)=(HBC(I,J,K)-HBC(I,J+1,K))/(DSC(I,J)*PI*RR(I,J,K)/180.)
      HWC(I,J,K)=(HWC(I,J,K)-HWC(I,J+1,K))/(DSC(I,J)*PI*RR(I,J,K)/180.)
      GOTO 754
  752 HBC(I,J,K)=(HBC(I,J-1,K)-HBC(I,J,K))/(DSC(I,J-1)*PI*RR(I,J,K)/180.
     C)
      HWC(I,J,K)=(HWC(I,J-1,K)-HWC(I,J,K))/(DSC(I,J-1)*PI*RR(I,J,K)/180.
     C)
  754 HBC(I,J,K)=HWC(I,J,K)-(F**2)*(HWC(I,J,K)-HBC(I,J,K))
      IF(HBC(I,J,K).LT.0)HBC(I,J,K)=ABS(HBC(I,J,K))
      HBC(I,J,K)=ACN(I,J)/SQRT(HBC(I,J,K))
      XK=0.446*(STD**0.34)/((F**0.15)*(HBC(I,J,K)/SQRT(981.))**0.15)
      YIC(I,J,K)=ALOG(YIC(I,J,K)/YOC(I,J,K))
      HBC(I,J,K)=(REQC(I,J,K)/(1.+(SQRT(981.)/(XK*HBC(I,J,K)))*(1.+YIC(I
     C,J,K))))*(1.+SQRT(981.)/(XK*HBC(I,J,K)))
      REQC(I,J,K)=XK*(HBC(I,J,K)-REQC(I,J,K))/YIC(I,J,K)
      REQC(I,J,K)=(REQC(I,J,K)**2)*ROO
      REQC(I,J,K)=REQC(I,J,K)/SHEAR
  750 CONTINUE
      WRITE(K3,15)
      WRITE(K3,16)ARAV,VAV,F,NS,NC,RAT
      DO 202 I=1,NS
      NN=NSL(I)+1
      MM=NWS(I)-1
      DO 202 J=1,NN
      DO 202 K=1,MM
      WRITE(K3,22)I,J,XIS(I,J,K),REQS(I,J,K)
  202 CONTINUE
      WRITE(K3,15)
      WRITE(K3,16)ARAV,VAV,F,NS,NC,RAT
      DO 203 I=1,NC
      NN=NSC(I)+1
```

```
            MM=NWC(I)-1
            DO 203 J=1,NN
            DO 203 K=1,MM
            WRITE(K3,22)I,J,XIC(I,J,K),REQC(I,J,K)
        203 CONTINUE
C
C           *******************************************************************
C
C                                  *************************
C                                  *************************
C                                  **                     **
C                                  **     SYMBOLS USED    **
C                                  **                     **
C                                  *************************
C                                  *************************
C
C
C           NS    NUMBER OF STRAIGHT CHANNELS
C           NC    NUMBER OF CURVED CHANNELS
C           H     HEAD OF WATER OVER V-NOTCH
C           CI    INITIAL BED LEVEL
C           CIB   FLUME BED LEVEL
C           WS    INITIAL WATER SURFACE LEVEL
C           R     MEAN RADIUS OF CURVATURES
C           SL    STRAIGHT CHANNEL LENGTHS
C           CA    CENTRAL ANGLES OF CURVATURE
C           NSL   NUMBER OF LONGITUDINAL SUBDIVISIONS IN STRAIGHT CHANNELS
C           NSC   NUMBER OF LONGITUDINAL SUBDIVISIONS IN CURVED CHANNELS
C           NWS   NUMBER OF CROSS SUBDIVISION IN STRAIGHT CHANNELS
C           NWC   NUMBER OF CROSS SUBDIVISION IN CURVED CHANNELS
C           DSL   LONGITUDINAL SUBDIVISION LENGTHS IN STRAIGHT CHANNELS
C
            RUN=3.
C
C           DSC   LONGITUDINAL SUBDIVISION ANGLES IN CURVED CHANNELS
C           WSL   CROSS SUBDIVISION LENGTHS IN STRAIGHT CHANNELS
C           WSC   CROSS SUBDIVISION LENGTHS IN CURVED CHANNELS
C           HBS   FINAL BED LEVELS IN STRAIGHT CHANNELS,TRANSFORMED TO HIGHTS
C                 OVER FLUMES BED IN C..1,HIGHTS OF BED AT THE MEASURING POINTS
C                 OVER THE FLUME BED IN C..4
C           HWS   FINAL WATER LEVELS IN STRAIGHT CHANNELS ,TRANSFORMED TO HIGHTS
C                 OVER FLUME BED IN C..1,WATER DEPTHS AT THE MEASURING POINTS
C                 OVER FLUME BED IN C..4
C           HBC   FINAL BED LEVELS IN CURVED CHANNELS ,TRANSFORMED TO HIGHTS
C                 OVER FLUME BED IN C..1,HIGHTS OF BED AT THE MEASURING POINTS
C                 OVER THE FLUME BED IN C..4
C           HWC   FINAL WATER LEVELS IN CURVED CHANNELS,TRANSFORMED TO HIGHTS
C                 OVER FLUME BED IN C..1,WATER DEPTHS AT THE MEASURING POINTS
C                 OVER THE FLUMES BED IN C..4
C           REQS  DOPPLER FREQUENCIES IN STRAIGHT CHANNELS,TRANSFORMED TO POINT
C                 VELOCITIES IN C..6
C           REQC  DOPPLER FREQUENCIES IN CURVED CHANNELS,TRANSFORMED TO POINT
C                 VELOCITIES IN C..6
C           RMSS  RMS-VOLTS IN STRAIGHT CHANNELS
C           RMSC  RMS-VOLTS IN CURVED CHANNELS
C           YOS   VERTICAL LENGTHS OF LASER BEAM FROM THE OUTER FLUME EDGE IN
C                 STRAIGHT CHANNELS,TRANSFORMED TO CORRESPONDING HIGHTS OVER
C                 FLUME BED IN C..4,WATER DEPTHS AT THE MEASURING POINTS IN C..-
C           YIS   VERTICAL LENGTHS OF LASER BEAM FROM THE INNER FLUME EDGE IN
C                 STRAIGHT CHANNELS,TRANSFORMED TO CORRESPONDING HIGHTS OVER
```

```
C             FLUME BED IN C..4.HIGHTS OF MEASURING POINTS OVER THE FLUME
C
        RUN=3.
C
C             BED IN C..4.HIGHTS OF MEASURING POINTS OVER CHANNELS BED IN C..
C       XOS   HORIZONTAL WIDTH OF LASER BEAM IN THE OUTER SIDE OF STRAIGHT
C             CHANNELS.TRANSFORMED TO TOTAL DISTANCES OF MEASURING POINTS
C             FROM THE INNER SIDE OF THE CHANNEL IN C..4
C       XIS   HORIZONTAL WIDTH OF LASER BEAM IN THE INNER SIDE OF STRAIGHT
C             CHANNELS.TRANSFORMED TO THE DISTANCES OF THE MEASURING POINT
C             TO THE INNER SIDE OF THE CHANNEL IN C..4
C       YOC   VERTICAL LENGTHS OF LASER BEAM FROM THE OUTER FLUME EDGE IN
C             CURVED CHANNELS.TRANSFORMED TO CORRESPONDING HIGHTS OVER THE
C             FLUME BED IN C..4.WATER DEPTHS AT THE MEASURING POINTS IN C..4
C       YIC   VERTICAL LENGTHS OF LASER BEAM FROM THE INNER FLUME EDGE IN
C             CURVED CHANNELS.TRANSFORMED TO CORRESPONDING HIGHTS OVER THE
C             FLUME BED IN C..4.HIGHTS OF MEASURING OI
C             FLUME BED IN C..4.HIGHTS OF MEASURING POINTS OVER FLUMES BED
C             IN C..4.HIGHTS OF MEASURING POINT OVER THE CHANNELS BED IN C..4
C       XOC   HORIZONTAL WIDTH OF LASER BEAM IN THE OUTER SIDE OF CURVED
C             CHANNELS .TRANSFORMED TO TOTAL DISTANCES OF MEASURING POINRS
C             FROM THE INNER SIDE OF THE CHANNEL IN C..4
C       XIC   HORIZONTAL WIDTH OF LASER BEAM IN THE INNER SIDE OF CURVED
C             CHANNELS.TRANSFORMED TO THE DISTANCE OF THE MEASURING POINTS
C             TO THE INNER SIDE OF THE CHANNEL IN C..4
C       AS    ELEMENTARY SCOURED OR DEPOSITED AREAS IN STRAIGHT CHANNELS.
C             TRANSFORMED TO CORRESPONDING VOLUMES IN C..2.ELEMENTARY WATER
C             CROSS SECTIONAL AREAS IN C..5
C       ASN   TOTAL SCOURED OR DEPOSITED AREAS IN STRAIGHT CHANNELS.TRANSFOR
C             TO CORRESPONDING VOLUMES IN C..2.TOTAL CROSS SECTIONAL AREAS
C             OF WATER IN C..5
C
        RUN=3.
C
C       AC    ELEMENTARY SCOURED OR DEOSITED AREAS IN CURVED CHANNELS.
C             TRANSFORMED TO CORRESPONDING VOLUMES IN C..2.ELEMENTARY WATER
C             CROSS SECTIONAL AREAS IN C..5
C       ACN   TOTAL SCOURED OR DEPOSITED AREAS IN CURVED CHANNELS.TRANSFORMED
C             TO CORRESPONDING VOLUMES IN C..2.TOTAL CROSS SECTIONAL AREAS
C             OF WATER IN C..5
C       B     RADIUS OF CURVATURES TO THE OUTER FLUME EDGE
C       XS    TOTAL DISTANCES FROM THE STARTING MEASURING SECTION TO THE
C             SLICE END IN STRAIGHT CHANNELS
C       XSC   TOTAL DISTANCES FROM THE STARTING MEASURING SECTION TO THE
C             SLICE CENTER IN STRAIGHT CHANNELS
C       XC    TOTAL DISTANCES FROM THE STARTING MEASURING SECTION TO THE
C             SLICE END IN CURVED CHANNELS
C       XCC   TOTAL DISTANCES FROM THE STARTING MEASURING SECTION TO THE
C             SLICE CENTER IN CURVED CHALLELS
C
C       ***************************************************************
C       ***************************************************************
C       ***************************************************************
        STOP
        END
C
$ENTRY
```

Appendix (B-2)

Computational analysis for Finite Fourier Series,Autoregressive Process,and Moving Average Models.

```
C      ****************************************************************
C      ****************************************************************
C      ****************************************************************
C
C      PART(2) OF THE PROGRAM PREPARED BY MAMDOUH ALY NOUH,CIVIL ENGINEERI
C      DEPARTMENT-OTTAWA UNIVERSITY,TO SIMULATE THE SHEAR STRESS DISTRIBUT
C      ON THE BED OF OPEN CHANNEL BENDS BY USING STOCHASTIC STATIONARY
C      PROCESS-KEPT.
C       THE SHEAR STRESS DATA POINTS ARE OBTAINED FROM THE SAME PROGRAM
C      PART(1) AND INTRODUCED IN THE SYSTEM ON PUNCHED CARDS
C
C      ****************************************************************
C      ****************************************************************
C      ****************************************************************
C      ****************************************************************
C
       DIMENSION X(5,33),Y(33,1),NA(5),NB(5),NCC(5),ND(5),A(33),B(33),PHA
      CSE(33),AMP(33),FREQ(33),SSPEC(33),SUMVAR(33),EST(33,17),COV(33),CO
      RR(33,8),SPP(33,7),XX(33,33),AA(33,33),AC(33,1),ZC(33,1),LL(33),MM(
      C33),DIV(33)
C
C      ****************************************************************
       READ(5,1)NR
       DO 8000 I=1,NR
 8000  READ(5,2)NA(I),NB(I),NCC(I),ND(I)
       DO 9000 I=1,NR
       NJ=NA(I)
 9000  READ(5,4)(X(I,J),J=1,NJ)
C
C      ****************************************************************
C      ****************************************************************
C
       WRITE(6,9001)
       WRITE(6,9003)
       BI=2.*3.14
       DO 1000 N=1,NR
       NP=NA(N)
       NH=NB(N)
       NNH=NH-2
       NS=ND(N)
       INT=NCC(N)
       WRITE(6,11)
       DO 9004 I=1,3
 9004  WRITE(6,21)
       WRITE(6,22)
       WRITE(6,22)
       DO 9005 I=1,3
 9005  WRITE(6,23)
       WRITE(6,8888)
       WRITE(6,8002)(X(N,J),J=1,NP)
C
C      ****************************************************************
C
C      CALCULATION OF THE MEAN
C
C      ****************************************************************
C
       XM=0.
```

```
      DO 30 J=1,NP
   30 XM=XM+X(N,J)
      XMEAN=XM/FLOAT(NP)
C
C     ******************************************************************
C
C     CALCULATION OF THE VARIANCE
C
C     ******************************************************************
      XV=0.
      DO 40 J=1,NP
   40 XV=XV+(X(N,J)-XMEAN)**2
      XVAR=XV/FLOAT(NP)
C
C     ******************************************************************
C
C     HARMONIC ANALYSIS
C
C     ******************************************************************
C
      DO 50 M=1,NH
      A(M)=0.
      B(M)=0.
      PHASE(M)=0.
      AMP(M)=0.
   50 FREQ(M)=0.
      AQ=0.
      FA=-1.
      NNH=NH+1
      DO 60 J=1,NNH
      JJ=J-1
      XJJ=JJ
      FREQ(J)=XJJ/FLOAT(NP)
      DO 70 K=1,NP
      IF(J.EQ.1.AND.NS.EQ.1)GOTO 75
      IF(JJ.EQ.NH.AND.NS.EQ.1)GOTO 17
      CO=BI*FREQ(J)*FLOAT(K)
      A(J)=A(J)+X(N,K)*COS(CO)
      B(J)=B(J)+X(N,K)*SIN(CO)
      GOTO 70
   17 AQ=AQ+FA*X(N,K)
      FA=-FA
   70 CONTINUE
      IF(JJ.EQ.NH.AND.NS.EQ.1)GOTO 37
      A(J)=(A(J)*2.)/FLOAT(NP)
      B(J)=(B(J)*2.)/FLOAT(NP)
      GOTO 74
   37 A(J)=AQ/FLOAT(NP)
      B(J)=0.
      GOTO 74
   75 A(J)=XMEAN
      B(J)=0.
   74 CONTINUE
      PHASE(J)=ATAN(-B(J)/A(J))*(180./3.14)
      AMP(J)=A(J)**2+B(J)**2
   60 CONTINUE
      DO 80 J=1,NH
      SSPEC(J)=0.
```

```
   80 SUMVAR(J)=0.
      SUMX=0.
      DO 90 J=1,NNH
      JJ=J-1
      SSPEC(J)=(AMP(J)*100.)/(2.*XVAR)
      IF(J.EQ.1)SSPEC(J)=(AMP(J)*100.)/XVAR
      NNN=NP/2
      IF(JJ.EQ.NNN)SSPEC(J)=(AMP(J)*100.)/XVAR
      SUMX=SUMX+SSPEC(J)
      SUMVAR(J)=SUMX
   90 CONTINUE
      WRITE(6,91)
      WRITE(6,92)
      WRITE(6,93)
      WRITE(6,94)
      WRITE(6,95)
      WRITE(6,96)
      WRITE(6,97)
      WRITE(6,96)
      DO 100 J=1,NNH
      L=J-1
      WRITE(6,98)L,A(J),B(J),AMP(J),PHASE(J),SSPEC(J),SUMVAR(J),FREQ(J)
  100 CONTINUE
      WRITE(6,96)
      WRITE(6,96)
      WRITE(6,99)XMEAN,XVAR
C
C     ************************************************************************
C
      WRITE(6,101)
      WRITE(6,102)
      WRITE(6,103)
      WRITE(6,104)
      JH=NH-1
      WRITE(6,106)(J,J=1,12)
      WRITE(6,102)
      WRITE(6,102)
      DO 107 K=1,NP
      XEST=0.
      NNH=NH-1
      DO 108 L=1,NH
      J=L+1
      CO=BI*FREQ(J)*FLOAT(K)
      XEST=XEST+A(J)*COS(CO)+B(J)*SIN(CO)
      M=J-1
      EST(K,M)=XEST+XMEAN
  108 CONTINUE
  107 CONTINUE
      DO 109 K=1,NP
      Y(K,1)=X(N,K)
  109 CONTINUE
      DO 112 K=1,NP
  112 WRITE(6,113)Y(K,1),(EST(K,I),I=1,12)
      WRITE(6,102)
      WRITE(6,102)
C
C     ************************************************************************
C
```

```
C       CORRELATION ANALYSIS
C
C       ********************************************************************
C
        WRITE(6,134)
        WRITE(6,131)
        WRITE(6,132)
        WRITE(6,133)
        WRITE(6,431)
        WRITE(6,133)
        WRITE(6,132)
        WRITE(6,135)
        WRITE(6,136)
        WRITE(6,137)
        WRITE(6,132)
        KM=NP-1
        DO 121 K=1,KM
        AX=0.
        NK=NP-K
        DO 122 J=1,NK
    122 AX=AX+(X(N,J)-XMEAN)*(X(N,(J+K))-XMEAN)
        AZ=1.96*SQRT(FLOAT(NK)-1.)
        COV(K)=AX/FLOAT(NP)
        COR(K,2)=COV(K)/XVAR
        COR(K,3)=(-1.+AZ)/FLOAT(NK)
        COR(K,4)=(-1.-AZ)/FLOAT(NK)
        WRITE(6,123)K,COV(K),COR(K,2),COR(K,3),COR(K,4)
    121 CONTINUE
        WRITE(6,132)
        WRITE(6,132)
        WRITE(6,609)
        NK=NP-1
        DO 601 I=1,NK
        XX(1,1)=1.
        II=I+1
        XX(1,II)=COR(I,2)
    601 CONTINUE
        DO 602 K=1,NP
        XX(K,1)=XX(1,K)
    602 CONTINUE
        DO 603 I=2,NP
        DO 603 K=1,NP
        K1=K+1
        K2=K-1
        I1=I-1
        IF(I.GE.K)GOTO 604
        XX(I,K)=XX(I1,K2)
        GOTO 603
    604 IF(I.GT.K)GOTO 606
        XX(I,K)=1.
        GOTO 603
    606 XX(I,K)=XX(K,I)
    603 CONTINUE
        DO 607 I=1,NP
    607 WRITE(6,608)(XX(I,K),K=1,NP)
        DO 705 I=1,NP
        DO 705 K=1,NP
    705 AA(I,K)=(XX(I,K)*XVAR)*100.
```

```
      WRITE(6,600)
      DO 706 I=1,NP
  706 WRITE(6,608)(AA(I,K),K=1,NP)
      WRITE(6,1111)
C
C     ******************************************************************
C
C     SPECTRAL ANALYSIS
C
C     ******************************************************************
C
      WRITE(6,141)
      WRITE(6,142)
      WRITE(6,143)
      WRITE(6,142)
      WRITE(6,144)
      WRITE(6,142)
      ACC=0.
      ASS=0.
      NNH=NH+1
      DO 145 I=1,NNH
      SUMA=0.
      SUMB=0.
      DO 146 J=1,KM
      AZ=COS(BI*FREQ(I)*FLOAT(J))
      SUMA=SUMA+COR(J,2)*AZ
      BWIN=1.-FLOAT(J)/FLOAT(NP)
      IF(FLOAT(J).GE.FLOAT(NP))BWIN=0.
  146 SUMB=SUMB+BWIN*COR(J,2)*AZ
      SPP(I,1)=FREQ(I)
      SPP(I,2)=2.*(1.+2.*SUMA)
      SPP(I,3)=2.*(1.+2.*SUMB)
      IF(I.EQ.1.OR.I.EQ.NH)GOTO 147
      ACC=ACC+SPP(I,2)
      ASS=ASS+SPP(I,3)
      GOTO 148
  147 ACC=ACC+0.5*SPP(I,2)
      ASS=ASS+0.5*SPP(I,3)
      IF(I.LT.NH)GOTO 145
      ACC=ACC/(2.*NH)
  148 ASS=ASS/(2.*NH)
  145 CONTINUE
      NNH=NH+1
      DO 151 I=1,NNH
  151 WRITE(6,152)SPP(I,1),SPP(I,2),SPP(I,3)
      WRITE(6,142)
      WRITE(6,142)
      WRITE(6,153)ACC,ASS
C
C
C
C     ******************************************************************
C
C     AUTOREGRESSIVE ANALYSIS_FIRST AND SECOND ORDER LINEAR MODELS
C
C     ******************************************************************
C
```

```
      WRITE(6,43)
      WRITE(6,44)
      PH1=COR(1,2)
      PH21=COR(1,2)*(1.-COR(2,2))/(1.-(COR(1,2)**2))
      PH22=(COR(2,2)-COR(1,2)**2)/(1.-COR(1,2)**2)
      WRITE(6,45)
      WRITE(6,46)PH1,PH21,PH22
      NK=NP-1
      DO 47 K=1,NK
   47 COR(K,5)=PH1**K
      NNH=NP+1
      DO 48 I=1,NNH
      XI=I-1.
      FREQ(I)=XI/FLOAT(NP)
   48 SPP(I,4)=2.*(1.-PH1**2)/(1.+PH1**2-2.*PH1*COS(2.*3.14*FREQ(I)))
      A1=PH21**2+4.*PH22
      IF(A1)51,52,53
   51 WRITE(6,54)
      R1=SQRT(-PH22)
      R2=ARCOS(ABS(PH21)/(2.*R1))
      R3=ATAN(((1.+R1**2)/(1.-R1**2))*TAN(R2*180./3.14))
      R4=(R2*180./3.14)/(2.*3.14)
      WRITE(6,7000)R1,R4,R3
      NK=NP-1
      DO 55 K=1,NK
   55 COR(K,6)=(R1**K)*COS(((R2*K)-R3)*(180./3.14))/COS(R3*180./3.14)
      GOTO 59
   52 NK=NP-1
      DO 56 K=1,NK
   56 COR(K,6)=COR(K,5)
      GOTO 59
   53 WRITE(6,58)
      G1=(PH21+SQRT(PH21**2+4.*PH22))/2.
      G2=(PH21-SQRT(PH21**2+4.*PH22))/2.
      WRITE(6,57)G1,G2
      NK=NP-1
      DO 61 K=1,NK
   61 COR(K,6)=(G1*(1.-G2**2)*G1**K-G2*(1.-G1**2)*G2**K)/((G1-G2)*(1.+G1
     C*G2))
   59 DO 62 K=1,NP
   62 DIV(K)=X(N,K)-XMEAN
      DI=0.
      DO 63 K=1,NP
   63 DI=DI+DIV(K)
      DIVM=DI/FLOAT(NP)
      DV=0.
      DO 64 K=1,NP
   64 DV=DV+(DIV(K)-DIVM)**2
      DIVAR=DV/FLOAT(NP)
      SYGMA=DIVAR*(1.-COR(1,2)*PH21-COR(2,2)*PH22)
      NNH=NH+1
      DO 65 J=1,NNH
   65 SPP(J,5)=(2.*SYGMA)/((1.+PH21**2+PH22**2-2.*PH21*(1.-PH22)*COS(2.*
     C3.14*FREQ(J))-2.*PH22*COS(4.*3.14*FREQ(J)))*XVAR)
      WRITE(6,311)
      WRITE(6,312)
      WRITE(6,313)
      WRITE(6,314)
```

```
      WRITE(6,312)
      WRITE(6,66)
      WRITE(6,67)
      WRITE(6,68)
      WRITE(6,312)
      KM=NP-1
      DO 71 K=1,KM
   71 WRITE(6,333)K,COR(K,2),COR(K,5),COR(K,6)
      WRITE(6,312)
      WRITE(6,312)
      WRITE(6,241)
      WRITE(6,242)
      WRITE(6,243)
      WRITE(6,242)
      WRITE(6,244)
      WRITE(6,242)
      NNH=NH+1
      DO 27 J=1,NNH
   27 WRITE(6,252)SPP(J,1),SPP(J,2),SPP(J,4),SPP(J,5)
      WRITE(6,242)
      WRITE(6,242)
C
C     *******************************************************************
C
C     ANALYSIS OF FIRST AND SECOND ORDER MARKOVIAN MODELS
C
C     *******************************************************************
C
      WRITE(6,7001)
      E=COR(1,2)
      F=COR(2,2)
      NG=10000
      DO 7005 J=1,NG
      I=J-NG/2
      XI=I/100.
      D=(XI**5)*(F**4)+(XI**4)*(3.*E*(F**3))+(XI**3)*(2.*F**4+F**3+(3.*(
     CE**2)*(F**2)))+(XI**2)*(4.*E*(F**3)+(2.*E*(F**2))+(E**3)*F)+XI*(3.
     C*(E**2)*(F**2)+((E**2)*F))+(E**3)*F
      XL=ABS(D)
      XXL=1./100.
      IF(XL.GT.XXL)GOTO 7005
      GOTO 7006
 7005 CONTINUE
 7006 SI=ABS(XI)
      IF(SI.GE.2)XI=1./XI
      THE21=XI
      THE22=(F*XI)/((F*XI)+E)
      DO 7007 J=1,NG
      I=J-NG/2
      XI=I/100.
      D=(XI**2)*E+XI+E
      XL=ABS(D)
      XXL=1./100.
      XXXL=2.*XXL
      IF(XL.GT.XXXL.AND.XL.GT.XXXL)GOTO 7007
      IF(XL.GT.XXXL.AND.XL.LE.XXXL)GOTO 7008
      GOTO 7008
 7007 CONTINUE
```

```
 7008 SI=ABS(XI)
      IF(SI.GE.2)XI=1./XI
      THE1=XI
      VARN=XVAR/(1.+THE1**2)
      VVRN=XVAR/(1.+THE21**2+THE22**2)
      NNH=NH+1
      DO 7009 J=1,NNH
      E=THE21
      F=THE22
      SPP(J,7)=2.*VVRN*(1.+E**2+F**2-2.*E*(1.-F)*COS(2.*3.14*(FREQ(J)))-
     C2.*F*COS(4.*3.14*FREQ(J)*(180./3.14)))/XVAR
      E=THE1
      F=0.
      SPP(J,6)=2.*VARN*(1.+E**2-2.*E*COS(3.14*FREQ(J)*(180./3.14)))/XVAR
 7009 CONTINUE
      WRITE(6,7002)THE1,THE21,THE22
      WRITE(6,241)
      WRITE(6,242)
      WRITE(6,243)
      WRITE(6,242)
      WRITE(6,244)
      WRITE(6,242)
      NNH=NH+1
      DO 7004 J=1,NNH
 7004 WRITE(6,252)SPP(J,1),SPP(J,2),SPP(J,6),SPP(J,7)
      WRITE(6,242)
      WRITE(6,242)
      WRITE(6,33)
      WRITE(6,31)
      WRITE(6,31)
      WRITE(6,31)
      WRITE(6,31)
 1000 CONTINUE
      DO 2000 N=1,NR
      NI=NP
      CALL MINV(XX,NI,YY,LL,MM)
      COR(NP,2)=0.
      DO 701 I=1,NP
  701 AC(I,1)=COR(I,2)
      CALL GMPRD(XX,AC,ZC,NP,NP,1)
      WRITE(6,134)
      WRITE(6,702)
      DO 703 I=1,NP
  703 WRITE(6,704)I,ZC(I,1)
 2000 CONTINUE
C
C     ***************************************************************
C
      WRITE(6,555)
C
C     ***************************************************************
C     ***************************************************************
C
C     FORMAT STATMENTS
C
C     ***************************************************************
C     ***************************************************************
C
```

```
      1 FORMAT(I2)
      2 FORMAT(4(I3))
      4 FORMAT(8F10.2)
     11 FORMAT('1',20(/),55X,'TIME SERIES ANALYSIS FOR;')
     21 FORMAT(55X,32('*'))
     22 FORMAT(60X,22('*'))
     23 FORMAT(68X,6('*'))
     31 FORMAT('1')
     32 FORMAT('1',///,60X,'ANALYSIS OF THE RESULTS'/60X,23('*')/60X,23('*
       C'))
     33 FORMAT('1',///,60X,'GENERAL ANALYSIS'/60X,16('*')/60X,16('*'))
     43 FORMAT('1',//////////,55X,'ANALYSIS OF LINEAR MODELS'/55X,25('*')/
       C55X,25('*')/55X,25('*'))
     44 FORMAT(/////,55X,'AUTOREGRESSIVE PROCESSES'/55X,24('*')/55X,24('*'
       C))
     45 FORMAT('1',/////,50X,'PARAMETERS FOR AUTOREGRESSIVE PROCESSES ARE:
       C'/50X,44('*')/50X,44('*'))
     46 FORMAT(////,20X,'FOR FIRST ORDER PHI=',F10.4,20X,'FOR SECOND ORDER
       C PHI=',F10.4,5X,'AND',F10.4)
     54 FORMAT(//////,70X,'THE ROOTS OF THE CHARACTERISTICS EQUATION ARE C
       COMPLEX'/70X,53('*'))
     57 FORMAT(///,70X,'THE ROOTS ARE :'/70X,14('*')/75X,F9.4/75X,F9.4)
     58 FORMAT(////,70X,'THE ROOTS OF THE CHARACTERISTICS EQUATION ARE REA
       CL'/70X,50('*'))
     66 FORMAT(40X,'**',2(10X,'*'),2X,'OUTOREG   PROCESS',2X,'**')
     67 FORMAT(40X,'**',3X,'LAG',4X,'*',1X,'OUTOCOR',2X,24('*'))
     68 FORMAT(40X,'**',2(10X,'*'),2X,'FIRST',3X,'*',3X,'SECOND',1X,'**')
     69 FORMAT(40X,'**',4(10X,'*'),'*'/40X,'**',4X,I2,4X,3('*',1X,F8.2,1X)
       C,'**')
     72 FORMAT('1',/////,40X,46('*'))
     73 FORMAT(40X,46('*'))
     91 FORMAT('1',//////////,20X,89('*'))
     92 FORMAT(20X,10('*'),69X,10('*'))
     93 FORMAT(20X,10('*'),12X,'ANALYSIS OF VARIANCE TABLE FOR GIVEN SERIE
       CS',14X,10('*'))
     94 FORMAT(20X,40('*'),3X,'NOUH',3X,39('*'))
     95 FORMAT(20X,40('*'),1X,'SH.STRESS',1X,38('*'))
     96 FORMAT(20X,89('*'))
     97 FORMAT(20X,'**',1X,'HARMONIC','*',2X,'COEF A',2X,'*',2X,'COEF B',2
       CX,'*','AMPLITUDE',1X,'*',2X,'PHASE',3X,'*',2X,'EX VAR',2X,'*','SUM
       C EX VAR','*','FREQUENCY','**')
     98 FORMAT(20X,'**',9X,6('*',10X),'*',9X,'**'/20X,'**',4X,I2,3X,6('*',
       C1X,F8.3,1X),'*',1X,F7.5,1X,'**')
     99 FORMAT(////////,20X,'SERIES MEAN VALUE=',F10.2,20X,'SERIES TOTAL V
       CARIANCE=',F10.2)
    101 FORMAT('1',//,10X,120('*'))
    102 FORMAT(10X,120('*'))
    103 FORMAT(10X,'**',8X,'*',46X,'ESTIMATED VALUES',45X,'**')
    104 FORMAT(10X,'**','OBSERVED',110('*'))
    106 FORMAT(10X,11('*'),12(1X,I2,'HAR',2X,'*'),'*')
    113 FORMAT(10X,'*',13('*',8X),'**'/10X,'**',13(2X,F5.2,1X,'*'),'*')
    123 FORMAT(40X,'**',5(10X,'*'),'*'/40X,'**',4X,I2,4X,4('*',1X,F8.2,1X)
       C,'**')
    131 FORMAT('1',////,40X,58('*'))
    132 FORMAT(40X,58('*'))
    133 FORMAT(40X,'**',54X,'**')
    134 FORMAT('1',//////////////////////,55X,'CORRELATION ANALYSIS'/55X,20(
       C'*')/55X,20('*'))
```

```
  135 FORMAT(40X,'**',3(10X,'*'),2X,'CONFIDENCE LIMITS',2X,'**')
  136 FORMAT(40X,'**',3X,'LAG',4X,'*',1X,'OUTOCCV.',1X,'*',1X,'OUTOCOR.'
     C,1X,24('*'))
  137 FORMAT(40X,'**',3(10X,'*'),2X,'UPPER',3X,'*',3X,'LOWER',2X,'**')
  141 FORMAT('1',/////////////,45X,51('*'))
  142 FORMAT(45X,51('*'))
  143 FORMAT(45X,'**',15X,'SPECTRAL ANALYSIS',15X,'**')
  144 FORMAT(45X,'**',3X,'FREQUENCY',3X,'*',3X,'SPECTRAL',4X,'*',1X,'SMO
     COTH SPECT',2X,'**')
  152 FORMAT(45X,'**',3(15X,'*'),'*'/45X,'**',3(2X,F10.4,3X,'*'),'*')
  153 FORMAT(////,65X,F10.4,6X,F10.4)
  241 FORMAT('1',/////////////,53X,67('*'))
  242 FORMAT(53X,67('*'))
  243 FORMAT(53X,'**',25X,'SPECTRAL ANALYSIS',21X,'**')
  244 FORMAT(53X,'**',3X,'FREQUENCY',3X,'*',3X,'OBSERVED',4X,'*',1X,'FIR
     CST PROCESS',1X,'*',1X,'SECOND PROCESS','**')
  252 FORMAT(53X,'**',4(15X,'*'),'*'/53X,'**',4(2X,F10.4,3X,'*'),'*')
  311 FORMAT('1',////,40X,47('*'))
  312 FORMAT(40X,47('*'))
  313 FORMAT(40X,'**',43X,'**')
  314 FORMAT(40X,'**',12X,'CORRELATION ANALYSIS',11X,'**')
  333 FORMAT(40X,'**',4(10X,'*'),'*'/40X,'**',4X,I2,4X,3('*',1X,F8.2,1X)
     C,'**')
  431 FORMAT(40X,'**',17X,'CORRELATICN ANALYSIS',17X,'**')
  600 FORMAT('1',/////,60X,'COVERIANCE MATRIX'/60X,17('*')/60X,17('*'))
  608 FORMAT(7X,24(F5.2),/)
  609 FORMAT('1',/////,60X,'CORRELATION MATRIX'/60X,18('*')/60X,18('*'))
  702 FORMAT('1',//////,30X,'PHI',37X,'OUTOCORRELATICN TERMS'/30X,'***',
     C40X,15('*')/30X,'***',40X,15('*'))
  704 FORMAT(31X,I2,42X,F10.6)
 6066 FORMAT(40X,'**',3(10X,'*'),2X,'MOVING AV PRCCESS',2X,'**')
 7000 FORMAT(/////,70X,'THE DAMPING FACTOR=',F10.4/70X,'THE FREQUENCY
     C   =',F10.4/70X,'THE PHASE            =',F10.4)
 7001 FORMAT('1',/////////////////////,50X,'FIRST AND SECOND MOVING AVARA
     CGE PROCESS'/50X,39('*')/50X,39('*'))
 7002 FORMAT(///,20X,'PARAMETER OF FIRST ORDER PROCESS',20X,'PARAMETERS
     CFOR SECOND ORDER PROCESS'/20X,32('*'),20X,35('*')///30X,F12.4,40X,
     CF10.4,5X,F10.2)
 8002 FORMAT(30X,8F10.2,/)
 8888 FORMAT('1',///////////,47X,'THE OBSERVATICNS OF THE SERIES ARE AS F
     COLLOW:'/47X,46('*')/47X,46('*'))
 9001 FORMAT('1',/////,55X,'FOURIER ANALYSIS FOR TIME SERIES'/55X,'PERIO
     CDGRAM-SPECTRUM-CORRLOGRAM'/55X,30('*')/55X,30('*'))
 9002 FORMAT(//,25X,'THIS ANALYSIS OF TIME SERIES IS BASED ON FOURIER TR
     CANSFORMATION(HARMONICS)'/20X,'NUMBER OF HARMONICS IS LIMITED TO ON
     CE HALF OF TOTAL NUMBER OF OBSERVATIONS IN EACH RUN'/20X,'NUMBER OF
     CLAGS USED IN CORRELATION ANALYSIS IS LIMITED TO ONE FOURTH TOTAL N
     CUMBER OF OBSERVATIONS'/20X,'NUMBER OF SETS IS LIMITED TO FIVE WIT
     C  (25)     DATA POINTS EACH'/20X,'BARTLETTS LAG WINDOW METHOD IS US
     CED IN SMOOTHING THE SPECTRUM'/20X,'FOR MORE LAGS USE OBEICUS VALUE
     CS TILL THE NUMBER OF OBSERVATIONS MINUS ONE')
 9003 FORMAT(/////,25X,'THE SYMBOLS USED IN THIS PROGRAM ARE AS FOLLOW:'
     C/20X,'NR=NUMBER OF DATA SETS'/20X,'NA=NUMBER OF DATA POINTS IN EAC
     CH SET'/20X,'NB=NUMBER OF OF HARMONICS IN EACH SET')
  555 FORMAT(//////,25X,'THIS ANALYSIS IS DONE BY MAMDOUH ALY NOUH'/20X,
     C'MARCH 18 TH,1977'/20X,'UNIVERSITY OF OTTAWA'/20X,'CIVIL ENGINEERI
     CNG DEPARTMENT',//////////////////////)
 1111 FORMAT(//,7X,'THE VARIANCE VALUES ARE MULTIPL BY 100'/7X,40('*'))
```

```
C
C
C     ******************************************************************
C     ******************************************************************
C     ******************************************************************
C     ******************************************************************
C
      STOP
      END
```

Appendix (C)

Figures

Appendix (C-1)

Stable Channel

Fig.6.11- Bed topography of stable straight channel.

NUMBER OF STRAIGHT CHANNELS= 2

NUMBER OF CURVED CHANNELS= 1

MEAN RADIUS TO WIDTH RATIO= 3.00

ST. CHANNEL NO.	NO. OF CROSS SECTION	BED LEVELS ACROSS THE SECTION-INITIAL BED LEVEL IS A REFERANCE						
1	1	0.00	-0.10	0.10	0.10	0.20	0.20	-0.10
1	2	0.00	0.00	0.00	0.25	0.25	0.30	0.00
1	3	0.10	-0.05	0.20	0.20	0.25	0.20	0.10
1	4	0.00	0.00	0.20	0.10	0.10	0.10	0.10
1	5	0.00	-0.10	0.10	0.20	0.20	0.20	0.10
1	6	0.10	-0.10	0.10	0.20	0.20	0.20	0.10
2	1	1.20	1.80	1.10	0.20	-1.00	-3.70	-4.80
2	2	0.00	1.00	1.45	1.00	-2.60	-4.60	-5.30
2	3	-0.10	-0.10	0.80	0.30	-1.80	-4.50	-5.10
2	4	-0.10	0.00	0.30	-0.20	-1.80	-4.00	-4.10
2	5	-0.10	0.20	0.70	-0.10	-1.80	-3.30	-3.00
2	6	-0.20	0.20	1.00	0.00	-1.70	-2.70	-2.50
2	7	0.10	0.10	1.00	0.30	-0.40	-1.60	-2.20
2	8	-0.20	0.25	1.20	0.80	-0.10	-1.30	-2.00
2	9	0.20	0.20	0.80	0.90	0.20	-0.90	-1.70
2	10	-0.15	-0.15	0.70	0.70	0.20	-1.10	-1.50
2	11	0.00	0.00	0.35	0.50	0.20	-1.10	-1.00
2	12	-0.20	0.00	0.40	0.50	0.20	0.00	-0.10
2	13	0.10	0.00	0.20	0.35	0.30	0.25	0.30
2	14	-0.10	-0.50	0.30	0.40	1.00	0.70	0.40
2	15	-0.20	-0.80	0.20	0.75	1.00	0.65	0.45
2	16	-0.10	-0.30	0.25	0.70	0.70	0.50	0.40
2	17	0.40	-0.10	0.50	0.40	0.50	0.50	0.40
2	18	0.00	0.20	0.20	0.20	0.20	0.30	0.50
2	19	0.20	0.10	0.10	0.00	0.20	0.30	0.40
2	20	0.20	-0.10	0.00	-0.10	0.00	0.10	0.30

Fig.C1.2-Bed topography of stable curved channel.

NUMBER OF STRAIGHT CHANNELS= 2

NUMBER OF CURVED CHANNELS= 1

MEAN RADIUS TO WIDTH RATIO= 3.00

****

CURVED CHANNEL NO.	NO. OF CROSS SECTION	BED LEVELS ACROSS THE SECTION-INITIAL BED LEVEL IS A REFERANCE						
1	1	0.10	-0.10	0.10	0.20	0.20	0.20	0.10
1	2	0.20	0.05	0.00	0.10	0.25	0.30	0.30
1	3	0.40	-0.35	-0.30	-0.40	0.00	0.00	0.00
1	4	0.80	-0.30	-0.90	-0.50	-0.30	-0.15	0.00
1	5	1.40	0.40	-0.20	-0.30	-0.75	-0.40	-0.10
1	6	1.85	1.00	0.00	-0.30	-0.50	-0.70	-0.80
1	7	1.20	1.80	1.10	0.20	-1.00	-3.70	-4.80

Fig.C1.3 -Water surface configuration of stable straight sand bed channel.

NUMBER OF STRAIGHT CHANNELS= 2

NUMBER OF CURVED CHANNELS= 1

MEAN RADIUS TO WIDTH RATIO= 3.00

****

ST. CHANNEL NO.=	NO. OF CROSS SECTION=	WATER LEVELS ACROSS THE SECTION-INITIAL WATER LEVEL IS A REFERANCE						
1	1	0.00	0.00	0.00	0.00	0.00	0.00	0.00
1	2	0.00	0.00	0.00	0.00	0.00	0.00	0.00
1	3	0.00	0.00	0.00	0.00	0.00	0.00	0.00
1	4	-0.10	-0.05	-0.05	0.00	0.00	0.00	0.00
1	5	0.00	-0.10	-0.10	-0.10	-0.10	-0.10	-0.10
1	6	0.00	-0.10	-0.05	-0.10	-0.10	-0.10	-0.10
2	1	-0.55	-0.50	-0.45	-0.35	-0.30	-0.10	0.00
2	2	-0.60	-0.65	-0.50	-0.40	-0.40	-0.30	-0.20
2	3	-0.40	-0.40	-0.30	-0.20	-0.20	-0.15	0.00
2	4	-0.30	-0.30	-0.30	-0.20	-0.20	-0.15	0.00
2	5	-0.20	-0.25	-0.20	-0.15	-0.25	-0.10	0.00
2	6	-0.30	-0.30	-0.20	-0.20	-0.20	-0.15	-0.20
2	7	-0.20	-0.20	-0.20	-0.20	-0.20	-0.20	-0.20
2	8	-0.20	-0.20	-0.20	-0.20	-0.20	-0.20	-0.20
2	9	-0.10	-0.20	-0.20	-0.10	-0.10	-0.10	-0.10
2	10	-0.10	-0.10	-0.10	-0.10	-0.10	-0.10	-0.10
2	11	-0.15	-0.15	-0.15	0.00	0.00	0.00	0.00
2	12	-0.10	-0.10	-0.10	-0.10	-0.10	-0.10	-0.05
2	13	-0.10	-0.10	-0.10	0.00	0.00	0.00	0.00
2	14	-0.10	-0.10	-0.15	-0.15	-0.20	-0.20	-0.20
2	15	-0.20	-0.20	-0.20	-0.20	-0.20	-0.20	-0.20
2	16	-0.20	-0.20	-0.20	-0.20	-0.20	-0.20	-0.20
2	17	0.00	-0.05	-0.10	-0.10	-0.20	-0.20	-0.20
2	18	-0.25	-0.30	-0.30	-0.30	-0.30	-0.30	-0.30
2	19	-0.40	-0.40	-0.40	-0.40	-0.40	-0.40	-0.40
2	20	-0.50	-0.50	-0.50	-0.50	-0.50	-0.50	-0.50

Fig.C1.4 - Water surface configuration of stable curved sand bed channel.

NUMBER OF STRAIGHT CHANNELS= 2

NUMBER OF CURVED CHANNELS= 1

MEAN RADIUS TO WIDTH RATIO= 3.00

****

CURVED CHANNEL NO.	NO. OF CROSS SECTION	WATER LEVELS ACROSS THE SECTION-INITIAL WATER LEVEL IS A REFERANCE						
1	1	0.00	-0.10	-0.05	-0.10	-0.10	-0.10	-0.10
1	2	-0.20	-0.20	-0.15	-0.10	0.00	0.05	0.05
1	3	-0.20	-0.20	-0.10	0.00	0.00	0.00	0.00
1	4	-0.30	-0.30	-0.30	-0.30	-0.20	-0.10	-0.10
1	5	-0.45	-0.35	-0.30	-0.20	-0.15	0.00	0.00
1	6	-0.50	-0.60	-0.50	-0.30	-0.25	-0.20	-0.10
1	7	-0.55	-0.50	-0.45	-0.35	-0.30	-0.10	0.00

Fig. C1.5 Stable cross sectional areas of water in stable straight sand bed channel.

NUMBER OF STRAIGHT CHANNELS= 2

NUMBER OF CURVED CHANNELS= 1

MEAN RADIUS TO WIDTH RATIO= 3.00

ST. CHANNEL NO.	N. OF CROSS SECTION	TOTAL CHANGE IN THE AREA	CHANGES IN THE AREAS 5-CMS INTERVAL					
1	1	2.25	-0.3	-0.0	0.5	0.7	1.0	0.2
1	2	4.00	0.0	0.0	0.6	1.3	1.4	0.8
1	3	4.50	0.1	0.4	1.0	1.1	1.1	0.7
1	4	2.75	0.0	0.5	0.7	0.5	0.5	0.5
1	5	3.25	-0.3	-0.0	0.7	1.0	1.0	0.7
1	6	3.50	-0.0	-0.0	0.7	1.0	1.0	0.7
2	1	-17.00	7.5	7.2	3.2	-2.0	-11.8	-21.3
2	2	-32.00	2.5	6.1	6.1	-4.0	-18.0	-24.8
2	3	-39.50	-0.5	1.7	2.8	-3.8	-15.8	-24.0
2	4	-39.00	-0.3	0.8	0.3	-5.0	-14.5	-20.3
2	5	-29.25	0.2	2.2	1.5	-4.8	-12.8	-15.8
2	6	-22.75	0.0	3.0	2.5	-4.3	-11.0	-13.0
2	7	-8.25	0.5	2.7	3.3	-0.3	-5.0	-9.5
2	8	-1.25	0.1	3.6	5.0	1.7	-3.5	-8.3
2	9	2.25	1.0	2.5	4.2	2.7	-1.8	-6.5
2	10	-2.38	-0.8	1.4	3.5	2.2	-2.3	-6.5
2	11	-2.75	0.0	0.9	2.1	1.7	-2.3	-5.3
2	12	4.75	-0.5	1.0	2.2	1.7	0.5	-0.3
2	13	6.50	0.2	0.5	1.4	1.6	1.4	1.4
2	14	10.25	-1.5	-0.5	1.7	3.5	4.2	2.7
2	15	9.62	-2.5	-1.5	2.4	4.4	4.1	2.7
2	16	10.00	-1.0	-0.1	2.4	3.5	3.0	2.2
2	17	11.00	0.7	1.0	2.2	2.2	2.5	2.2
2	18	6.75	0.5	1.0	1.0	1.0	1.3	2.0
2	19	5.00	0.7	0.5	0.2	0.5	1.3	1.7
2	20	0.75	0.2	-0.3	-0.3	-0.3	0.2	1.0

Fig. C1.6 -Stable cross sectional areas of water in stable curved sand bed channel.

NUMBER OF STRAIGHT CHANNELS= 2

NUMBER OF CURVED CHANNELS= 1

MEAN RADIUS TO WIDTH RATIO= 3.00

****

CURVED CHANNEL NO.	NO. OF CROSS SECTION	TOTAL CHANGE IN THE AREA	CHANGES IN THE AREAS 5-CMS INTERVAL					
1	1	3.50	-0.0	-0.0	0.7	1.0	1.0	0.7
1	2	4.75	0.6	0.1	0.2	0.9	1.4	1.5
1	3	-4.25	0.1	-1.6	-1.8	-1.0	0.0	0.0
1	4	-8.75	1.3	-3.0	-3.5	-2.0	-1.1	-0.4
1	5	-3.00	4.5	0.5	-1.3	-2.6	-2.9	-1.3
1	6	0.12	7.1	2.5	-0.8	-2.0	-3.0	-3.8
1	7	-17.00	7.5	7.2	3.2	-2.0	-11.8	-21.3

Fig.C1.7 -Scoured and deposited volumes of sand in stable straight sand bed channel.

NUMBER OF STRAIGHT CHANNELS= 2

NUMBER OF CURVED CHANNELS= 1

MEAN RADIUS TO WIDTH RATIO= 3.00

ST. CHANNEL NO.	N. OF CROSS SECTION	TOTAL CHANGE IN THE VOL.	CHANGES IN THE VOLS. 5-CMS INTERVAL					
1	1	23.91	-1.0	-0.0	4.3	7.6	9.1	3.8
1	2	43.18	0.6	1.9	8.3	12.1	12.7	7.6
1	3	27.73	0.5	3.3	6.7	6.2	6.2	4.8
1	4	34.50	-1.4	2.9	8.6	8.6	8.6	7.2
1	5	11.81	-0.4	-0.0	2.6	3.5	3.5	2.6
2	1	-159.25	32.5	43.5	30.5	-19.5	-96.7	-149.5
2	2	-525.53	14.7	57.9	65.2	-57.0	-248.1	-358.3
2	3	-302.23	-2.9	9.6	11.5	-33.7	-116.5	-170.4
2	4	-348.08	-0.0	15.3	8.9	-49.7	-139.0	-183.6
2	5	-132.08	0.6	13.3	10.2	-22.9	-60.3	-73.0
2	6	-118.11	1.9	21.9	21.9	-17.1	-61.0	-85.7
2	7	-36.20	2.4	24.3	31.4	5.7	-32.4	-67.6
2	8	6.35	7.1	38.9	58.7	28.6	-33.3	-93.7
2	9	-0.79	1.6	24.6	49.2	31.7	-25.4	-82.6
2	10	-23.06	-3.4	10.1	25.3	18.0	-20.3	-52.9
2	11	11.40	-2.8	10.7	24.9	19.9	-10.0	-31.4
2	12	85.72	-1.9	11.4	27.6	25.7	14.3	8.6
2	13	127.63	-9.5	-0.0	23.8	39.1	42.9	31.4
2	14	176.89	-35.6	-17.8	36.7	70.1	74.5	48.9
2	15	149.54	-26.7	-12.4	36.2	60.0	54.3	38.1
2	16	186.69	-2.2	7.8	41.1	51.1	48.9	40.0
2	17	112.89	7.9	12.7	20.7	20.7	23.8	27.0
2	18	89.53	9.5	11.4	9.5	11.4	19.0	28.6
2	19	51.12	8.9	2.2	-0.0	2.2	13.3	24.4

Fig. C1.8-Scoured and deposited volumes of sand in stable curved sand bed channel.

NUMBER OF STRAIGHT CHANNELS= 2

NUMBER OF CURVED CHANNELS= 1

MEAN RADIUS TO WIDTH RATIO= 3.00

CURVED CHANNEL NO.	NO. OF CROSS SECTION	TOTAL CHANGE IN THE VOL.	CHANGES IN THE VOLS. 5-CMS INTERVAL					
1	1	88.06	4.3	0.9	8.2	17.8	26.7	30.2
1	2	19.58	10.1	-20.8	-22.1	-2.0	24.5	29.9
1	3	-283.68	27.5	-94.4	-111.7	-67.8	-27.4	-9.9
1	4	-359.06	152.5	-67.4	-132.2	-134.7	-123.5	-53.7
1	5	-166.86	384.3	100.5	-68.7	-165.0	-219.9	-198.0
1	6	-899.42	579.3	390.4	102.3	-168.9	-648.6	-1153.9

Fig. C1.9 - Water Depths in Stable Straight Sand Bed Channel

```
FLOW CHARACTERISTICS
**********************
**********************
AVARAGE CROSS SECTIONAL AREA=     127.97
MEAN VELOCITY=          31.62
FROUDE NUMBER=           3.49
NUMBER OF STRAIGHT CHANNELS= 2
NUMBER OF CURVED CHANNELS= 1
MEANRADIUS TO WIDTH RATIO= 3.00
************************************
************************************
```

ST. CHANNEL NO.	NO. OF CROSS SECTION	CROSS DISTANCE	WATER LEVEL	BED LEVEL	WATER DEPTH
2	7	3.81	10.00	6.10	3.90
2	7	9.14	10.00	6.10	3.90
2	7	17.15	10.00	6.49	3.51
2	7	21.63	10.00	6.10	3.90
2	7	26.55	10.00	6.10	3.90
2	8	3.69	10.00	6.13	3.87
2	8	9.83	10.00	6.25	3.75
2	8	16.19	10.00	6.47	3.53
2	8	21.63	10.00	6.17	3.83
2	8	26.67	10.00	6.17	3.83
2	9	3.69	10.03	6.20	3.83
2	9	9.52	10.00	6.20	3.80
2	9	16.63	10.00	6.40	3.61
2	9	21.29	10.02	6.20	3.82
2	9	26.67	10.02	6.20	3.82
2	10	3.81	10.10	5.85	4.25
2	10	9.68	10.10	5.85	4.25
2	10	16.19	10.10	6.05	4.05
2	10	21.24	10.10	5.85	4.25
2	10	26.67	10.10	5.85	4.25
2	11	2.95	10.05	6.00	4.05
2	11	9.83	10.05	6.00	4.05
2	11	15.73	10.05	6.05	4.00
2	11	21.91	10.05	6.00	4.05
2	11	26.13	10.05	6.00	4.05
2	12	2.95	10.10	5.92	4.18
2	12	9.83	10.10	6.00	4.10
2	12	15.99	10.10	6.08	4.02
2	12	21.63	10.10	5.94	4.16
2	12	26.55	10.10	5.94	4.16
2	13	2.95	10.10	6.04	4.06
2	13	9.14	10.10	6.01	4.09
2	13	16.71	10.10	6.07	4.03
2	13	21.63	10.10	6.03	4.07
2	13	26.67	10.10	6.03	4.07
2	14	3.79	10.10	5.60	4.50
2	14	9.52	10.10	5.51	4.59
2	14	16.45	10.09	5.74	4.35
2	14	17.23	10.10	5.65	4.45
2	14	26.48	10.10	5.57	4.53
2	15	3.39	10.00	5.39	4.61
2	15	9.68	10.00	5.21	4.79
2	15	16.45	10.00	5.50	4.50
2	15	20.96	10.00	5.36	4.64
2	15	25.72	10.00	5.37	4.63
2	16	3.39	10.00	5.76	4.24
2	16	9.52	10.00	5.71	4.29
2	16	15.99	10.00	5.81	4.19
2	16	21.91	10.00	5.74	4.26
2	16	26.19	10.00	5.75	4.25
2	17	3.28	10.17	6.07	4.10
2	17	8.99	10.15	5.93	4.22
2	17	[illegible]	10.15	6.02	4.13
2	[illegible]	[illegible]	[illegible]	6.17	4.21

Fig. C1.9-Cont.

ST. CHANNEL NO.	NO. OF CROSS SECTION	CROSS DISTANCE	WATER LEVEL	BED LEVEL	WATER DEPTH
1	1	0.00	10.20	6.00	4.20
1	1	5.00	10.20	5.90	4.30
1	1	10.00	10.20	6.10	4.10
1	1	15.00	10.20	6.10	4.10
1	1	20.00	10.20	6.20	4.00
1	1	25.00	10.20	6.20	4.00
1	1	30.00	10.20	5.90	4.30
1	2	0.00	10.20	6.00	4.20
1	2	5.00	10.20	6.00	4.20
1	2	10.00	10.20	6.00	4.20
1	2	15.00	10.20	6.25	3.95
1	2	20.00	10.20	6.25	3.95
1	2	25.00	10.20	6.30	3.90
1	2	30.00	10.20	6.00	4.20
1	3	0.00	10.20	6.10	4.10
1	3	5.00	10.20	5.95	4.25
1	3	10.00	10.20	6.20	4.00
1	3	15.00	10.20	6.20	4.00
1	3	20.00	10.20	6.25	3.95
1	3	25.00	10.20	6.20	4.00
1	3	30.00	10.20	6.10	4.10
1	4	0.00	10.10	6.00	4.10
1	4	5.00	10.15	6.00	4.15
1	4	10.00	10.15	6.20	3.95
1	4	15.00	10.20	6.10	4.10
1	4	20.00	10.20	6.10	4.10
1	4	25.00	10.20	6.10	4.10
1	4	30.00	10.20	6.10	4.10
1	5	0.00	10.20	6.00	4.20
1	5	5.00	10.10	5.90	4.20
1	5	10.00	10.10	6.10	4.00
1	5	15.00	10.10	6.20	3.90
1	5	20.00	10.10	6.20	3.90
1	5	25.00	10.10	6.20	3.90
1	5	30.00	10.10	6.10	4.00
1	6	0.00	10.20	6.10	4.10
1	6	5.00	10.10	5.90	4.20
1	6	10.00	10.15	6.10	4.05
1	6	15.00	10.10	6.20	3.90
1	6	20.00	10.10	6.20	3.90
1	6	25.00	10.10	6.20	3.90
1	6	30.00	10.10	6.10	4.00
2	1	0.00	9.65	7.20	2.45
2	1	5.00	9.70	7.80	1.90
2	1	10.00	9.75	7.10	2.65
2	1	15.00	9.85	6.20	3.65
2	1	20.00	9.90	5.00	4.90
2	1	25.00	10.10	2.30	7.80
2	1	30.00	10.20	1.20	9.00
2	2	0.00	9.60	6.00	3.60
2	2	5.00	9.55	7.00	2.55
2	2	10.00	9.70	7.45	2.25
2	2	15.00	9.80	7.00	2.80
2	2	20.00	9.80	3.40	6.40
2	2	25.00	9.90	1.40	8.50
2	2	30.00	10.00	0.70	9.30
2	3	0.00	9.80	5.90	3.90
2	3	5.00	9.80	5.90	3.90
2	3	10.00	9.90	6.80	3.10
2	3	15.00	10.00	6.30	3.70
2	3	20.00	10.00	4.20	5.80
2	3	25.00	10.05	1.50	8.55
2	3	30.00	10.20	0.90	9.30

Fig.Cl.9 -Cont.

ST. CHANNEL NO.	NO. OF CROSS SECTION	CROSS DISTANCE	WATER LEVEL	BED LEVEL	WATER DEPTH
2	4	0.00	9.90	5.90	4.00
2	4	5.00	9.90	6.00	3.90
2	4	10.00	9.90	6.30	3.60
2	4	15.00	10.00	5.80	4.20
2	4	20.00	10.00	4.20	5.80
2	4	25.00	10.05	2.00	8.05
2	4	30.00	10.20	1.90	8.30
2	5	0.00	10.00	5.90	4.10
2	5	5.00	9.95	6.20	3.75
2	5	10.00	10.00	6.70	3.30
2	5	15.00	10.05	5.90	4.15
2	5	20.00	9.95	4.20	5.75
2	5	25.00	10.10	2.70	7.40
2	5	30.00	10.20	3.00	7.20
2	6	0.00	9.90	5.80	4.10
2	6	5.00	9.90	6.20	3.70
2	6	10.00	10.00	7.00	3.00
2	6	15.00	10.00	6.00	4.00
2	6	20.00	10.00	4.30	5.70
2	6	25.00	10.05	3.30	6.75
2	6	30.00	10.00	3.50	6.50
2	7	0.00	10.00	6.10	3.90
2	7	5.00	10.00	6.10	3.90
2	7	10.00	10.00	7.00	3.00
2	7	15.00	10.00	6.30	3.70
2	7	20.00	10.00	5.60	4.40
2	7	25.00	10.00	4.40	5.60
2	7	30.00	10.00	3.80	6.20
2	8	0.00	10.00	5.80	4.20
2	8	5.00	10.00	6.25	3.75
2	8	10.00	10.00	7.20	2.80
2	8	15.00	10.00	6.80	3.20
2	8	20.00	10.00	5.90	4.10
2	8	25.00	10.00	4.70	5.30
2	8	30.00	10.00	4.00	6.00
2	9	0.00	10.10	6.20	3.90
2	9	5.00	10.00	6.20	3.80
2	9	10.00	10.00	6.80	3.20
2	9	15.00	10.10	6.90	3.20
2	9	20.00	10.10	6.20	3.90
2	9	25.00	10.10	5.10	5.00
2	9	30.00	10.10	4.30	5.80
2	10	0.00	10.10	5.85	4.25
2	10	5.00	10.10	5.85	4.25
2	10	10.00	10.10	6.70	3.40
2	10	15.00	10.10	6.70	3.40
2	10	20.00	10.10	6.20	3.90
2	10	25.00	10.10	4.90	5.20
2	10	30.00	10.10	4.50	5.60
2	11	0.00	10.05	6.00	4.05
2	11	5.00	10.05	6.00	4.05
2	11	10.00	10.05	6.35	3.70
2	11	15.00	10.20	6.50	3.70
2	11	20.00	10.20	6.20	4.00
2	11	25.00	10.20	4.90	5.30
2	11	30.00	10.20	5.00	5.20
2	12	0.00	10.10	5.80	4.10
2	12	5.00	10.10	6.00	4.10
2	12	10.00	10.10	6.40	3.70
2	12	15.00	10.10	6.50	3.60
2	12	20.00	10.10	6.20	3.90

Fig.C1.9 -Cont.

ST. CHANNEL NO.	NO. OF CROSS SECTION	CROSS DISTANCE	WATER LEVEL	RED LEVEL	WATER DEPTH
2	12	25.00	10.10	6.00	4.10
2	12	30.00	10.15	5.90	4.25
2	13	0.00	10.10	6.10	4.00
2	13	5.00	10.10	6.00	4.10
2	13	10.00	10.10	6.20	3.90
2	13	15.00	10.20	6.35	3.85
2	13	20.00	10.20	6.30	3.90
2	13	25.00	10.20	6.25	3.95
2	13	30.00	10.20	6.30	3.90
2	14	0.00	10.10	5.90	4.20
2	14	5.00	10.10	5.50	4.60
2	14	10.00	10.05	6.30	3.75
2	14	15.00	10.05	6.40	3.65
2	14	20.00	10.00	7.00	3.00
2	14	25.00	10.00	6.70	3.30
2	14	30.00	10.00	6.40	3.60
2	15	0.00	10.00	5.80	4.20
2	15	5.00	10.00	5.20	4.80
2	15	10.00	10.00	6.20	3.80
2	15	15.00	10.00	6.75	3.25
2	15	20.00	10.00	7.00	3.00
2	15	25.00	10.00	6.65	3.35
2	15	30.00	10.00	6.45	3.55
2	16	0.00	10.00	5.90	4.10
2	16	5.00	10.00	5.70	4.30
2	16	10.00	10.00	6.25	3.75
2	16	15.00	10.00	6.70	3.30
2	16	20.00	10.00	6.70	3.30
2	16	25.00	10.00	6.50	3.50
2	16	30.00	10.00	6.40	3.60
2	17	0.00	10.20	6.40	3.80
2	17	5.00	10.15	5.90	4.25
2	17	10.00	10.10	6.50	3.60
2	17	15.00	10.10	6.40	3.70
2	17	20.00	10.00	6.50	3.50
2	17	25.00	10.00	6.50	3.50
2	17	30.00	10.00	6.40	3.60
2	18	0.00	9.95	6.00	3.95
2	18	5.00	9.90	6.20	3.70
2	18	10.00	9.90	6.20	3.70
2	18	15.00	9.90	6.20	3.70
2	18	20.00	9.90	6.20	3.70
2	18	25.00	9.90	6.30	3.60
2	18	30.00	9.90	6.50	3.40
2	19	0.00	9.80	6.20	3.60
2	19	5.00	9.80	6.10	3.70
2	19	10.00	9.80	6.10	3.70
2	19	15.00	9.80	6.00	3.80
2	19	20.00	9.80	6.20	3.60
2	19	25.00	9.80	6.30	3.50
2	19	30.00	9.80	6.40	3.40
2	20	0.00	9.70	6.20	3.50
2	20	5.00	9.70	5.90	3.80
2	20	10.00	9.70	6.00	3.70
2	20	15.00	9.70	5.90	3.80
2	20	20.00	9.70	6.00	3.70
2	20	25.00	9.70	6.10	3.60
	[illegible]	[illegible]	9.70	6.30	3.40

Fig.C1.9 -Cont.

```
FLOW CHARACTERISTICS
********************
********************
AVARAGE CROSS SECTIONAL AREA=     127.97
MEAN VELOCITY=        31.62
FROUDE NUMBER=         0.49
NUMBER OF STRAIGHT CHANNELS= 2
NUMBER OF CURVED CHANNELS= 1
MEANRADIUS TO WIDTH RATIO= 3.00
***********************************
***********************************
```

ST. CHANNEL NO.	NO. OF CROSS SECTION	CROSS DISTANCE	WATER LEVEL	BED LEVEL	WATER DEPTH
2	18	3.81	9.91	6.15	3.76
2	18	10.32	9.90	6.20	3.70
2	18	15.97	9.91	6.16	3.75
2	18	20.96	9.91	6.16	3.75
2	18	26.67	9.91	6.17	3.74
2	19	2.95	9.80	6.14	3.66
2	19	9.52	9.80	6.10	3.70
2	19	15.97	9.80	6.10	3.70
2	19	20.96	9.80	6.13	3.67
2	19	25.72	9.80	6.14	3.66
2	20	2.86	9.70	6.03	3.67
2	20	9.19	9.70	5.92	3.78
2	20	15.97	9.70	5.94	3.76
2	20	20.96	9.70	6.01	3.69
2	20	25.72	9.70	6.01	3.69

Fig. C1.10 -Water depths in stable curved sand bed channel.

```
FLOW CHARACTERISTICS
********************
********************
AVARAGE CROSS SECTIONAL AREA=     127.97
MEAN VELOCITY=      31.62
FROUDE NUMBER=       0.49
NUMBER OF STRAIGHT CHANNELS= 2
NUMBER OF CURVED CHANNELS= 1
MEANRADIUS TO WIDTH RATIO= 3.00
***********************************
***********************************
```

CURVED CHANNEL NO.	NO. OF CROSS SECTION	CROSS DISTANCE	WATER LEVEL	BED LEVEL	WATER DEPTH
1	1	3.75	10.12	5.95	4.18
1	1	9.86	10.10	5.90	4.20
1	1	16.63	10.12	5.97	4.15
1	1	21.24	10.12	5.94	4.18
1	1	26.61	10.12	5.93	4.18
1	2	3.87	10.00	6.08	3.92
1	2	10.82	10.01	6.04	3.97
1	2	18.80	10.01	6.05	3.95
1	2	25.04	10.01	6.04	3.97
1	2	26.28	9.99	6.12	3.88
1	3	4.35	10.00	5.75	4.25
1	3	11.18	10.02	5.66	4.36
1	3	17.56	10.01	5.70	4.31
1	3	24.17	10.02	5.68	4.34
1	3	27.90	10.01	5.70	4.32
1	4	3.75	9.90	5.97	3.93
1	4	9.83	9.90	5.71	4.19
1	4	17.27	9.90	5.43	4.47
1	4	22.73	9.90	5.83	4.07
1	4	27.43	9.90	5.85	4.05
1	5	3.93	9.83	6.61	3.22
1	5	10.99	9.86	6.28	3.58
1	5	18.68	9.85	6.37	3.48
1	5	23.60	9.85	6.37	3.48
1	5	27.53	9.84	6.45	3.40
1	6	4.62	9.61	7.06	2.54
1	6	10.82	9.62	6.84	2.78
1	6	18.38	9.61	6.91	2.70
1	6	24.38	9.62	6.86	2.75
1	6	27.53	9.61	6.95	2.66
1	7	4.48	9.69	7.74	1.96
1	7	10.32	9.70	7.76	1.95
1	7	17.15	9.70	7.75	1.95
1	7	23.45	9.70	7.75	1.95
1	7	28.06	9.70	7.75	1.95

Fig. C1.10 cont.

CURVED CHANNEL NO.	NO. OF CROSS SECTION	CROSS DISTANCE	WATER LEVEL	BED LEVEL	WATER DEPTH
1	1	0.00	10.20	6.10	4.10
1	1	5.00	10.10	5.90	4.20
1	1	10.00	10.15	6.10	4.05
1	1	15.00	10.10	6.20	3.90
1	1	20.00	10.10	6.20	3.90
1	1	25.00	10.10	6.20	3.90
1	1	30.00	10.10	6.10	4.00
1	2	0.00	10.00	6.20	3.80
1	2	5.00	10.00	6.05	3.95
1	2	10.00	10.05	6.00	4.05
1	2	15.00	10.10	6.10	4.00
1	2	20.00	10.20	6.25	3.95
1	2	25.00	10.25	6.30	3.95
1	2	30.00	10.25	6.30	3.95
1	3	0.00	10.00	6.40	3.60
1	3	5.00	10.00	5.65	4.35
1	3	10.00	10.10	5.70	4.40
1	3	15.00	10.20	5.60	4.60
1	3	20.00	10.20	6.00	4.20
1	3	25.00	10.20	6.00	4.20
1	3	30.00	10.20	6.00	4.20
1	4	0.00	9.90	6.80	3.10
1	4	5.00	9.90	5.70	4.20
1	4	10.00	9.90	5.10	4.80
1	4	15.00	9.90	5.50	4.40
1	4	20.00	10.00	5.70	4.30
1	4	25.00	10.10	5.85	4.25
1	4	30.00	10.10	6.00	4.10
1	5	0.00	9.75	7.40	2.35
1	5	5.00	9.85	6.40	3.45
1	5	10.00	9.90	5.80	4.10
1	5	15.00	10.00	5.70	4.30
1	5	20.00	10.05	5.25	4.80
1	5	25.00	10.20	5.60	4.60
1	5	30.00	10.20	5.90	4.30
1	6	0.00	9.70	7.85	1.85
1	6	5.00	9.60	7.00	2.60
1	6	10.00	9.70	6.00	3.70
1	6	15.00	9.90	5.70	4.20
1	6	20.00	9.95	5.50	4.45
1	6	25.00	10.00	5.30	4.70
1	6	30.00	10.10	5.20	4.90
1	7	0.00	9.65	7.20	2.45
1	7	5.00	9.70	7.80	1.90
1	7	10.00	9.75	7.10	2.65
1	7	15.00	9.85	6.20	3.65
1	7	20.00	9.90	5.00	4.90
1	7	25.00	10.10	2.30	7.80
1	7	30.00	10.20	1.20	9.00

Fig. FC1.11 - Dimensionless cross sectional areas of water in stable curved sand bed channel.

```
FLOW CHARACTERISTICS
********************
********************
AVARAGE CROSS SECTIONAL AREA=     127.97
MEAN VELOCITY=      31.62
FROUDE NUMBER=       0.49
NUMBER OF STRAIGHT CHANNELS= 2
NUMBER OF CURVED CHANNELS= 1
MEANRADIUS TO WIDTH RATIO= 3.00
***********************************
***********************************
```

CURVED CHANNEL NO.	NO. OF CROSS SECTION	DIMENSIONLESS AREA OF WATER
1	1	0.94
1	2	0.93
1	3	1.00
1	4	1.00
1	5	0.96
1	6	0.90
1	7	1.04

Fig. C1.12 -Dimensionless cross sectional areas of water in stable straight sand bed channel.

```
FLOW CHARACTERISTICS
*******************
*******************
AVARAGE CROSS SECTIONAL AREA=     127.97
MEAN VELOCITY=       31.62
FROUDE NUMBER=        0.49
NUMBER OF STRAIGHT CHANNELS= 2
NUMBER OF CURVED CHANNELS= 1
MEANRADIUS TO WIDTH RATIO= 3.00
**********************************
**********************************
```

ST. CHANNEL NO.	NO.OF CROSS SECTION	DIMENSIONLESS AREA OF WATER
1	1	0.97
1	2	0.95
1	3	0.95
1	4	0.96
1	5	0.94
1	6	0.94
2	1	1.04
2	2	1.13
2	3	1.24
2	4	1.24
2	5	1.17
2	6	1.11
2	7	1.00
2	8	0.95
2	9	0.94
2	10	0.98
2	11	0.99
2	12	0.93
2	13	0.92
2	14	0.87
2	15	0.86
2	16	0.86
2	17	0.87
2	18	0.86
2	19	0.85
2	20	0.86

Appendix (C-2)

Stochastic Analysis

For

Path (1)-5.0 cms.From Inner

Wall,Bend Central Angle= 60

Fig. C2.1 -Dimensionless shear stress values along Path(1).

```
THE OBSERVATIONS OF THE SERIES ARE AS FOLLOW:
***********************************************
***********************************************
```

1.00	1.40	1.85	2.10	1.90	1.80	1.25	1.10
0.95	0.80	0.80	0.80	0.80	0.80	0.80	1.00
1.00	1.10	1.15	1.20	1.20	1.20	1.25	1.27
1.28	1.40	1.45	1.40	1.10	1.05	1.00	0.90

```
                              FOURIER ANALYSIS FOR TIME SERIES
                              PERIODGRAM-SPECTRUM-CORRLOGRAM
                              ******************************
                              ******************************

     THE SYMBOLS USED IN THIS PROGRAM ARE AS FOLLOW:
NR=NUMBER OF DATA SETS
NA=NUMBER OF DATA POINTS IN EACH SET
NB=NUMBER OF OF HARMONICS IN EACH SET
```

```
TIME SERIES ANALYSIS FCR;Path(1)
********************************
********************************
********************************
     **********************
     **********************
             ******
             ******
             ******
```

Fig. C2.2 -Harmonic analysis for the series in Path(1).

ANALYSIS OF VARIANCE TABLE FOR GIVEN SERIES
NCUH
SH.STRESS

HARMONIC	COEF A	COEF B	AMPLITUDE	PHASE	EX VAR	SUM EX VAR	FREQUENCY
0	1.191	0.0	1.418	0.0	1257.982	1257.982	0.0
1	0.234	-0.003	0.055	0.646	24.356	1282.338	0.03125
2	-0.132	0.257	0.084	62.793	37.075	1319.412	0.06250
3	-0.226	0.063	0.055	15.489	24.349	1343.762	0.09375
4	-0.154	-0.001	0.024	-0.468	10.473	1354.234	0.12500
5	-0.038	-0.042	0.003	-47.664	1.401	1355.635	0.15625
6	0.011	-0.025	0.001	65.809	0.334	1355.969	0.18750
7	0.016	-0.030	0.001	61.244	0.507	1356.476	0.21875
8	0.013	-0.021	0.001	58.692	0.266	1356.742	0.25000
9	-0.019	-0.026	0.001	-54.011	0.469	1357.211	0.28125
10	0.004	-0.016	0.000	76.732	0.113	1357.324	0.31250
11	0.004	0.000	0.000	-3.058	0.006	1357.330	0.34375
12	-0.001	0.016	0.000	85.997	0.120	1357.450	0.37500
13	-0.033	0.008	0.001	13.695	0.506	1357.956	0.40625
14	-0.003	-0.010	0.000	-75.855	0.050	1358.006	0.43750
15	0.005	-0.011	0.000	64.943	0.070	1358.075	0.46875
16	0.017	0.0	0.000	0.0	0.253	1358.328	0.50000

Fig. C2.3 -Predicted dimensionless shear stress values along the Path(1).

OBSERVED	ESTIMATED VALUES 1HAR	2HAR	3HAR	4HAR	5HAR	6HAR	7HAR	8HAR	9HAR	10HAR	11HAR	12HAR
1.00	1.42	1.40	1.24	1.13	1.08	1.06	1.03	1.01	0.99	0.97	0.97	0.98
1.40	1.41	1.49	1.47	1.46	1.44	1.41	1.39	1.38	1.40	1.41	1.41	1.39
1.85	1.38	1.57	1.68	1.78	1.81	1.81	1.83	1.85	1.86	1.87	1.87	1.88
2.10	1.35	1.61	1.82	1.97	2.02	2.05	2.08	2.10	2.06	2.05	2.04	2.05
1.90	1.32	1.61	1.84	1.95	1.98	2.00	2.00	1.98	1.98	1.98	1.98	1.97
1.80	1.28	1.55	1.74	1.74	1.72	1.71	1.68	1.66	1.70	1.71	1.71	1.73
1.25	1.23	1.45	1.53	1.42	1.37	1.34	1.33	1.35	1.34	1.32	1.32	1.31
1.10	1.19	1.32	1.26	1.11	1.06	1.05	1.08	1.09	1.07	1.06	1.06	1.06
0.95	1.14	1.17	0.99	0.88	0.89	0.91	0.93	0.91	0.93	0.95	0.95	0.96
0.80	1.10	1.01	0.78	0.78	0.83	0.85	0.83	0.82	0.84	0.83	0.83	0.81
0.80	1.06	0.87	0.66	0.77	0.82	0.82	0.79	0.81	0.78	0.77	0.77	0.78
0.80	1.02	0.77	0.65	0.80	0.81	0.78	0.79	0.80	0.80	0.81	0.82	0.82
0.80	0.99	0.71	0.72	0.83	0.79	0.77	0.80	0.78	0.81	0.81	0.81	0.79
0.80	0.97	0.70	0.84	0.84	0.79	0.80	0.80	0.79	0.78	0.77	0.77	0.79
0.80	0.96	0.74	0.96	0.85	0.84	0.87	0.84	0.86	0.83	0.84	0.84	0.83
1.00	0.96	0.82	1.05	0.90	0.93	0.94	0.93	0.94	0.96	0.96	0.96	0.96
1.00	0.96	0.94	1.09	0.98	1.04	1.02	1.04	1.02	1.04	1.03	1.03	1.04
1.10	0.98	1.06	1.09	1.09	1.11	1.09	1.11	1.10	1.07	1.08	1.08	1.07
1.15	1.00	1.18	1.08	1.19	1.16	1.16	1.14	1.16	1.15	1.16	1.16	1.17
1.20	1.03	1.28	1.08	1.23	1.18	1.20	1.17	1.18	1.21	1.20	1.20	1.20
1.20	1.06	1.35	1.12	1.23	1.19	1.21	1.22	1.20	1.19	1.20	1.20	1.18
1.20	1.10	1.38	1.19	1.20	1.21	1.20	1.24	1.23	1.19	1.21	1.20	1.22
1.25	1.15	1.37	1.29	1.19	1.24	1.21	1.22	1.25	1.26	1.25	1.25	1.24
1.27	1.19	1.33	1.39	1.23	1.28	1.26	1.23	1.25	1.27	1.27	1.27	1.27
1.28	1.24	1.26	1.44	1.33	1.32	1.34	1.32	1.30	1.27	1.29	1.29	1.30
1.40	1.28	1.20	1.43	1.42	1.37	1.40	1.42	1.41	1.39	1.38	1.39	1.37
1.45	1.32	1.14	1.35	1.45	1.40	1.41	1.44	1.46	1.49	1.48	1.48	1.49
1.40	1.36	1.10	1.22	1.37	1.37	1.34	1.34	1.35	1.35	1.37	1.37	1.37
1.10	1.39	1.10	1.08	1.19	1.24	1.22	1.18	1.16	1.13	1.13	1.13	1.12
1.05	1.41	1.13	0.99	0.99	1.05	1.05	1.05	1.04	1.04	1.03	1.03	1.05
1.00	1.42	1.20	0.98	0.87	0.89	0.91	0.94	0.97	1.00	1.01	1.01	1.00
0.90	1.42	1.29	1.06	0.91	0.67	0.89	0.90	0.92	0.90	0.90	0.91	0.90

Fig. C2.4 -Correlation analysis for the dimensionless shear stress observed values in Path(1).

CORRELATION ANALYSIS

LAG	UUTOCOV.	LUTCCOR.	CONFIDENCE LIMITS	
			UPPER	LOWER
1	0.09	0.84	0.31	-0.38
2	0.06	0.57	0.32	-0.39
3	0.03	0.27	0.32	-0.39
4	0.00	0.01	0.33	-0.40
5	-0.02	-0.16	0.33	-0.41
6	-0.03	-0.24	0.34	-0.42
7	-0.03	-0.30	0.34	-0.42
8	-0.04	-0.33	0.35	-0.43
9	-0.04	-0.35	0.36	-0.44
10	-0.04	-0.34	0.36	-0.45
11	-0.04	-0.31	0.37	-0.47
12	-0.03	-0.25	0.38	-0.48
13	-0.02	-0.19	0.39	-0.49
14	-0.01	-0.12	0.39	-0.50
15	-0.01	-0.06	0.40	-0.52
16	-0.00	-0.02	0.41	-0.54
17	0.00	0.03	0.42	-0.56
18	0.01	0.07	0.43	-0.58
19	0.01	0.11	0.45	-0.60
20	0.02	0.16	0.46	-0.63
21	0.02	0.19	0.47	-0.65
22	0.02	0.20	0.49	-0.69
23	0.02	0.15	0.50	-0.73
24	0.01	0.07	0.52	-0.77
25	-0.01	-0.05	0.54	-0.83
26	-0.02	-0.14	0.56	-0.90
27	-0.02	-0.15	0.58	-0.98
28	-0.01	-0.11	0.60	-1.10
29	-0.01	-0.06	0.59	-1.26
30	-0.00	-0.01	0.48	-1.48
31	0.00	0.02	-1.00	-1.00

Fig. C2.5 -Spectral analysis for the dimensionless shear stress observed values in Path(1).

SPECTRAL ANALYSIS

FREQUENCY	SPECTRAL	SMCOTH SPECT
0.0	-0.0000	1.9000
0.0313	7.8740	8.5494
0.0625	11.8363	10.7561
0.0938	7.7229	5.5287
0.1250	3.3012	2.7934
0.1563	0.4297	1.2311
0.1875	0.1054	0.5729
0.2188	0.1605	0.3166
0.2500	0.0832	0.1771
0.2813	0.1377	0.2073
0.3125	0.0322	0.1812
0.3438	0.0032	0.1485
0.3750	0.0452	0.1268
0.4063	0.1610	0.1653
0.4375	0.0113	0.0977
0.4688	0.0174	0.1128
0.5000	0.1618	0.1992

Fig. C2.6 -Estimated autoregressive parameters for the series in Path(1).

```
PARAMETERS FOR AUTCREGRESSIVE PRCCESSES ARE:
********************************************
********************************************

FCR FIRST ORDER PHI=    0.8408          FOR SECCND ORDER PHI=    1.2243     AND    -0.4561


THE RCOTS OF THE CHARACTERISTICS EQUATION ARE COMPLEX
*****************************************************


THE DAMPING FACTOR=     0.6753
THE FREGUENCY     =     3.9808
THE PHASE         =    -0.3445
```

Fig. C2.7 - Theoretical and observed autocorrelation analysis.

CORRELATION ANALYSIS

LAG	OUTCOR	CUTOREG PROCESS FIRST	CUTOREG PROCESS SECOND
1	0.84	0.84	0.78
2	0.57	0.71	0.59
3	0.27	0.59	0.43
4	0.01	0.50	0.31
5	-0.16	0.42	0.22
6	-0.24	0.35	0.15
7	-0.30	0.30	0.10
8	-0.33	0.25	0.07
9	-0.35	0.21	0.04
10	-0.34	0.18	0.03
11	-0.31	0.15	0.02
12	-0.25	0.12	0.01
13	-0.19	0.10	0.01
14	-0.12	0.09	0.00
15	-0.06	0.07	0.00
16	-0.02	0.06	0.00
17	0.03	0.05	0.00
18	0.07	0.04	0.00
19	0.11	0.04	-0.00
20	0.16	0.03	-0.00
21	0.19	0.03	-0.00
22	0.20	0.02	-0.00
23	0.15	0.02	-0.00
24	0.07	0.02	-0.00
25	-0.05	0.01	-0.00
26	-0.14	0.01	-0.00
27	-0.15	0.01	-0.00
28	-0.11	0.01	-0.00
29	-0.06	0.01	-0.00
30	-0.01	0.01	-0.00
31	0.02	0.00	-0.00

Fig.C2.8 -Theoretical spectral analysis of autoregressive process.

SPECTRAL ANALYSIS

FREQUENCY	OBSERVED	FIRST PROCESS	SECOND PROCESS
0.0	-0.0000	23.1248	8.6378
0.0313	7.8740	10.1715	8.7897
0.0625	11.8363	3.8254	8.0108
0.0938	7.7229	1.9002	5.0783
0.1250	3.3012	1.1329	2.5020
0.1563	0.4297	0.7592	1.2334
0.1875	0.1054	0.5517	0.6667
0.2188	0.1605	0.4254	0.3979
0.2500	0.0832	0.3437	0.2591
0.2813	0.1377	0.2882	0.1816
0.3125	0.0322	0.2495	0.1357
0.3438	0.0032	0.2221	0.1071
0.3750	0.0452	0.2025	0.0889
0.4063	0.1610	0.1888	0.0772
0.4375	0.0113	0.1798	0.0699
0.4688	0.0174	0.1747	0.0659
0.5000	0.1618	0.1730	0.0646

Fig.C2.9 -Theoretical spectral analysis of moving average process.

SPECTRAL ANALYSIS

FREQUENCY	OBSERVED	FIRST PROCESS	SECOND PROCESS
0.0	-0.0000	1.9200	1.7811
0.0313	7.8740	1.9367	1.9498
0.0625	11.8363	1.9799	1.8331
0.0938	7.7229	2.0314	1.8957
0.1250	3.3012	2.0698	1.9477
0.1563	0.4297	2.0791	1.8543
0.1875	0.1054	2.0553	2.0385
0.2188	0.1605	2.0084	1.8935
0.2500	0.0832	1.9580	2.0530
0.2813	0.1377	1.9251	2.0135
0.3125	0.0322	1.9236	2.0171
0.3438	0.0032	1.9539	2.1409
0.3750	0.0452	2.0035	2.0046
0.4063	0.1610	2.0517	2.1920
0.4375	0.0113	2.0782	2.0610
0.4688	0.0174	2.0721	2.1471
0.5000	0.1618	2.0358	2.1553

Appendix (C-3)

Velocity Distributions in Sand Bed Curved Channels

VELOCITY DISTRIBUTIONS IN SAND BED CURVED CHANNELS

Vertical velocity distributions in a sand bed channel have been investigated, recently, by Mahmood[64]. He found that the velocity-defect law can be used to describe the vertical velocity profiles in the outer layers in such channels and also in the case of flat beds. Von Karman's coefficient, κ, in the outer layers is found to be related to the total suspended load as well as to the parameters representing the shape, concentration and angularity of the bed forms.

According to the stated assumptions in this study, namely: that the bed profile, along any path, is gradually-varying and smooth and that, in the case of curved channels of large radius of curvature to width ratio, the distribution of longitudinal velocity components in the bend will remain approximately the same as that in the straight channel upstream, the velocity-defect law (Eq. 3.1.2.2) can be used, with Von Karman's coefficient as a variable (Eq. 3.1.2.6), to describe the vertical velocity profiles in the channel system.

However, to examine the applicability of these laws, in the study Von Karman's coefficients are computed (Eq. 3.1.2.6) and a comparison between the velocity-defect law (Eq. 3.1.2.2) and measured point velocities in the corresponding vertical has been made (Fig. C3.1 and Fig. C3.2, respectively).

FIGURE C3.1

Distributions of von Karman's Coefficient κ

Run Number 2

Central Bend Angle = 60°

von Karman's Coefficient				
Path 1	Path 2	Path 3	Path 4	Path 5
0.51	0.51	0.51	0.51	0.51
0.52	0.51	0.51	0.48	0.48
0.52	0.51	0.51	0.50	0.48
0.53	0.52	0.50	0.50	0.49
0.53	0.52	0.52	0.50	0.50
0.53	0.52	0.52	0.50	0.50
0.52	0.52	0.52	0.50	0.50
0.52	0.52	0.52	0.51	0.50
0.52	0.52	0.52	0.51	0.51
0.51	0.52	0.52	0.51	0.51
0.50	0.52	0.52	0.52	0.52
0.48	0.52	0.52	0.52	0.53
0.47	0.52	0.52	0.53	0.53
0.48	0.52	0.52	0.53	0.53
0.48	0.52	0.52	0.52	0.53
0.49	0.52	0.52	0.52	0.53
0.48	0.52	0.51	0.52	0.52
0.48	0.52	0.51	0.52	0.52
0.49	0.52	0.51	0.52	0.52
0.49	0.52	0.51	0.52	0.52
0.50	0.51	0.51	0.51	0.52
0.49	0.51	0.51	0.51	0.51
0.49	0.50	0.51	0.51	0.51
0.50	0.50	0.50	0.51	0.51
0.50	0.50	0.50	0.50	0.50
0.50	0.50	0.50	0.50	0.50
0.50	0.50	0.50	0.50	0.49
0.50	0.49	0.49	0.48	0.48
0.49	0.48	0.49	0.49	0.48
0.49	0.49	0.49	0.49	0.49
0.46	0.48	0.48	0.48	0.49
0.48	0.49	0.48	0.48	0.49

Fig. 63.2. Typical theoretical and measured vertical velocity profiles

a) Straight channel at its centerline (Path 3-Section 26)

b) Curved channel (Path 5-Section 13)

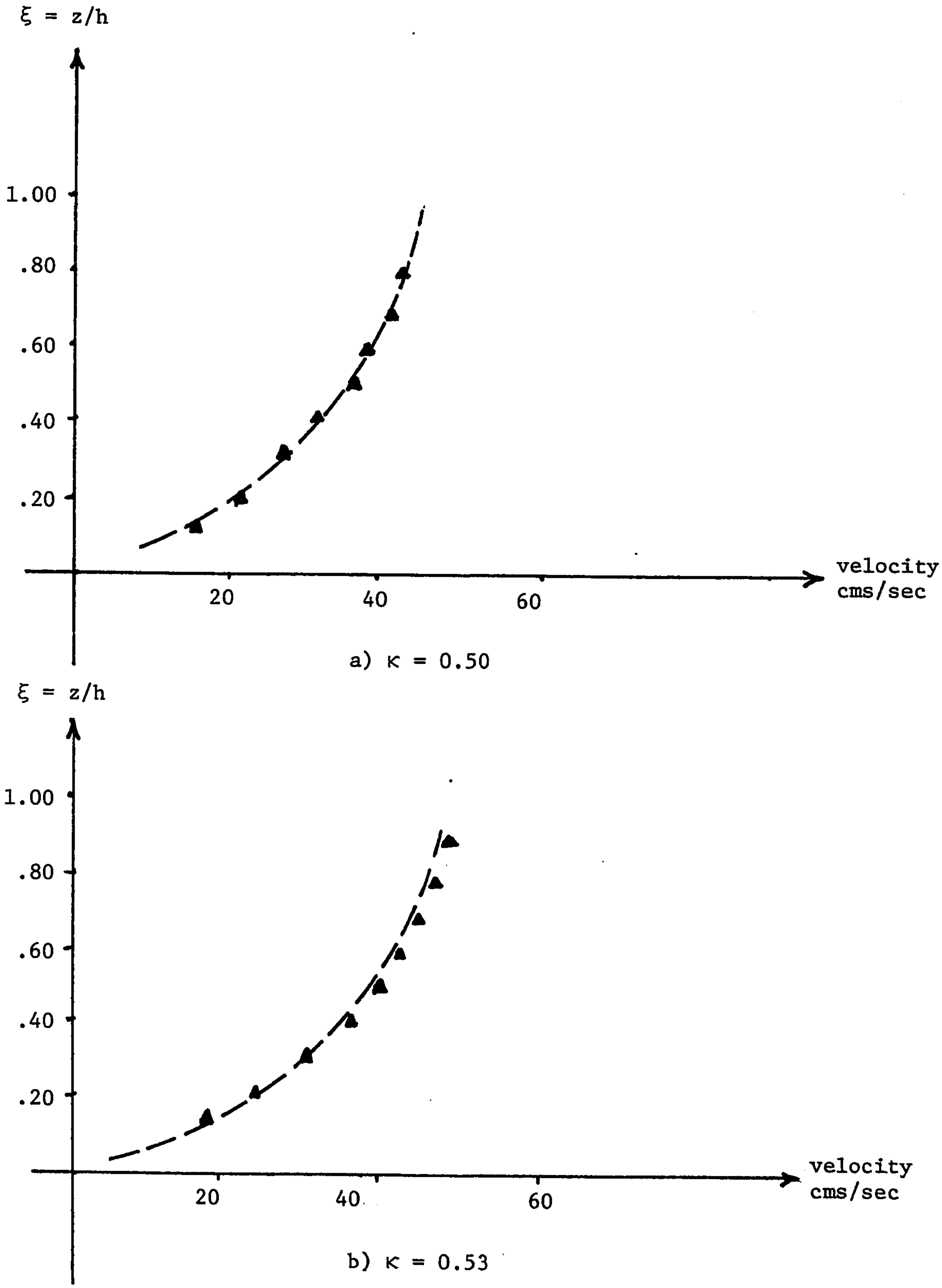

a) $\kappa = 0.50$

b) $\kappa = 0.53$

RESUME

Boundary shear stress distribution, in a fully-developed open channel flow, is predominantly a function of the velocity distribution in the flow field. The velocity distribution in a curved channel section (river bend) differs substantially from that in the preceding "straight". This is largely due to the presence of a strong helicoidal flow pattern in the bend (generated by the flowline curvature) - the effects of which may persist for a considerable distance downstream from same.

These so-called "secondary-currents", which govern the distribution of boundary shear stress (and hence the general bed topography) in the vicinity of channel bends, constitute only one factor in a highly complex problem in river engineering, namely that of sediment transportation.

In an alluvial stream, where non-cohesive materials constitute a larger percentage of the total sediment complex, this secondary flow phenomenon is the prime mechanism responsible for the establishment of the "meander" profile of the main channel. This has become, in many instances, an important economic consideration (in overall river management) in that substantial areas of valuable agricultural lands are lost in the erosion process.

Furthermore, subsequent deposition of material, (initially eroded along the outer bank of a river bend), near the inner bank downstream from the bend can present problems of equal importance. For example: dredged navigation channels may become blocked through silting and river intake/out fall structures might suffer similar consequences.

....2

These complex interrelated processes of erosion, transportation and deposition of material are governed, to a large degree, by the shear stress distribution at the sediment/water interface as is the stable channel bed configuration under "regime" flow conditions.

A major criticism that can be made concerning recent fundamental studies in this area is the fact that theories developed for the prediction of boundary shear stress distribution are only applicable to the bend sections themselves. They do not extend to the straight channel reaches (immediately following the bends) where, as has been mentioned earlier, the secondary currents remain a significant flow feature. Moreover, these same theories are based on an assumed uniform tractive force distribution on the channel bed - an assumption that normally does not reflect the true situation in a natural watercourse.

Other recent laboratory investigations, while reporting boundary shear stress values in channel bends, do not provide a methodology to facilitate prediction of the steady-state distribution therein. Furthermore, the data reported in these studies may be subject to inherent errors introduced by the nature of the instrumentation employed in the investigations.

In view of the aforementioned limitations in existing theories and related laboratory studies on this subject it was felt that further work in this area was warranted. In particular there was a need to develop a more comprehensive predictive model that would include those portions of the straight channel reaches, downstream from the bends, that continue to be influenced by the secondary currents generated in the latter.

....3

In the present study a stochastic-type numerical model is developed to facilitate prediction of the distribution of shear stress on the stable sand bed of a bend in an open channel and that portion of the straight channel reach (immediately following the bend) along which the secondary flow, generated in the bend section, remains a significant flow feature.

The overall investigation, which included laboratory studies on a physical model of the system, also presents a new method for determining actual boundary shear stress based on single-point velocity measurements in the flow field.

The physical model a 0.30 m wide rectangular channel, 10.0 m long contained an adjustable bend section, (mean radius of curvature to width ratio = 3.0), approximately 2.0 m downstream from the channel inlet. Central bend angles of 45°, 60° and 75° and a Froude Number (F) ≃ 0.50 were adopted in the study.

Point velocity measurements in the test section were obtained with a high degree of accuracy and without local disturbance to the flow field using the Laser Doppler Anemometer system.

Shear stress distributions, within the test section, were expressed in dimensionless format (i.e., local boundary shear stress values were related to the corresponding theoretical uniform stress value for a straight infinitely-wide channel).

Prediction of the steady-state distribution of bed shear stress in the three different bend sections was generated, (along paths that were parallel to the channel centerline), by the different

....4

mathematical models considered using the respective upstream (initial) channel boundary conditions.

Comparison between predicted and actual (steady-state) shear stress distributions were used to examine the relative merits of the numerical models developed for this purpose.

The results of this study indicate that shear stress distribution, along any path parallel to the channel centerline, can be predicted, to any required accuracy using Finite Fourier Series.

Furthermore, to ensure an acceptable degree of accuracy, a minimum number of harmonics is recommended. This number is found to be dependent on the position of any path (relative to the channel centerline) and also on the channel geometry; for example the number increases as the radius of curvature and bend central angle decreases.

Moreover, a second order autoregressive process appears to be appropriate in the analysis, and the autocorrelation function for all paths is found to be of the damped sine wave or damped exponential wave character. This conclusion is reflected in the periodic behaviour of the change in the bed shear stress along any path in the system.